NATIONAL CENTER FOR EARTHQUAKE ENGINEERING RESEARCH

State University of New York at Buffalo

Low-Level Dynamic Characteristics of Four Tall Flat-Plate Buildings in New York City

by

H. Gavin, S. Yuan, J. Grossman, E. Pekelis, and K. Jacob

conducted at

Department of Civil Engineering and Operations Research
School of Engineering and Applied Sciences
Princeton University
Princeton, New Jersey 08544

and

Lamont-Doherty Earth Observatory
of Columbia University
Palisades, New York 10964

Technical Report NCEER-92-0034

December 28, 1992

This research was conducted at Princeton University and Lamont-Doherty Earth Observatory and was partially supported by the National Science Foundation under Grant No. BCS 90-25010 and the New York State Scie ler Grant No. NEC-91029.

NOTICE

Low-Level Dynamic Characteristics of Four Tall Flat-Plate Buildings in New York City

by

H. Gavin[1], S. Yuan[2], J. Grossman[3], E. Pekelis[4] and K. Jacob[5]

December 28, 1992

Technical Report NCEER-92-0034

NCEER Project Numbers 91-1011 and 91-1031

NSF Master Contract Number BCS 90-25010
and
NYSSTF Grant Number NEC-91029

1 Research Engineer, Department of Civil Engineering and Operations Research, Princeton University
2 Associate Professor, Department of Engineering Mechanics, Tongji University, China
3 Vice President, Rosenwasser/Grossman Consulting Engineers
4 Staff Associate, Lamont-Doherty Earth Observatory
5 Senior Research Scientist in Seismology and Tectonics, Lamont-Doherty Earth Observatory

NATIONAL CENTER FOR EARTHQUAKE ENGINEERING RESEARCH
State University of New York at Buffalo
Red Jacket Quadrangle, Buffalo, NY 14261

PREFACE

The National Center for Earthquake Engineering Research (NCEER) was established to expand and disseminate knowledge about earthquakes, improve earthquake-resistant design, and implement seismic hazard mitigation procedures to minimize loss of lives and property. The emphasis is on structures in the eastern and central United States and lifelines throughout the country that are found in zones of low, moderate, and high seismicity.

NCEER's research and implementation plan in years six through ten (1991-1996) comprises four interlocked elements, as shown in the figure below. Element I, Basic Research, is carried out to support projects in the Applied Research area. Element II, Applied Research, is the major focus of work for years six through ten. Element III, Demonstration Projects, have been planned to support Applied Research projects, and will be either case studies or regional studies. Element IV, Implementation, will result from activity in the four Applied Research projects, and from Demonstration Projects.

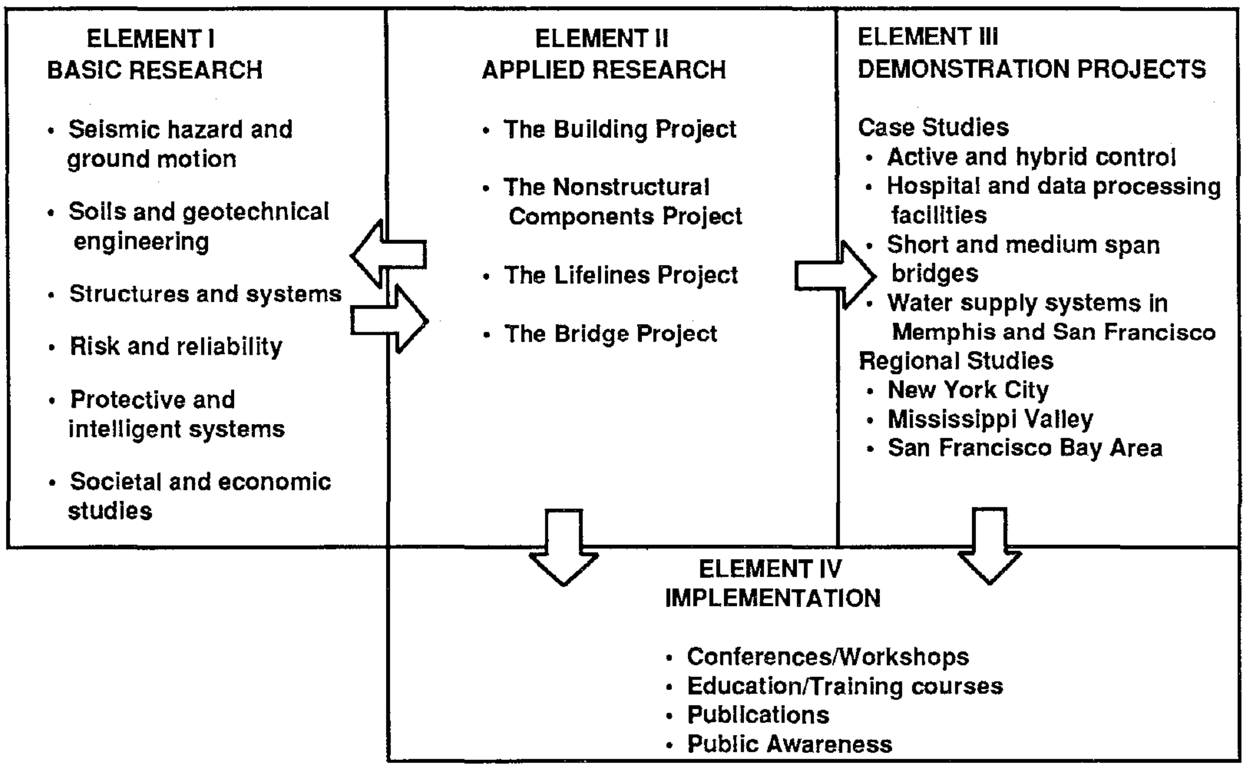

Research in the **Building Project** focuses on the evaluation and retrofit of buildings in regions of moderate seismicity. Emphasis is on lightly reinforced concrete buildings, steel semi-rigid frames, and masonry walls or infills. The research involves small- and medium-scale shake table tests and full-scale component tests at several institutions. In a parallel effort, analytical models and computer programs are being developed to aid in the prediction of the response of these buildings to various types of ground motion.

Two of the short-term products of the **Building Project** will be a monograph on the evaluation of lightly reinforced concrete buildings and a state-of-the-art report on unreinforced masonry.

The **structures and systems program** constitutes one of the important areas of research in the **Building Project**. Current tasks include the following:

1. Continued testing of lightly reinforced concrete external joints.
2. Continued development of analytical tools, such as system identification, idealization, and computer programs.
3. Perform parametric studies of building response.
4. Retrofit of lightly reinforced concrete frames, flat plates and unreinforced masonry.
5. Enhancement of the IDARC (inelastic damage analysis of reinforced concrete) computer program.
6. Research infilled frames, including the development of an experimental program, development of analytical models and response simulation.
7. Investigate the torsional response of symmetrical buildings.

*The evaluation of existing buildings for seismic effects has been one of the main goals of the **Building Project**. The primary emphasis has been on concrete structures that were designed only for gravity loads. One problem in the evaluation and design of structures for dynamic loads is the accurate analytical representation of the stiffness and damping properties. This report presents the results of field tests on four flat-plate structures, which are a very common type of structural system in the East. Such tests on real buildings include the effects of the interaction of walls with the other elements. The low-level ambient wind vibration tests help the calibration of analytical methods, especially in the determination of the effective width of floor slabs.*

ABSTRACT

Many reinforced concrete structures utilize flat plates to provide lateral resistance when architectural constraints prevent wide-spread use of shear-walls. Understanding the resistance of flat-plate frames to large lateral loads is important for serviceability as well as seismic vulnerability assessment of hundreds of buildings on the East Coast. In February of 1991, the authors collected ambient vibration measurements to study the behavior of four flat plate, reinforced concrete structures in Manhattan ranging from 27 to 52 stories. All but one structure rests on a rock supported foundation. This report presents the development of ambient vibration analysis software based on the fast Fourier transform. Long ambient vibration records allow accurate power spectrum estimation. A robust peak picking method, also tailored for ambient vibration data, facilitates the interpretation of auto-power and phase spectra. Damping estimates based on spectral peak band-widths are very sensitive to bias and leakage errors in the spectrum estimate. However, root-mean-square statistics of acceleration as well as of velocity and displacement can reasonably be estimated from the auto-power spectrum of response acceleration. Measured fundamental periods are shorter than those calculated from the 1982 UBC formula, but are longer than those calculated from the 1988 UBC Code or the proposed NYC Seismic Code. The results presented herein provide a base-line set of periods, deflections, and damping ratios to be compared to results expected to be obtained during strong winds. Periods estimated from ambient, mostly wind-induced vibration measurements are used to calibrate finite element models of the structures, and are compared to values calculated from code design rules. A future goal of this on-going research is to relate effective flat plate width to lateral load level at service load levles, i.e., between ambient conditions and strong winds. Estimating dynamic parameters under various loading conditions coupled with ultimate load tests on model structures is intended to reveal the load-dependent stiffness of these structures.

ACKNOWLEDGEMENTS

The structural engineering firm of Rosenwasser/Grossman, P.C., initiated this study, designed the buildings, and arranged access to them. The researchers thank the owners of the four buildings tested, The DeMatteis Organization, Grand Palais Associates, and Rose Associates, for their cooperation in this study. Financial support for this project was provided by Rosenwasser/Grossman, P.C., and The National Center for Earthquake Engineering Research under grant No's. NCEER 91-1011 and 91-1031.

Preceding page blank

TABLE OF CONTENTS

LIST OF ILLUSTRATIONS

LIST OF TABLES

SECTION 1
INTRODUCTION

Since the late 1960's, building codes for tall structures in New York City have increasingly emphasized structural resistance to wind and other lateral loads. Forthcoming New York City Building Code revisions will include seismic provisions and will increase the lateral design loads for many tall structures. Many high-rise structures in New York City are residential, especially in the upper stories. Architectural constraints in high-rise apartment buildings preclude the prevalent usage of shear walls to resist lateral forces. Consequently, in order to enhance their lateral resistance, several hundred buildings have incorporated, and rely upon, flat plates. In the structures studied herein, the flat-plate system is designed to resist a considerable portion of the lateral loads, the remainder of which is carried by shear walls interacting with the frame. In existing design codes for seismically active regions of the country, the base shear resistance of the structure is prescribed as a function of the structure's first natural period. Codes provide simplified formulas for estimating a building's fundamental period at its ultimate capacity. However, the actual dynamic properties of the structure at service load levels and at limit state levels may differ considerably from values estimated using codified formulas. Periods computed in the design process, which correspond to a 100-year wind producing roof deflection of H/400, are longer than the measured ambient periods, which correspond to deflections as small as H/ 2,000,000. In addressing wind response, serviceability considerations, and occupant comfort, extensive dynamic measurements of some of the tallest structures in New York City, such as the World Trade Center (aspect ratio = 6), and several other slender concrete structures (aspect ratio $\geq$10), have been undertaken in the past [Grossman 1990]. However, many moderately sized buildings, between 30 and 60 stories, have, as of yet, been overlooked by such dynamic analyses. The current trend toward more slender structures and reduced foot-print areas could result in greater sway in, albeit, shorter structures, and present an engineering challenge not found in squatter, although taller buildings. The combined conditions of the reduction in shear wall areas, more slender structures, consideration of occupant comfort, and more demanding codes with respect to lateral loads call for a method to assess the strength of flat plates in resisting lateral loads at ultimate conditions, as well as the behavior of flat-plate structures at service load levels. This report presents work in progress to meet these challenges. The ambient vibration measurements of this study are being compared to partially completed detailed computer modeling by the designers of the four "as built" reinforced concrete flat-plate framed structures. The design methodology used in the comparison [Grossman, 1987] was fine tuned in a parallel study [Grossman, in progress] using ultimate laboratory load tests of flat-plate sub-structures [Moehle, 1990].

Of key interest is the contribution of several structural and non-structural elements to the structure's lateral resistance, and the degradation of the lateral resistance at greater deflections. The dependency of parameters such as the effective flat-plate width, the effective shear wall stiffness, and the effective coupling-beam moment of inertia, on the deflection of the structure is uncertain, and needs to be determined reliably.

For purposes of comparing lateral sway among different buildings, roof deflections can be expressed as a fraction of the total height of the structure, H. For example, typical roof deflections under ambient conditions are less than H/800, the 100-year wind deflections are on the order of H/400, and seismic deflections should not exceed H/200.

The scale of these structures virtually precludes forced response experiments and traditional modal analysis. Nonetheless, ambient vibrations are very informative and have certain advantages, namely:

1. The length of time for data recording can be arbitrarily large, allowing for long-duration spectral averages and, hence, improved spectral resolution.

2. Structures vibrating in ambient conditions (at small amplitudes) behave more linearly than structures responding to earthquakes. Structural parameters, estimated from response records alone, are time-invariant if the excitation is stationary and the structure exhibits linear elastic behavior over the course of a single measurement record.
3. The variance of the response acceleration is nearly independent of the section of the data record being analyzed. Adjusting the recorder gains to the known signal level before recording begins, maximizes the signal-to-noise ratio of the recording, without the risk of clipping the data.
4. Comparing the motion of the structure subjected to forces during strong winds to predetermined thresholds of human comfort or perception is useful in assessing serviceability.

The immediate objectives of this study are to:

1. Develop parameter estimation software for the analysis of ambient vibration measurements from large scale structural systems. The software package computes auto-power spectra and phase spectra between a "measurement" or "response" sensor and a "reference" sensor. It also picks spectral peaks, a feature which facilitates the estimation of the following dynamic parameters: natural frequency, amplitude, phase, damping ratio, and root-mean-square displacement, velocity, and acceleration. The programs require discrete building-response (output) time-records only.
2. Verify the results from the programs developed in step 1 with a parallel but independently developed routine. Verify the root-mean-square computations with small-scale tests on laboratory models.
3. Compare experimentally estimated periods with periods computed (in a parallel study) by finite-element modeling of the "as-built" structure.
4. Establish a set of base-line parameters for comparison with future tests during different

wind conditions.

The long-range objectives of this study are to:

1. Assess the actual contribution of flat-plates, shear walls, and coupling beams to the overall lateral stiffness in four similar, reinforced concrete structures.
2. Compare the buildings' compliance with current and proposed New York City design codes for wind and seismic forces respectively.
3. Compare the natural periods of structures under construction to their periods after some wind storms. Model the measured buildings in their "as built" condition using state of the art software not available to the design team at the time the structures were designed. Investigate the influence of partitions and cladding on the building's response to lateral loads.
4. Investigate the influence of foundations and soil conditions on the measured building response at different periods.

In conducting the measurements and analysis, the researchers enlisted equipment and expertise from the Lamont-Doherty Geological Observatory of Columbia University (L-DGO), and from the Department of Civil Engineering and Operations Research of Princeton University. The buildings measured were designed by the firm of Rosenwasser/Grossman, P.C. L-DGO has a wide interest in the measurement and analysis of earthquake-induced ground motions. It provided the geophones, accelerometers, recording instruments, and some of the pre-processing and analysis hardware used in this study. Professor Shi Yuan's experience in ambient vibration analysis expedited the development of a systematic and robust software package. The spectral analysis routines were written at Princeton University's Department of Civil Engineering and Operations Research, and verified by methods independently developed at L-DGO.

Following this introduction, Section 2 contains a description of the four buildings chosen for the study. Section 3 reviews the standard code procedures of estimating a building's period. Sections 4 and 5 present the measurement and experimental data analysis methods respectively. Section 6 compares the finite-element results to the experimental results. Section 7 discusses the research underway to evaluate the resistance of flat plates to lateral loads, and Section 8 contains the conclusions.

SECTION 2
DESCRIPTION OF THE BUILDINGS

The four reinforced-concrete frame structures each represent a common type of east-coast construction; the design philosophy for all the buildings requires using flat plates to improve resistance to lateral forces. Buildings A and B were under construction during the measurements. Building A is a new building and was clad up to two-thirds its height at the time of the measurements; it was not occupied. It had interior partitions up to the 45^{th} floor. The partitions' mass was positioned (stored) in the upper stories, although the partitions were not yet installed. Building B was a new, bare, unclad, and unoccupied concrete frame at the time of the measurements. Buildings C and D were completed and occupied during the measurements; they both had brick cladding. Building D was constructed during the mid 1970's, was topped-out but remained partially un-clad for several years during the 1970's recession. It was finished several years later and is now fully occupied. Figures 2-1 to 2-4 describe the typical structural floor plans, the elevation views of the four buildings, and other pertinent information. Table 2-I summarizes some of the building features.

TABLE 2-I Overview of the Four Buildings

	A	B	C	D
Number of Stories	52	40	27	48
Effective building height	486 ft.	423 ft.	248 ft.	460 ft.
Inter-story height	9'-0.5"	9'-8"	8'-8"	8'-10"
Foot Print (NSxEW)	112' x 92'	80.5' x 90'	80' x 121'	176' x 145'
Aspect Ratio (NS, EW)	4.3 5.3	5.3 4.7	3.1 2.1	2.6 3.2
Foundation	piles	rock	rock	rock
Number of Load-Bearing Columns	31	27	42	54
Thickness of the floor slab	8.5 in.	8.5 in.	8 in.	8 in.

Building A is the only building of the four utilizing a pile foundation. Twenty-five feet of fill overlays 90 to 130 feet of poorly graded, saturated sands with little silt, having standard penetration test blow counts (N values) ranging between medium compact (10 < N < 30) at the top 50 feet of the sand strata to compact (N > 30) at the deeper strata (> 75') where the piles were fetched. These strata occupy a portion of the southern end of Manhattan. They have a long history of settlement of existing buildings when, at adjacent lots, displacement piles are driven (by impact hammers) to support new structures. Augured piles were therefore recommended for Building A when in close proximity to adjacent existing structures, in order to reduce settlement that would have been caused by the vibration from impact hammers. However, the augured piles were difficult to control during the construction period because of loss of ground into the augured shaft.

The water table is approximately 10 feet below the fill (35' to 40' below street level) and liquefaction of the top strata, while a remote possibility, needed not to be considered for this structure in accordance with the existing or newly proposed NYC Code. Piles are long (90 feet minimum for the augured piles and about 110 feet for the driven pipe piles). Even if some liquefaction were to occur, it is unlikely that it would cause the loss of building support. S3 = 1.5 would have been the appropriate site category and coefficient for this structure had it been designed according to the now newly proposed NYC Seismic Code. The building's design preceded the proposed NYC Seismic Code.

Buildings B and D are supported by spread footings, bearing on rock of class 3-65 and 2-65 [20-40 ton/sq.ft. capacity] and the proposed NYC Seismic Code assigns a site coefficient of So = 0.67 for such sites. Building C is supported on spread footings and short piles to rock [class 3-65, 20 ton/sq.ft.] and its site coefficient will require further study (but is likely to be S1 = 1.0) .

All four buildings are considered by the proposed NYC Seismic Code to be Dual Systems having concrete shear walls with concrete Ordinary Moment Resisting Frame [OMRF (Rw = 5)].

Concrete ordinary moment resisting frames (OMRF's) are, in these cases, flat plates without spandrel beams. This system became popular in eastern U.S. cities after the Second World War, initially with spandrel beams, but since the 1970's often without them. The flat plate is therefore an important lateral load-resisting structural member.

Shear-wall frame interaction is present in all four structures. In building A, for example, about 50% of the total lateral overturning moment is resisted by shear deformation of the columns and slabs and the remainder by flexural action of the coupled structural walls. Recent laboratory testing [Hwang and Moehle 1990, 1991a, 1991b] and a sensitivity review [Grossman 1991] allow determination of the flat-plate effectiveness at different lateral load levels. Other studies [Grossman 1987, Moehle and Wallace 1990] provide recommendations to estimate the structural wall stiffness acting under varied gravity and lateral loads. A follow-up study will attempt to verify these earlier studies by comparing the measured dynamic properties of the structures with the computed dynamic properties obtained using the methodologies proposed in Section 7 to estimate stiffnesses.

The flat plates were designed to support a considerable portion of the lateral loads in addition to gravity loads. The column-slab joints were designed to transfer large moments and continuity of bottom mat reinforcing was required to account for reversal of moments. In these structures the integrity requirements of the 1989 ACI Code were generally observed, even though they were constructed before such requirements became mandatory.

FIGURE 2-1 BUILDING A - Typical Floor Plan and Elevation

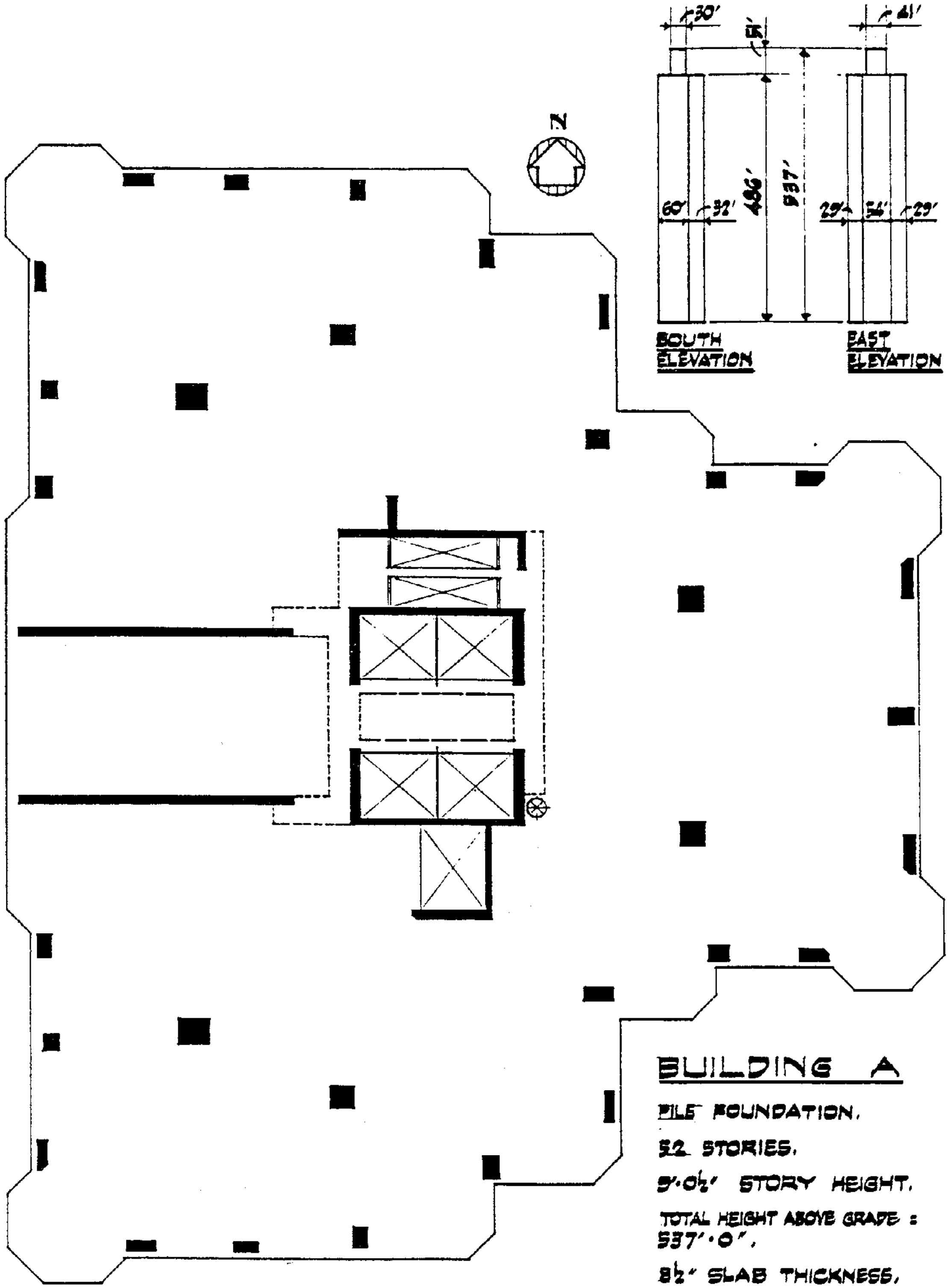

FIGURE 2-2 BUILDING B - Typical Floor Plan and Elevation

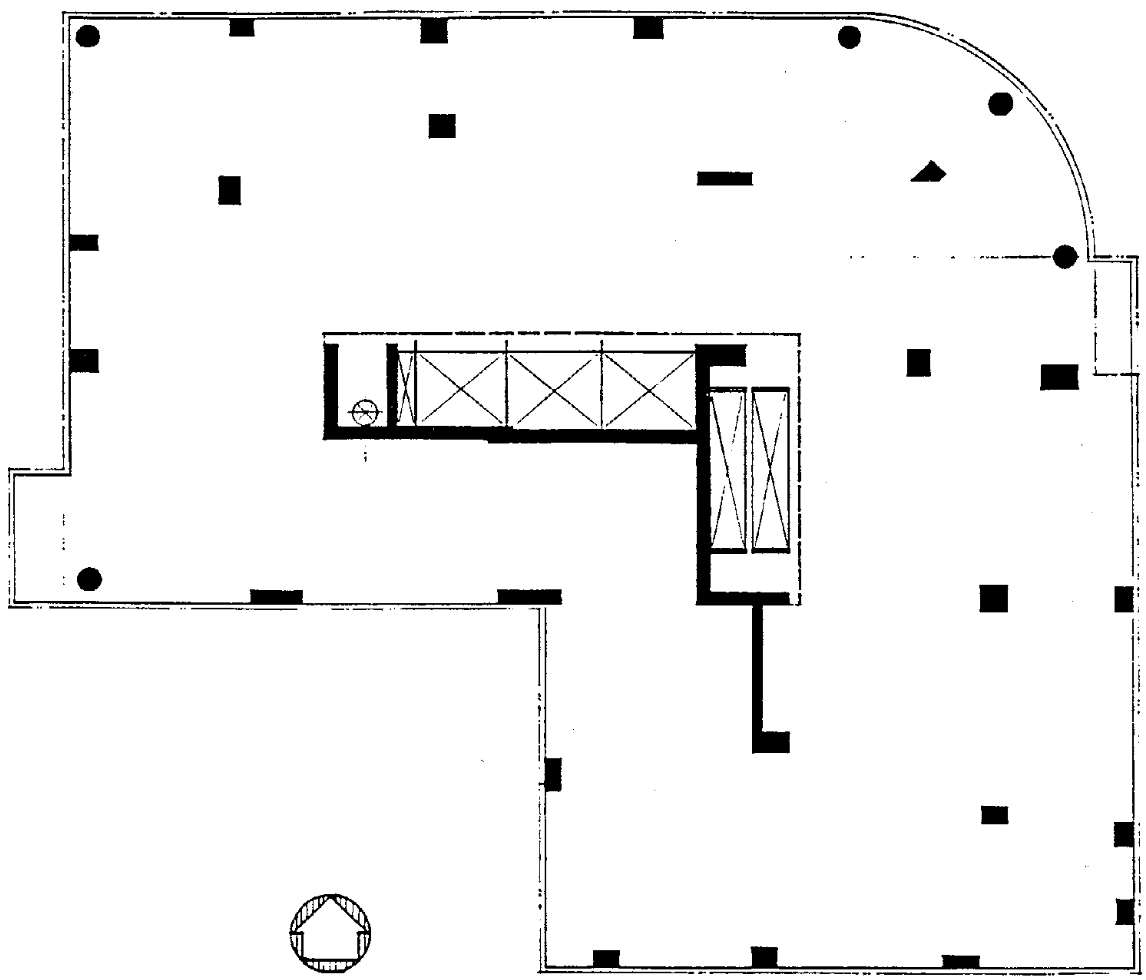

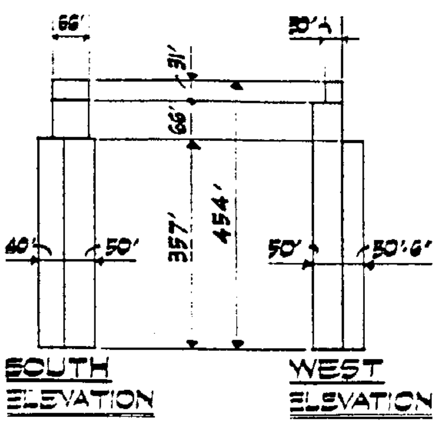

BUILDING B

40 TON/SQ. FT. ROCK FOUNDATION.
40 STORIES.
9'-8" = STORY HEIGHT.
TOTAL HEIGHT ABOVE GRADE = 454'-0".
8½' = SLAB THICKNESS.

FIGURE 2-3 BUILDING C - Typical Floor Plan and Elevation

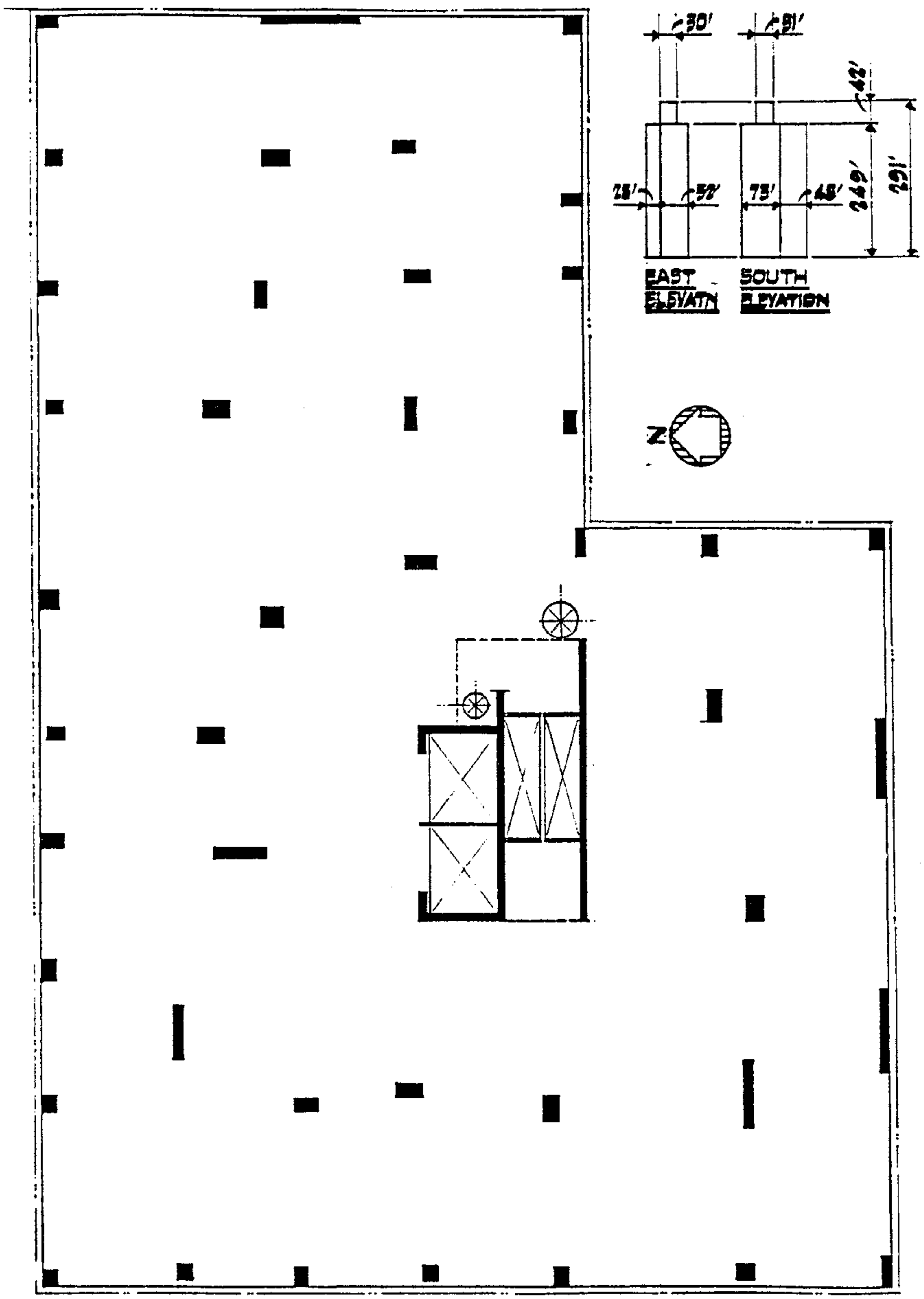

BUILDING C

TOTAL HEIGHT ABOVE GRADE : 291'-0"

8" SLAB THICKNESS.

FTGS TO 20 TON ROCK & 105 TON PILES.

27 STORIES.

8'-8' STORY HEIGHT.

FIGURE 2-4 BUILDING D - Typical Floor Plan and Elevation

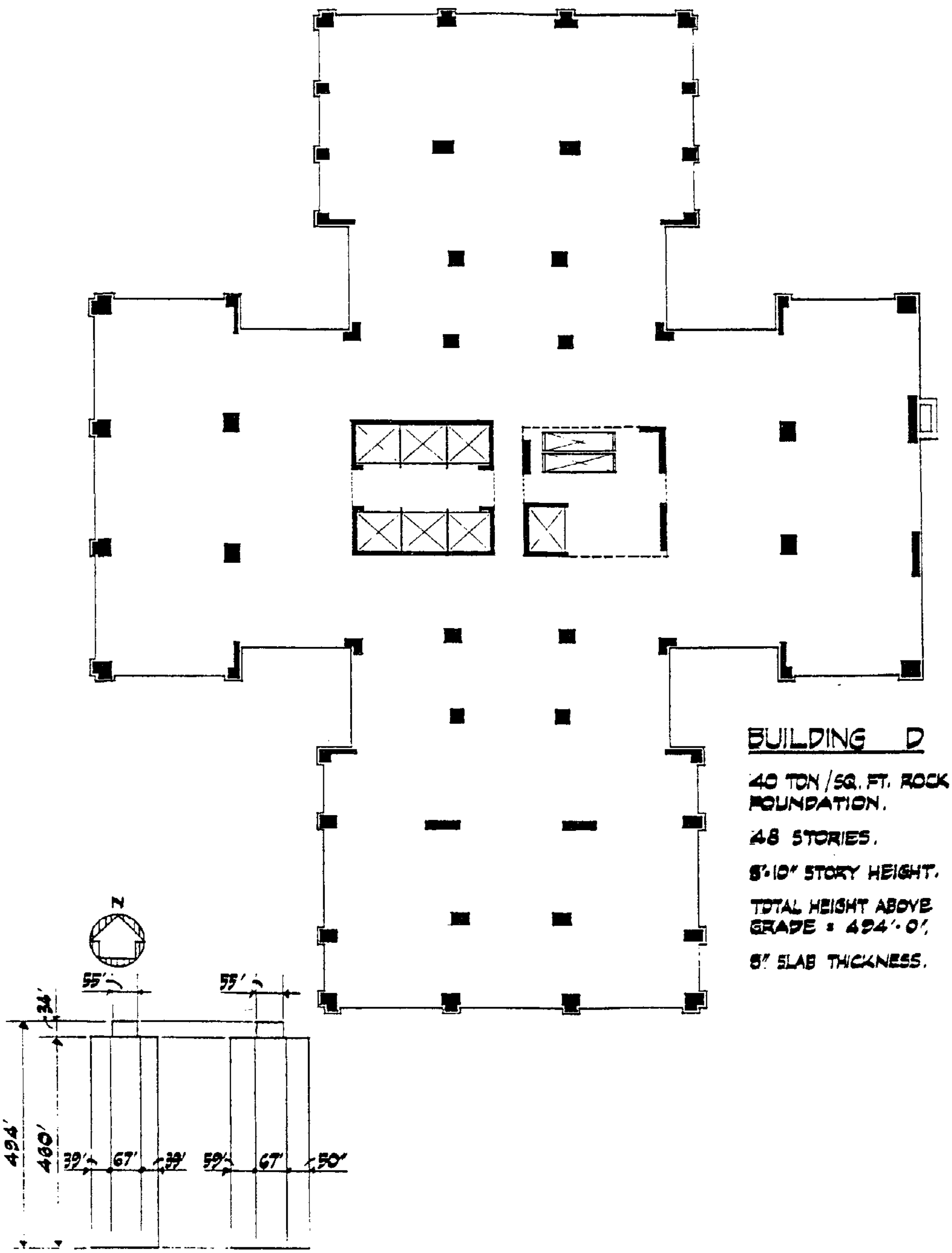

SECTION 3
CODE-PRESCRIBED ESTIMATION OF FUNDAMENTAL PERIODS

In order to estimate the lateral forces acting on a structure it is necessary first to estimate its fundamental period. Several factors contribute to the uncertainty of the estimation of fundamental periods from design plans, such as: variations in the modulus of elasticity, section dimensions, stripping operations, creep, and shrinkage. Over the life of the structure, cracks in structural members and disengagement of the partitions reduce the stiffness of the structure and lead to greater uncertainty of the periods. It is therefore difficult during the design stage to predict the dynamic properties of a structure at an arbitrary point in its service life. Without accurate estimates of fundamental periods, results from wind-tunnel experiments lead to inaccuracies in wind-related design requirements. Furthermore, the design base-shear for earthquake resistant design is a function of the structure's period. The applicable national or local Codes must be consulted to determine the empirical lower bound fundamental periods in order to establish the minimum lateral load requirements. It is apparent at this time that such Codes have not settled on a uniform method to determine the periods. The West Coast experience has been influencing this empirical approach which more accurately describes the stiffer structures designed to withstand large seismic forces in California. An exception is the earlier 1982 UBC Code.

The Uniform Building Code of 1982 specified that the period of a multi-story framed building can be estimated by dividing the total number of stories by ten [Blume, 1979]. This method results in longer periods than those measured in this study.

$$\text{1982 UBC} \qquad T = N/10 \tag{3.1}$$

N = number of stories of the building

The 1988 version of the Uniform Building Code allows for one of two methods to be used in computing the natural period. The first method (Method A) takes the material of the building into account.

1988 UBC $\quad T = C_t\,(h_n)^{3/4}$ (3.2)

$C_t = 0.020$ for dual moment resisting frames and eccentric braced frames;

$C_t = 0.1 / \sqrt{A_c}$ for structures with concrete or masonry shear walls;

$A_c = \sum A_e[0.2 + (D_e/h_n)^2]$ and depends upon the dimensions of the shear walls;

A_e is the minimum cross sectional shear area in any horizontal plane in the first story, in square feet, of a shear wall. D_e is the length in feet of shear wall in the first story in the direction parallel to the applied forces. A_c is the combined effective area, in square feet, of the shear walls of the first story of a structure. h_n is the effective height in feet above the base of the building [UBC 1988]. The effective height of the building, h_n, accounts for reduction in floor area at high floor levels, roof equipment, and elevator housings on the roof. The second method (Method B) specifies a Rayleigh-Ritz approach to determine the period.

East Coast experience has led to less stiff structures because of moderate lateral load requirements as well as the tendency of eastern construction to be taller and more slender. The proposed New York City seismic provisions modify the 1988 UBC Code by assigning $C_t = 0.035$ for frame concrete structures and by adjusting C_t for dual systems as follows:

$C_t = 0.020$ when $h_n \leq 160$ ft.

$C_t = 0.030$ when $h_n \geq 400$ ft.

Linear interpolation is permitted for intermediate heights.

This method results in shorter periods than those measured in this study. Table 3-I summarizes these results.

TABLE 3-I Comparison of Code-based Estimation of Fundamental Periods to the Measured Values in Ambient Conditions.

BLDG.	Height h_n	1982 UBC	1988 UBC (A)	Proposed NYC	Measured Ambient N-S	Measured Ambient E-W
A	486'	5.3 s	2.07 s	3.11 s	4.47 s	4.53 s
B	423'	4.1 s	1.87 s	2.80 s	3.98 s	2.79 s
C	249'	2.8 s	1.25 s	1.41 s	1.94 s	1.69 s
D	460'	4.9 s	1.99 s	2.98 s	3.76 s	3.88 s

In comparing periods from code equations with measured ambient periods, it should be noted that the equations in the design code are meant to describe the structure in its ultimate state, for example, story drift of H/200, whereas the measured ambient periods correspond to story drifts of much less than H/1000. Stiffness degradation at larger story drifts will result in longer periods than those measured when the building is in ambient conditions.

Note that the code equations are really not meant to provide accurate estimates of the fundamental period, but for finding the proper design force level, as prescribed by a design spectrum. To be conservative, the periods from code formulas should therefore be less than the measured periods under ambient conditions, which applied in the 1988 UBC Code and the proposed NYC Seismic Code. (See Table 3-I.)

SECTION 4
INSTRUMENTATION AND MEASUREMENT PROCEDURES

In all four buildings, Terra Technology SSA-302 triaxial force-balance accelerometers were the sensors used to measure horizontal and vertical accelerations at various floor levels. Kinemetrics 5-second seismometers were used to measure the velocity motion of the foundation. The Terra Tech accelerometers exhibit excellent linearity by virtue of the feed-back control of the seismic mass. In addition, the fluid damped design makes them very rugged. Triaxial accelerometers were placed at different floor levels in the buildings. Two triaxial accelerometers on the same floor near the top of the building allowed the identification of torsional modes. In buildings A and B, the deployed accelerometers measured to ±0.2g full scale. In buildings C and D, the accelerometers measured to ±2.0g full scale. PRS-4 synchronous, digital, 12-bit, auto-scaling, battery powered recorders sampled, digitized, and recorded the data. Each recorder has 1 Mega-byte of RAM for data storage. There was one PRS-4 recorder per triaxial accelerometer. The PRS-4's are especially well suited for temporary instrumentation of large scale structures because they have synchronized (±1 milli-second) internal clocks, therefore they can operate independently from one another, do not require any interconnecting cables, and are ruggedized. The PRS-4 units were pre-programmed to sample simultaneously at a pre-specified time of day, sample rate, and duration. The wind was very light during the measurements of buildings A and B but was 35 knots during the measurements of buildings C and D. This is evidenced by much heavier participation of the lower frequencies for buildings C and D. The following table summarizes the instrumentation location and the data acquisition on the four structures. In Table 4-I, B stands for basement, E and W for east and west positions of the floor plan. Sensor locations not in either the east or west positions were placed near the center of the floor plan.

TABLE 4-I Measurement Locations and Data Acquisition

BLDG.	SENSOR LOCATIONS - FLOOR NUMBER							SAMPLE RATE	TIME
A	B	10	20	30	40	52E	52W	50 / sec	20 min.
B	B	10	20	30	36E	36W	40	25 / sec	40 min.
C	B	6	28	29E	29W			25 / sec	30 min.
D	B	10	51	51E	51W			25 / sec	30 min.

Measurements from Building A were taken on February 4, 1991; those from Building B were taken on February 7, 1991. Buildings C and D were measured on February 22, 1991. Buildings A and B were measured a second time on August 15, 1991. Appendix B contains the results from the first set of measurements. For completeness, the results from the second set of measurements are included in Appendix C.

After each test, the data was transferred via a Compaq portable PC to a network of Sun Spark stations for analysis. After formatting the data into the proper ASCII format, auto-power and phase spectra were estimated. Peak picking software facilitated the spectral analysis.

SECTION 5
DATA ANALYSIS AND SPECTRAL PARAMETER ESTIMATION

Ideally, estimation of the parameters of a system is accomplished by fitting a model of the system to simultaneously sampled input and output data records. While the costs associated with artificial, measurable excitation of civil engineering structures are high, parameters estimated from forced-vibration tests are accurate and indicative of the nature of the structure itself [Ho 1989]. The force-levels required for uniform excitation of high-rise structures requires expensive and elaborate test arrangements, including reaction-mass servo-hydraulic actuators in many cases. Furthermore, forcing the structural response to levels significantly greater than ambient levels may risk non-linear behavior and subsequent damage to the structure, if measurement feedback is not used to limit the actuator excitation. Because of these experimental difficulties, and in light of the relative ease of collecting ambient vibration measurements as described in Section 4, the four high-rise structures were measured in ambient conditions.

If certain assumptions regarding the characteristics of the excitation to the structure, the structural behavior, and the response measurements hold, then the analysis of ambient vibration measurements will yield more meaningful results [Luz, 1992]. These assumptions are:

1. The excitation is sufficiently broad band and stochastic to uniformly excite at least the lowest 20 to 30 modes of the three-dimensional structure. In each of these structures the lower resonant frequencies range from 0.2 Hertz to 5 Hertz. Spatially uncorrelated excitations also helps reduce the chances of disproportionate energy concentration in certain modes.
2. The measured acceleration responses are at least weakly stationary. This permits meaningful time averages of the auto-power and cross-power spectra. The response

will be stationary if the excitation (wind pressure) is stationary, and the structure behaves linearly.

3. The resonant modes are lightly damped and the resonant frequencies are distinct and well separated. In this condition, spectral peak amplitudes have negligible contribution from out-of-band resonances. The figures in Appendices B and C verify that these assumptions hold.
4. Samples of the vibration measurements are simultaneous in time at all measurement locations. This condition is essential for proper cross-power spectral estimation. The test hardware guarantees nearly simultaneous sampling, as is indicated in Section 4.

If the above assumptions are warranted, frequencies with maximum spectral power (peak frequencies) can be interpreted as structural natural frequencies. In ambient conditions, tall buildings in urban areas are excited by wind turbulence and mechanical equipment. Wind pressures are spatially and temporally less correlated in turbulent flow than in laminar flow, but the spectra of turbulent velocity fluctuations decreases logarithmically with frequency [Simiu and Scanlan 1986]. Wind pressures are not uniformly distributed along the height of these high-rise structures. And because many of these buildings rise above the surrounding structures, the spectrum of wind velocites near the tops of the buildings can be qualitatively different from those in the lower stories. Since the auto-power spectra can not be normalized by the (unmeasured) wind forces, the spatial distribution of structural vibrations corresponding to a particular modal frequency are termed "operational deflection shapes." An operational deflection shape (ODS) is defined as the spatial distribution of peak spectral amplitudes at a resonant frequency.

Parameter estimation methods that implement an input-output ARMA model of the system were tested for ambient vibration applications [Ghanem, 1991]. However, the parameters resulting from such methods often depend upon assumptions regarding initial conditions, excitation, and measurement noise. In addition, these methods are more computationally intensive than methods based on the Fast Fourier Transform (FFT). Frequency domain analysis is especially useful for ambient vibration data, since the long durations of data allow for a considerable amount of averaging while maintaining a very high resolution of frequencies. Small frequency increments, Δf, are necessary to characterize low frequency peaks. Computer programs tailored for spectral estimation from multi-measurement ambient data were written to first estimate power and phase spectra, then use these spectra to pick the peak frequencies, amplitudes, and to estimate damping, RMS acceleration, RMS velocity, and RMS displacement. To verify the operation of the programs described above, an almost identical method was implemented independently at Columbia University's Lamont-Doherty Geological Observatory. Consistent results confirmed the accuracy of the programs.

5.1 Spectrum Estimation

Acceleration data are digitized and sampled with a sample interval of Δt seconds. $a(t) = a(i\Delta t)$, $i=1...P$, where P is the total number of points in the digitized data record. The data record is divided into K overlapping sample functions, a_k, $k=1...K$, of N (a power of 2) points each. The sample functions overlap each other by 50% of their length.

$$a_k(i\Delta t) = a((j+i)\Delta t), \quad j = \frac{N(k-1)}{2}, \quad k=1\cdots K, \quad i=1\cdots N \tag{5.1}$$

Each sample function is multiplied by the Hanning window, w .

$$\tilde{a}_k(i\Delta t) = a_k(i\Delta t)\, w_i \tag{5.2}$$

$$w_i = \frac{1}{2} - \frac{1}{2}\cos\left(\frac{2\pi(i-1)}{N-1}\right) \tag{5.3}$$

The complex valued discrete Fourier transform (DFT) of each segment is computed using the Cooley-Tukey (decimation in time) algorithm with the Danielson-Lanczos lemma to calculate the transforms [Oppenheim 1979, Press 1988]. This radix-2 method of computing the discrete Fourier transform is one of a variety of Fast Fourier Transform (FFT) methods. The Fourier transform is defined for both positive and negative frequencies. K FFT's are computed from each of two time records: a response acceleration record, $y(i\Delta t)$, at an elevated floor; and a reference acceleration record, $x(i\Delta t)$ near the base of the building. For proper phase spectrum estimation, it is essential that the samples for the x and y time records be simultaneous. Each record is segmented and windowed as the FFT's, $\tilde{X}_k$ and $\tilde{Y}_k$, are computed. Windowing the data reduces the leakage error in the FFT.

$$\tilde{X}_k(j\Delta f) = \sum_{i=1}^{N} \tilde{x}_k(i\Delta t)e^{-\mathit{i}\,2\pi ij/N} \tag{5.4}$$

$$\tilde{Y}_k(j\Delta f) = \sum_{i=1}^{N} \tilde{y}_k(i\Delta t)e^{-\mathit{i}\,2\pi ij/N} \tag{5.5}$$

Where the italic "*i* " in the exponent is the imaginary number and should not be confused with the non-italic index, "i." The discrete frequency interval is $\Delta f = 1/(N\Delta t)$, and $j=1...N/2$. The discrete, one-sided, auto power spectrum, $G_{yy}(j\Delta f)$, and cross power spectrum, $G_{xy}(j\Delta f)$, are computed by averaging the auto-power and cross power spectra of the K overlapping sample functions.

$$G_{yy}(j\Delta f) = \frac{1}{NK\sum_{i=1}^{N} w_i^2} \sum_{k=1}^{K} \left[\left|\tilde{Y}_k(j\Delta f)\right|^2 + \left|\tilde{Y}_k(-j\Delta f)\right|^2 \right] \tag{5.6}$$

$$G_{xy}(j\Delta f) = \frac{1}{NK\sum_{i=1}^{N} w_i^2} \sum_{k=1}^{K} \left[\tilde{X}_k(j\Delta f)\tilde{Y}_k^*(j\Delta f) + \tilde{X}_k^*(-j\Delta f)\tilde{Y}_k(-j\Delta f) \right] \tag{5.7}$$

The asterisk (*) indicates the complex conjugate of the variable. The factor in the denominator of equations (5.6) and (5.7) results in a normalization such that

$$\sum_{j=1}^{N/2} G_{yy}(j\Delta f) = \frac{1}{P}\sum_{i=1}^{P} \left[y(i\Delta t)\right]^2 \tag{5.8}$$

The phase spectrum is calculated using the cross power spectrum with respect to the lowest measured floor (usually the tenth in these buildings). The discrete phase spectrum, $\theta(j\Delta f)$ is defined by

$$\theta(j\Delta f) = \arctan\left(\frac{\mathrm{Re}\left(G_{xy}(j\Delta f)\right)}{\mathrm{Im}\left(G_{xy}(j\Delta f)\right)}\right) \tag{5.9}$$

The phase spectrum evaluated at peak frequencies of the auto power spectrum is almost always within 5° of either 0° or 180°. The power and phase spectra are given in Appendix B. The results of an analysis of a second set of measurements for Buildings A and B are included in Appendix C. Program AMB, listed in Appendix D, computes the auto-power spectrum and the phase spectrum given a pair of vibration records.

5.2 Parameter Estimation

Structural resonant frequencies are estimated in each auto spectrum by curve-fitting a quadratic to the three largest values in the regions of peak spectral power, and calculating the coordinates of the peak of the quadratic. The curve-fit is exact since three points uniquely determine a quadratic; no least squares or maximum likelihood methods are needed for this estimation. Since the power and phase spectra are not transfer or transmittance functions, traditional modal analysis curve-fitting methods [Ho 1989, Richardson 1982, Richardson 1985, Vold 1990] cannot be employed, nor can many other methods which rely on an input-output model of the structure [DiPasquale 1987, Ewins 1984, Ghanem 1991, Ho 1989]. Nevertheless, since points in the power spectrum are usually asymmetrically spaced around the peak frequency, the frequency of the true largest power spectrum value usually does not coincide with the sampled peak frequency; the true peak frequency is usually within one frequency interval of the largest data value (see Figure 5-1.) By fitting a quadratic to the three largest points in the spectrum, the peak coordinates may be estimated easily.

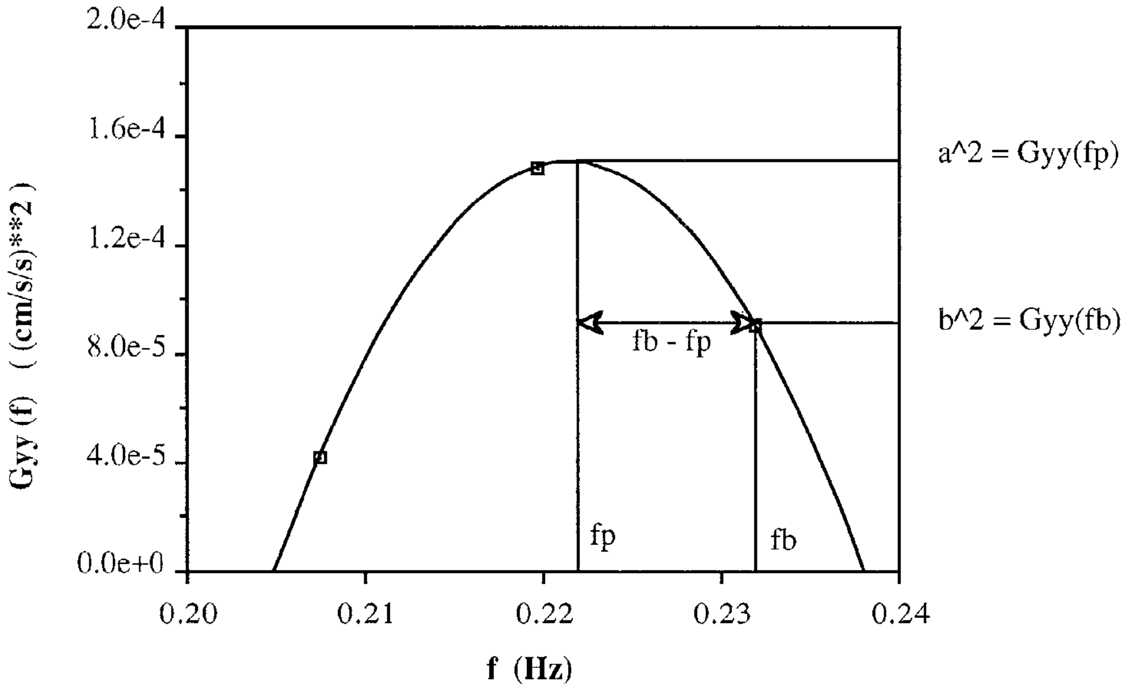

Figure 5-1 Quadratic Curve-fit to the Auto-power Spectral Peak

$G_{yy}(f) = c_0 + c_1 f + c_2 f^2$

Peak Frequency: $f_p = c_1 / (2c_2)$, Peak Amplitude: $G_{yy}(f_p) = c_0 + c_1^2 / (4c_2)$.

The variables a^2 and b^2 are used in Appendix A.

Given the coordinates of the largest sampled peak, (f_2, $G_{yy}(f_2)$), and the two adjacent coordinates, (f_1, $G_{yy}(f_1)$) and (f_3, $G_{yy}(f_3)$), a quadratic, $G_{yy}(f) = c_0 + c_1 f + c_2 f^2$, passing through all three points is computed by solving

$$\begin{Bmatrix} G_{yy}(f_1) \\ G_{yy}(f_2) \\ G_{yy}(f_3) \end{Bmatrix} = \begin{bmatrix} 1 & f_1 & f_1^2 \\ 1 & f_2 & f_2^2 \\ 1 & f_3 & f_3^2 \end{bmatrix} \begin{Bmatrix} c_0 \\ c_1 \\ c_2 \end{Bmatrix} \tag{5.10}$$

for c_0, c_1, and c_2 using Gauss-Jordan inversion with partial pivoting. The estimated peak frequency is $f_p = c_1 / (2c_2)$. The estimated peak amplitude is $G_{yy}(f_p) = c_0 - c_1^2 / (4c_2)$.

The structural damping ratio is calculated using the band-width of the auto power spectrum. The peak coordinate estimated from the curve-fit, $G_{yy}(f_p)$, and the auto power spectrum data at a point near the half-peak level, $G_{yy}(f_b)$, are used to compute the damping ratio (refer to Figure 5-1). Band-width formulae for computing damping ratios are derived from the analytic expression of the dynamic amplification factor of a SDOF structure under steady-state harmonic motion (for details see Appendix A). The amplification factor is defined in terms of displacements and assumes viscous damping [Beards 1983, Paz 1985]. Since our power spectra are computed from acceleration data, and the normalization is given by equation (5.8), dividing each point by $(2\pi f)^4$ results in displacement spectra. Assuming that the structure behaves linearly, has viscous damping, and has a stationary, steady-state, narrow-band response, that acceleration power spectra are normalized as in equation (5.8), and that the computed auto-power spectrum has no bias or leakage errors, then the following expression results in an approximate damping estimate.

$$\zeta = \frac{|f_b - f_p|}{f_p\sqrt{\left(\frac{f_b}{f_p}\right)^4 \frac{G_{yy}(f_p)}{G_{yy}(f_b)} - 1}} \qquad (5.11)$$

The curve-fit peak coordinate is $(f_p, G_{yy}(f_p))$; the coordinate at the band-width level is $(f_b, G_{yy}(f_b))$. The band-width frequency coordinate, f_b, is always taken to be greater than the peak frequency, f_p; and the band-width amplitude is no greater than 70% of the peak amplitude. This method of frequency estimation and damping calculation allows for the frequency data to be asymmetrically spaced around the peak and uses exact data values when appropriate. Equation (5.11) is a conservative approximation which ignores higher order terms (see Appendix A). Recently, FFT-based averaged spectrum estimation methods have been applied to the problem of damping estimation of long span suspension bridges [Jones 1990, Littler 1991].

For finite lengths of data, there is a trade-off between the error in the spectral amplitudes and the spectral resolution of any FFT-based spectrum estimation routine [Gade 1988]. The variance of a spectrum with fine spectral resolution is larger than the variance of an averaged spectrum with coarse spectral resolution computed from a data set of a fixed length [Press 1988]. The normalized standard error of a spectral estimate is $K^{-1/2}$, where K is the number spectral averages [Bendat 1986]. However, spectral bias errors result from averaging spectra and have the effect of widening spectral peaks. An estimate of the bias error of a spectral estimate is $E_b = -\Delta f/(6\zeta f)^2$ where Δf is the frequency resolution of the spectrum, and f and ζ are the frequency and damping ratio associated with a peak in the spectrum [Bendat 1986]. The bias can be somewhat controlled by the shape of the window function. In choosing a window function, there is a trade off between the narrowness of the peak and side-lobe amplitudes; so windows that produce narrow peaks are not always advantageous. Other spectrum estimation methods, employing multiple orthogonal window functions, have been shown to reduce bias errors more effectively [Thompson 1982, Park 1987].

In an effort to find the combination of the window function and number of averages which gives a spectrum with an appropriate band-width, several approaches were employed. All approaches used the same simulated acceleration response record of a linear SDOF system of a known natural frequency and damping ratio. The linear acceleration method was used to simulate the acceleration response record [Paz 1985]. Spectra of the resulting simulated acceleration response record were computed using various window functions and numbers of averages. Method 1 simply compared the known damping ratio to the damping ratio computed using equation (5.11). Methods 2 and 3 compared the bandwidth factor, q, computed from a closed form solution to the band-width factors computed from spectral moments, equation

(5.13), and from envelope statistics, equation (5.14). Three expressions of the band-width factor, q, are [Vanmarcke 1972]

$$q^2 = 1 - \frac{1}{1-\zeta^2}\left[1 - \frac{1}{\pi}\tan^{-1}\left(\frac{2\zeta\sqrt{1-\zeta^2}}{1-2\zeta^2}\right)\right]^2 \tag{5.12}$$

$$q^2 = 1 - \frac{\lambda_1^2}{\lambda_0\lambda_2} \tag{5.13}$$

$$q = \frac{\sigma_{\dot{r}}}{\sigma_{\dot{x}}} \tag{5.14}$$

where ζ is the damping ratio, and λ_i is the i^{th} spectral moment of the auto-power spectrum.

$$\lambda_i = \sum_{j=1}^{N/2} (j\Delta f)^i G_{yy}(j\Delta f) \tag{5.15}$$

$\sigma_{\dot{r}}$ and $\sigma_{\dot{x}}$ are computed using envelope statistics. $\sigma_{\dot{r}}$ and $\sigma_{\dot{x}}$ are the standard deviations of the time rates of change of the random processes x and r respectively. The envelope of the random process is r, and x is computed as the modulous of the complex quantity $x + i\,\hat{x}$, where $\hat{x}$ is the Hilbert transform of x and can be computed in the frequency domain or in a finite impulse response filter form in the time domain [Bendat 1986, Boashash 1987, Deutsch 1969, Rao 1990]. The impulse response function of the Hilbert transform is

$$h(t) = \frac{1}{\pi t} \tag{5.16}$$

The Fourier transform of $\hat{x}(t)$ is $\hat{X}(f)$ and the Fourier transform of x(t) is X(f).

$$\hat{X}(f) = \left\{ \begin{array}{c} i\,X(f) \ \text{ if } f > 0 \\ 0 \ \text{ if } f = 0 \\ -i\,X(f) \ \text{ if } f > 0 \end{array} \right\} \tag{5.17}$$

After computing $\hat{X}(f)$ from equation (5.17), $\hat{x}(t)$ is computed using the inverse Fourier transform of $\hat{X}(f)$. The time derivatives of the processes are computed using the central difference rule.

$$\dot{x}_j = \frac{x_{j+1} - x_{j-1}}{2\Delta t} \tag{5.18}$$

Figure 5-2 shows a portion of the simulated acceleration response record, its envelope function, and the power spectrum of the simulated acceleration record.

No combination of window function and frequency interval resulted in a very good match for all three methods of band-width comparison simultaneously. The final decision on what level of averaging and window function to use was based largely on the results from Method 1. Since the frequency values are of much greater interest in this study, a finer spectral resolution was favored. From these considerations, a frequency interval of approximately 0.0061 Hz and the Hanning window function were chosen to be suitable. This resulted in 13 spectral averages for Building A, 28 spectral averages for Building B, 20 averages for Building C, and 20 for Building D. A more rigorous analysis would take advantage of multi-taper methods [Park 1987, Thompson 1982] and would be an interesting topic for further study. These methods result in spectral estimates which have much smaller bias errors.

In summary, spectral band-widths can be determined to a large extent by computational errors in peak regions of the spectrum. If the auto-power spectrum is calculated with little regard to the sources of these errors, damping estimates from band-width measures may have little physical significance. In addition, damping estimates from band-width measures of ambient vibration data are contingent upon implicit assumptions, are subject to data processing effects, and therefore are used only as comparative measures within this analysis.

5.3 Root-Mean-Square Computations

Since the auto power spectra are normalized as in equation (5.8), the square root of the sum of the power spectrum points is the root-mean-square acceleration of the record, provided that the time history was demeaned or high-pass filtered prior to power spectrum computation. More importantly, however, root-mean-square velocity or displacement can be obtained if each spectral data point is divided by $(2\pi f)^2$ or $(2\pi f)^4$, respectively. Root mean squared displacement computations in the frequency domain are contingent upon the following assumptions:

1. The original discrete acceleration record can be represented by a Fourier series expansion.
2. Each power spectrum coordinate equals the amplitude squared of the corresponding Fourier series term.
3. Term by term integration of the Fourier series representing the acceleration record results in a Fourier series representing the velocity record. And term by term integration of the Fourier series representing the velocity record represents the displacement record.

Root-mean-squared (RMS) displacement computations are most sensitive to low-frequency accelerations. Power spectra often contain low frequency biases due to low-frequency noise in the measured acceleration records. Since low-frequency biases in the power spectrum result in gross over-estimates of RMS velocity and especially RMS displacement, all power spectrum values below 1 rad/sec (0.159 Hz) are divided by 1 instead of $(2\pi f)^2$ or $(2\pi f)^4$, thereby attenuating the very low-frequency noise. (For small values of f, the function $1/(2\pi f)^4$ becomes very large.) 1 rad/sec (Period = 6.28 sec) is a reasonable lower bound for structural oscillations of the buildings in this study. The equations for frequency domain calculation of the root mean square equations are:

$$\text{RMS-acc} = \left[\sum_{j=1}^{N/2} G_{yy}(j\Delta f)\right]^{\frac{1}{2}} \tag{5.18}$$

$$\text{RMS-vel} = \left[\sum_{j=1}^{N/2} \frac{G_{yy}(j\Delta f)}{\omega^2} \right]^{\frac{1}{2}} \tag{5.19}$$

$$\text{RMS-dsp} = \left[\sum_{j=1}^{N/2} \frac{G_{yy}(j\Delta f)}{\omega^4} \right]^{\frac{1}{2}} \tag{5.20}$$

where

$$\omega = \begin{Bmatrix} 2\pi j\Delta f \text{ if } j\Delta f \geq 0.159 \\ 2\pi\, 0.159 \text{ if } j\Delta f < 0.159 \end{Bmatrix} \tag{5.21}$$

Alternately, integrating acceleration time histories numerically results in velocity and displacement time histories. Numerical integration can be unstable if the record to be integrated contains frequencies greater than $1/(4\Delta t)$ Hz [Hamming 1989]. To estimate RMS displacement from recorded acceleration time records, the authors found that the following procedure was sufficiently accurate:

1. Demean the acceleration time record by subtracting the average acceleration from all data points.
2. Low-pass filter the acceleration time record with a cut-off frequency at $1/(5\Delta t)$ Hz. A non-recursive Kaiser filter was implemented in these analyses [Hamming 1989].
3. Integrate the demeaned, filtered, acceleration data once using Tick's rule [Hamming 1989]. Tick's rule is accurate and stable up to $1/(4\Delta t)$ Hz.
4. Band-pass filter the integrated acceleration record between 0.15 Hz and $1/(5\Delta t)$ Hz.
5. Integrate again using Tick's rule and find the RMS value of the 'displacement' time record.

These methods were verified in the laboratory by measuring and recording simultaneous acceleration and displacement time histories of a SDOF system excited randomly by base accelerations. A linear voltage displacement transducer (LVDT) measured the mass's deflections while a force balance accelerometer measured the mass's accelerations. RMS displacement was computed in three ways: directly from the recorded displacement time records, in the frequency domain using the acceleration power spectrum and equations (5.20) and (5.21), and in the time domain from the five-step process outlined above. The resulting RMS values were within 2% of each other. Comparable results between the time and frequency domain methods using the ambient vibration data collected from the measured structures in New York City provided further confirmation of the accuracy of the frequency domain approach. Table 5-I compares the measured RMS displacement and the computed RMS displacements for the SDOF structure tested in the laboratory. RMS displacement values computed from the 52nd floor of Building A are indicated in the second row of Table 5-I.

TABLE 5-I Validation of the Frequency Domain RMS Computation Method

	Measured Displacement	Frequency Domain	Time Domain
SDOF-RMS	0.591 in.	0.588 in.	0.578 in.
NYC - RMS		0.112 cm	0.130 cm

To facilitate the analysis of the power spectra and phase spectra computed by program AMB, program PEAK was written. This program passes through the spectral data several times to compute RMS quantities, pick peaks, sort the peaks by increasing frequency, fit a quadratic to the peaks, and estimate values for the peak frequencies, amplitudes, and damping ratios. To qualify as a peak, the power spectrum data must satisfy all of the following conditions:

1. The power spectrum frequency coordinate must lie within a user-specified frequency band.
2. The amplitude must be larger than any other point not already identified as a peak.

3. The derivative of the spectrum with respect to frequency must change signs at a peak.
4. The frequency at a peak must be outside of a user-specified frequency buffer around any previously identified adjacent peak. This helps in eliminating picking large side-lobes as legitimate peaks.

In estimating the damping ratio, the spectral coordinate used for the band-width estimation is no greater than 70% of the peak amplitude. The source code for program PEAK is included in Appendix E.

FIGURE 5-2
Simulated Acceleration Response, Computed Envelope, and Estimated Power Spectrum

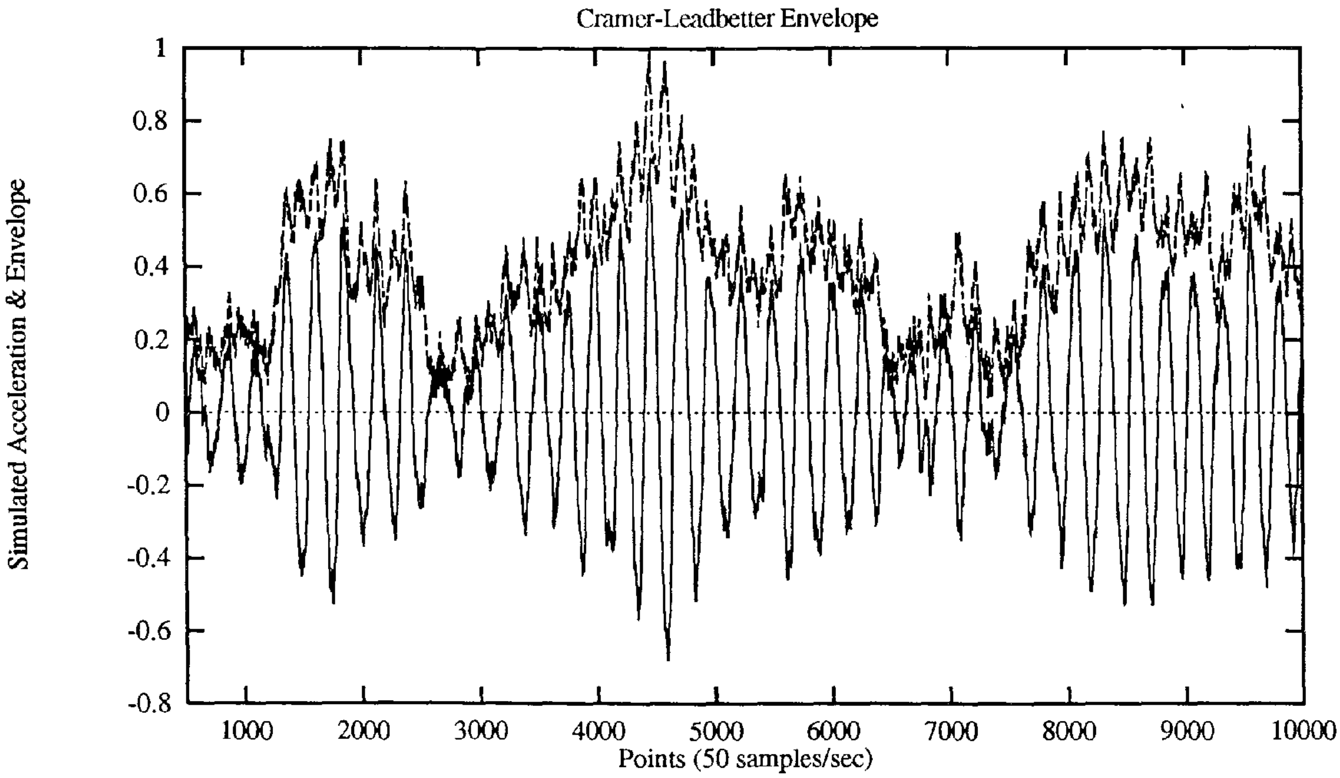

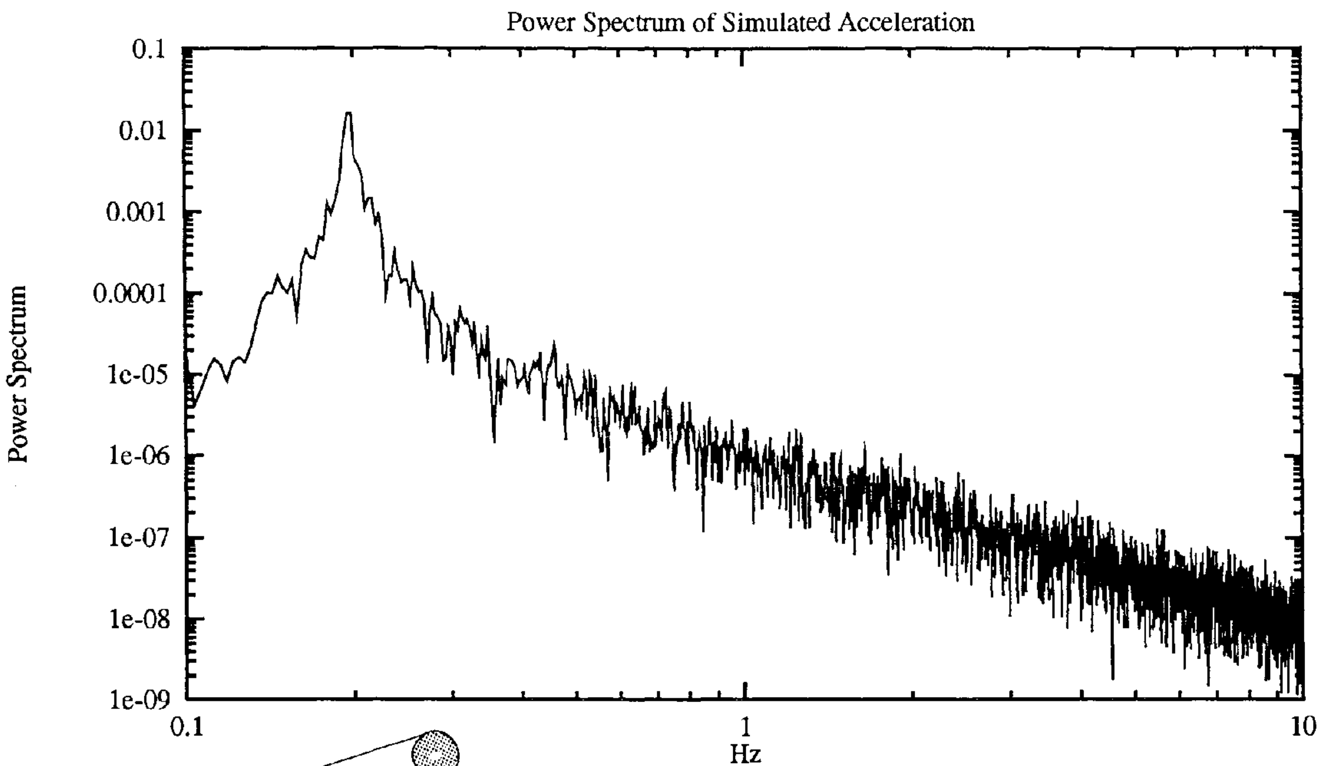

SECTION 6
DYNAMIC PARAMETERS

Table 6-I compares the periods and amplitudes of the ambient measurements resulting from an analysis using the methods described in Section 5 with those from finite-element dynamic analysis, and with code-formula estimates. The finite-element analysis is preliminary, reflecting engineering judgment as to the flat-slab width, effective shear wall stiffness, and effective coupling-beam moment of inertia.

The wind was very light during the measurements of Buildings A and B but was 35 knots during the measurements of Buildings C and D. This is evidenced by heavier modal participation in the lower frequencies for Buildings C and D. The concentration of spectral energy in the lower frequencies in Buildings C and D made the higher frequencies in Buildings C and D more difficult to identify.

Lengthy ambient vibration records improved power spectrum estimation by allowing a fine frequency resolution while averaging several spectra together. Most spectra were 2048 points long and were averaged up to 28 times. This enhanced the estimation of the natural periods, and damping ratios. The output files from program PEAK, which analyzed the power spectrum and phase spectrum data files, are shown with their corresponding spectra in Appendix B.

Figures 6-1 to 6-10 illustrate the "operational deflected shapes" (ODS) of the four buildings. Note that these are not normalized mode shapes since the spectral amplitude of ambient vibration measurements cannot be normalized by the spectral excitation amplitudes. "Operational deflected shapes" is the term used by the modal analysis community to describe the spatial description of the amplitude of vibration at resonant frequencies under operating conditions. Operational deflection shapes corresponded well to engineering judgment. That is, for the most part, the number of inflection points in the ODS is one less than the number of the associated resonant frequency for that ODS. Furthermore, ODS amplitudes are larger in the lower resonant frequencies.

The root mean squared (RMS) displacement values presented in Table 6-I are not the first mode RMS values, but are computed using equation (5.20). RMS velocity and acceleration values, along with plots of acceleration response amplitude and phase spectra are given in Appendices B and C. Measured RMS accelerations were much less than the threshold of perception (0.005 g or 5 cm/sec^2 [Simiu and Scanlan 1986]).

TABLE 6-I Dynamic Parameters Estimated by Ambient Vibration Measurements, by Finite Element Analysis, and by Code.

	Measured Period (sec)	Measured Damping(%)	RMS Disp. (cm)	F.E.A.* Period (sec)	1988 U.B.C. Period(sec)
BUILDING A					
1 N-S	4.47	2.0	0.0108	5.2	2.07
2 N-S	1.32	1.0		1.6	
3 N-S	0.71	0.2		0.8	
1 E-W	4.53	2.8	0.0071	4.6	2.07
2 E-W	1.23	1.0		1.3	
3 E-W	0.64	0.7		0.7	
1 TORSION	3.41	0.7		4.1	
2 TORSION	1.10	0.8		1.4	
3 TORSION	0.49	0.3		0.8	
BUILDING B					
1 N-S	3.98	2.4	0.0118	3.93	1.87
2 N-S	1.00	0.5		1.06	
3 N-S	0.57	0.8		0.59	
1 E-W	2.79	1.0	0.0066	2.63	1.87
2 E-W	0.80	0.7		0.80	
3 E-W	0.46	0.5		0.47	
1 TORSION	3.49	1.5		3.20	
2 TORSION	1.21	1.0		1.15	
3 TORSION	1.07	1.0		0.69	
BUILDING C					
1 N-S	1.94	1.4	0.0189	N/A**	1.25
2 N-S	0.66	0.7			
1 E-W	1.69	2.7	0.0063		1.25
2 E-W	0.57	1.2			
1 TORSION	1.32	1.3			
2 TORSION	0.70	0.9			
BUILDING D					
1 N-S	3.76	4.7	0.0520	N/A**	1.99
2 N-S	1.26	1.2			
3 N-S	0.68	0.6			
1 E-W	3.88	5.6	0.0825		1.99
2 E-W	1.17	1.1			
1 TORSION	2.91	2.4			
2 TORSION	0.83	0.7			

* Computed periods were obtained using K_d=2.0 in equation (7.1) for flat slabs and uncracked sections for columns, walls and beams [Grossman, in progress].
** N/A indicates that these values are not available, this work is in progress by the designers.

Figure 6-1
Building A; North-South Accelerations

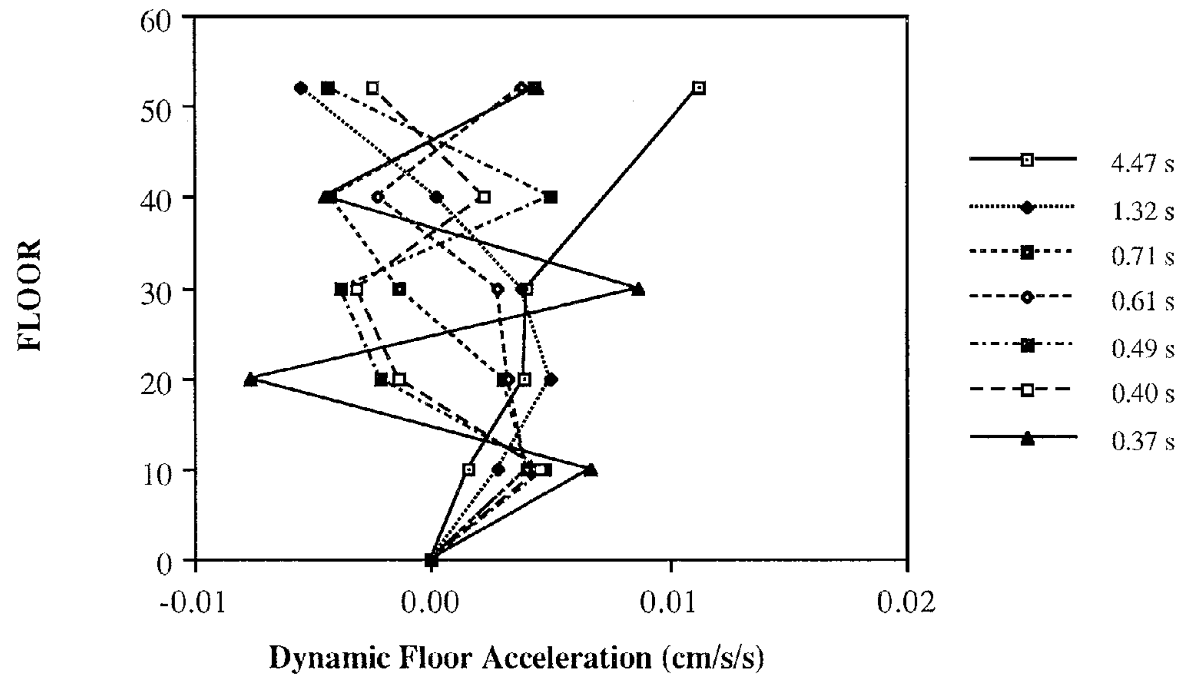

Figure 6-2
Building A; East-West Accelerations

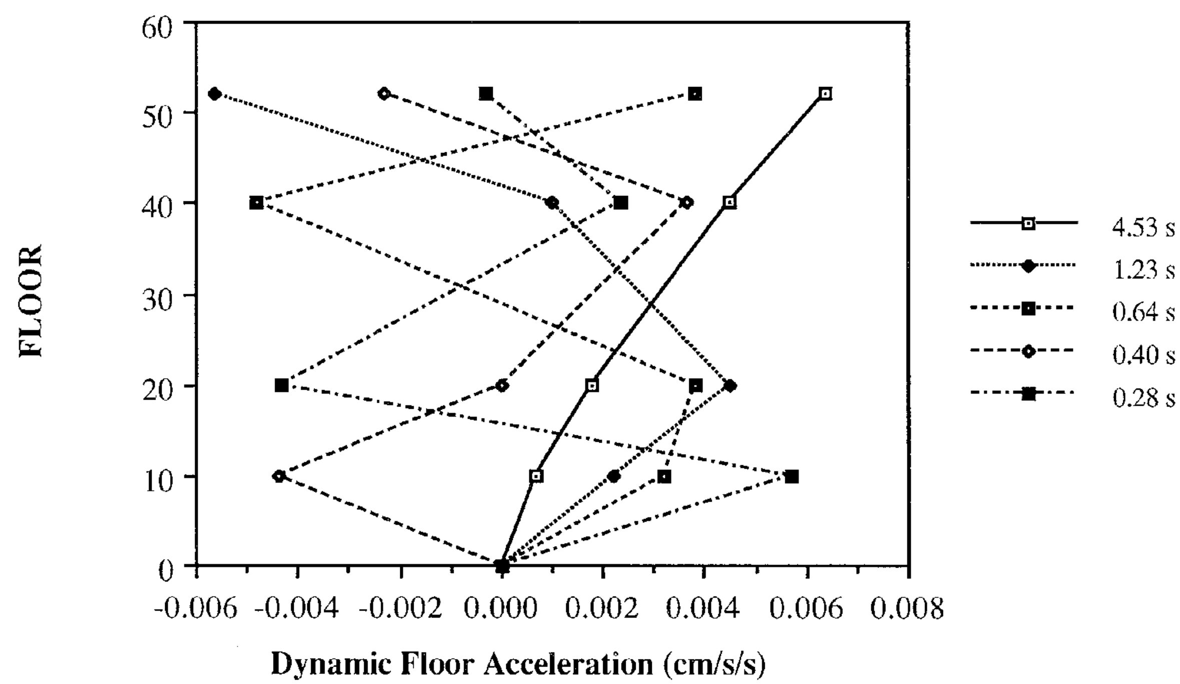

Figure 6-3
Building A; North-South Displacements

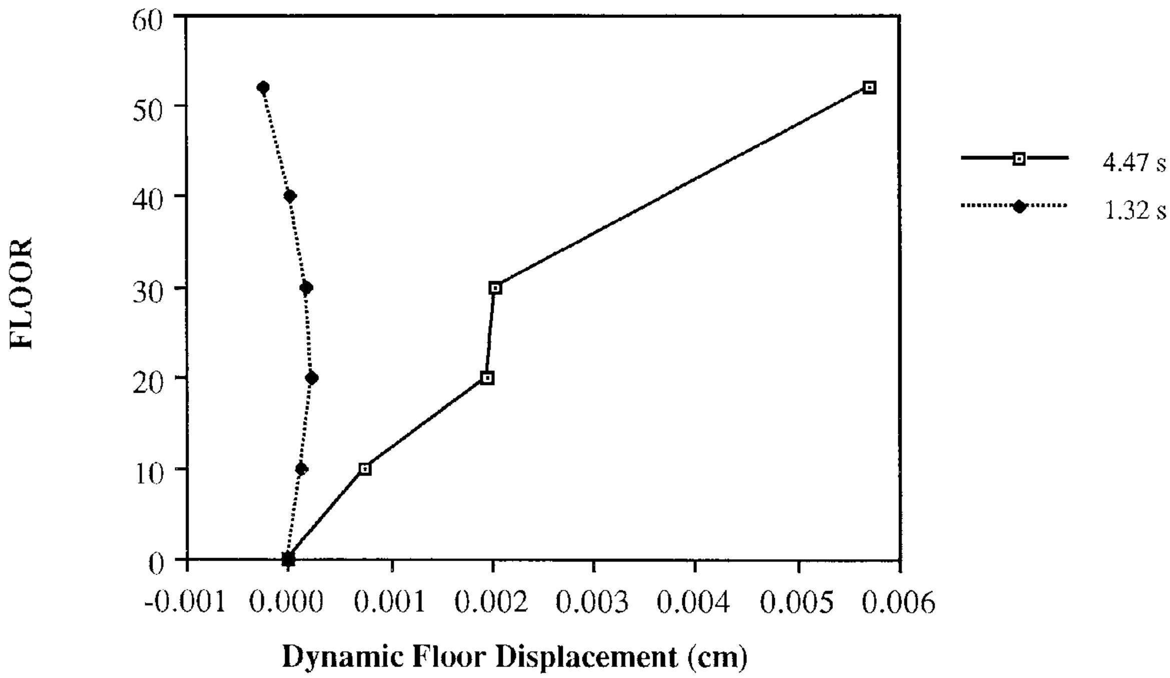

Figure 6-4
Building A; East-West Displacements

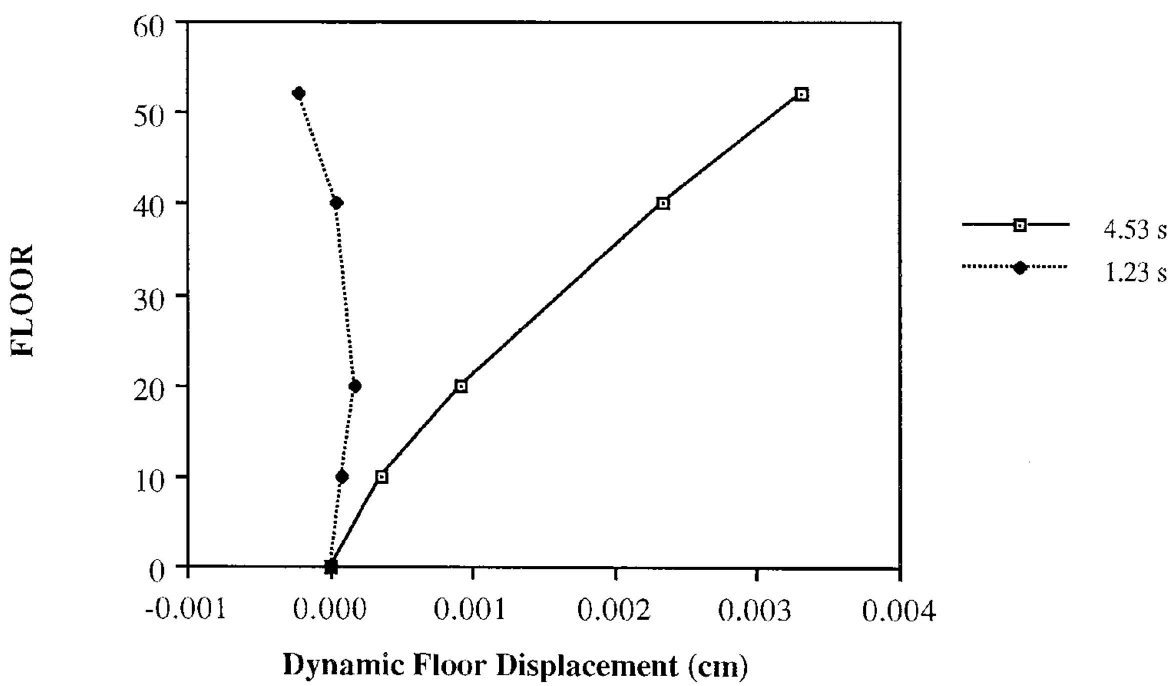

Figure 6-5
Building A; North-South Displacements

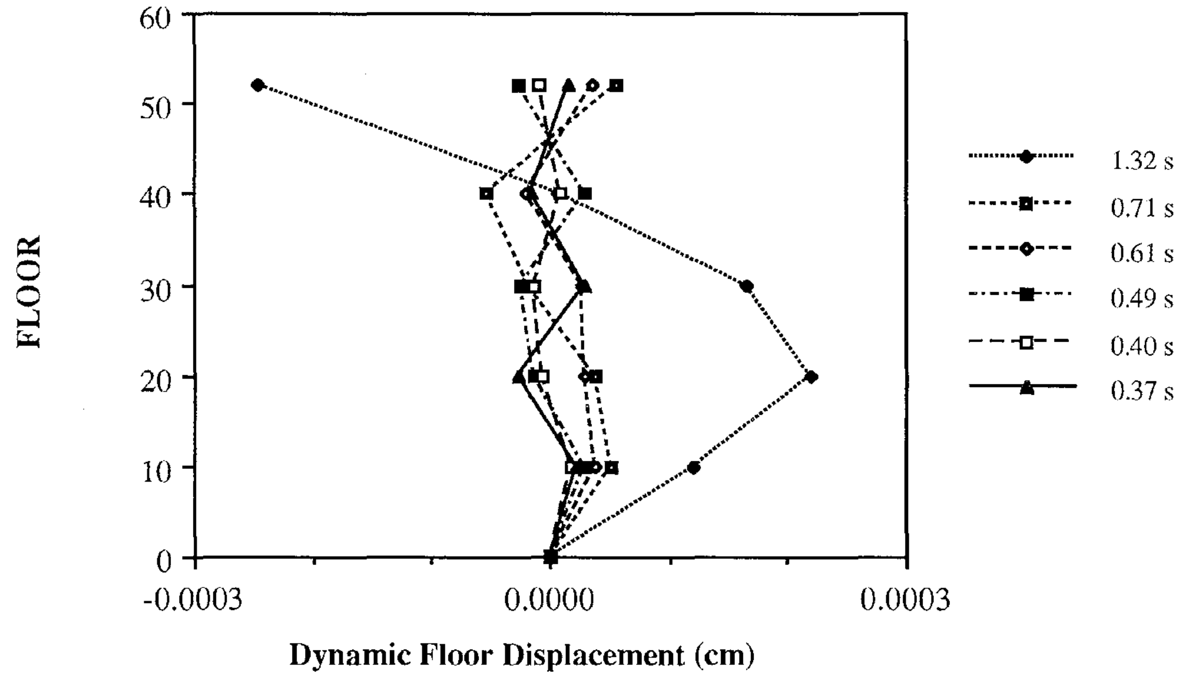

Figure 6-6
Building A; East-West Displacements

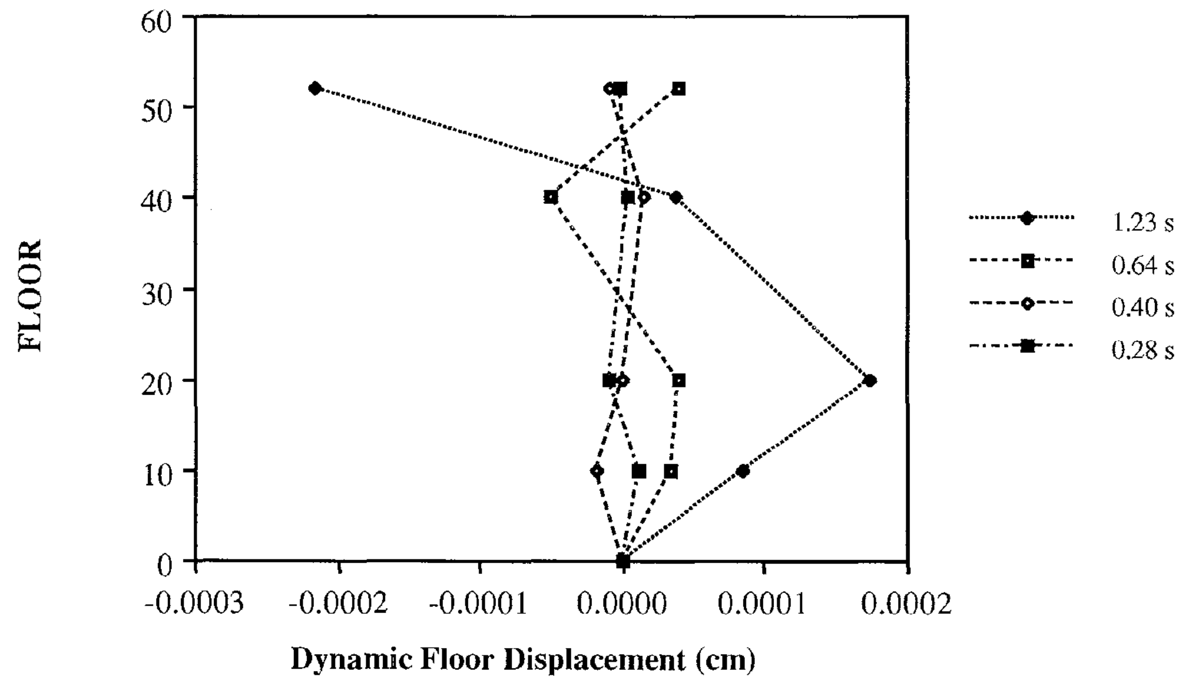

Figure 6-7
Building B; North South Accelerations

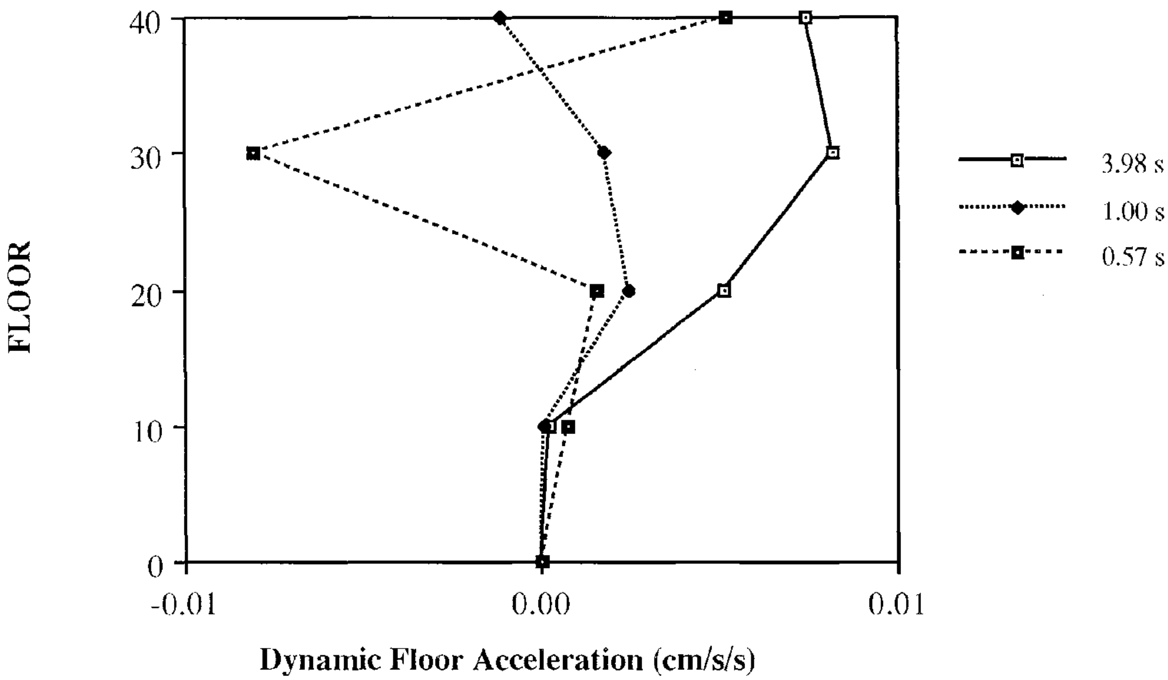

Figure 6-8
Building B; East-West Accelerations

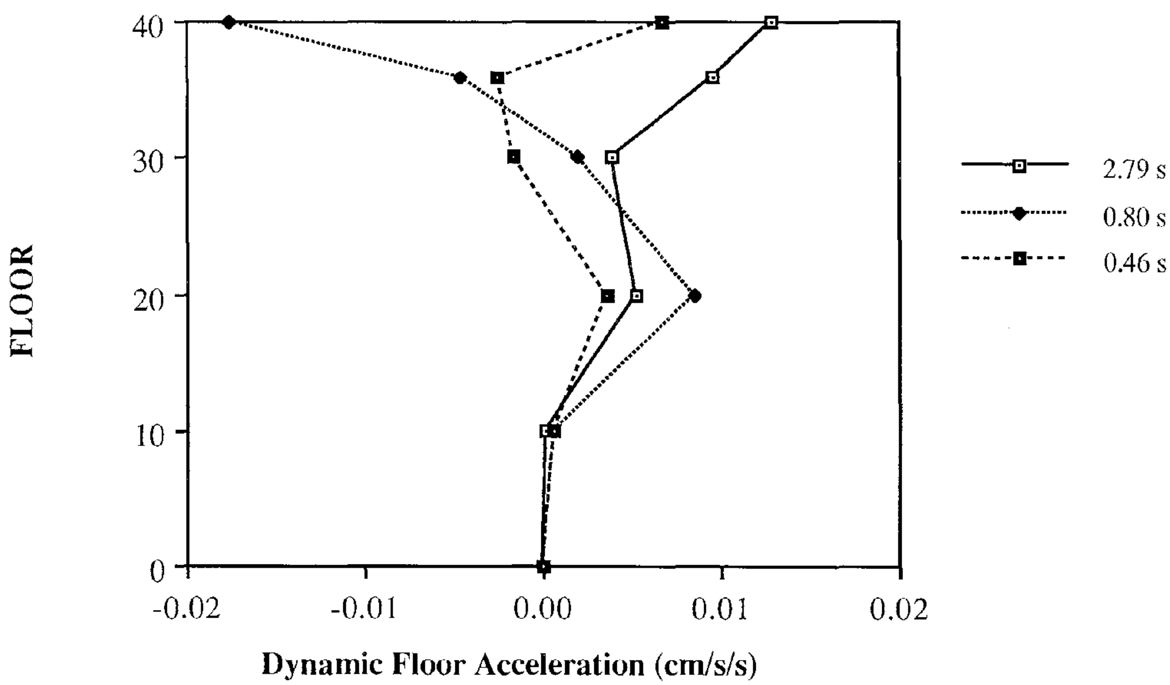

Figure 6-9
Building B; North-South Displacements

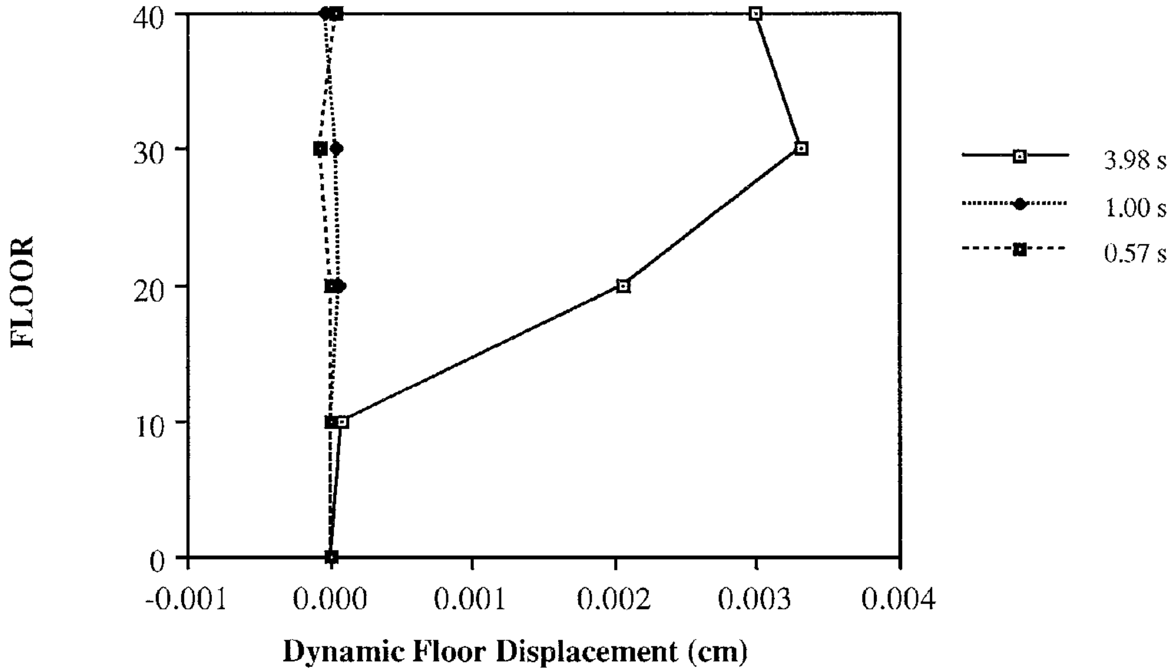

Figure 6-10
Building B; East-West Displacements

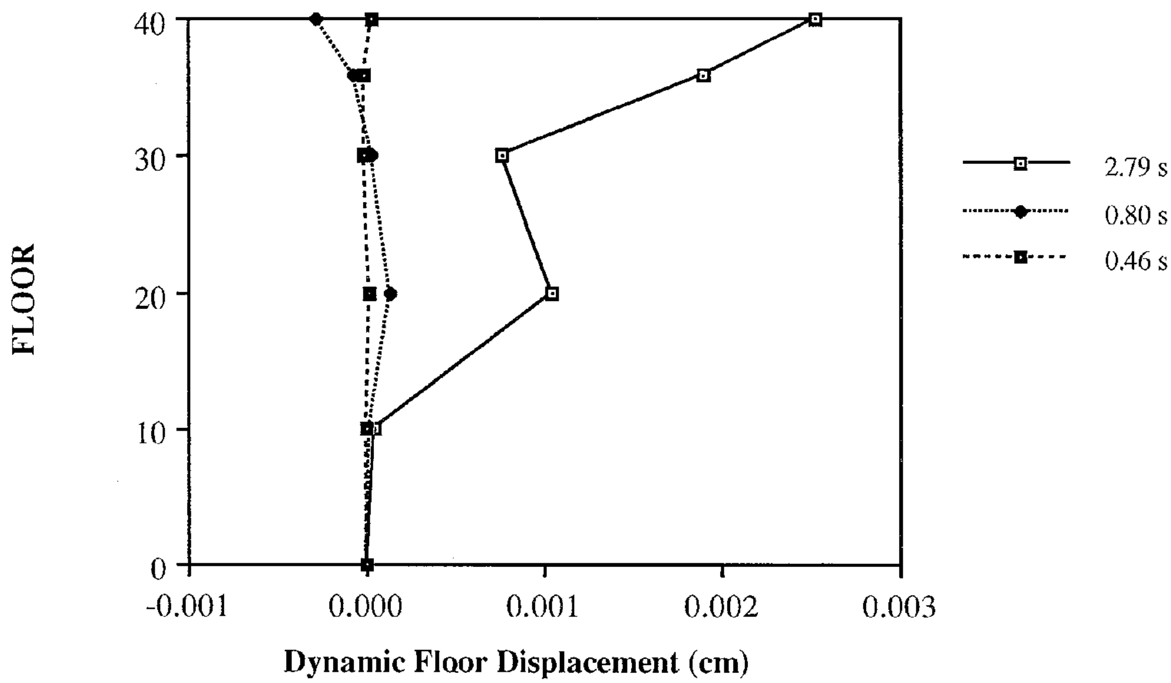

SECTION 7
RESISTANCE OF FLAT PLATE SYSTEMS TO LATERAL FORCES

In high-rise buildings that are constrained architecturally from the prevalent usage of windowless structural walls, buildings that have columns which do not fall in a regular grid pattern, and buildings that have a structural system determined by interior floor-plans, flat plates have been designed to resist lateral forces. Forming costs for flat plates are also less those for beam-drops. However, the lateral resistance that flat plates provide is not clearly understood. The approach engineers should choose in the design of flat plate systems, when the flat plate is intended to provide lateral resistance, is not precisely specified in ACI 318-83 [ACI-318 Code 1983]. The Equivalent Frame Method was evaluated by the late Professor Vanderbilt [Vanderbilt 1981]. But disagreement in the 1983 ACI Code Committee 318 regarding its suitability resulted in the inclusion of both Equivalent Frame and Effective Width methods in the ACI 318-83 code. (See commentary [ACI-318 Commentary 1983] Section 13.3.1.2 .) A lack of pertinent test data caused great uncertainty in the detailing of connections between plates and supporting columns in order for the plate to develop its full moment capacity. The discussions during the development of the 1983 Code concerning flat plate design for lateral forces led the Reinforced Concrete Research Council (RCRC) to assign researchers to tasks aimed at better understanding flat plate behavior. One of the tasks was motivated by the recent inclusion of moderate seismic requirements in many states East of the Rocky Mountains.

A methodology describing the effective width, αl_2, of flat plates at interior supports [Grossman, 1987] was verified and adjusted [Grossman, in progress] to results of laboratory tests [Moehle 1990] is as follows (for notation consult ACI 318):

$$\alpha\, l_2 = K_d\left[0.3\, l_1 + C_1\frac{l_2}{l_1} + \frac{(C_2 - C_1)}{2}\right]\frac{d}{0.9\, h} \qquad (7.1)$$

with limits

$$0.2\ K_d\ l_2 \leq \alpha\ l_2 \leq 0.5\ K_d\ l_2 \qquad (7.2)$$

where K_d depends on the load level and the computed drift index. Additional adjustments at the edge of the plate, and at side and corner supports were also recommended but not duplicated here. The K_d values were calibrated from the flat plate substructure tests [Moehle, 1990] and *tentatively* (pending additional field measurements) may be taken equal to:

At ambient conditions	K_d = 1.5 - 2.0
H/800	K_d = 1.1
H/400	K_d = 1.0
H/200	K_d = 0.8

A future goal of the current measurements and analyses of wind excited response of the four full-scale buildings will be to verify the appropriate values for K_d at smaller drift ratios (< H/800) and to confirm the values of K_d interpolated from the substructure tests when possible. Computed dynamic properties (using K_d=2.0) for two measured structures [Grossman, in progress] are summarized in Table 6-I.

More intimate knowledge of the fundamental periods and damping in actual flat plate structures is needed to better estimate seismic lateral loads, soil-structure interaction, and serviceability of tall structures. These issues will bear more weight when the need to retrofit existing structures (not designed for seismic loads), becomes pertinent. The research presented herein is the initial phase of work toward the task of correlating the design methods developed for flat-plate structures and shear walls with measured ambient dynamic properties. This correlation will implement ETABS models of the "as-built" condition of the measured models. Douglas and Ried [1982] calibrated similar SAP models to the measured bridge dynamic parameters, and their methods will be implemented here.

The approach starts by deriving a quadratic relationship between M parameters (P_i, i=1...M) and N significant structural variables (X_k, k=1...N). In this analysis, the parameters, P_i, are the natural periods. The structural variables, X_k, are the effective plate width, the effective shear wall area, and the effective coupling beam moment of inertia. M must be at least as large as N. Analytic parameters, obtained from an ETABS computation as a function of the structural variables, are denoted P_i; while measured parameters, obtained from ambient dynamic measurements are denoted PM_i. The fitting of the ETABS model to the measured parameters, PM_i, by adjusting the structural variables, X_k, follows the following steps.

1. Specify a base-line value, $X^b{}_k$, an upper bound, $X^u{}_k$, and a lower bound, $X^l{}_k$, for each structural variable. $X^l{}_k < X^b{}_k < X^u{}_k$.
2. Run ETABS 2N+1 times. For each run, each X_k changes from $X^b{}_k$ to $X^l{}_k$ to $X^u{}_k$ one at a time. Each run computes different set of M parameters (periods). Parameters computed by varying the structural variables are denoted PQ^i. There are three sets of parameters corresponding to each structural variable, corresponding to $X^b{}_k$, $X^l{}_k$, and $X^u{}_k$ respectively.

$$
\begin{aligned}
PQ_1^i &= P_i\left(X_1^b \cdots X_N^b\right)\\
PQ_2^i &= P_i\left(X_1^l \cdots X_N^b\right)\\
PQ_3^i &= P_i\left(X_1^u \cdots X_N^b\right)\\
&\vdots\\
PQ_{2N+1}^i &= P_i\left(X_1^b \cdots X_N^u\right)
\end{aligned}
\qquad (7.3)
$$

3. Derive a quadratic equation describing how each parameter, PQ^i, varies with changes in the N structural variables. The quadratic form of PQ^i is given by

$$
PQ^i = C^i + \sum_{k=1}^{N}\left(X_k A_k^i + X_k^2 B_k^i\right) \qquad (7.4)
$$

The constant polynomial coefficients, $A_k{}^i$, $B_k{}^i$, and C^i, of the quadratic can be found by solving

$$\begin{Bmatrix} PQ_1^i \\ PQ_2^i \\ PQ_3^i \\ \vdots \\ PQ_{2N+1}^i \end{Bmatrix} = \begin{bmatrix} 1 & X_1^b \cdots X_N^b & X_1^{b^2} \cdots X_N^{b^2} \\ 1 & X_1^l \cdots X_N^b & X_1^{l^2} \cdots X_N^{b^2} \\ 1 & X_1^u \cdots X_N^b & X_1^{u2} \cdots X_N^{b^2} \\ & \vdots & \\ 1 & X_1^b \cdots X_N^u & X_1^{b2} \cdots X_N^{u2} \end{bmatrix} \begin{Bmatrix} C^i \\ A_1^i \\ \vdots \\ A_N^i \\ B_1^i \\ \vdots \\ B_N^i \end{Bmatrix} \tag{7.5}$$

using, for example, singular value decomposition.

4. If each PQ^i can be put in terms of a quadratic function of the structural variables, the structural variables corresponding to the measured parameters can be found in a least squares sense. Using the polynomial expressions for PQ^i given by equations (7.4) and (7.5), an error function can be written

$$E^2 = \sum_{i=1}^{M} (PM_i - PQ^i)^2 \tag{7.6}$$

Equation (7.6) is minimized by setting the partial derivatives of E^2 with respect to X_k equal to zero and obtaining N equations to solve for the N different structural variables, X_k. There are a variety of numerical minimization procedures which can accomplish this task.

5. Once a set of the structural variables has been identified, the procedure can be repeatedly refined by using the identified values of X_k as $X_k{}^b$ and diminishing the difference between $X_k{}^u$ and $X_k{}^l$. This will refine and reduce the uncertainty in the true structural parameters, X_k.

By correlating ETABS models to natural periods measured under various wind conditions, including very strong winds, and by including recent static tests on flat-plate/column models, it is anticipated that criteria for degradation of ambient stiffness to stiffness at load levels anticipated during seismic events will be established. Top story displacements during strong winds may be on the order of H/800 or H/1000. Recent static tests on scaled flat plate substructures indicates the degradation of lateral resistance for drifts corresponding to H/800, H/400, H/200 and larger. The laboratory study fine tuned an empirical formula, equation (7.1), relating the effective width at interior supports of the flat plate to the load level, causing a defined top story drift. The purpose of the research at hand is to confirm the laboratory results at lower load levels by identifying the effective plate width of full scale structures subjected to various load levels. Once verified, this stiffness degradation can be used in seismic vulnerability assessment of many flat-plate and shear-wall structures East of the Rocky Mountains.

SECTION 8
CONCLUSIONS

1. Vibration measurement analysis of high-rise structures in ambient conditions is useful in revealing the differences between the as-built characteristics of the structure and the design representation of the building. The analyses of measurements from four reinforced concrete flat plate structures in Manhattan ranging from 27 stories to 52 stories are presented in this report. The aspect ratios of the structures ranged from 2.1 to 5.3. The four structures were in various phases of construction at the time of the measurements.
2. Using modular, synchronized (to within 1 millisecond), digital data recorders simplifies the instrumentation of large scale structures. These recorders do away with the task of running cables between remote sensors and a central recording unit. Hence, measurements can be taken unobtrusively and with no interruption in construction. All the structures were measured with triaxial force-balance accelerometers in at least four locations. Data was collected at 25 or 50 samples per second.
3. Ambient vibration measurements were analyzed using software tailored for this purpose. The auto-power spectrum and phase spectrum are estimated using fast Fourier transforms and a windowing method. Interpretation of the spectral estimates was enhanced by peak-picking software, also tailored for ambient structural vibration analysis.
4. Recording long lengths of ambient vibration data allows for several spectral averages which enhances spectral resolution. Curve-fitting the spectral peaks with a quadratic further improves the precision of the estimated periods. Measured ambient fundamental periods from all four buildings are shorter than those given by the 1982 Uniform Building Code, but are longer than fundamental periods estimated using formulas in the 1988 Uniform Building Code, and the proposed NYC Seismic Code. Fundamental

periods range from 1.69 seconds in the shortest building to 4.53 seconds in the tallest building.

5. Ambient vibration analysis using spectral analysis methods is robust. However results derived from spectral band-width measures, such as damping ratios, should be viewed with extreme caution. Bias and leakage errors in the spectrum estimates affects band-width measures strongly. Damping estimates in ambient conditions reported in this study range from 0.2% in the higher modes to 5.6% in the fundamental mode.

6. Three methods for assessing the artificial widening of spectral peaks due to averaging and windowing finite lengths of discrete data are reviewed. These methods can be used as explicit guidelines in choosing target frequency intervals, and required data record lengths for a specific application. Comparing damping ratios computed from the spectra of simulated acceleration records with the known damping ratios is the most robust method for choosing the proper level of frequency resolution and spectral averages. Future analyses using multi-taper spectral estimation methods, in which the data is repeatedly windowed with orthogonal weighting functions, should result in spectra with less bias.

7. The computation of root mean square (RMS) acceleration and RMS displacement from normalized power spectra of acceleration data was confirmed using a small-scale laboratory test in which acceleration and displacement were measured and recorded simultaneously. Root mean square displacements range from 0.007 cm under very light wind to 0.08 cm under stronger winds. The tallest buildings were measured only under light winds.

8. The first mode alone cannot account for the total motion of tall structures in ambient conditions. Indeed, the higher modes often participate more strongly in the lower floors. Dynamic measurements are very useful in evaluating the higher mode response of the structure. The participation of lower modes is heavier during strong winds. So

the total displacement response to strong wind can be estimated using the first mode alone within acceptable error margins.

9. Differences in periods estimated from ambient vibration measurements and preliminary finite element analysis can be reconciled by fitting uncertain quantities, such as effective flat-plate widths, in the finite element model. In so doing, the effective flat plate width can be related to lateral load level under service load conditions.

10. Fitting flat plate widths in the finite element model to measured periods can give a better understanding of the contribution of flat plates to the lateral resistance in tall buildings, and how this resistance changes with higher load levels.

11. The data presented herein is part of an on-going study of the behavior of flat-plate reinforced concrete structures. Fundamental periods from these tests will be compared to periods from future tests under different wind conditions or different stages of construction. Combining the results of these studies with the results of destructive tests of flat-plate substructures will lead to a method for evaluating the behavior of high-rise flat-plate structures at large drift ratios (H/200).

SECTION 9

REFERENCES

1. ACI Committee 318, "Building Code Requirements for Reinforced Concrete (ACI 318-77)," American Concrete Institute, Detroit MI, 1977.

2. ACI Committee 318, "Building Code Requirements for Reinforced Concrete (ACI 318-83)," American Concrete Institute, Detroit MI, 1983.

3. ACI Committee 318, "Commentary on Building Code Requirements for Reinforce Concrete (ACI 318-83)," American Concrete Institute, Detriot MI, 1983.

4. Beards, C.F., Structural Vibration Analysis, John Wiley and Sons, New York, 1983.

5. Bendat, J.S., and Piersol, A.G., Random Data: Analysis and MEasurement Procedures, 2nd ed., John Wiley and Sons, New York, 1986.

6. Blume, J.A. and Honda, K.K, *"Dynamic Characteristics of Reinforced Concrete Buildings,"* in Vibrations of Concrete Structures, American Concrete Institute, Detroit MI, 1979, pp 79-108.

7. Boashash, B., and Black, P.J., *"An Efficient Real-Time Implementation of the Wigner-Ville Distribution"* IEEE Transactions on Acoustics, Speech, and Signal Processing, Vol. ASSP-35, No. 11, November 1987.

8. Corotis, R.B., Vanmarcke, E.H., and Cornell, C.A., *"First Passage of Nonstationary Random Processes,"* J. of the Engineering Mechanics Division, ASCE, April 1972, pp 401-414.

9. Corotis, R.B., and Vanmarcke, E.H., *"Time-Dependent Spectral COntent of System Response,"* J. of the Engineering Mechanics Division, ASCE, EM5, October 1975, pp 623-637.

10. Deutsch, Ralph, System Analysis Techniques, Prentice Hall, Englewood Cliffs, NJ, 1969

11. DiPasquale, E. and Cakmak, A.S. *"Detection and Assessment of Seismic Structural Damage,"* NCEER Technical Reprot NCEER-87-0015, National Center for Earthquake Engineering Research, State University of New York at Buffalo, August 25, 1987.

12. Douglas, B.M. and Reid, W.H. *"Dynamic Tests and Systems Identification of Bridges,"* ASCE Journal of the Structural Division, Vol. 108, No. ST10, October, 1982.

13. Ewins, D.J., Modal Testing: Theory and Practice, John Wiley and Sons, New York, 1984, pp 82-85.

14. Gade, S. and Herlufsen, H., *"Windows to FFT Analysis,"* Sound and Vibration Magazine, March 1988, pp 14-22.

15. Ghanem, R. and Gavin, H. *"Experimental Verification of A Number of System Identification Algorithms,"* NCEER Technical Report 91-0024, National Center for Earthquake Engineering Research, State University of New York at Buffalo, September 19, 1991.

16. Grossman, Jacob S., *"Verification of Proposed Design Methodologies for Effective width of Slabs in Slab-Column Frames,"* in progress awaiting additional field measurements at intermediate wind loads.

17. Grossman, Jacob S., *"Slender Concrete Structures – The New Edge,"* ACI Structural Journal, Vol. 87, No. 1, Jan-Feb 1990, pp 39-52

18. Grossman, Jacob S., *"Reinforced Concrete Design,"* Building Structural Design Handbook, R.N. White and C.G. Salmon, editors. John Wiley & Sons, New York, 1987, Chapter 22, pp 699-786.

19. Hamming, R.W. Digital Filters, 3rd ed., Prentice-Hall, Englewood Cliffs NJ, 1989.

20. Harris, C.M., ed., Shock and Vibration Handbook, 3rd ed., McGraw Hill, New York, 1988.

21. Ho, I-K. and Aktan, A.E, *"Linearized Identification of Buildings With Cores for Seismic Vulnerability Assessment,"* NCEER Technical Report 89-0041, National Center for Earthquake Engineering Research, State University of New York at Buffalo, November 1, 1989.

22. Hwang, S.J. and Moehle, J.P., *"An Experimental Study of Flat-Plate Structures Under Vertical and Lateral Loads,"* Report No. UCB/SEMM-90/11, Department of Civil Engineering, University of California, Berkeley, Berkeley California, July 1990, pp 271.

23. Hwang, S.J., and Moehle, J.P., *"Test of Nine-Panel Flat-Plate Structure,"* Submitted to RCRC for review.

24. Hwang, S.J., and Moehle, J.P., *"Frame Models for Laterally Loaded Slab-Column Frames,"* Submitted to RCRC for review.

25. International Conference of Building Officials, Uniform Building Code 1988 Edition, Whittier, CA, Fifth Printing May 1988

26. Jacob, Klaus H., *"Seismic Hazards and the Effects of Soils on Ground Motions for the Greater New York City Metropolitan Region,"* Proceedings of the Continuing Education Seminar of the NYC Metropolitan Section of the ASCE, November 14+14, 1990, New York City.

27. Jones, N.P. and Spartz, C.A., *"Structural Damping Estimation for Long-Span Bridges,"* J. of Engineering Mechanics, Vol. 116, No. 11, November, 1990, pp. 2414-2433.

28. Littler, J.D., *"Discussion of Structural Damping Estimation for Long-Span Bridges,"* by N.P. Jones, and C.A. Spartz, J. of Engineering Mechanics, Vol. 116, No. 11, November 1990.

29. Luz, E. and Wallasschek, J. *"Experimental Modal Analysis Using Ambient Vibration,"* International Journal of Analytical and Experimental Modal Analysis, Vol. 7, No. 1, Jan. 1992, pp 29-39.

30. Macdonald, A.J., Wind Loading on Buildings, John Wiley and Sons, New York, 1975.

31. Moehle, J.P., Wallace, J.W., Martinez-Cruzado, J., *"Implications of Strong Motion Data For Design of Reinforced Concrete Bearing Wall Buildings,"* Report No. UCB/SEMM-90-01, Department of Civil Engineering, University of California, Berkeley California, June 1990.

32. Oppenheim, A.V. and Schafer, R.W. Digital Signal Processing, Prentice-Hall, Englewood Cliffs NJ, 1979.

33. Park, J., Lindberg, C.R., and Thomson, D.J., *"Multiple-taper Spectral analysis of terrestrial free oscillations: part I,"* Geophysical Journal of the Royal Astronomical Society, Vol. 91, pp. 755-794, 1987.

34. Paz, M., Structural Dynamics, 2nd ed., Van Nostrands Reinhold Co., New York, 1985.

35. Press, W.H., Flannery, B.P., Teukolsky, S.A., and Vetterling, W.T., Numerical Recipes in C - The Art of Scientific Computing, Cambridge University Press, Cambridge, 1988.

36. Simiu, E. and Scanlan, R.H., Wind Effects on Structures, 2nd ed., John Wiley and Sons, New York, 1986.

37. Rao, P., Taylor, F., and Harrison, G., *"Real-Time Monitoring of Vibration Using the Wigner Distribution"* Sound and Vibration Magazine, May 1990.

38. Richardson, M.H. and Formenti, D.L. *"Parameter Estimation from Frequency Response Measurements Using Rational Fraction Polynomials,"* 1st International Modal Analysis Conference, Orlando FL, 1982.

39. Richardson, M.H. and Formenti, D.L. *"Global Curve Fitting of Frequency Response Measurements Using the Rational Fraction Polynomial Method,"* 3rd International Modal Analysis Conference, Orlando FL, 1985.

40. Thompson, D.J., *"Spectrum Estimation and Harmonic Analysis,"* Proceedings of the IEEE, Vol. 70, No. 9, pp. 1055-1096, September 1982.

41. Vanderbilt, D.M. *"Equivilant Frame Analysis of Unbraced Reinforced Concrete Buildings for Static Lateral Loads,"* Structural Research Report No. 36, Civil Engineering Department, Colorado State University, Fort Collins CO, June 1981.

42. Vanmarcke, Erik H., *"Properties of Spectral Moments with Applications to Random Vibration,"* J. of the Engineering Mechanics Division, ASCE, April 1972, pp 425-446.

43. Vanmarcke, Erik H., Random Fields: Analysis and Synthesis, MIT Press, Cambridge, MA, 1984.

44. Vold, H. *"Numerically Robust Frequency Domain Modal Parameter Estimation,"* Sound and Vibration Magazine, January 1990

APPENDIX A

DERIVATION OF TWO DAMPING ESTIMATORS

Textbook formulae for damping estimation using impulse response functions or spectral bandwidths should be used with caution when applied to experimentally obtained discrete data. This appendix contains the derivation of these two common damping estimators and assesses their suitability to experimental data from large-scale structures [Beards 1983, Paz 1985].

A.1 Time Domain

In the time domain, damping is often estimated using the logarithmic decrement. Consider the SDOF displacement response to an impulse.

$$x(t) = A_0 e^{-\omega_n \zeta t} \sin\left(\omega_n \sqrt{1-\zeta^2}\, t - \varphi\right) \qquad \text{(A.1)}$$

This is a sinusoidal oscillation with exponentially decreasing amplitude. The response displacement reaches adjacent relative maxima at times t_1 and t_2, with displacements A_1 and A_2. $t_2 - t_1 = \tau$. The variable τ is the damped natural period.

$$\frac{A_1}{A_2} = \frac{e^{-\omega_n \zeta t_1}}{e^{-\omega_n \zeta (t_1+\tau)}} = e^{-\omega_n \tau} \qquad \text{(A.2)}$$

By definition,

$$\omega_n \sqrt{1-\zeta^2}\, \tau = 2\pi \qquad \text{(A.3)}$$

Defining the logarithmic decrement, δ,

$$\delta = \ln\left(\frac{A_1}{A_2}\right) \qquad \text{(A.4)}$$

taking the natural log of both sides of equation (A.2), and substituting equation (A.3) results in an expression for damping.

$$\zeta = \frac{\delta}{\sqrt{4\pi^2 + \delta^2}} \tag{A.5}$$

If the damping is purely viscous then several oscillations may be used to compute the logarithmic decrement.

$$\delta = \frac{1}{n} \ln\left(\frac{A_1}{A_{n+1}}\right) \tag{A.6}$$

Equation (A.5) is exact. In its derivation, no expressions were truncated and no terms were ignored. If the damping is viscous, then δ will not depend upon the strain, deflection, temperature, or strain rate. In this case, δ will be constant with respect to the section of the data record chosen for analysis. In addition, the logarithmic decrement may be computed using acceleration amplitudes directly if the response is purely single mode. However, several damping mechanisms usually contribute to the total damping and each mechanism's contribution usually is *not* independent of strain, deflection, temperature, and strain rate. Often, damping ratios computed with the initial, large motion, response are larger than those computed using the subsequent, smaller amplitude, motion. Further experimental complications arise from the fact that impulse decay measurements are often polluted with higher mode response, and that low frequency noise can seriously distort the results. Additionally, large, purely impulsive forces are difficult to generate in high-rise structures and damping ratios for higher modes are very difficult to obtain using this technique.

A.2 Frequency Domain

Frequency domain damping evaluation, although simpler experimentally, requires many more mathematical assumptions than does evaluation of damping in the time domain.

Consider the dynamic amplification of a SDOF system responding to steady state harmonic excitation of circular frequency ω. If the response quantity is acceleration, the dynamic amplification factor is

$$\frac{\ddot{x}}{x_{st}} = \frac{\omega^2}{\sqrt{\left(1 - \Omega^2\right)^2 + \left(2\zeta\Omega\right)^2}} \tag{A.7}$$

where $\Omega = \omega/\omega_n$. The peak of the function described by equation (A.7) occurs when

$$\Omega = \sqrt{1 - 2\zeta^2} \tag{A.9}$$

and has the value of

$$a = \frac{\ddot{x}}{x_{st}} = \frac{\omega^2}{2\zeta\sqrt{1 - \zeta^2}} \tag{A.10}$$

The value of the acceleration frequency response function, equation (A.7), at the frequency $\Omega = 1 + \Delta\Omega/2$ is

$$b = \frac{\left(1 + \frac{\Delta\Omega}{2}\right)^2 \omega_n^2}{\sqrt{\left[1 - \left(1 + \frac{\Delta\Omega}{2}\right)^2\right]^2 + \left[2\zeta\left(1 + \frac{\Delta\Omega}{2}\right)^2\right]^2}} \tag{A.11}$$

Values for a^2 and b^2 are indicated graphically in Figure 5-1. Since the eventual aim is to compute damping estimates from power spectra, the ratio of the squares of equations (A.10) and (A.11) is

$$\frac{a^2}{b^2} = \frac{\left(1 - 2\zeta^2\right)\left\{\left[1 - \left(1 + \frac{\Delta\Omega}{2}\right)^2\right]^2 + \left[2\zeta\left(1 + \frac{\Delta\Omega}{2}\right)\right]^2\right\}}{4\zeta^2\left(1 - \zeta^2\right)\left(1 + \frac{\Delta\Omega}{2}\right)^4} \tag{A.12}$$

Solving for ζ^2, we obtain

$$\zeta^2 = \frac{(1 - \varepsilon_2)\left(\Delta\Omega + \frac{\Delta\Omega^2}{4}\right)^2 + \frac{a^2}{b^2}\varepsilon_1\varepsilon_4}{4\left(\frac{a^2}{b^2}\varepsilon_4 + \varepsilon_3 - 1\right)} \tag{A.13}$$

where

$$\varepsilon_1 = 4\zeta^4 \tag{A.14}$$

$$\varepsilon_2 = 4\left(\zeta^2 - \zeta^4\right) \tag{A.15}$$

$$\varepsilon_3 = \Delta\Omega + \frac{\Delta\Omega^2}{4} \tag{A.16}$$

and

$$\varepsilon_4 = \left\{ \begin{array}{c} \left(1 + \frac{\Delta\Omega}{2}\right)^4 \text{ if the data is acceleration} \\ \\ 1 \text{ if the data is displacement} \end{array} \right\} \tag{A.17}$$

For small values of damping, $\varepsilon_1 < \varepsilon_2 < \varepsilon_3 < \varepsilon_4$. Neglecting higher order terms, such as $\Delta\Omega^2$ with respect to $\Delta\Omega$, and both $\Delta\Omega^2$ and $\Delta\Omega$ compared to 1, and assuming the power spectrum data is from an acceleration record, ε_1 , ε_2 , and ε_3 are set to zero, and

$$\zeta = \frac{\Delta\Omega}{2\sqrt{\frac{a^2}{b^2}\left(1 + \frac{\Delta\Omega}{2}\right)^4 - 1}} \tag{A.18}$$

which is equivalent to equation (5.11).

The truncated formula, (5.11) or (A.18), results in lower damping estimates than using the exact formula, (A.13) - (A.17). This under-estimate of the damping is recovered (in part if not entirely) by the artificial widening of the spectral peaks caused by windowing the time domain data before computing the FFT's [Oppenheim 1979, Press 1988]. Using equation (5.11) or (A.18) for damping estimation from power spectra of acceleration data is contingent upon the following assumptions:

1. The damping is small (< 10%) and the damping mechanism is viscous. For damping < 2%, the truncation effects are insignificant.

2. The original discrete acceleration record can be represented by a Fourier series.
3. Each power spectrum coordinate equals the amplitude squared of the corresponding Fourier series term.
4. The response is narrow band, stationary, and steady-state and the structure behaves linearly.
5. Power spectrum computation does not appreciably widen the spectral peaks. This is often the over-riding assumption.

In summary, damping estimates from impulse responses are the most accurate, if an adequately strong and brief impulse can be generated. The absence of forced response experiments requires frequency domain estimates. These estimates are often upper bounds due to artificial peak widening in the process of computing averaged windowed power spectra.

APPENDIX B

POWER SPECTRA, PHASE SPECTRA,

ESTIMATED FREQUENCIES, AND ESTIMATED DAMPING RATIOS:

FIRST SET OF MEASUREMENTS

Parameters reported in Section 6 are estimated from the spectra shown in Appendix B. This data will serve as a base-line set of measurements for comparison to parameters obtained from measurements in stronger winds. The measurement dates are as follows:

Building A:	February 4, 1991
Building B:	February 7, 1991
Building C:	February 22, 1991
Building D:	February 22, 1991

FIGURE B-1

BUILDING A - Power and Phase Spectra of Measured Acceleration

Measurement	Date	February 4, 1991
Measurement	Sensor Location	10th Floor, Center
Reference	Sensor Location	20th Floor, Center
	Sensor Direction	North-South

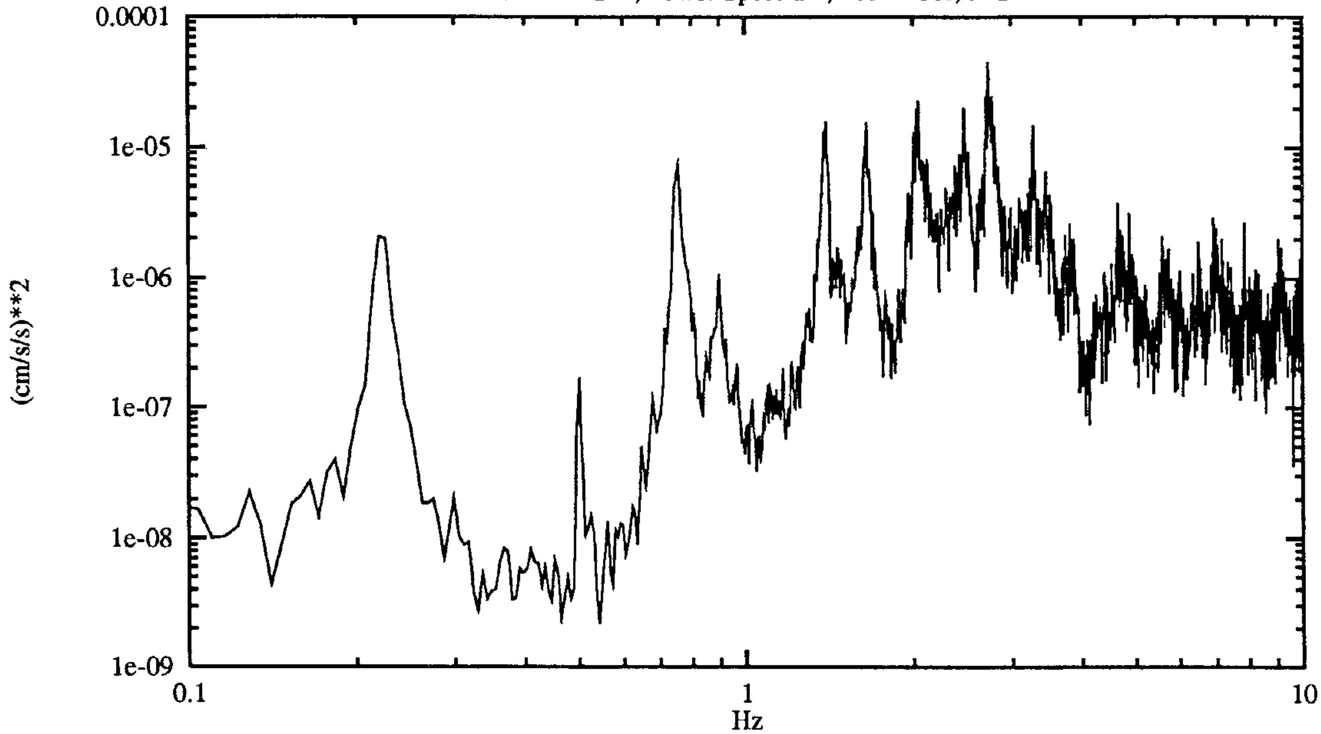

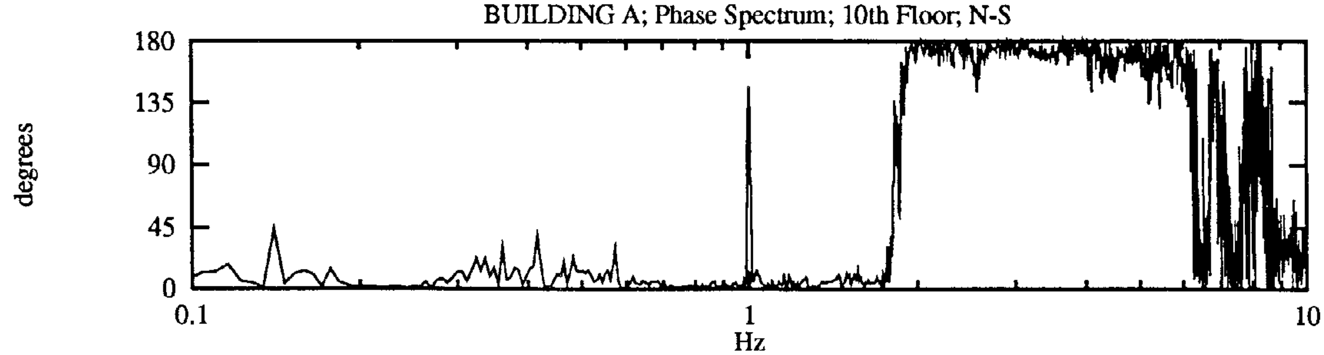

Peaks In G10.20n

Hz-data		Hz-fit	Amp^2-data	Amp^2-fit	Phase	Damping %
0.2197	N1	0.2225	2.0383e-06	2.1789e-06	0	2.1
0.5005	T1	0.5003	1.6904e-07	1.6921e-07	13	0.7
0.7568	N2	0.7556	7.3875e-06	7.4916e-06	1	1.0
0.8972	T2	0.8966	1.0517e-06	1.0561e-06	2	0.8
1.3977	N3	1.3964	1.5605e-05	1.5914e-05	5	0.5
1.6541		1.6532	1.5315e-05	1.5557e-05	4	0.3
2.0447		2.0434	2.2421e-05	2.2650e-05	176	0.4
2.4658		2.4665	2.0156e-05	2.0266e-05	170	0.5
2.7283		2.7277	4.5020e-05	4.4823e-05	176	0.2
3.2837		3.2828	1.4461e-05	1.4782e-05	170	0.1

RMS-acc	RMS-vel	RMS-dsp
5.441e-02	3.752e-03	1.620e-03

FIGURE B-2

BUILDING A - Power and Phase Spectra of Measured Acceleration

Measurement	Date	February 4, 1991
Measurement	Sensor Location	20th Floor, Center
Reference	Sensor Location	10th Floor, Center
	Sensor Direction	North-South

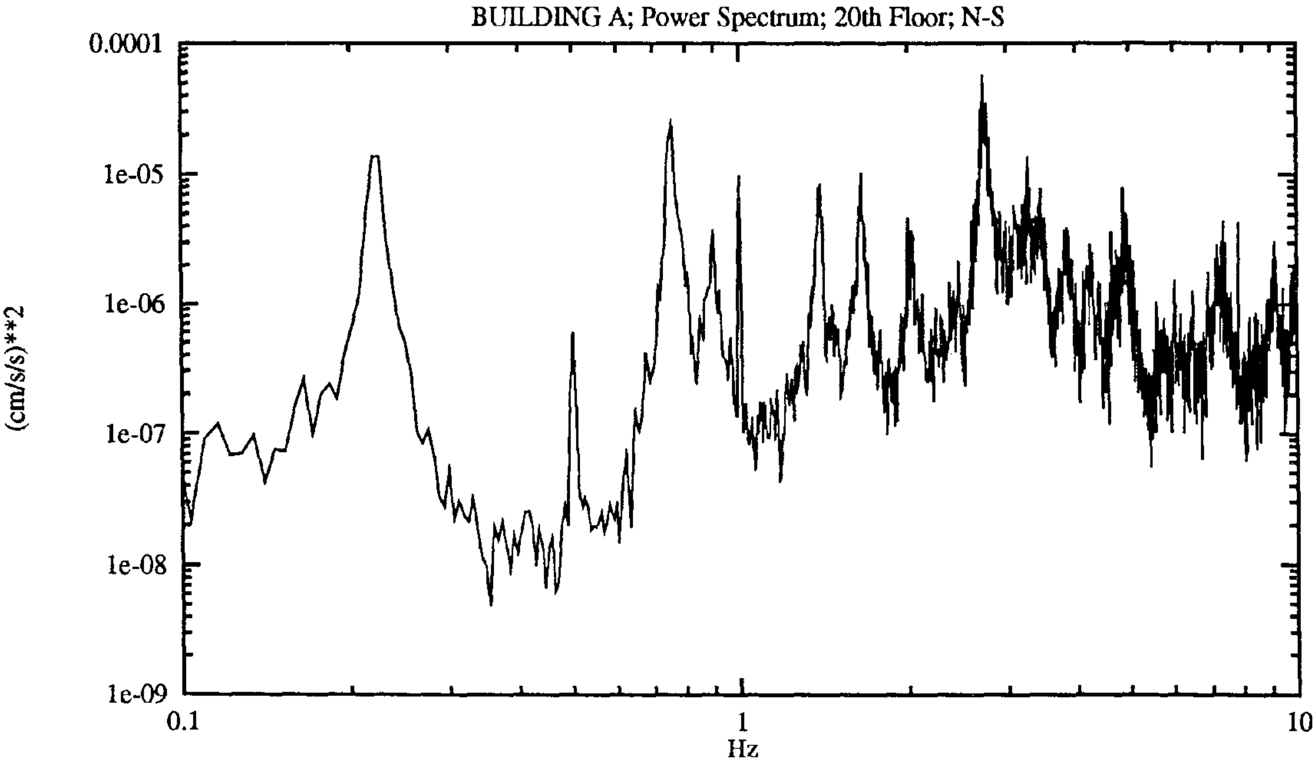

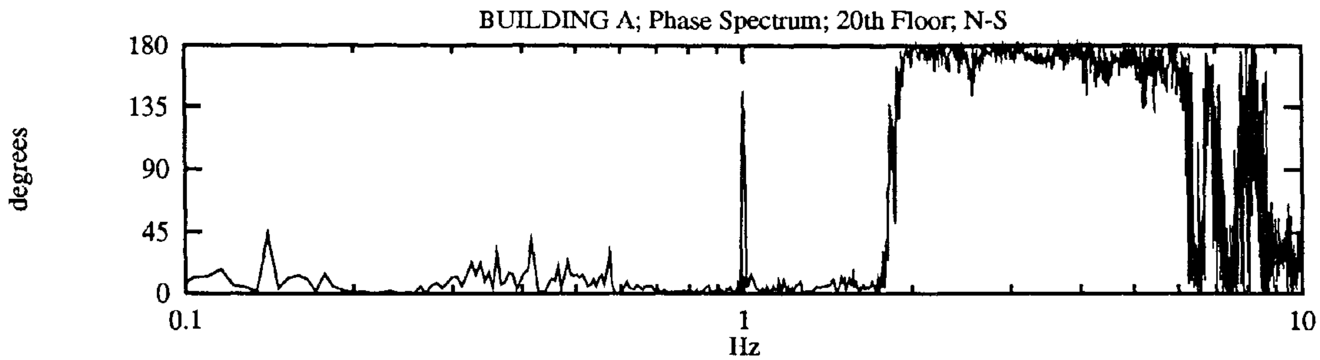

Peaks In G20.10n

Hz-data		Hz-fit	Amp^2-data	Amp^2-fit	Phase	Damping %
0.2197	N1	0.2227	1.3643e-05	1.4678e-05	0	2.0
0.5005	T1	0.5003	5.9826e-07	5.9837e-07	13	0.8
0.7568	N2	0.7554	2.4299e-05	2.4699e-05	1	1.0
0.8972	T2	0.8968	3.7739e-06	3.7812e-06	2	0.8
1.0010		1.0005	9.8104e-06	9.8497e-06	147	0.3
1.3977	N3	1.3963	8.4339e-06	8.5831e-06	5	0.6
1.6541		1.6534	1.0178e-05	1.0252e-05	4	0.4
2.0020		2.0015	4.7157e-06	4.7535e-06	168	0.4
2.7283		2.7275	5.8616e-05	5.8174e-05	176	0.2
3.2837		3.2825	1.3784e-05	1.4305e-05	170	0.1
3.4607		3.4602	7.7546e-06	7.7486e-06	170	0.2

RMS-acc	RMS-vel	RMS-dsp
5.380e-02	6.087e-03	3.827e-03

FIGURE B-3

BUILDING A - Power and Phase Spectra of Measured Acceleration

Measurement	Date	February 4, 1991
Measurement	Sensor Location	30th Floor, Center
Reference	Sensor Location	10th Floor, Center
	Sensor Direction	North-South

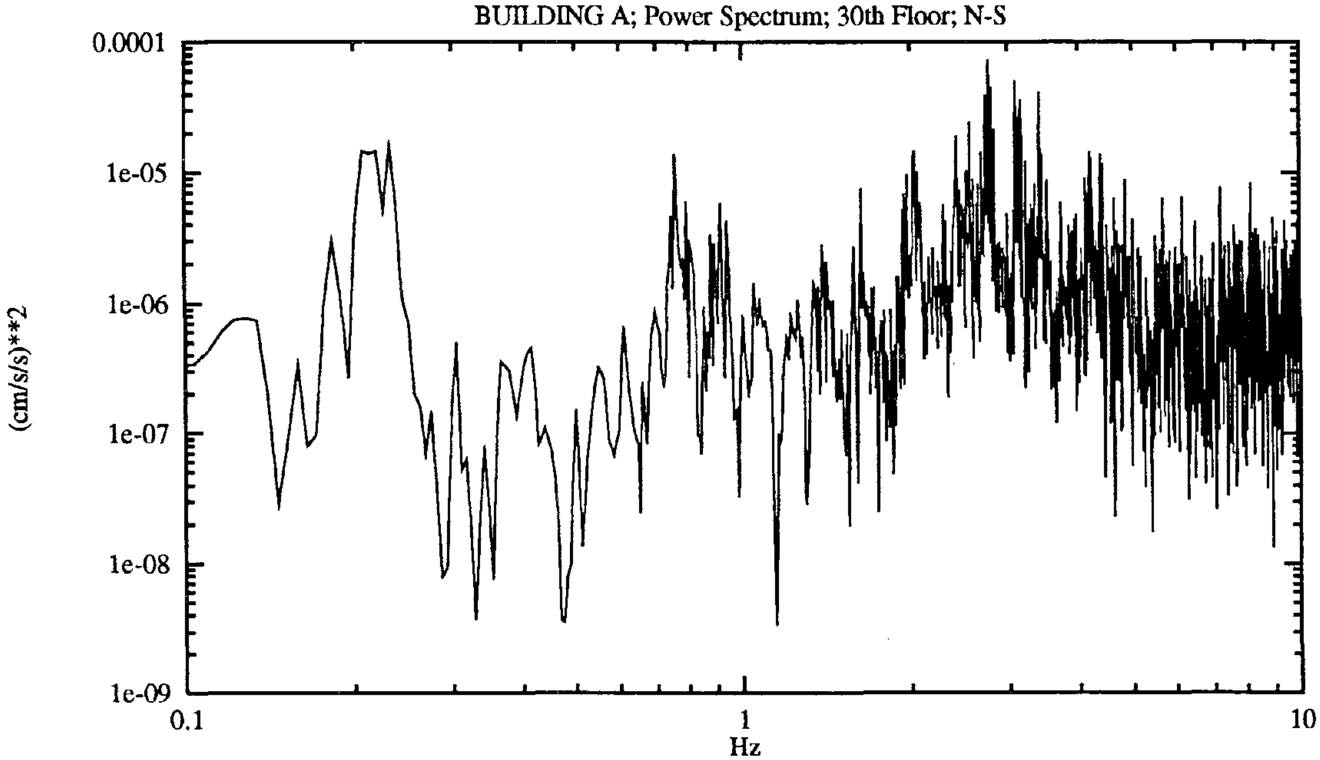

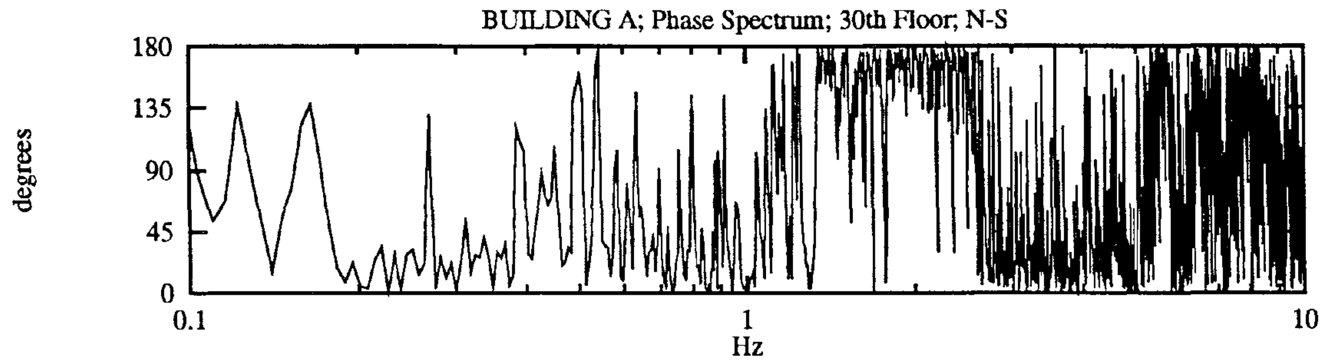

Peaks In G30.10n

Hz-data	Hz-fit	Amp^2-data	Amp^2-fit	Phase	Damping %
0.2319 N1	0.2321	1.5934e-05	1.5941e-05	28	1.8
0.7568 N2	0.7575	1.3971e-05	1.4096e-05	105	0.6
0.9155	0.9152	5.8761e-06	5.8860e-06	144	0.4
1.6357	1.6357	7.6040e-06	7.6294e-06	63	0.1
1.9775	1.9775	9.6823e-06	9.6560e-06	146	0.1
2.7710	2.7719	7.3553e-05	7.5340e-05	173	0.2
3.1006	3.0998	5.0418e-05	5.0545e-05	36	0.1

RMS-acc	RMS-vel	RMS-dsp
6.615e-02	8.571e-03	6.473e-03

FIGURE B-4

BUILDING A - Power and Phase Spectra of Measured Acceleration

Measurement	Date	February 4, 1991
Measurement	Sensor Location	40th Floor, Center
Reference	Sensor Location	10th Floor, Center
	Sensor Direction	North-South

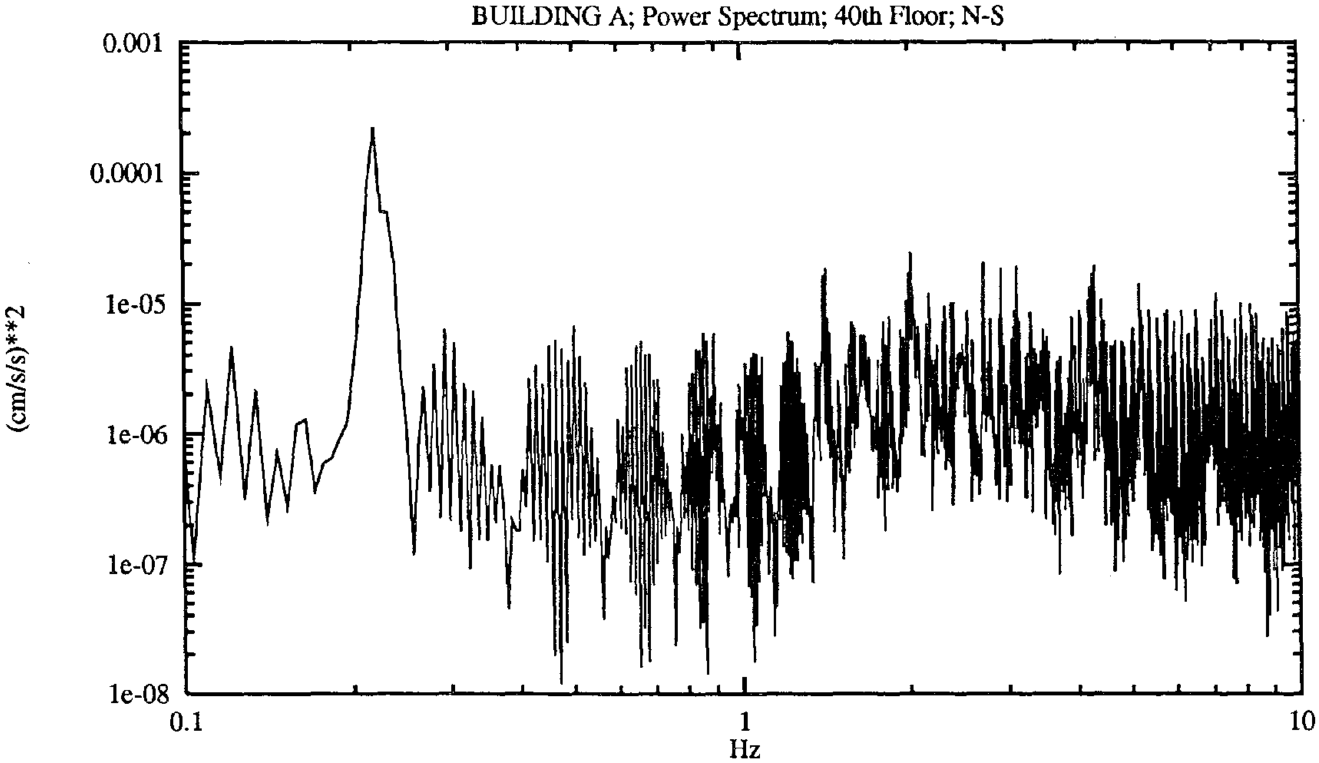

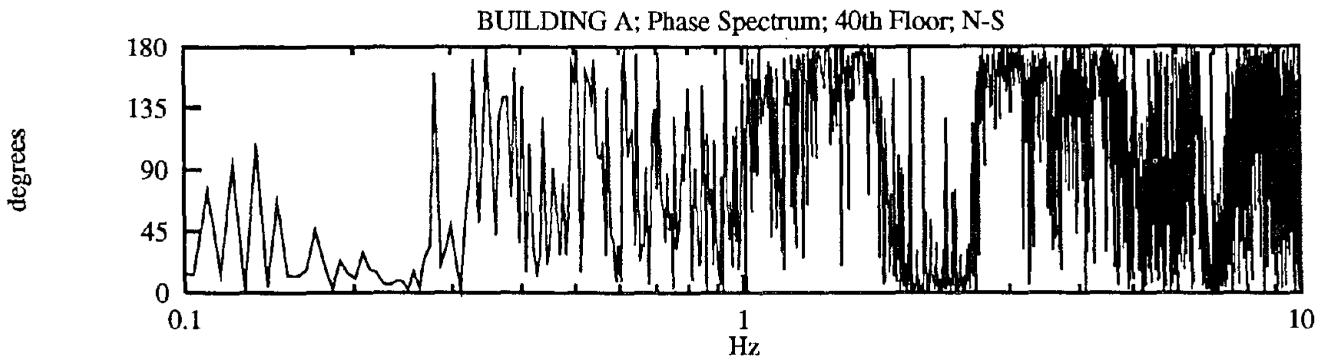

Peaks In G40.10n

Hz-data	Hz-fit	Amp^2-data	Amp^2-fit	Phase	Damping %
0.2197 N1	0.2194	2.2120e-04	2.2162e-04	15	1.5
1.4160	1.4160	1.8379e-05	1.8299e-05	179	0.1
2.0142	2.0140	2.4589e-05	2.4557e-05	5	0.2

RMS-acc	RMS-vel	RMS-dsp
8.417e-02	1.721e-02	1.272e-02

FIGURE B-5

BUILDING A - Power and Phase Spectra of Measured Acceleration

Measurement	Date	February 4, 1991
Measurement	Sensor Location	52nd Floor, Center
Reference	Sensor Location	10th Floor, Center
	Sensor Direction	North-South

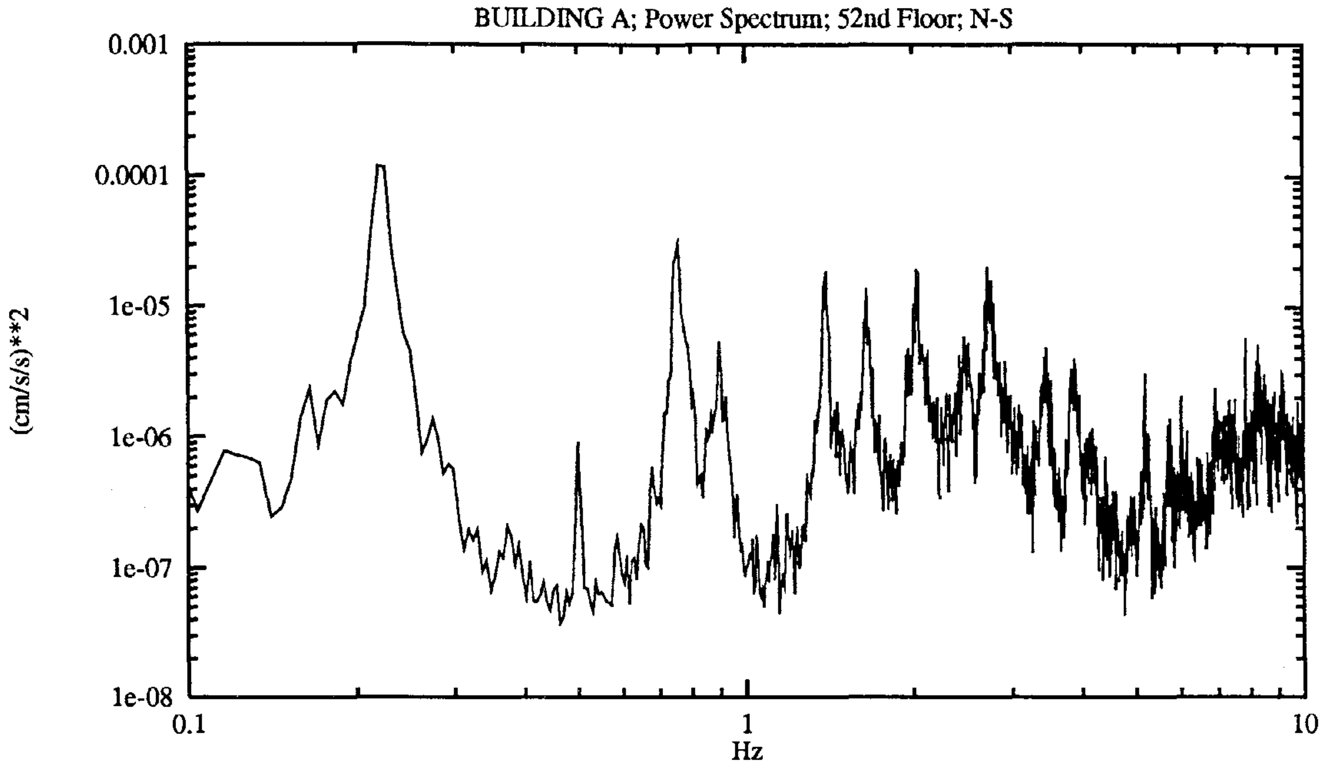

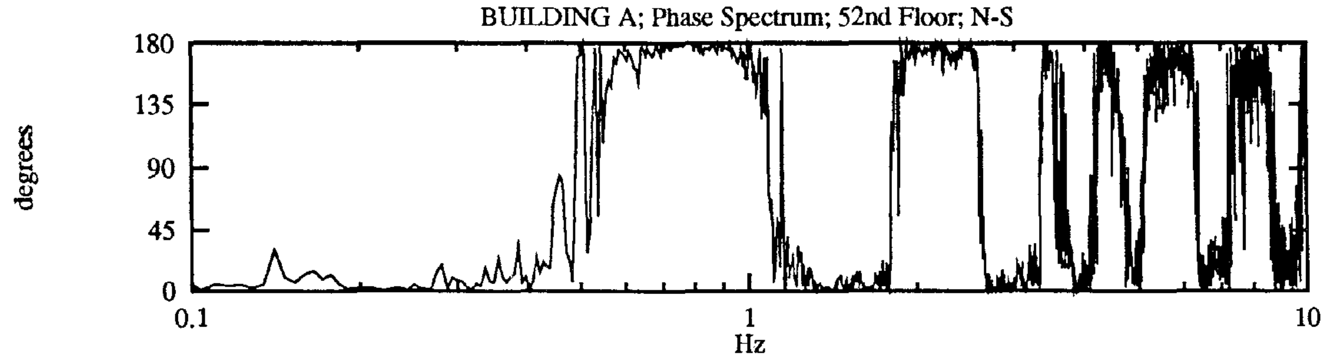

Peaks In G52.10n

Hz-data		Hz-fit	Amp^2-data	Amp^2-fit	Phase	Damping %
0.2197	N1	0.2227	1.1880e-04	1.2786e-04	0	2.0
0.5005	T1	0.5004	9.1953e-07	9.1968e-07	172	0.7
0.7568	N2	0.7555	3.0521e-05	3.0920e-05	179	1.0
0.8972	T2	0.8971	5.3543e-06	5.3532e-06	179	0.8
1.3977	N3	1.3959	1.8528e-05	1.9073e-05	1	0.6
1.6541		1.6535	1.3813e-05	1.3947e-05	3	0.3
2.0325		2.0330	1.9264e-05	1.9312e-05	176	0.8
2.4658		2.4676	5.8860e-06	6.0052e-06	176	0.7
2.7283		2.7274	2.0158e-05	2.0146e-05	4	0.2
3.4607		3.4607	4.8732e-06	5.0068e-06	163	0.1
3.8818		3.8817	4.0096e-06	3.9339e-06	6	0.1

RMS-acc	RMS-vel	RMS-dsp
5.674e-02	1.486e-02	1.078e-02

FIGURE B-6

BUILDING A - Power and Phase Spectra of Measured Acceleration

Measurement	Date	February 4, 1991
Measurement	Sensor Location	10th Floor, Center
Reference	Sensor Location	20th Floor, Center
	Sensor Direction	East-West

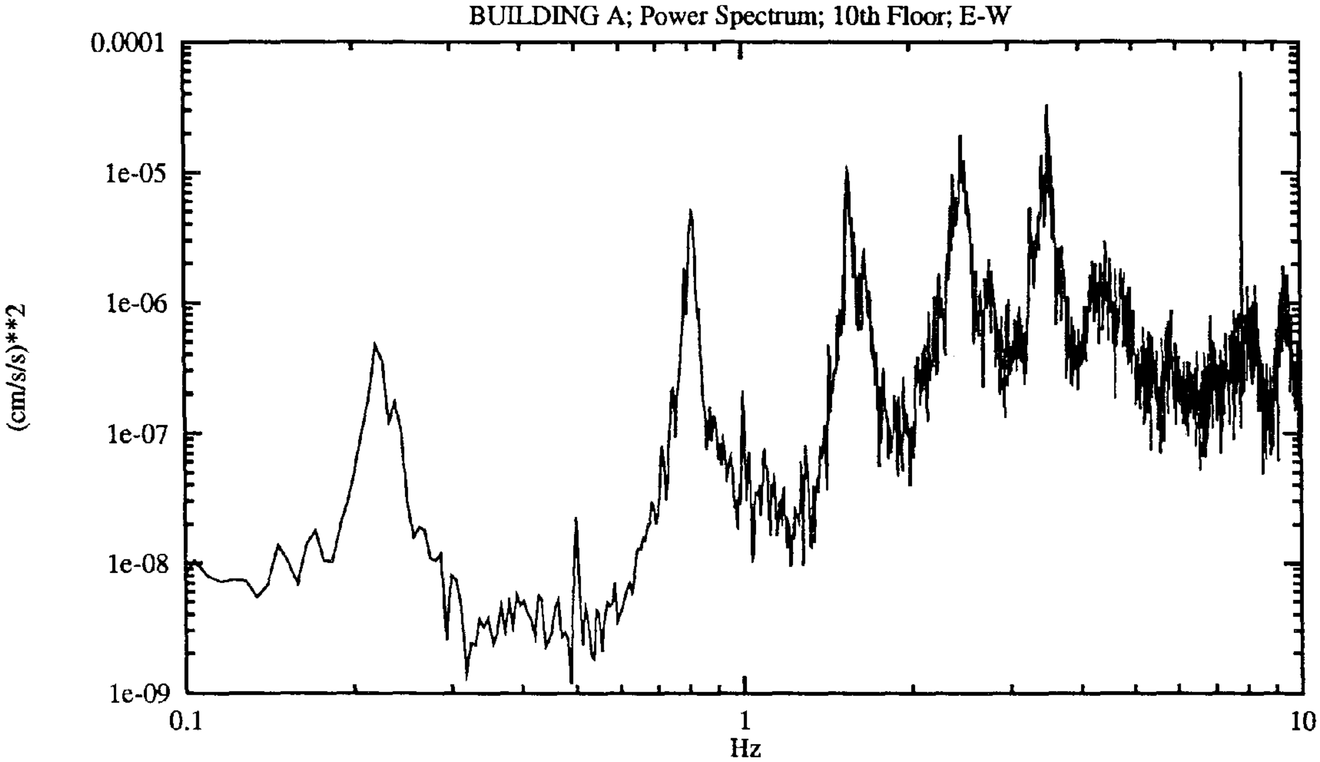

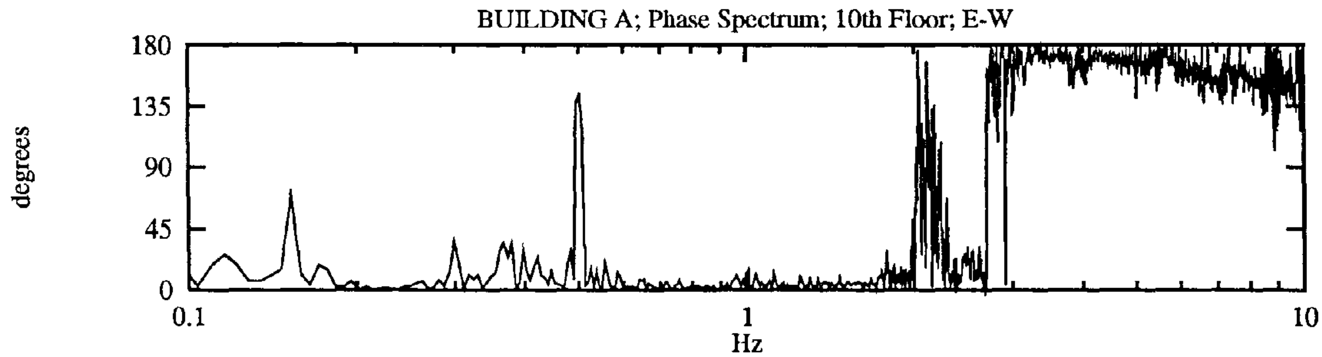

Hz-data	Hz-fit	Amp^2-data	Amp^2-fit	Phase	Damping %
0.2197	0.2211	4.7275e-07	4.8324e-07	1	2.5
0.5005	0.5002	2.2547e-08	2.2577e-08	143	0.7
0.8118	0.8127	4.8938e-06	4.9155e-06	3	1.0
1.5503	1.5512	1.0232e-05	1.0259e-05	4	0.7
2.4658	2.4670	1.9098e-05	1.9372e-05	23	0.5
3.5217	3.5213	3.3054e-05	3.2663e-05	171	0.3

RMS-acc	RMS-vel	RMS-dsp
4.156e-02	2.618e-03	1.233e-03

FIGURE B-7

BUILDING A - Power and Phase Spectra of Measured Acceleration

Measurement	Date	February 4, 1991
Measurement	Sensor Location	20th Floor, Center
Reference	Sensor Location	20th Floor, Center
	Sensor Direction	East-West

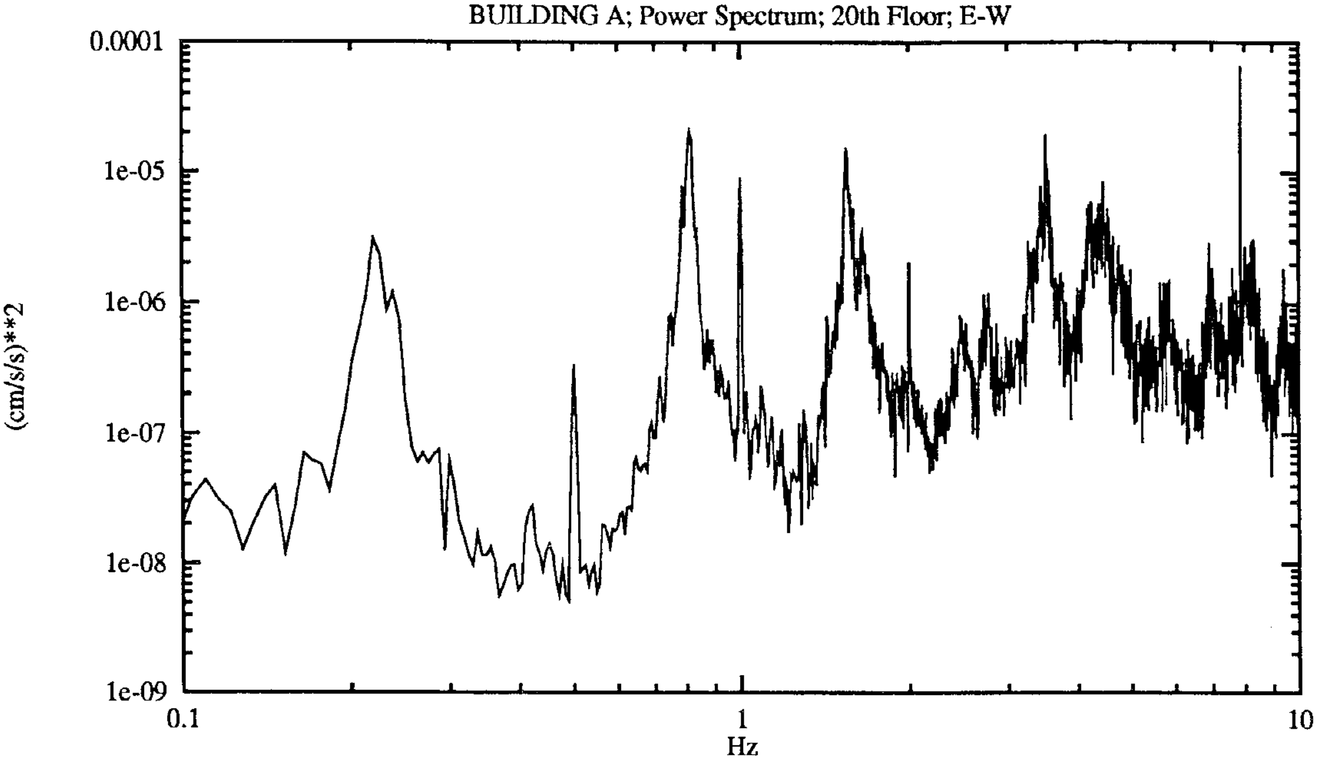

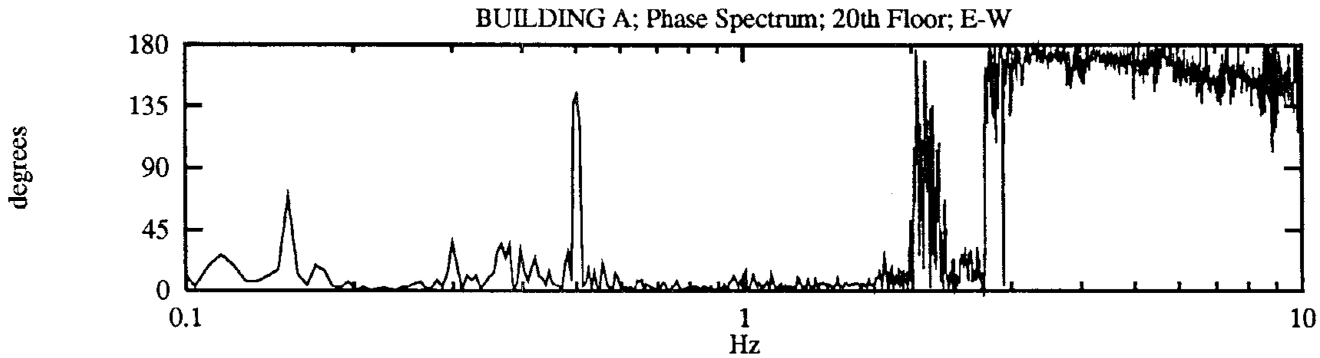

Peaks In G20.10e

Hz-data	Hz-fit	Amp^2-data	Amp^2-fit	Phase	Damping %
0.2197	0.2210	3.0824e-06	3.1450e-06	1	2.7
0.5005	0.5003	3.3415e-07	3.3434e-07	143	0.7
0.8118	0.8127	2.0372e-05	2.0452e-05	3	0.9
0.9216	0.9231	3.0714e-07	3.1129e-07	4	1.3
1.5503	1.5519	1.4445e-05	1.4566e-05	4	0.7
3.5217	3.5211	1.9257e-05	1.8835e-05	171	0.2

RMS-acc	RMS-vel	RMS-dsp
4.255e-02	3.975e-03	2.341e-03

FIGURE B-8

BUILDING A - Power and Phase Spectra of Measured Acceleration

Measurement	Date	February 4, 1991
Measurement	Sensor Location	40th Floor, Center
Reference	Sensor Location	10th Floor, Center
	Sensor Direction	East-West

BUILDING A; Power Spectrum; 40th Floor; E-W

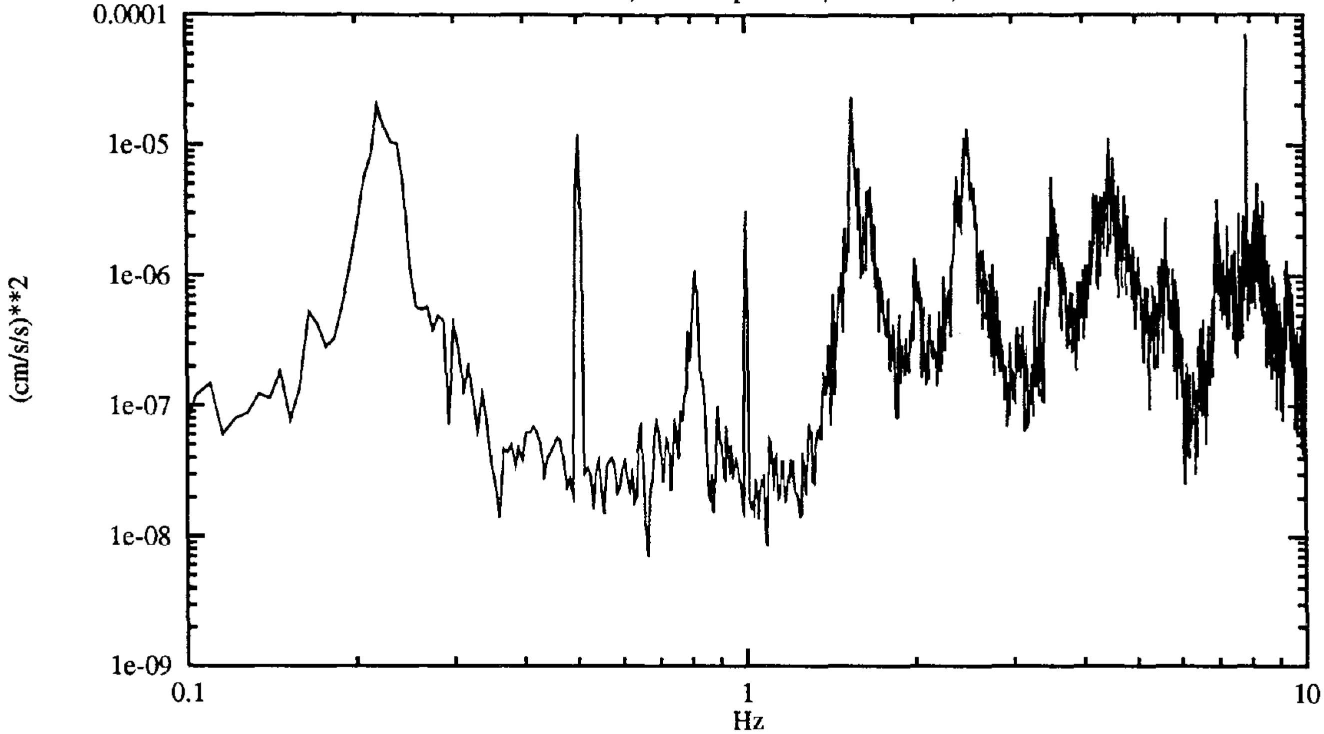

BUILDING A; Phase Spectrum; 40th Floor; E-W

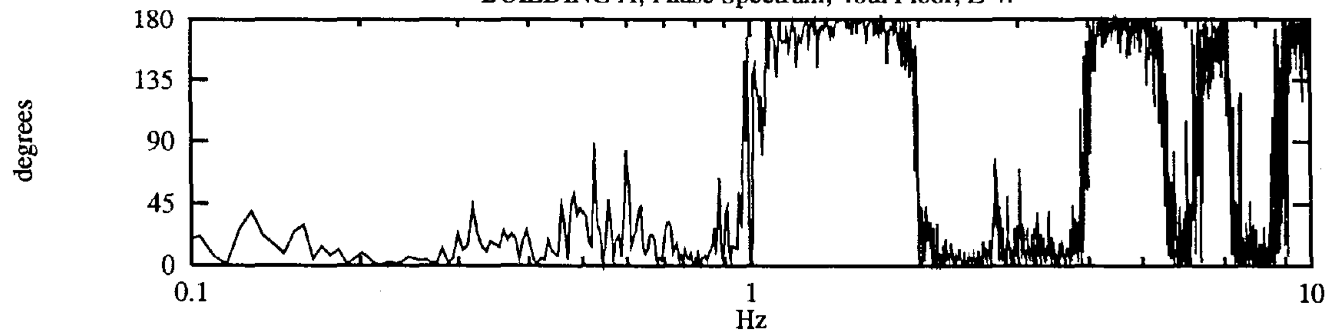

Peaks In G40.10e

Hz-data	Hz-fit	Amp^2-data	Amp^2-fit	Phase	Damping %
0.2197	0.2206	2.0189e-05	2.0377e-05	1	2.9
0.5005	0.5004	1.1825e-05	1.1828e-05	38	0.6
0.8118	0.8117	1.0042e-06	1.0040e-06	0	1.0
1.5503	1.5498	2.3042e-05	2.3127e-05	170	0.5
2.4902	2.4898	1.3338e-05	1.3351e-05	5	1.0
3.5217	3.5207	5.6267e-06	5.6326e-06	5	0.3
4.4556	4.4550	1.1168e-05	1.1206e-05	177	0.2

RMS-acc	RMS-vel	RMS-dsp
4.503e-02	7.520e-03	5.459e-03

FIGURE B-9

BUILDING A - Power and Phase Spectra of Measured Acceleration

Measurement	Date	February 4, 1991
Measurement	Sensor Location	52nd Floor, Center
Reference	Sensor Location	10th Floor, Center
	Sensor Direction	East-West

BUILDING A; Power Spectrum; 52nd Floor; E-W

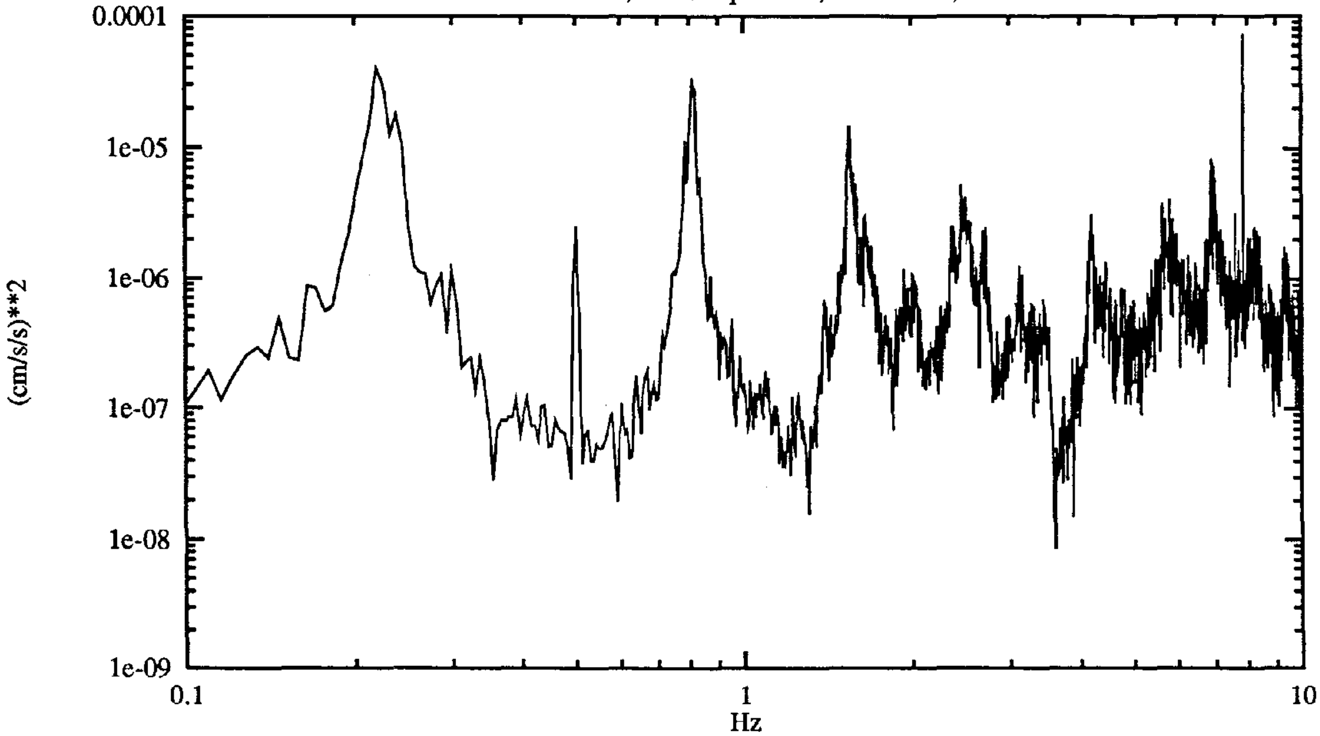

BUILDING A; Phase Spectrum; 52nd Floor; E-W

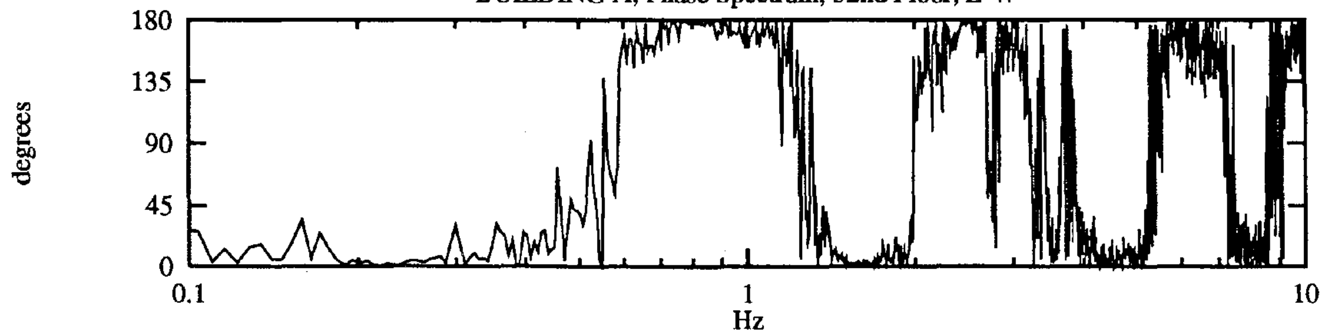

Peaks In G52.10e

Hz-data	Hz-fit	Amp^2-data	Amp^2-fit	Phase	Damping %
0.2197	0.2211	3.9923e-05	4.0730e-05	0	2.9
0.5005	0.5003	2.5103e-06	2.5127e-06	39	0.7
0.8118	0.8129	3.1305e-05	3.1509e-05	177	0.9
1.5503	1.5508	1.4744e-05	1.4767e-05	2	0.7
2.4658	2.4663	5.2409e-06	5.2899e-06	177	0.5

RMS-acc	RMS-vel	RMS-dsp
4.274e-02	9.882e-03	7.046e-03

FIGURE B-10

BUILDING B - Power and Phase Spectra of Measured Acceleration

Measurement	Date	February 7, 1991
Measurement	Sensor Location	10th Floor, Center
Reference	Sensor Location	20th Floor, Center
	Sensor Direction	North-South

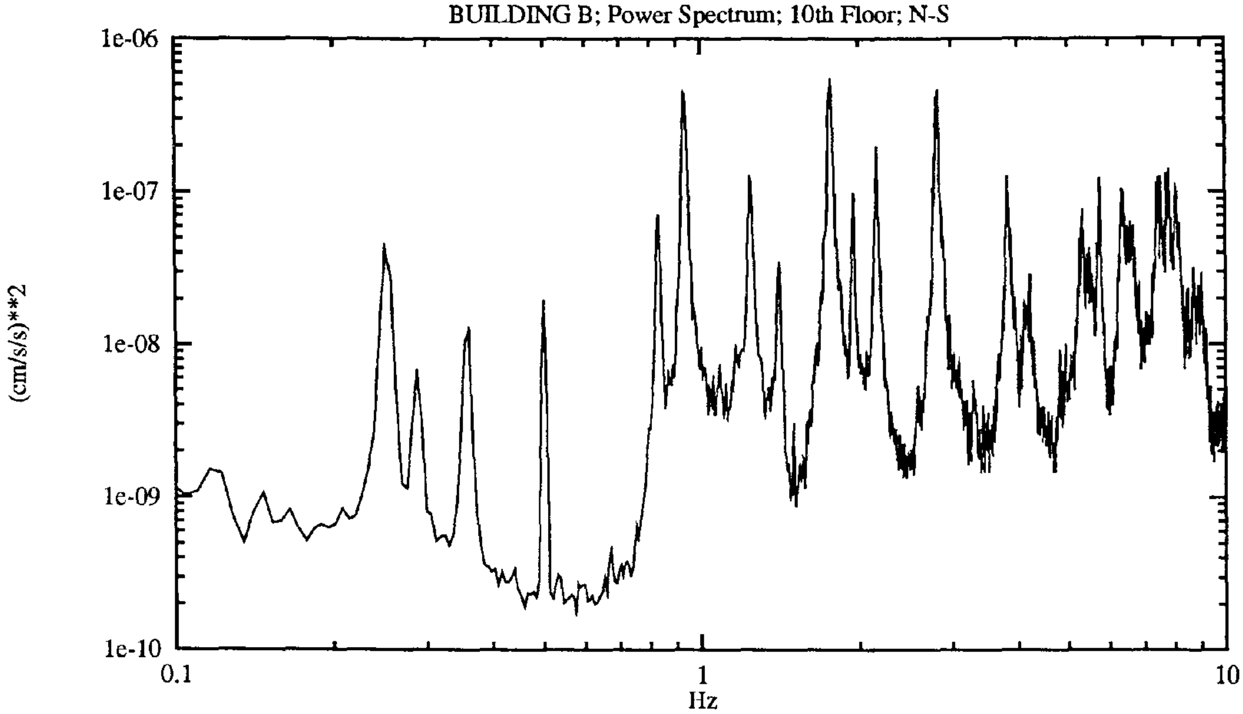

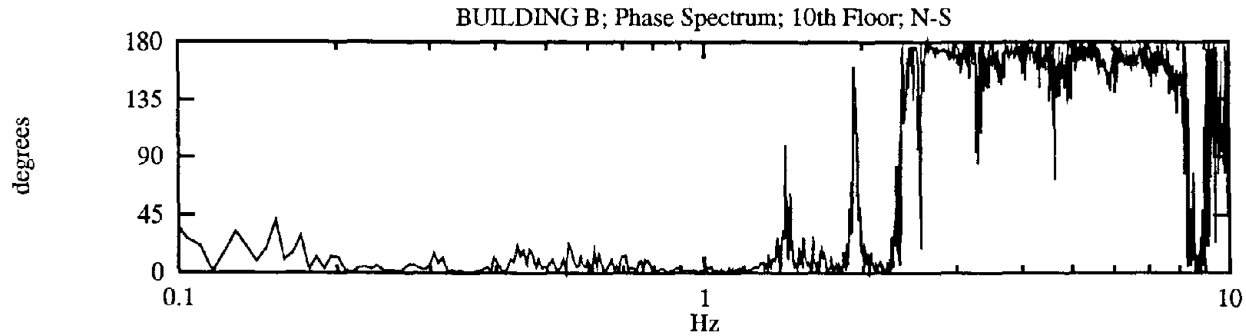

Peaks In G10.20n

Hz-data		Hz-fit	Amp^2-data	Amp^2-fit	Phase	Damping %
0.2502		0.2513	4.2749e-08	4.3379e-08	2	2.4
0.2869	T1	0.2868	6.8865e-09	6.8867e-09	4	1.7
0.3601		0.3581	1.2578e-08	1.3211e-08	0	1.1
0.5005		0.5002	1.9753e-08	1.9776e-08	6	0.6
0.8301	T2	0.8290	7.1446e-08	7.2032e-08	3	0.9
0.9277	T3	0.9304	4.4073e-07	4.6869e-07	2	1.0
1.2451		1.2474	1.2162e-07	1.2538e-07	5	0.7
1.4099	T4	1.4102	3.5103e-08	3.5187e-08	33	0.8
1.7700		1.7685	5.0356e-07	5.0757e-07	3	0.9
1.9531	T5	1.9518	9.7993e-08	9.8953e-08	93	0.5
2.1667		2.1655	1.9735e-07	1.9884e-07	3	0.5
2.8259		2.8246	4.6336e-07	4.6566e-07	173	0.5
3.8208		3.8215	1.2677e-07	1.2526e-07	170	0.5
3.9490		3.9483	2.0414e-08	2.0140e-08	176	0.6
4.2297		4.2301	2.9024e-08	2.8871e-08	172	0.2

RMS-acc	RMS-vel	RMS-dsp
6.440e-03	5.138e-04	2.807e-04

FIGURE B-11

BUILDING B - Power and Phase Spectra of Measured Acceleration

Measurement	Date	February 7, 1991
Measurement	Sensor Location	20th Floor, Center
Reference	Sensor Location	10th Floor, Center
	Sensor Direction	North-South

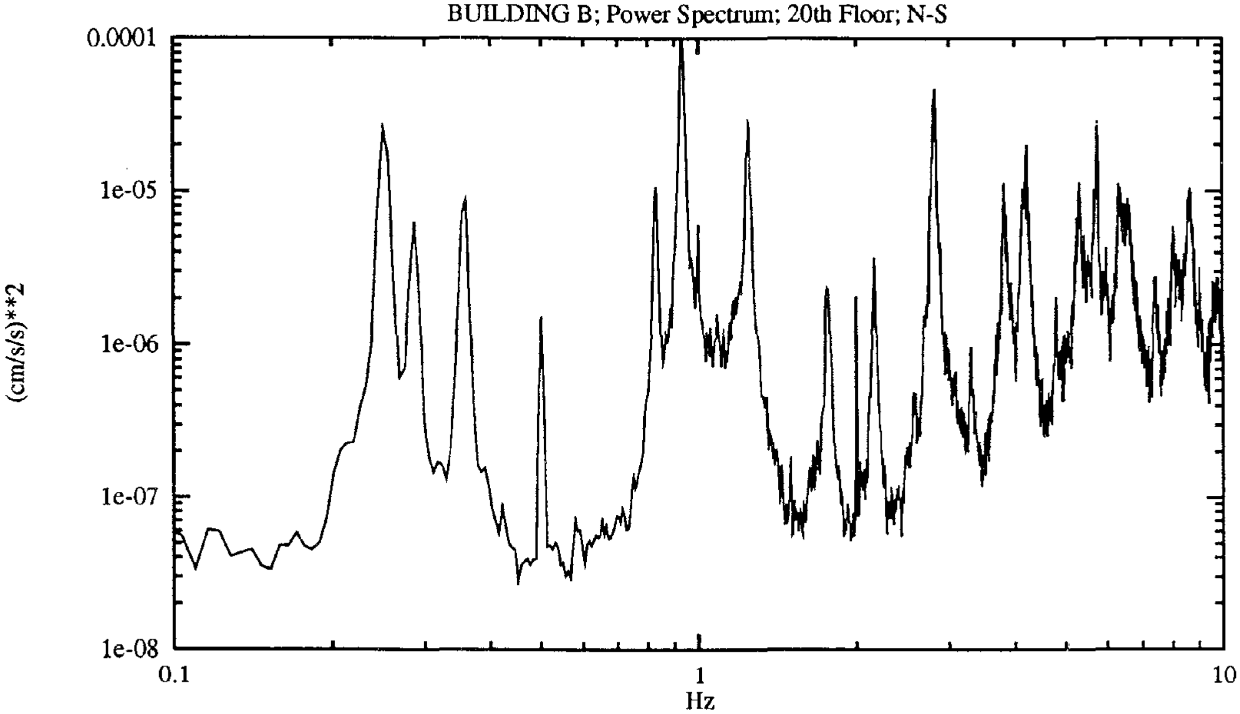

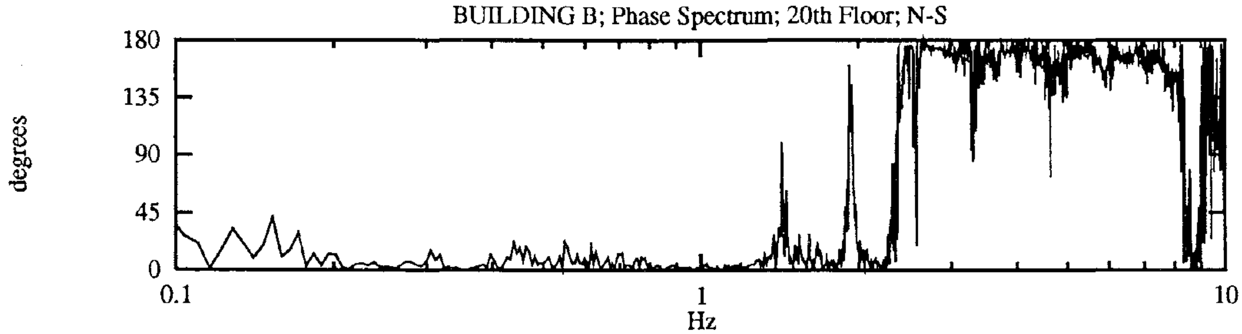

Peaks In G20.10n

Hz-data		Hz-fit	Amp^2-data	Amp^2-fit	Phase	Damping %
0.2502		0.2512	2.5807e-05	2.6146e-05	2	2.4
0.2869	T1	0.2868	6.3026e-06	6.3032e-06	4	1.5
0.3601		0.3582	8.7874e-06	9.2266e-06	0	1.0
0.5005		0.5003	1.5105e-06	1.5125e-06	6	0.7
0.8301	T2	0.8291	1.0673e-05	1.0759e-05	3	0.9
0.9277	T3	0.9305	9.8234e-05	1.0461e-04	2	1.0
1.0010		1.0006	6.0538e-06	6.0722e-06	1	0.4
1.2451		1.2471	2.7618e-05	2.8193e-05	5	0.7
1.7639		1.7656	2.3443e-06	2.3525e-06	3	1.1
2.0020		2.0008	2.0530e-06	2.0713e-06	18	0.1
2.1667		2.1657	3.7088e-06	3.7327e-06	3	0.5
2.8259		2.8243	4.6485e-05	4.6968e-05	173	0.5
3.3020	T6	3.3001	9.6800e-07	9.8720e-07	130	0.3
3.8208		3.8216	1.1379e-05	1.1444e-05	170	0.4
3.9490		3.9485	2.5657e-06	2.5779e-06	176	0.9
4.2297		4.2305	2.0037e-05	2.0742e-05	172	0.2

RMS-acc	RMS-vel	RMS-dsp
6.756e-02	7.412e-03	3.940e-03

FIGURE B-12

BUILDING B - Power and Phase Spectra of Measured Acceleration

Measurement	Date	February 7, 1991
Measurement	Sensor Location	30th Floor, Center
Reference	Sensor Location	10th Floor, Center
	Sensor Direction	North-South

BUILDING B; Power Spectrum; 30th Floor; N-S

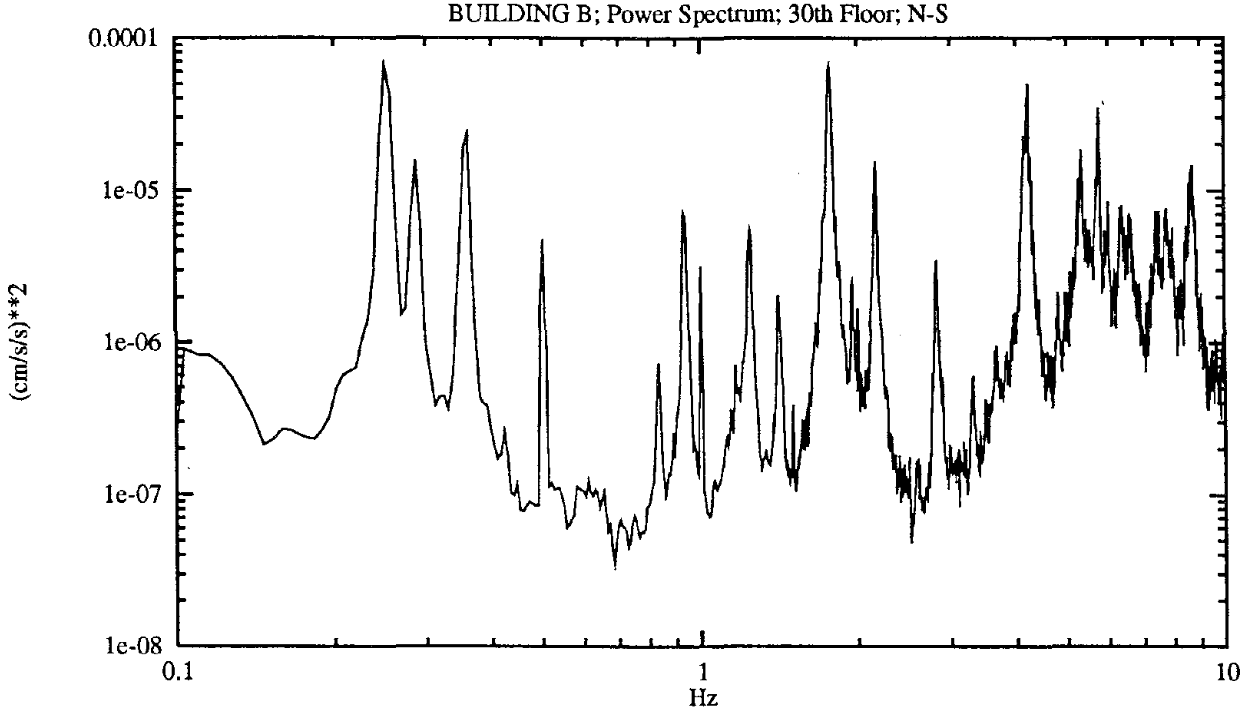

BUILDING B; Phase Spectrum; 30th Floor; N-S

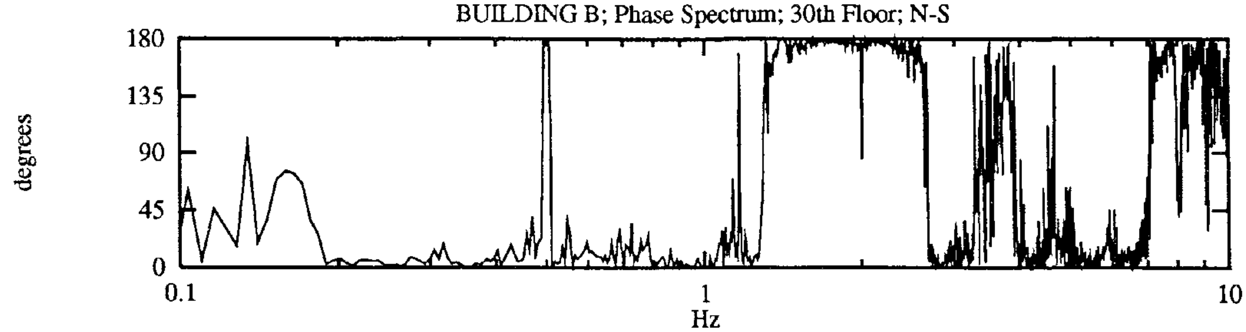

Peaks In G30.10n

Hz-data		Hz-fit	Amp^2-data	Amp^2-fit	Phase	Damping %
0.2502		0.2512	6.6898e-05	6.7841e-05	2	2.4
0.2869	T1	0.2868	1.5822e-05	1.5823e-05	5	1.5
0.3601		0.3581	2.3460e-05	2.4650e-05	1	1.0
0.5005		0.5002	4.7395e-06	4.7460e-06	179	0.7
0.8301	T2	0.8292	7.3327e-07	7.3761e-07	8	0.9
0.9277	T3	0.9303	7.1502e-06	7.5772e-06	2	1.0
1.0010		1.0004	3.1658e-06	3.1888e-06	2	0.3
1.2451		1.2461	5.4706e-06	5.4948e-06	8	0.7
1.4099	T4	1.4102	2.0440e-06	2.0452e-06	179	0.8
1.7700		1.7684	6.4706e-05	6.5267e-05	177	0.9
1.9531	T5	1.9509	2.5350e-06	2.6040e-06	176	0.6
2.1667		2.1655	1.5456e-05	1.5646e-05	178	0.5
2.8259		2.8247	3.4983e-06	3.5167e-06	2	0.5
4.2297		4.2306	4.9969e-05	5.0545e-05	2	0.2
5.3284		5.3288	1.8501e-05	1.8835e-05	2	0.3
5.7556		5.7557	3.4598e-05	3.4332e-05	8	0.4

RMS-acc	RMS-vel	RMS-dsp
7.292e-02	1.007e-02	6.318e-03

FIGURE B-13

BUILDING B - Power and Phase Spectra of Measured Acceleration

Measurement	Date	February 7, 1991
Measurement	Sensor Location	40th Floor, Center
Reference	Sensor Location	10th Floor, Center
	Sensor Direction	North-South

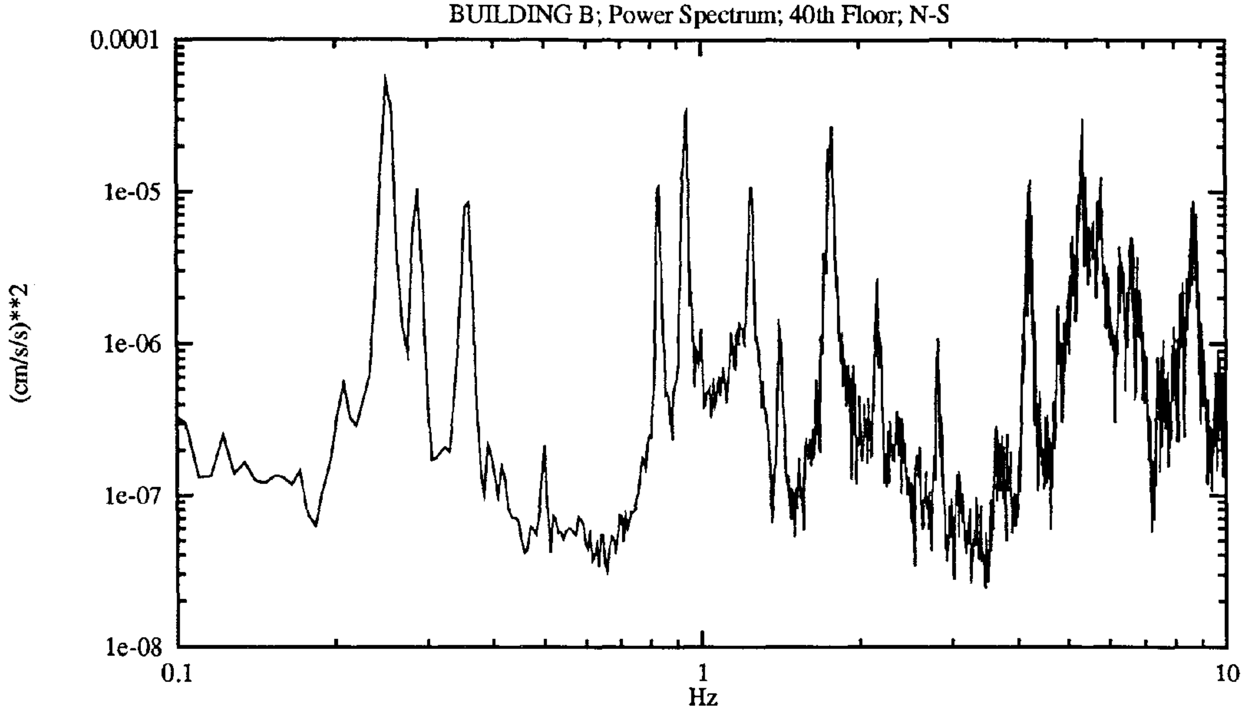

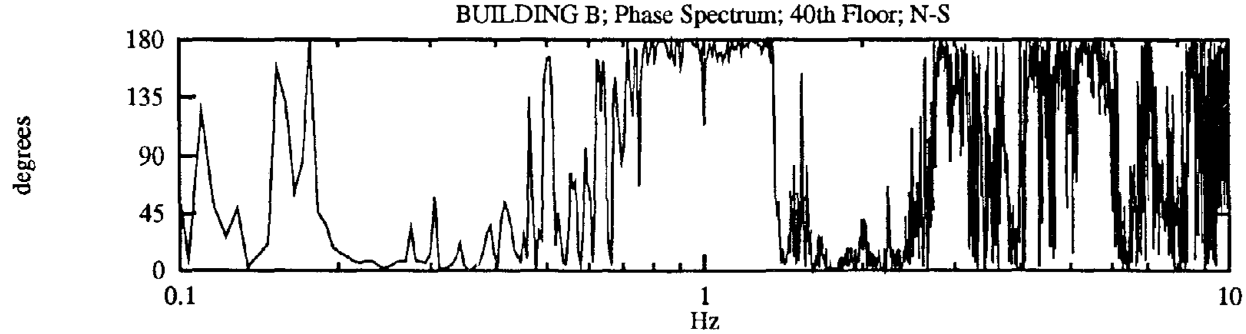

Peaks In G40.10n

Hz-data		Hz-fit	Amp^2-data	Amp^2-fit	Phase	Damping %
0.2502		0.2512	5.4492e-05	5.5306e-05	3	2.3
0.2869	T1	0.2864	1.0573e-05	1.0610e-05	7	1.4
0.3601		0.3575	8.4301e-06	9.0357e-06	1	1.3
0.5005		0.4997	2.1479e-07	2.1647e-07	165	1.0
0.8301	T2	0.8275	1.0780e-05	1.1347e-05	179	0.9
0.9399	T3	0.9375	3.3593e-05	3.5822e-05	179	0.5
1.0010		1.0000	1.2520e-06	1.2666e-06	114	0.6
1.2451		1.2452	1.0732e-05	1.0732e-05	179	0.8
1.4099	T4	1.4120	1.3258e-06	1.3672e-06	17	0.8
1.7761		1.7749	2.7003e-05	2.7299e-05	2	0.5
2.1667		2.1640	2.4450e-06	2.6226e-06	0	0.3
2.8259		2.8246	1.0786e-06	1.0878e-06	169	0.3
4.2358		4.2331	1.1243e-05	1.1802e-05	177	0.3
5.3528		5.3518	3.0246e-05	3.1471e-05	174	0.1
5.8044		5.8030	1.2482e-05	1.2875e-05	178	0.2

RMS-acc	RMS-vel	RMS-dsp
5.206e-02	8.614e-03	5.405e-03

FIGURE B-14

BUILDING B - Power and Phase Spectra of Measured Acceleration

Measurement	Date	February 7, 1991
Measurement	Sensor Location	10th Floor, Center
Reference	Sensor Location	20th Floor, Center
	Sensor Direction	East-West

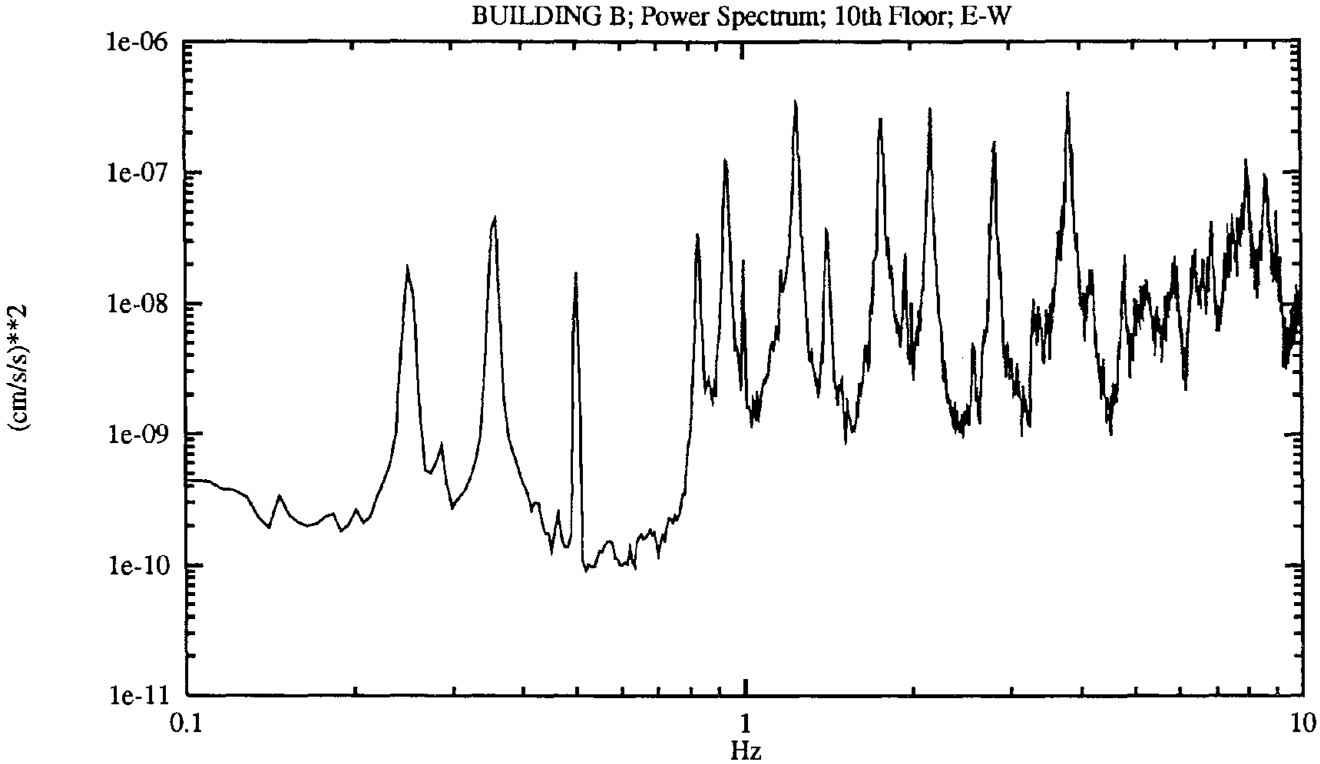

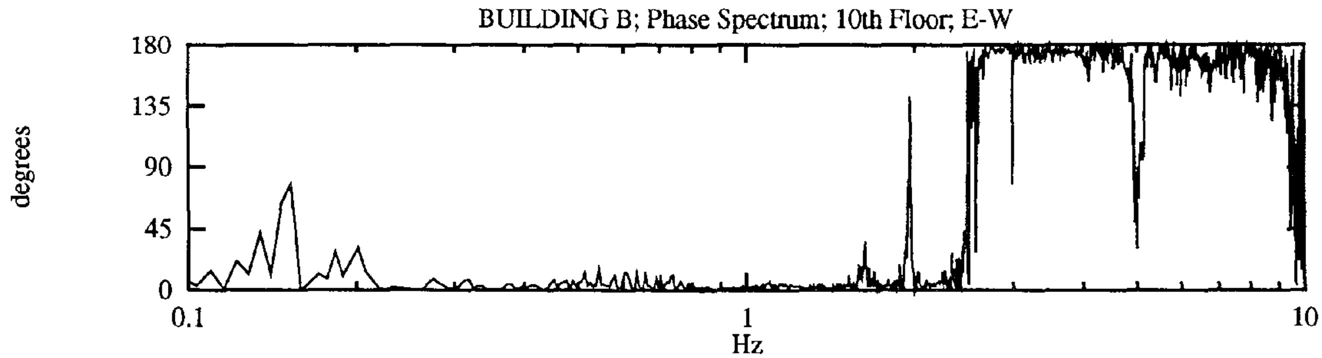

Peaks In G10.20e

Hz-data		Hz-fit	Amp^2-data	Amp^2-fit	Phase	Damping %
0.2502		0.2512	1.8296e-08	1.8515e-08	0	2.4
0.3601		0.3581	4.4522e-08	4.6886e-08	1	1.0
0.5005		0.5002	1.7424e-08	1.7455e-08	5	0.6
0.8301	T2	0.8294	3.4397e-08	3.4517e-08	3	0.9
0.9277	T3	0.9303	1.2379e-07	1.3108e-07	2	1.0
1.0010		1.0006	2.1840e-08	2.1915e-08	0	0.3
1.2451		1.2469	3.3531e-07	3.4040e-07	2	0.7
1.4099	T4	1.4124	3.6174e-08	3.7195e-08	0	0.8
1.7700		1.7693	2.6096e-07	2.6147e-07	3	0.8
2.1667		2.1650	3.0756e-07	3.1199e-07	5	0.5
2.8259		2.8245	1.7293e-07	1.7416e-07	175	0.5
3.8208		3.8210	4.0677e-07	4.0419e-07	174	0.4

RMS-acc	RMS-vel	RMS-dsp
5.927e-03	4.261e-04	2.158e-04

FIGURE B-15

BUILDING B - Power and Phase Spectra of Measured Acceleration

Measurement	Date	February 7, 1991
Measurement	Sensor Location	20th Floor, Center
Reference	Sensor Location	10th Floor, Center
	Sensor Direction	East-West

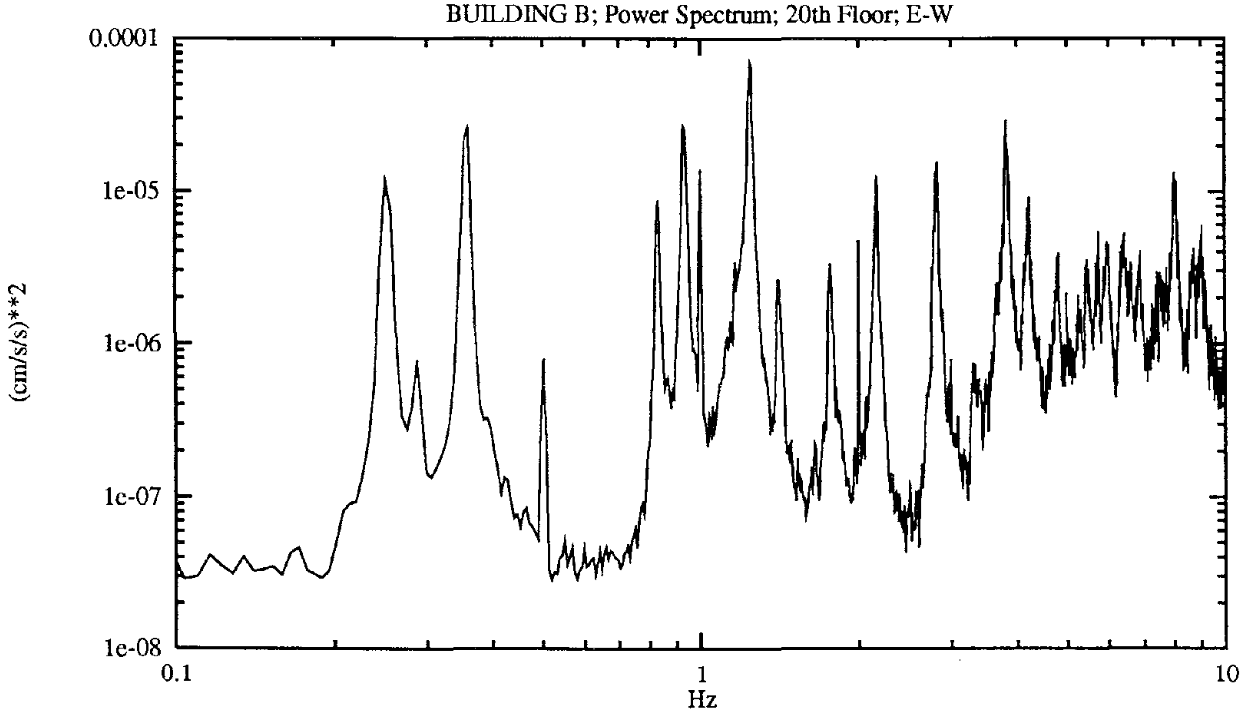

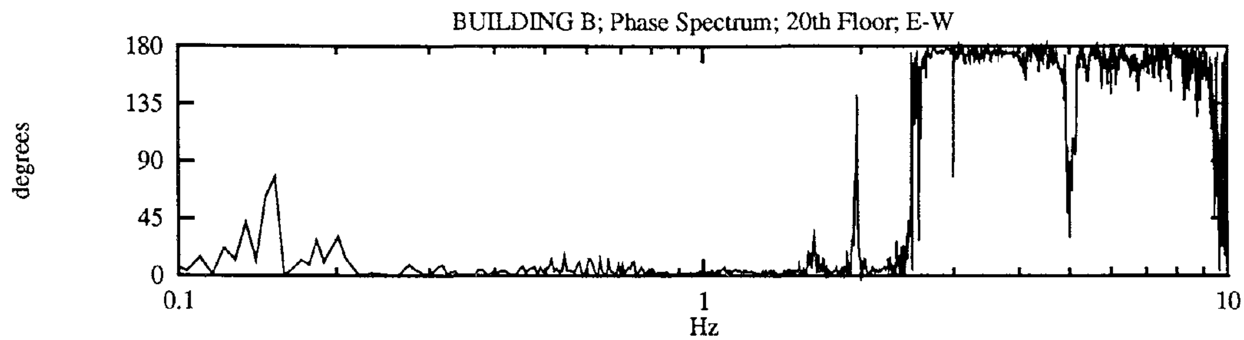

Peaks In G20.10e

Hz-data	Hz-fit	Amp^2-data	Amp^2-fit	Phase	Damping %
0.2502	0.2512	1.1862e-05	1.2006e-05	0	2.3
0.3601	0.3580	2.6226e-05	2.7731e-05	1	1.0
0.5005	0.5002	8.0354e-07	8.0466e-07	5	0.7
0.8301 T2	0.8294	8.7261e-06	8.7582e-06	3	0.9
0.9277 T3	0.9303	2.6870e-05	2.8476e-05	2	1.0
1.0010	1.0005	1.3890e-05	1.3977e-05	0	0.3
1.2451	1.2470	6.9901e-05	7.1168e-05	2	0.7
1.4160 T4	1.4130	2.6314e-06	2.7325e-06	1	0.9
1.7700	1.7696	3.3644e-06	3.3714e-06	3	0.8
2.0020	2.0006	4.8394e-06	4.9472e-06	4	0.1
2.1667	2.1648	1.2643e-05	1.2964e-05	5	0.5
2.8259	2.8245	1.5691e-05	1.5736e-05	175	0.5
3.8208	3.8209	2.9261e-05	2.9325e-05	174	0.4
4.2297	4.2321	9.2176e-06	9.5367e-06	176	0.3

RMS-acc	RMS-vel	RMS-dsp
6.011e-02	6.332e-03	2.996e-03

FIGURE B-16

BUILDING B - Power and Phase Spectra of Measured Acceleration

Measurement	Date	February 7, 1991
Measurement	Sensor Location	30th Floor, Center
Reference	Sensor Location	10th Floor, Center
	Sensor Direction	East-West

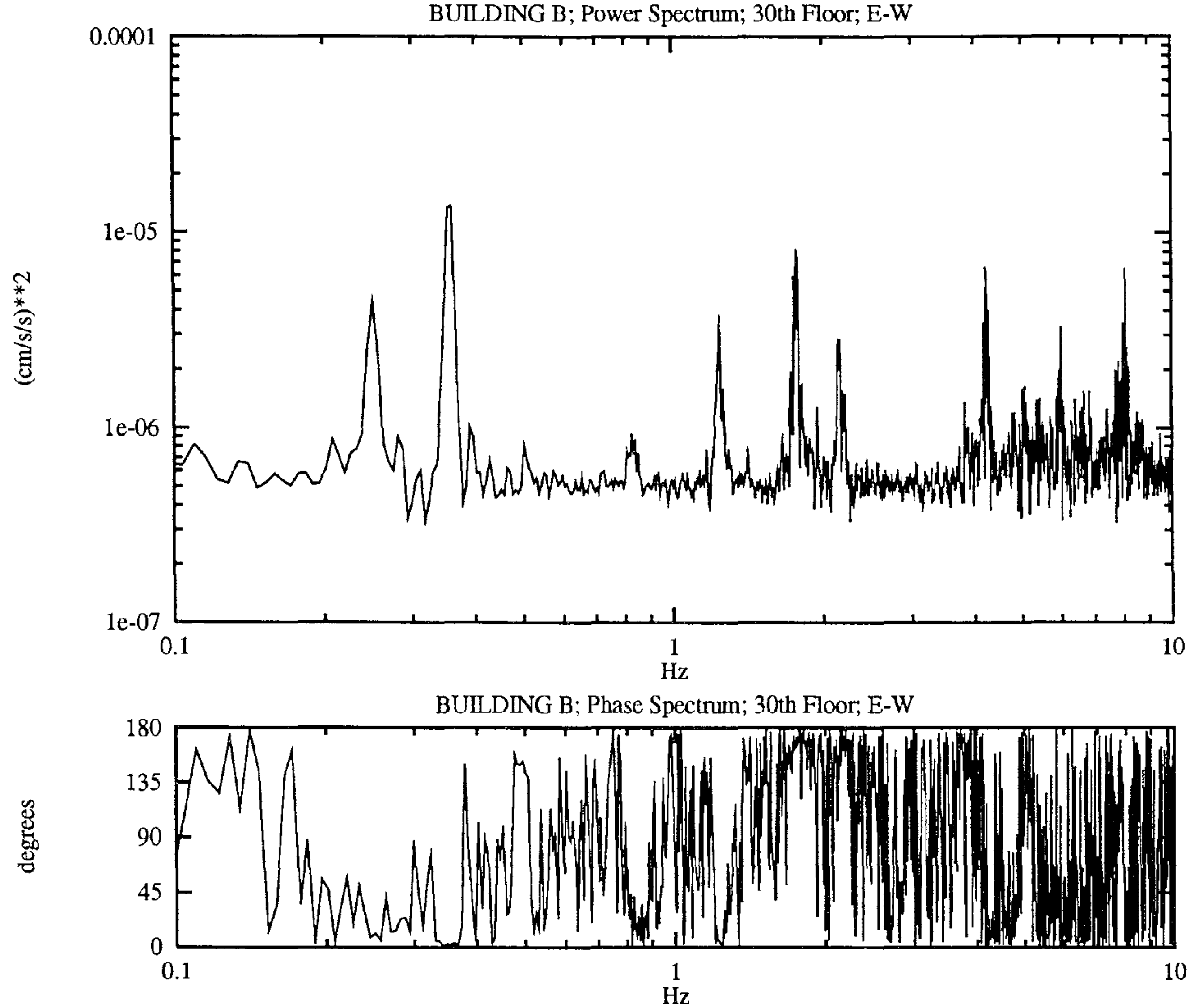

Peaks In G30.10e

Hz-data	Hz-fit	Amp^2-data	Amp^2-fit	Phase	Damping %
0.2502	0.2503	4.4746e-06	4.4745e-06	11	2.4
0.3601	0.3571	1.3679e-05	1.4858e-05	4	1.4
0.8240 T2	0.8244	9.3133e-07	9.3202e-07	42	2.6
1.2390	1.2389	3.7996e-06	3.7923e-06	3	0.5
1.7700	1.7713	8.1924e-06	8.2552e-06	179	0.8
2.1423	2.1443	2.8611e-06	2.9057e-06	176	1.0

RMS-acc	RMS-vel	RMS-dsp
3.998e-02	7.270e-03	5.872e-03

FIGURE B-17

BUILDING B - Power and Phase Spectra of Measured Acceleration

Measurement	Date	February 7, 1991
Measurement	Sensor Location	40th Floor, Center
Reference	Sensor Location	10th Floor, Center
	Sensor Direction	East-West

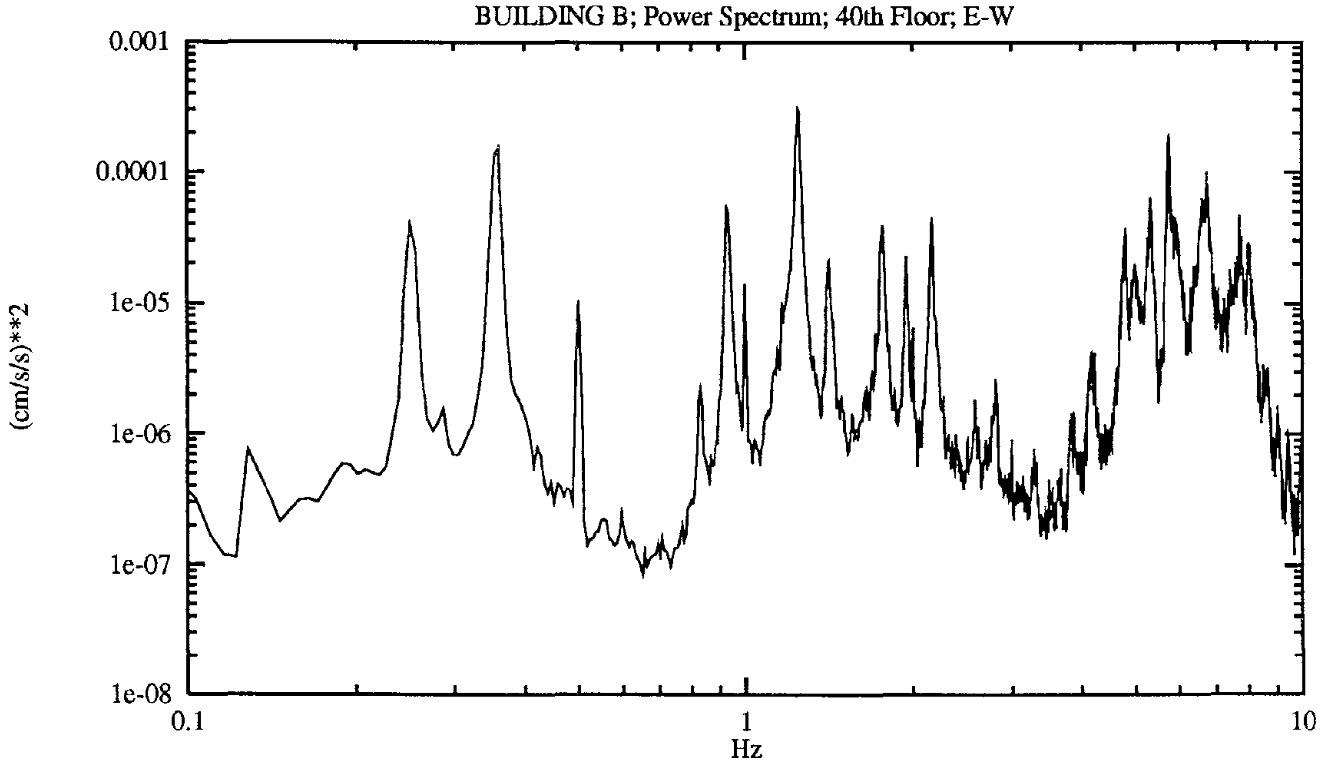

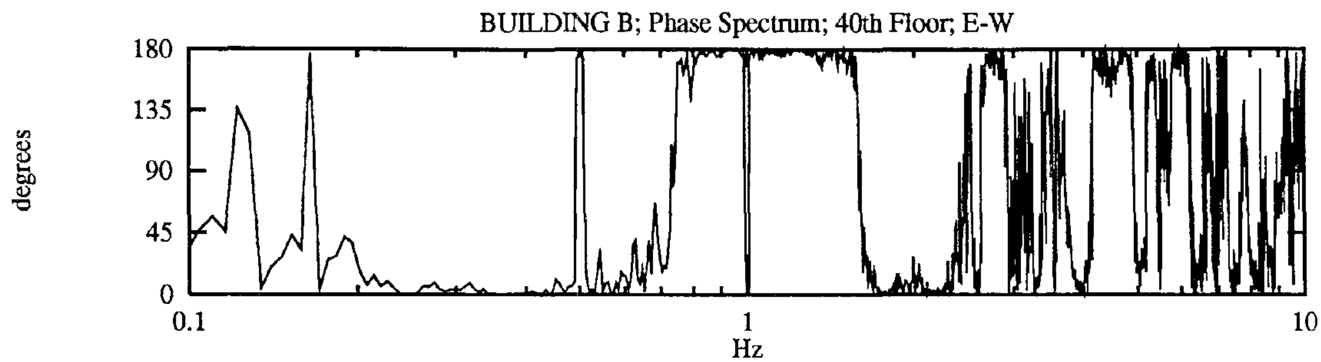

Peaks In G40.10e

Hz-data		Hz-fit	Amp^2-data	Amp^2-fit	Phase	Damping %
0.2502		0.2512	4.0316e-05	4.0822e-05	0	2.4
0.3601		0.3579	1.5520e-04	1.6442e-04	0	1.0
0.5005		0.5002	1.0364e-05	1.0379e-05	176	0.6
0.8301	T2	0.8294	2.2624e-06	2.2687e-06	177	1.0
0.9277	T3	0.9303	5.3396e-05	5.6475e-05	180	1.0
1.0010		1.0004	1.3866e-05	1.3977e-05	2	0.3
1.2451		1.2471	3.0377e-04	3.0994e-04	179	0.7
1.4160	T4	1.4135	2.0855e-05	2.1517e-05	177	0.8
1.7700		1.7689	3.9637e-05	3.9935e-05	2	0.8
1.9531	T5	1.9522	2.2500e-05	2.2650e-05	8	0.6
2.1667		2.1655	4.5414e-05	4.5776e-05	1	0.5

RMS-acc	RMS-vel	RMS-dsp
1.322e-01	1.333e-02	6.581e-03

FIGURE B-18

BUILDING B - Power and Phase Spectra of Measured Acceleration

Measurement	Date	February 7, 1991
Measurement	Sensor Location	36th Floor, East
Reference	Sensor Location	36th Floor, West
	Sensor Direction	North-South

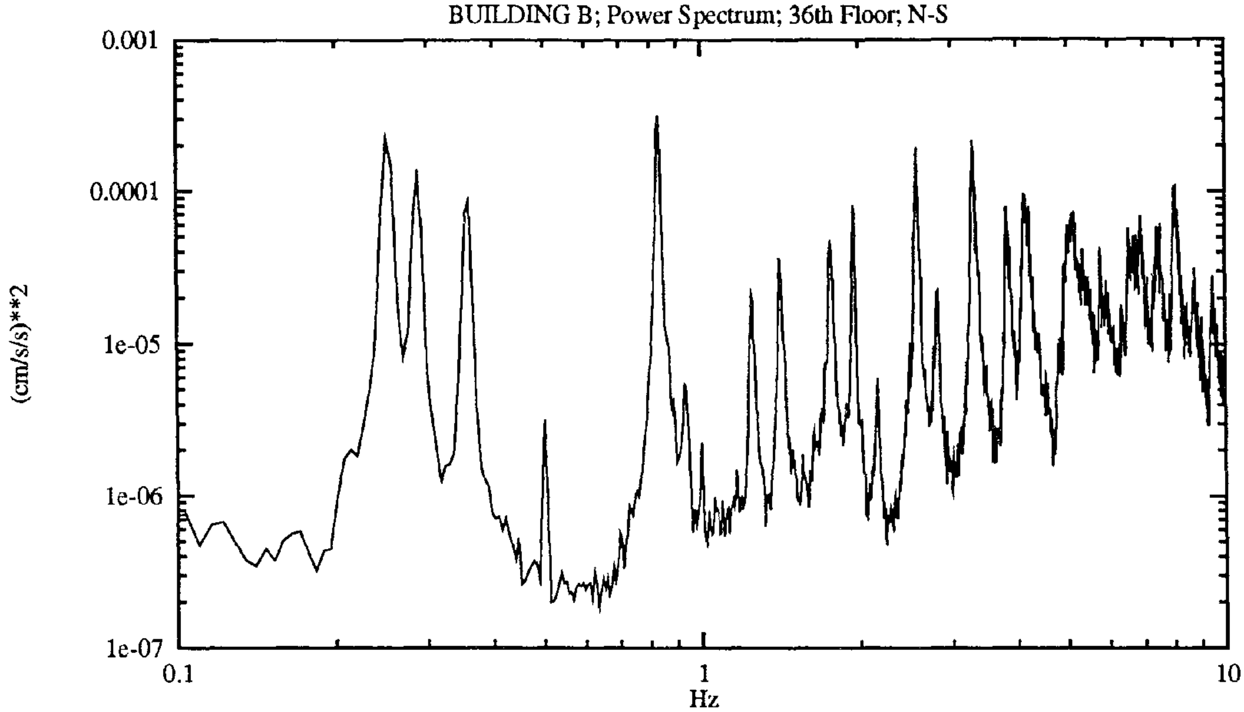

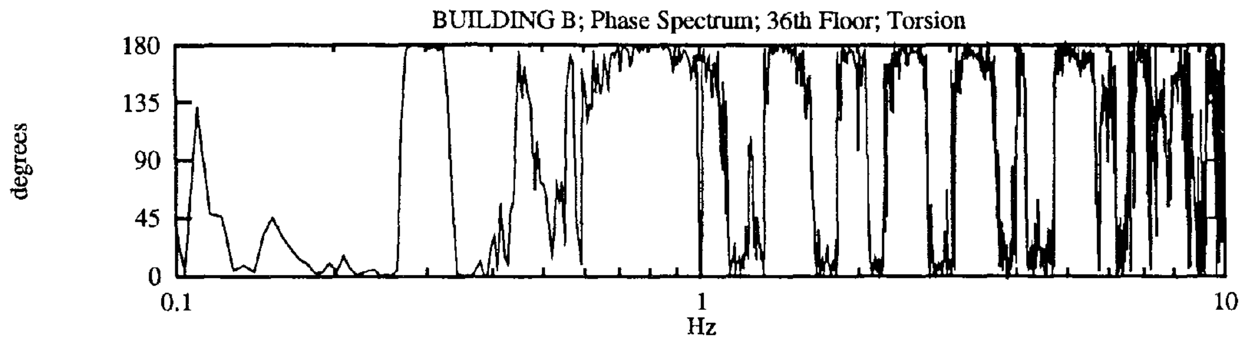

Peaks In G36w.36en

Hz-data		Hz-fit	Amp^2-data	Amp^2-fit	Phase	Damping %
0.2502		0.2512	2.2667e-04	2.2942e-04	2	2.4
0.2869	T1	0.2868	1.3903e-04	1.3904e-04	180	1.6
0.3601		0.3581	8.7529e-05	9.1955e-05	1	1.0
0.5005		0.5002	3.1643e-06	3.1674e-06	71	0.7
0.8301	T2	0.8288	3.1950e-04	3.2389e-04	179	0.9
0.9277	T3	0.9304	5.3538e-06	5.5768e-06	170	1.2
1.0010		1.0000	2.1989e-06	2.2259e-06	8	0.5
1.2451		1.2470	2.1100e-05	2.1651e-05	91	0.8
1.4099	T4	1.4127	3.5441e-05	3.6925e-05	177	0.7
1.7639		1.7650	4.5221e-05	4.5329e-05	5	0.8
1.9531	T5	1.9521	7.9733e-05	8.0347e-05	175	0.5
2.1667		2.1654	5.9476e-06	5.9903e-06	3	0.5
2.5757	T6	2.5757	1.9286e-04	1.9264e-04	175	0.3
2.8259		2.8251	2.2969e-05	2.3007e-05	8	0.5
3.3020	T7	3.3027	2.1444e-04	2.1553e-04	174	0.4
3.8208		3.8222	7.8104e-05	7.8201e-05	1	0.6
4.1382		4.1370	9.6194e-05	9.5367e-05	159	1.2

RMS-acc	RMS-vel	RMS-dsp
1.850e-01	2.066e-02	1.179e-02

FIGURE B-19

BUILDING C - Power and Phase Spectra of Measured Acceleration

Measurement	Date	February 22, 1991
Measurement	Sensor Location	6th Floor, Center
Reference	Sensor Location	28th Floor, Center
	Sensor Direction	North-South

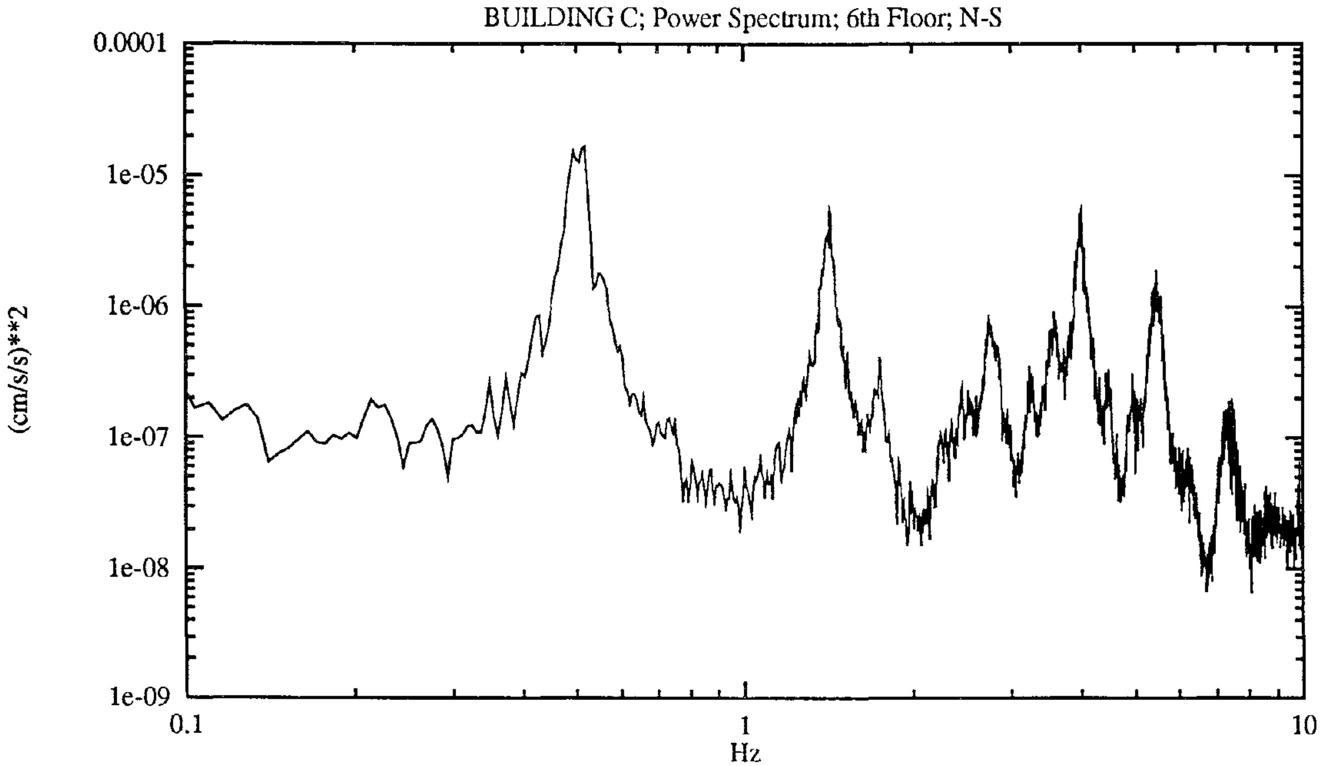

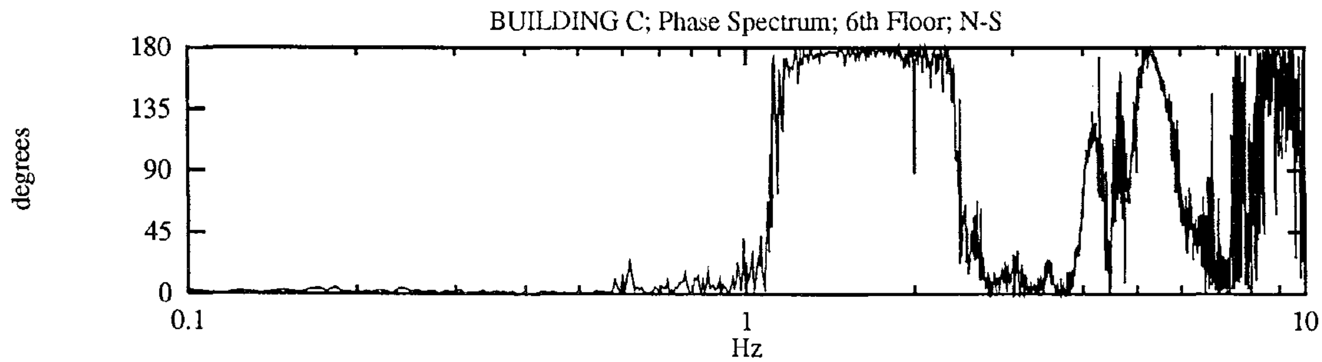

Peaks In G6.28n

Hz-data		Hz-fit	Amp^2-data	Amp^2-fit	Phase	Damping %
0.5188	N1	0.5162	1.6565e-05	1.7408e-05	0	1.4
1.4221	T2	1.4241	5.4219e-06	5.5581e-06	177	0.6
1.5259	N2	1.5257	4.5955e-07	4.5914e-07	178	0.7
2.7344	T4	2.7336	8.6550e-07	8.6427e-07	3	1.8
4.0222	T5	4.0209	5.4778e-06	5.4985e-06	78	0.5
5.4749	N3	5.4720	1.8704e-06	1.9670e-06	162	0.3

RMS-acc	RMS-vel	RMS-dsp
2.288e-02	4.878e-03	3.068e-03

FIGURE B-20

BUILDING C - Power and Phase Spectra of Measured Acceleration

Measurement	Date	February 22, 1991
Measurement	Sensor Location	28th Floor, Center
Reference	Sensor Location	6th Floor, Center
	Sensor Direction	North-South

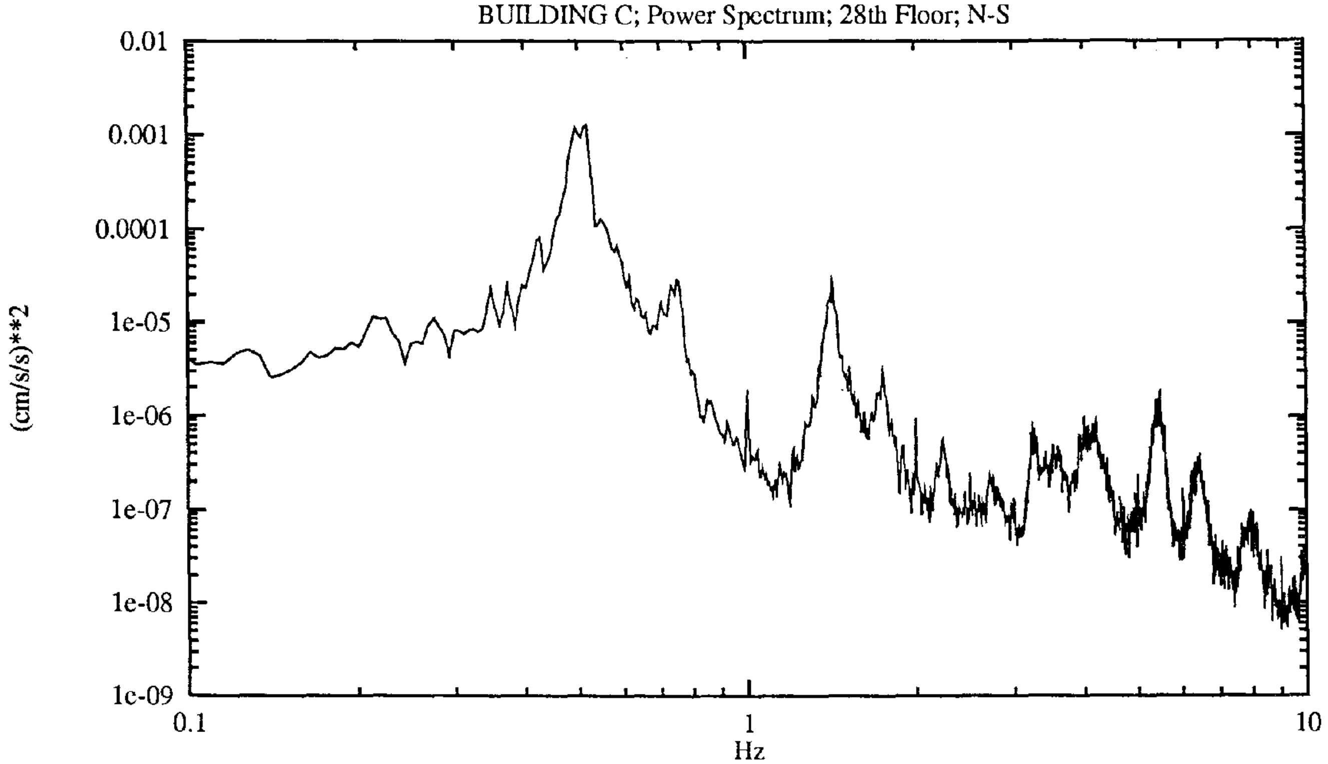

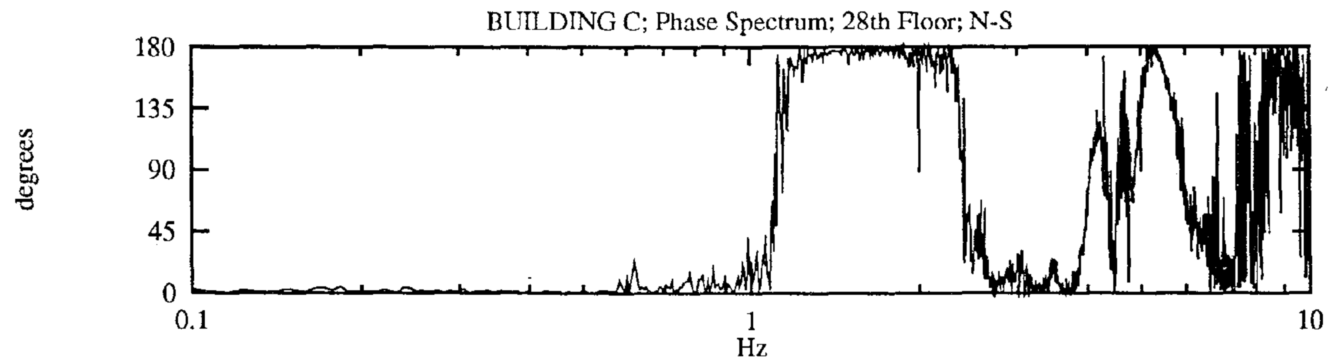

Peaks In G28.6n

Hz-data		Hz-fit	Amp^2-data	Amp^2-fit	Phase	Damping %
0.5188	N1	0.5162	1.2670e-03	1.3330e-03	0	1.4
0.7507	T1	0.7533	2.8378e-05	2.9229e-05	4	1.6
1.4221	T2	1.4241	2.7987e-05	2.8670e-05	177	0.7
1.7456		1.7453	3.0109e-06	3.0138e-06	177	1.1
5.4749	N3	5.4728	1.6624e-06	1.6987e-06	162	0.3

RMS-acc	RMS-vel	RMS-dsp
1.080e-01	3.532e-02	1.527e-02

FIGURE B-21

BUILDING C - Power and Phase Spectra of Measured Acceleration

Measurement	Date	February 22, 1991
Measurement	Sensor Location	6th Floor, Center
Reference	Sensor Location	28th Floor, Center
	Sensor Direction	East-West

BUILDING C; Power Spectrum; 6th Floor; E-W

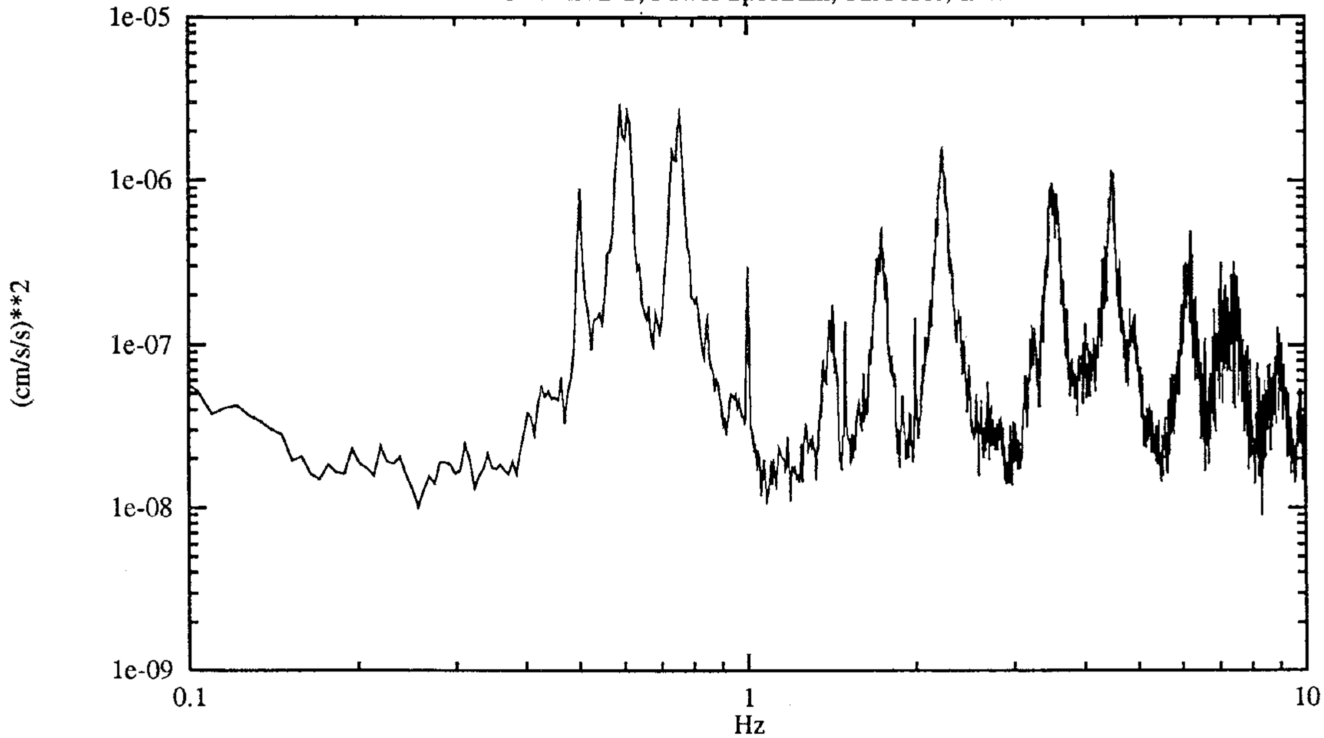

BUILDING C; Phase Spectrum; 6th Floor; E-W

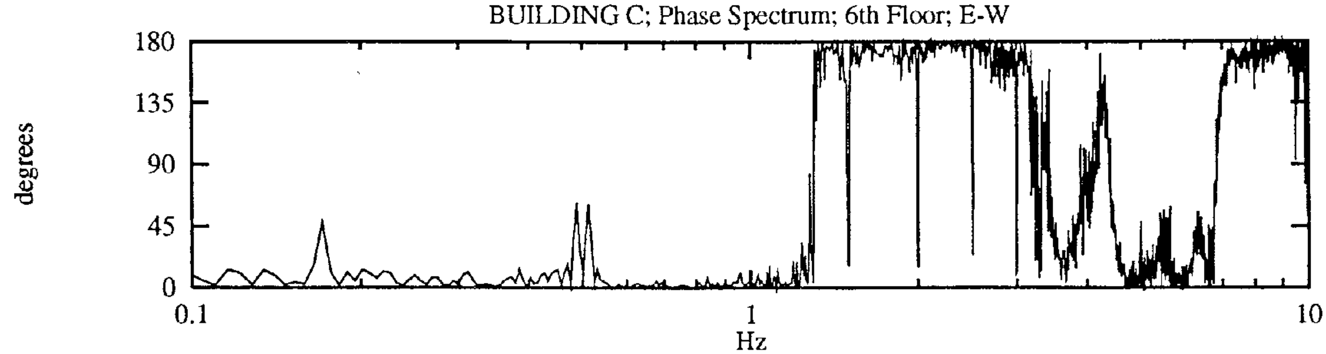

Peaks In G6.28e

Hz-data	Hz-fit	Amp^2-data	Amp^2-fit	Phase	Damping %
0.5005	0.5004	8.9375e-07	8.9360e-07	10	0.9
0.5920	0.5924	2.9490e-06	2.9523e-06	1	3.3
0.7568	0.7559	2.5533e-06	2.5667e-06	2	1.3
0.8118	0.8102	1.9406e-07	1.9581e-07	4	2.1
1.0010	1.0006	2.9809e-07	2.9895e-07	7	0.4
1.4221	1.4238	1.7510e-07	1.7881e-07	171	0.6
1.7456	1.7435	4.9491e-07	5.0385e-07	175	1.1
2.2400	2.2384	1.5507e-06	1.5581e-06	177	1.3
3.5156	3.5162	9.6818e-07	9.6858e-07	38	1.1
3.5828	3.5825	8.3206e-07	8.3447e-07	19	1.0
4.4800	4.4825	1.1470e-06	1.1474e-06	45	0.9

RMS-acc	RMS-vel	RMS-dsp
1.660e-02	2.044e-03	1.168e-03

FIGURE B-22

BUILDING C - Power and Phase Spectra of Measured Acceleration

Measurement	Date	February 22, 1991
Measurement	Sensor Location	28th Floor, Center
Reference	Sensor Location	6th Floor, Center
	Sensor Direction	East-West

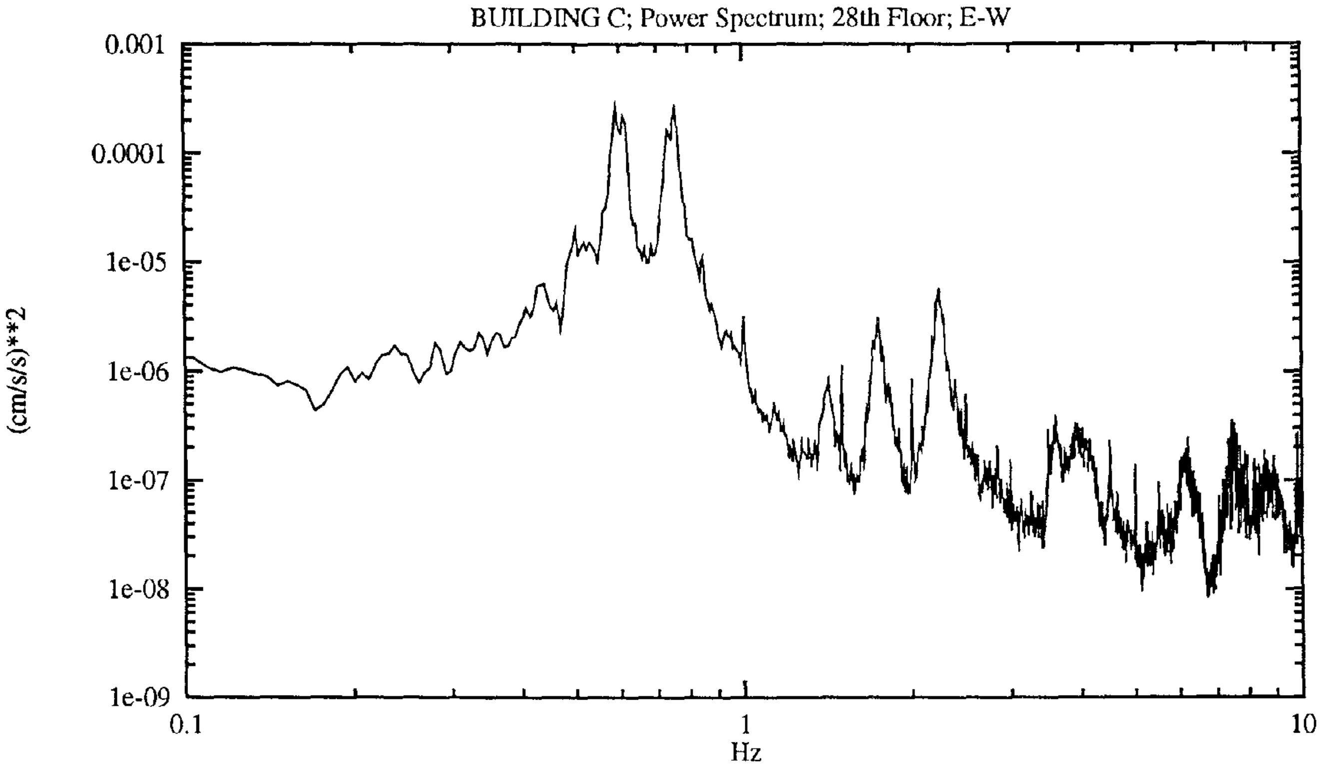

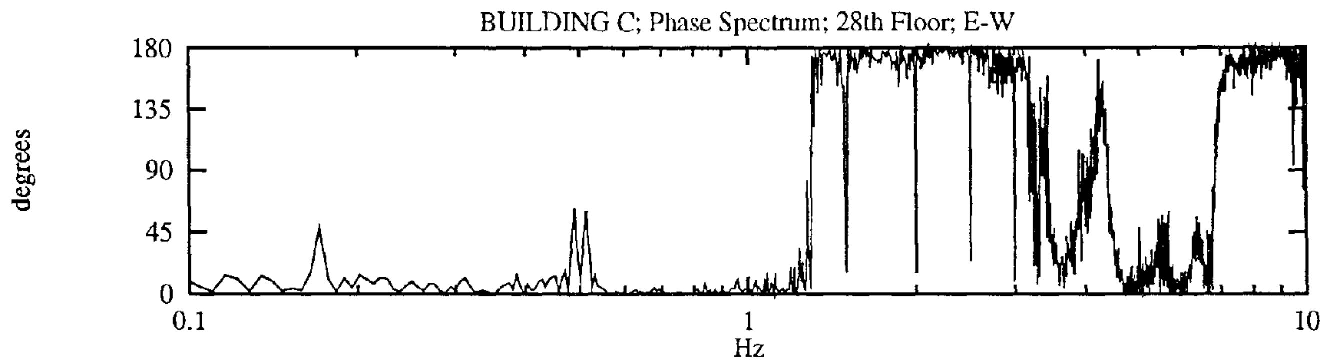

Peaks In G28.6e

Hz-data	Hz-fit	Amp^2-data	Amp^2-fit	Phase	Damping %
0.5920 E1	0.5922	2.6638e-04	2.6637e-04	1	2.2
0.7568 T1	0.7562	2.5561e-04	2.5630e-04	2	1.2
1.0010	1.0012	3.1784e-06	3.1851e-06	7	0.7
1.4221 T2	1.4219	8.8905e-07	8.8848e-07	171	1.3
1.5015 E2	1.5007	1.1213e-06	1.1288e-06	16	0.2
1.7395 E3	1.7423	3.0454e-06	3.1516e-06	172	1.3
2.2400 E4	2.2425	5.6826e-06	5.6941e-06	177	1.3

RMS-acc	RMS-vel	RMS-dsp
6.280e-02	1.582e-02	6.321e-03

FIGURE B-23

BUILDING C - Power and Phase Spectra of Measured Acceleration

Measurement	Date	February 22, 1991
Measurement	Sensor Location	29th Floor, West
Reference	Sensor Location	29th Floor, East
	Sensor Direction	North-South

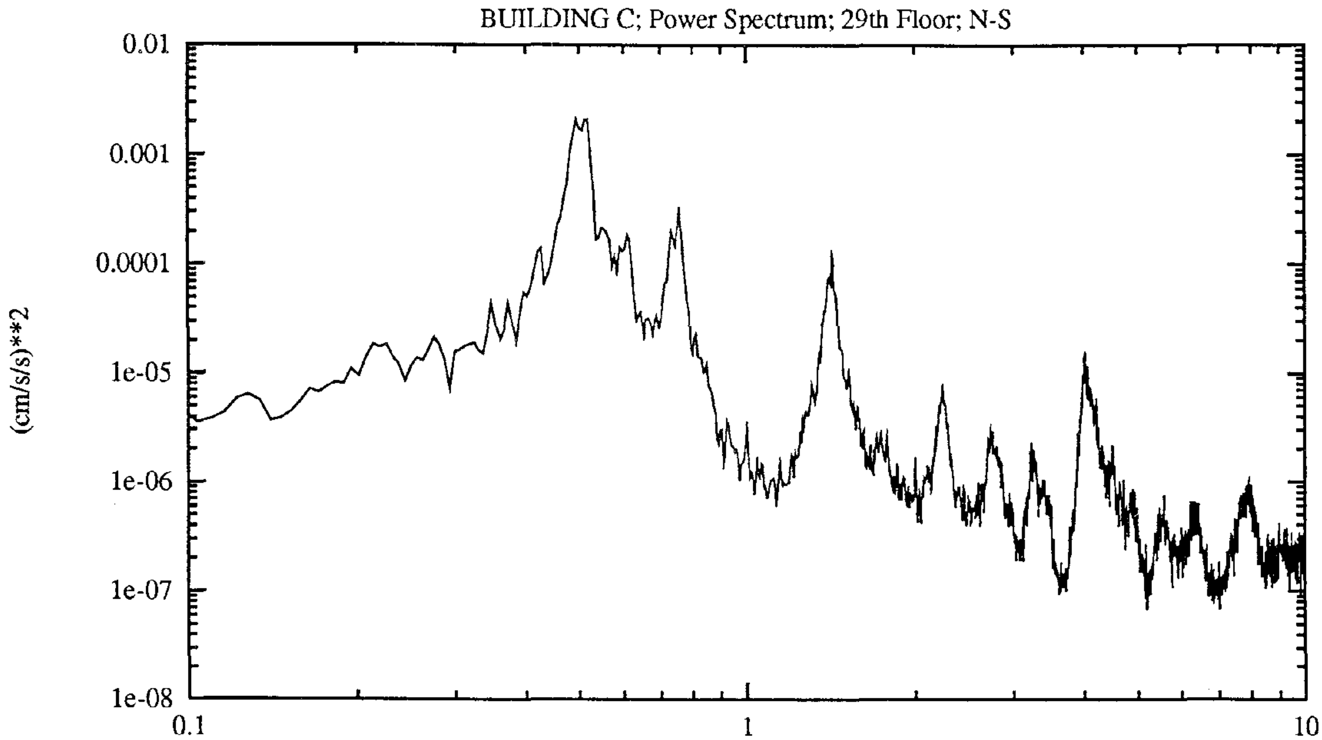

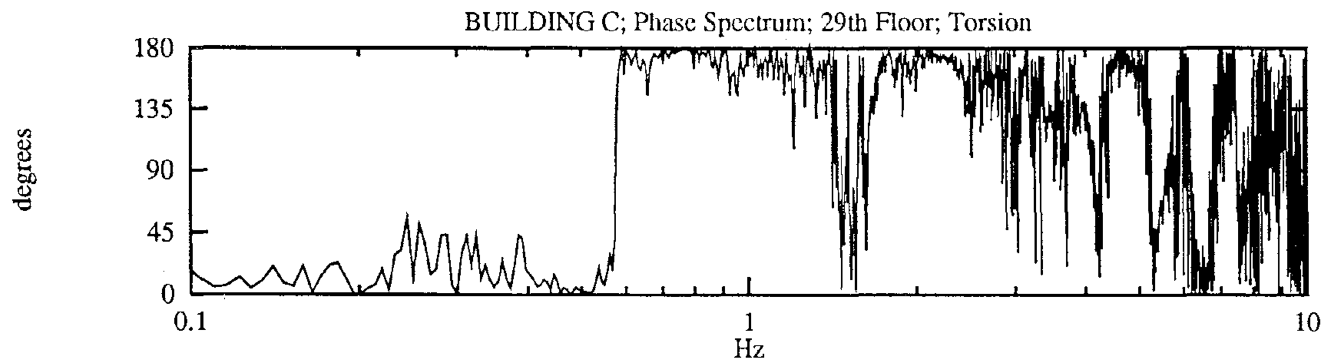

Peaks In G29w.29en

Hz-data		Hz-fit	Amp^2-data	Amp^2-fit	Phase	Damping %
0.5188	N1	0.5158	2.1116e-03	2.2473e-03	2	1.5
0.7568	T1	0.7568	2.9631e-04	2.9635e-04	179	1.3
1.4221	T2	1.4240	1.2100e-04	1.2374e-04	178	0.7
2.2400	T3	2.2375	7.7551e-06	7.8529e-06	175	1.5
2.7344	T4	2.7320	3.2104e-06	3.2857e-06	178	1.3
3.2349		3.2347	2.2786e-06	2.2352e-06	94	0.2
4.0222	T5	4.0211	1.4396e-05	1.4484e-05	139	0.6

RMS-acc	RMS-vel	RMS-dsp
1.549e-01	4.747e-02	1.890e-02

FIGURE B-24

BUILDING D - Power and Phase Spectra of Measured Acceleration

Measurement	Date	February 22, 1991
Measurement	Sensor Location	10th Floor, Center
Reference	Sensor Location	51st Floor, Center
	Sensor Direction	North-South

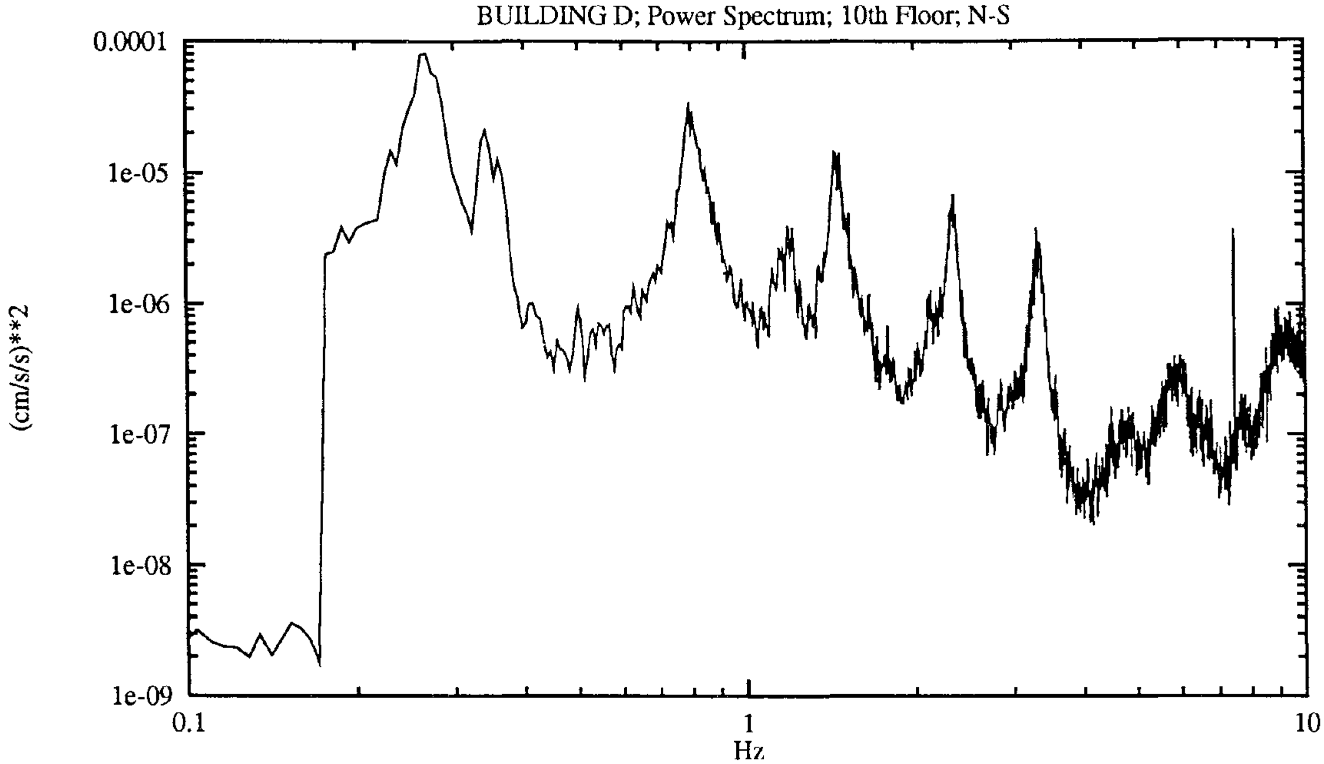

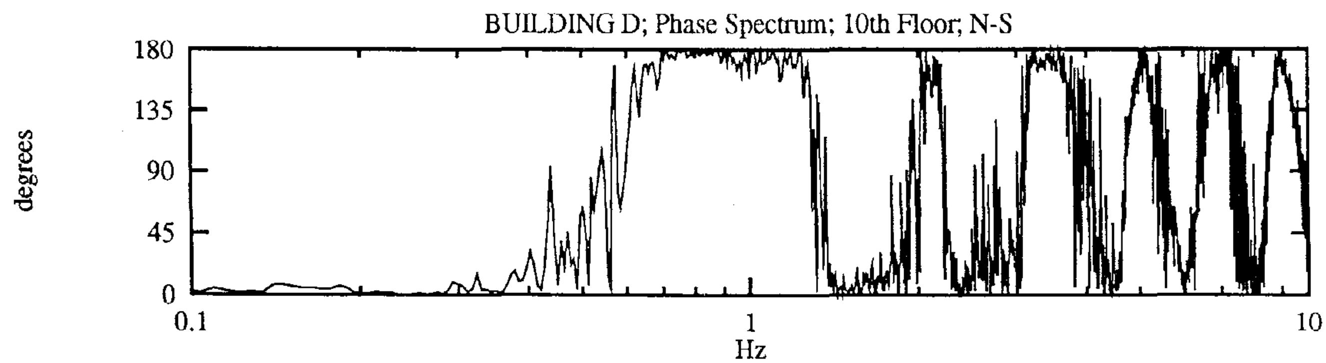

Peaks In G10.51n

Hz-data		Hz-fit	Amp^2-data	Amp^2-fit	Phase	Damping %
0.2686	N1	0.2660	8.1053e-05	8.3365e-05	1	5.7
0.3418	T1	0.3413	2.0928e-05	2.0962e-05	2	2.8
0.7935	N2	0.7926	3.1094e-05	3.1233e-05	176	1.2
1.1902	T2	1.1902	3.8834e-06	3.8855e-06	178	1.2
1.4465	N3	1.4491	1.4324e-05	1.4625e-05	4	1.1
2.3499	T3	2.3482	6.8481e-06	6.9141e-06	6	0.4
3.3142	T4	3.3156	3.7621e-06	3.7849e-06	171	0.3

RMS-acc	RMS-vel	RMS-dsp
4.324e-02	1.525e-02	8.904e-03

FIGURE B-25

BUILDING D - Power and Phase Spectra of Measured Acceleration

Measurement	Date	February 22, 1991
Measurement	Sensor Location	51st Floor, Center
Reference	Sensor Location	10th Floor, Center
	Sensor Direction	North-South

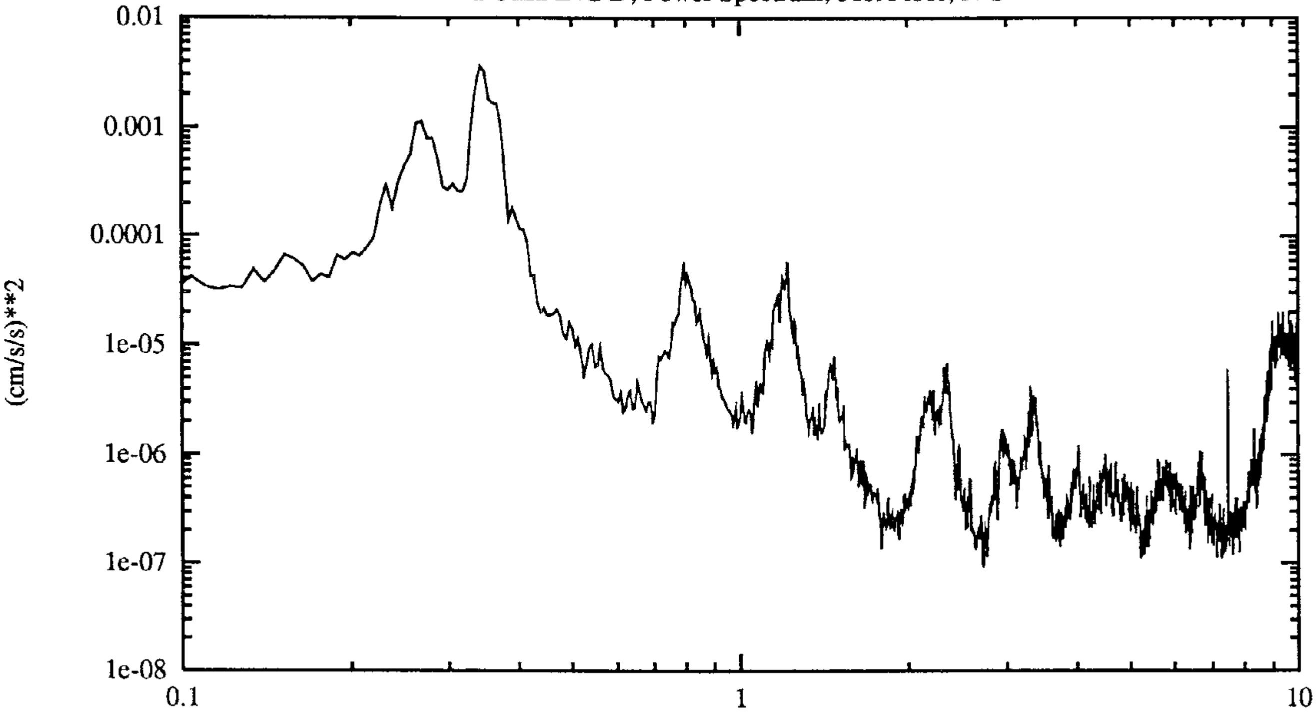

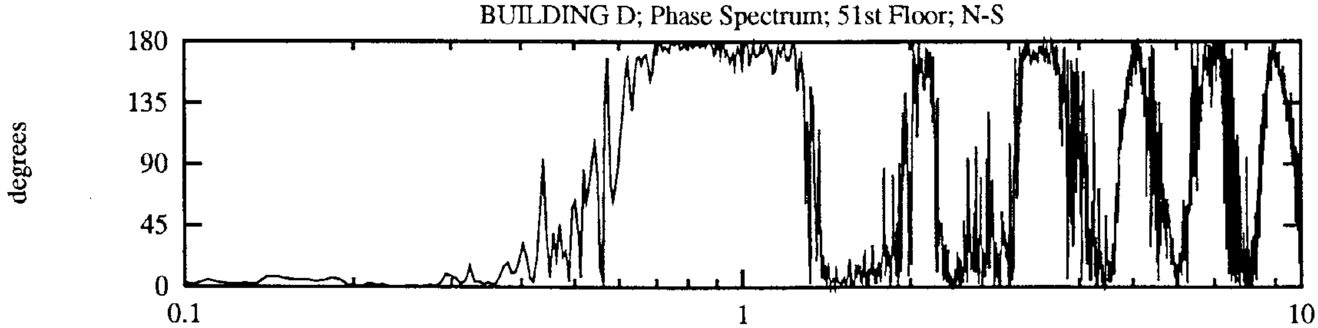

Peaks In G51.10n

Hz-data		Hz-fit	Amp^2-data	Amp^2-fit	Phase	Damping %
0.2686	N1	0.2663	1.1406e-03	1.1693e-03	1	3.8
0.3418	T1	0.3434	3.5929e-03	3.6454e-03	2	2.7
0.7935	N2	0.7929	5.2582e-05	5.2661e-05	176	1.2
1.2146	T3	1.2148	5.7150e-05	5.7101e-05	167	0.7
1.4771	N3	1.4766	7.9147e-06	7.9274e-06	6	0.6
2.1423		2.1427	3.4101e-06	3.4422e-06	169	3.3
2.3499	T3	2.3491	6.8024e-06	6.7651e-06	6	0.6
3.3142	T4	3.3167	3.8288e-06	3.9488e-06	171	0.2

RMS-acc	RMS-vel	RMS-dsp
1.811e-01	8.682e-02	5.197e-02

FIGURE B-26

BUILDING D - Power and Phase Spectra of Measured Acceleration

Measurement	Date	February 22, 1991
Measurement	Sensor Location	10th Floor, Center
Reference	Sensor Location	51st Floor, Center
	Sensor Direction	East-West

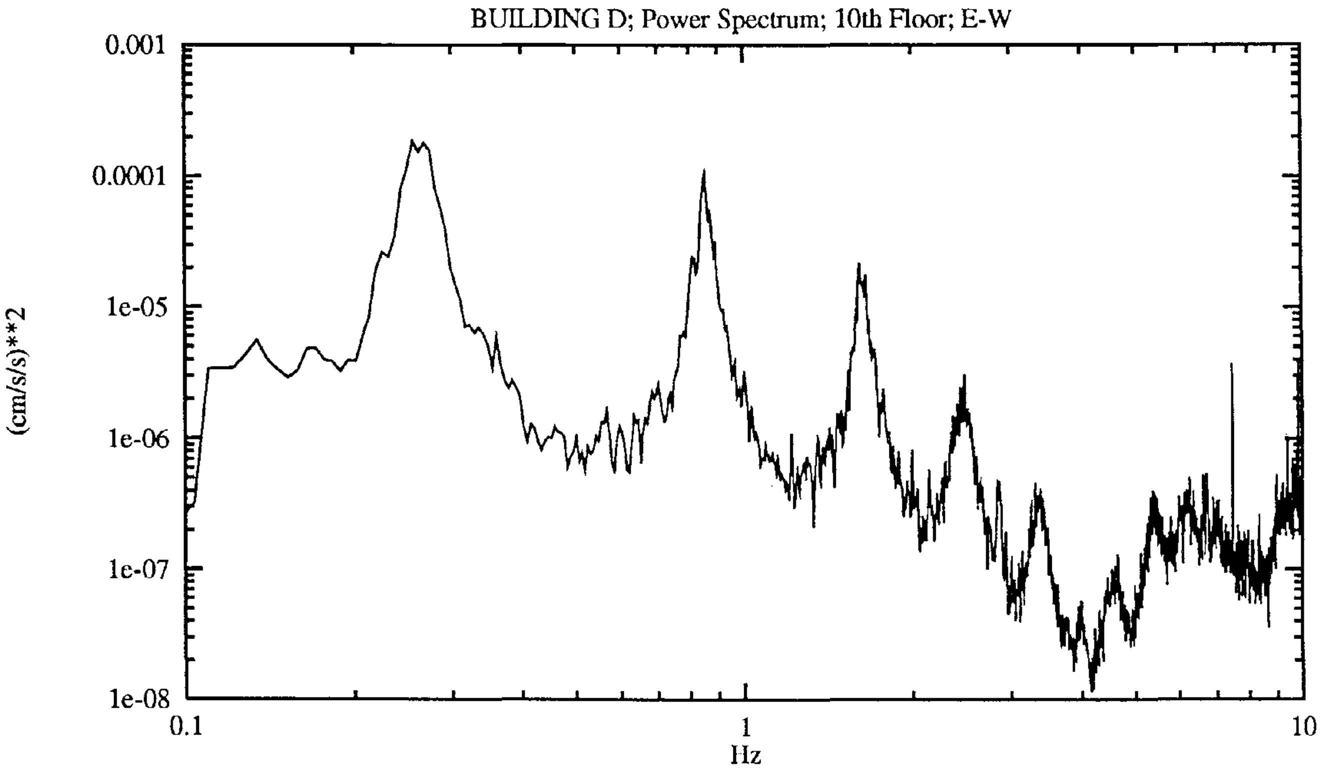

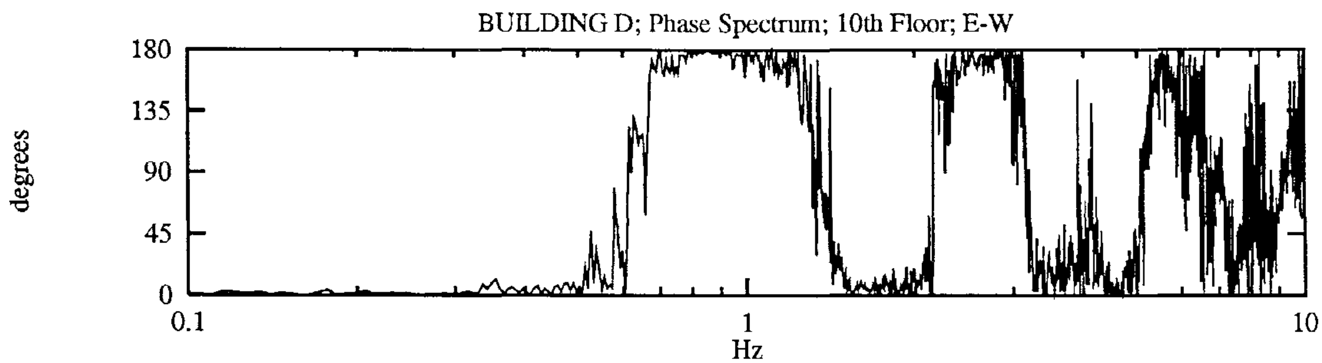

Peaks In G10.51e

Hz-data		Hz-fit	Amp^2-data	Amp^2-fit	Phase	Damping %
0.2563	E1	0.2575	1.8771e-04	1.8965e-04	1	6.0
0.8545	E2	0.8531	1.0513e-04	1.0663e-04	179	1.0
1.6174	E3	1.6161	2.1657e-05	2.1815e-05	6	1.6
2.4902	E4	2.4897	3.0756e-06	3.0994e-06	170	0.3
3.3203	T4	3.3189	4.6188e-07	4.5821e-07	12	0.3

RMS-acc	RMS-vel	RMS-dsp
5.490e-02	2.386e-02	1.531e-02

FIGURE B-27

BUILDING D - Power and Phase Spectra of Measured Acceleration

Measurement	Date	February 22, 1991
Measurement	Sensor Location	51st Floor, Center
Reference	Sensor Location	10th Floor, Center
	Sensor Direction	East-West

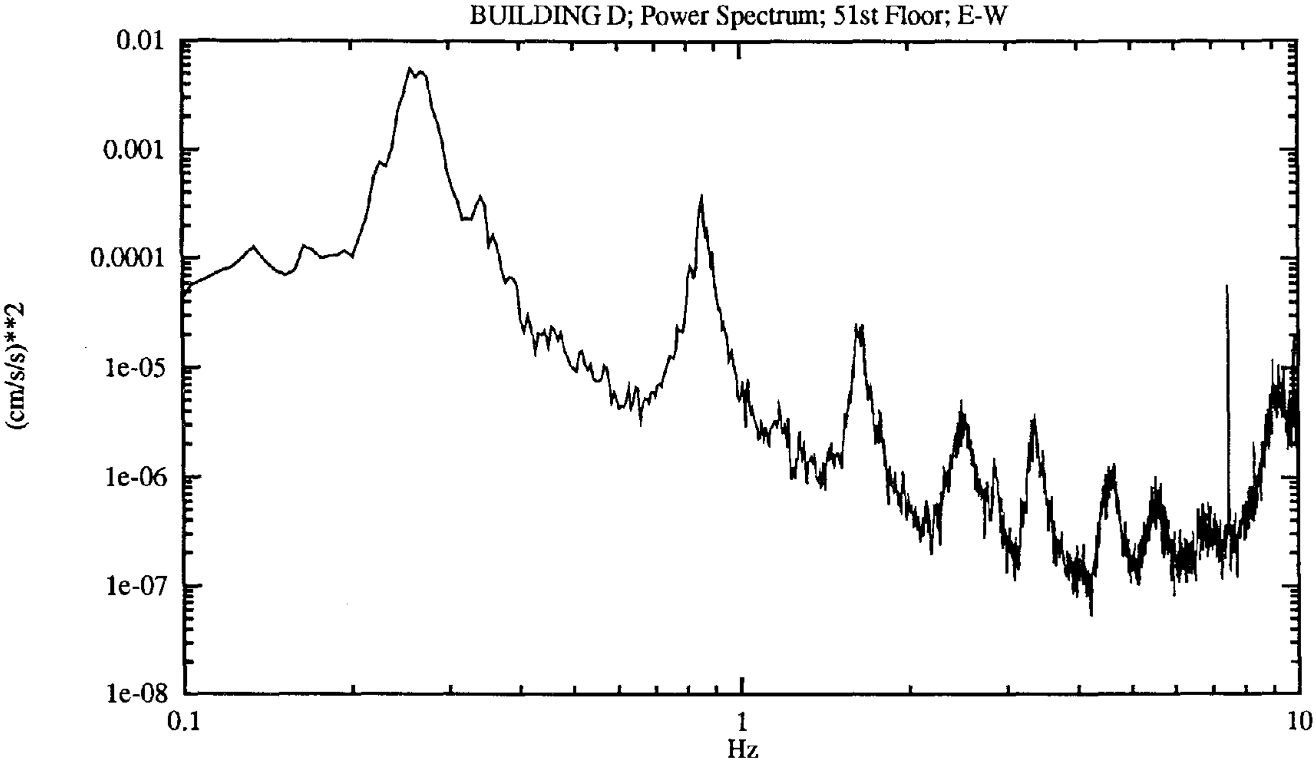

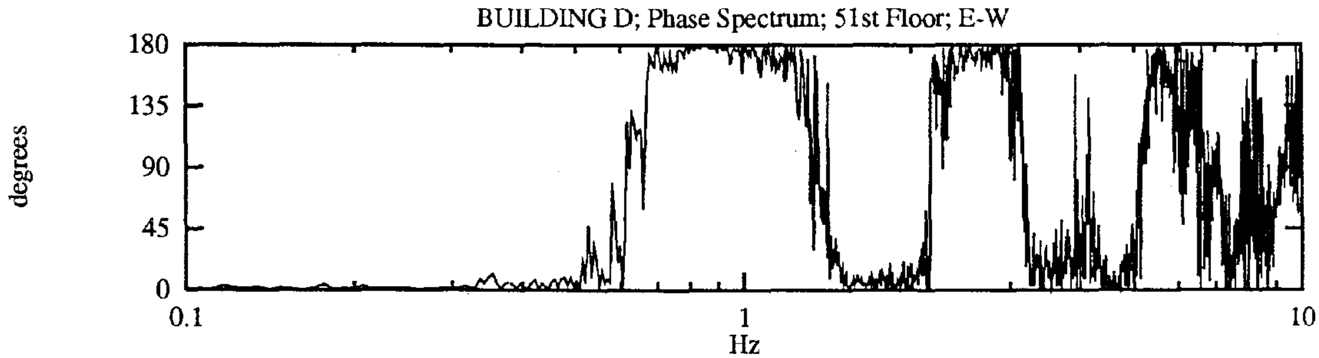

Peaks In G51.10e

Hz-data		Hz-fit	Amp^2-data	Amp^2-fit	Phase	Damping %
0.2563	E1	0.2575	5.6205e-03	5.6789e-03	1	5.9
0.3418	T1	0.3419	3.6986e-04	3.6991e-04	5	2.4
0.8545	E2	0.8531	3.6434e-04	3.6907e-04	179	1.0
1.6174	E3	1.6169	2.5655e-05	2.5660e-05	6	2.4
2.4902	E4	2.4896	5.1716e-06	5.1856e-06	170	0.3
3.3630	T4	3.3633	3.3579e-06	3.3528e-06	24	1.0

RMS-acc	RMS-vel	RMS-dsp
2.166e-01	1.259e-01	8.251e-02

FIGURE B-28

BUILDING D - Power and Phase Spectra of Measured Acceleration

Measurement	Date	February 22, 1991
Measurement	Sensor Location	51st Floor, South
Reference	Sensor Location	51st Floor, North
	Sensor Direction	East-West

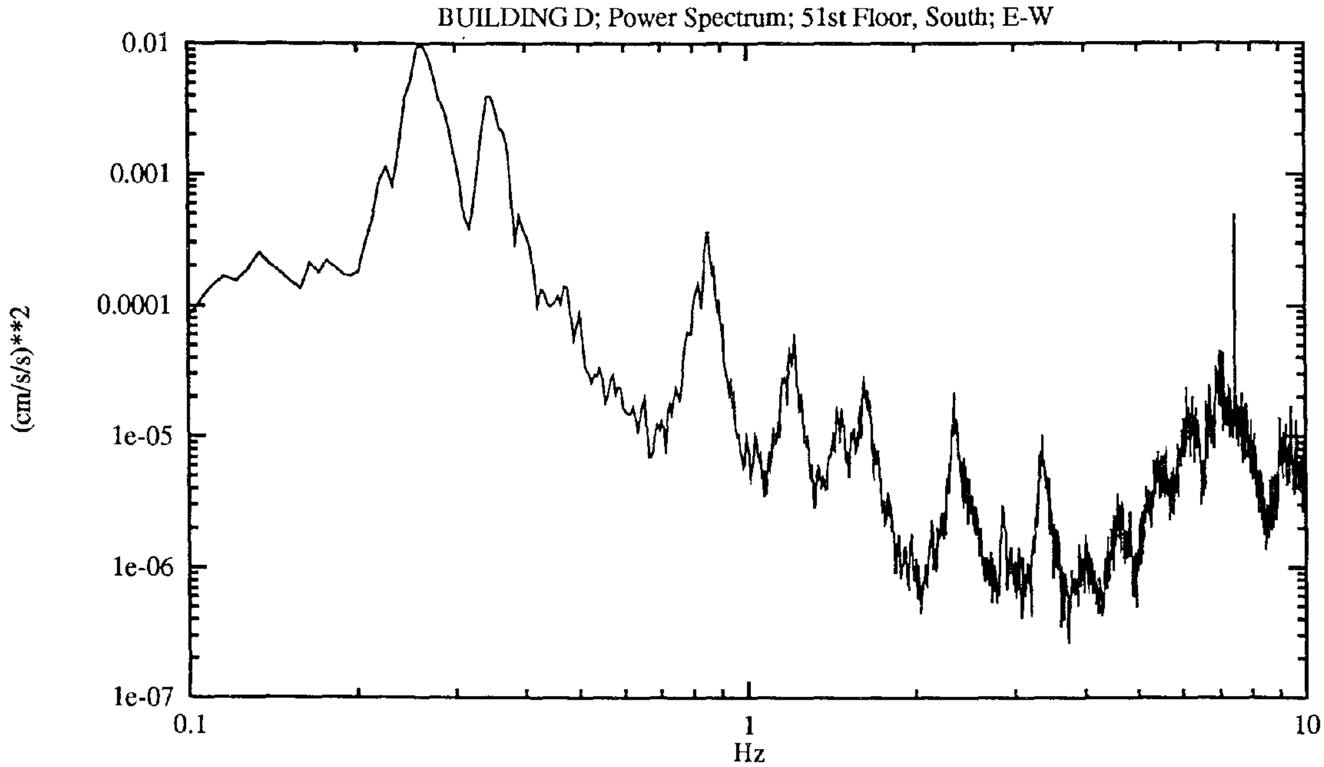

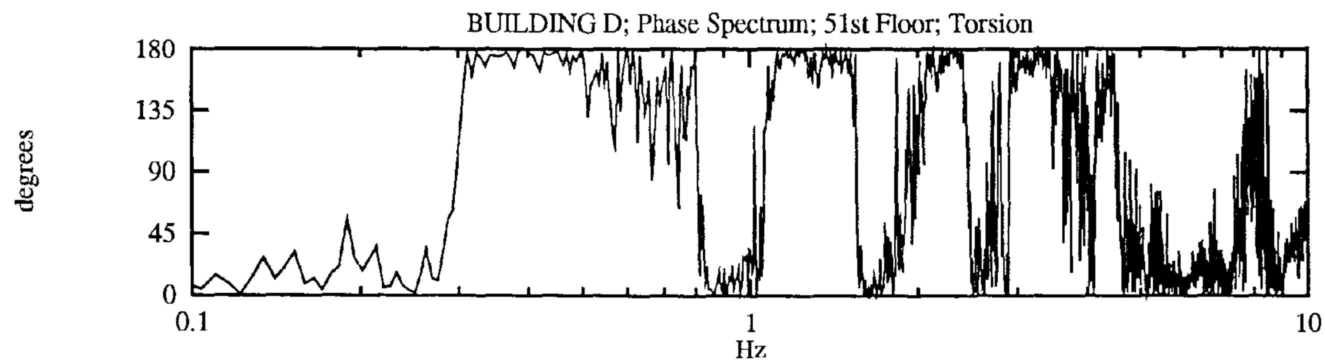

Peaks In G51s.51ne

Hz-data		Hz-fit	Amp^2-data	Amp^2-fit	Phase	Damping %
0.2625	E1	0.2606	9.6744e-03	9.7719e-03	34	5.0
0.3479	T1	0.3450	3.9176e-03	4.0276e-03	175	4.1
0.8545	E2	0.8516	3.6310e-04	3.7861e-04	3	1.3
1.2146	T2	1.2143	6.0564e-05	6.0499e-05	179	0.7
1.6174	E3	1.6160	2.6603e-05	2.6822e-05	1	1.6
2.3499	T3	2.3489	2.1690e-05	2.1636e-05	176	0.4
3.3569	T4	3.3577	1.0105e-05	1.0192e-05	177	0.5

RMS-acc	RMS-vel	RMS-dsp
3.221e-01	1.743e-01	1.117e-01

APPENDIX C

POWER SPECTRA, PHASE SPECTRA, ESTIMATED FREQUENCIES, AND ESTIMATED DAMPING RATIOS: SECOND SET OF MEASUREMENTS

A second set of measurements from Buildings A and B were collected at later dates, when the buildings were at a different stage of construction. Although parameters estimated from these measurements are not presented in Section 6, the spectra are included in Appendix C for completeness and for reference in future reports. The measurement dates are as follows:

Building A:	August 15, 1991
Building B:	August 15, 1991

FIGURE C-1

BUILDING A - Power and Phase Spectra of Measured Acceleration

Measurement	Date	August 15, 1991
Measurement	Sensor Location	52nd Floor, Center
Reference	Sensor Location	52nd Floor, West
	Sensor Direction	North-South

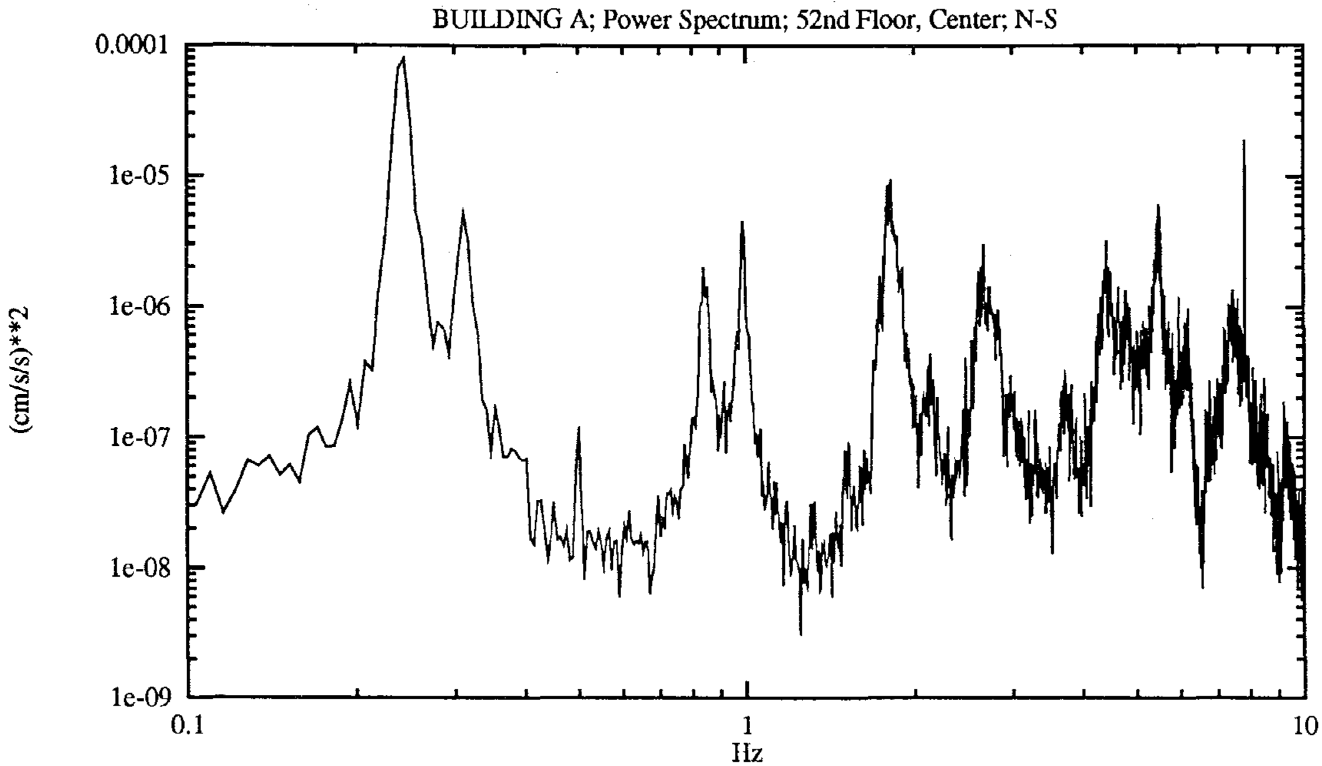

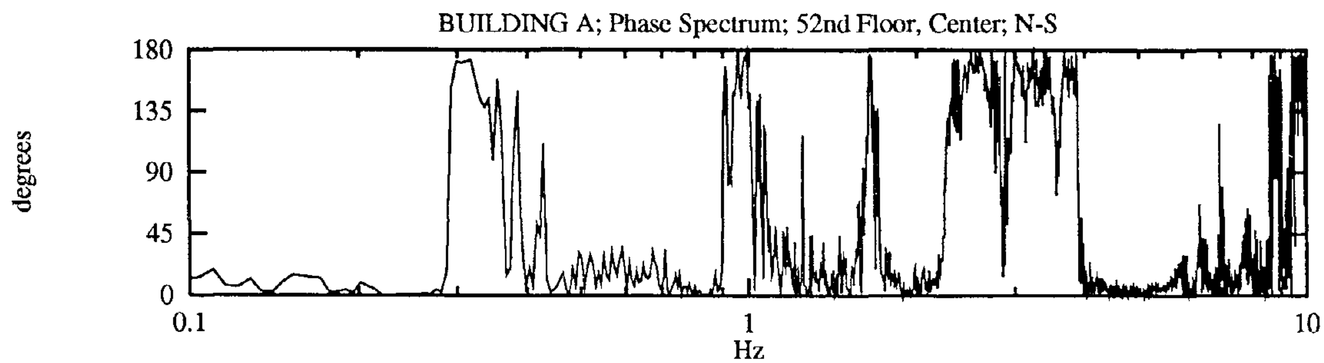

Peaks In G52cwn

Hz-data	Hz-fit	Amp^2-data	Amp^2-fit	Phase	Damping %
0.2441	0.2422	7.9021e-05	8.2292e-05	1	2.1
0.3113 T1	0.3117	5.2324e-06	5.2452e-06	171	2.0
0.5005	0.5000	1.1987e-07	1.2037e-07	27	0.7
0.8423	0.8426	2.0020e-06	2.0061e-06	0	0.9
0.9888	0.9894	4.5475e-06	4.5672e-06	174	0.7
1.8188	1.8185	9.4055e-06	9.3579e-06	10	0.4
2.1362	2.1379	4.4307e-07	4.5169e-07	13	0.4
2.6672 T5	2.6673	3.0255e-06	3.0100e-06	163	0.3

RMS-acc	RMS-vel	RMS-dsp
3.100e-02	9.962e-03	6.538e-03

FIGURE C-2

BUILDING A - Power and Phase Spectra of Measured Acceleration

Measurement	Date	August 15, 1991
Measurement	Sensor Location	52nd Floor, Center
Reference	Sensor Location	52nd Floor, West
	Sensor Direction	East-West

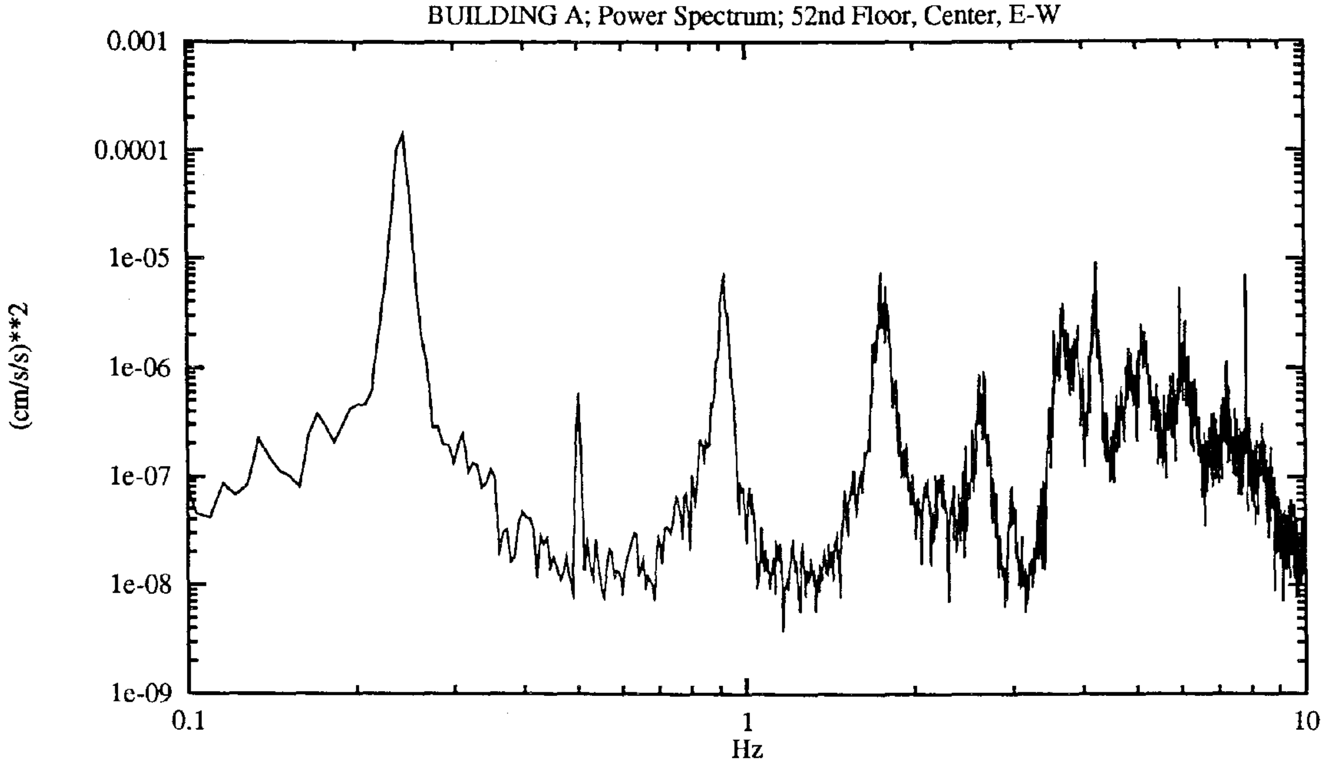

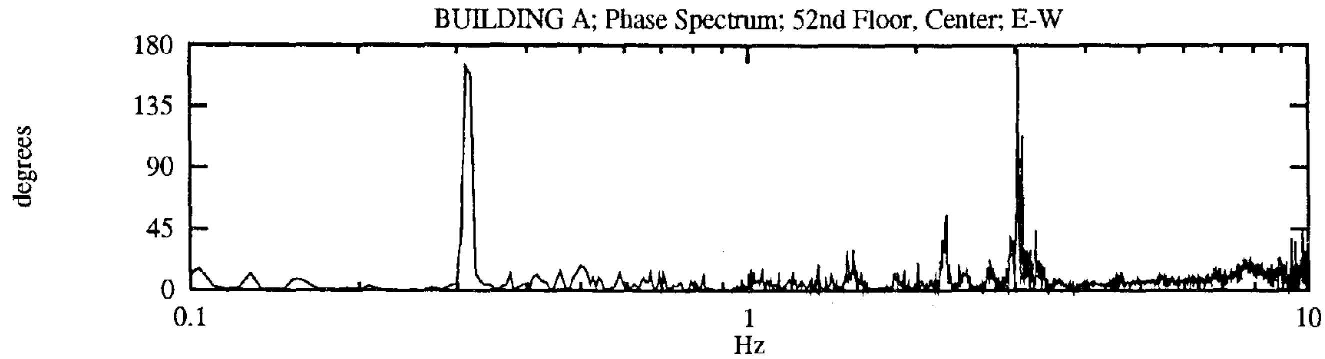

Peaks In G52cwe

Hz-data		Hz-fit	Amp^2-data	Amp^2-fit	Phase	Damping %
0.2441		0.2428	1.4131e-04	1.4474e-04	0	1.8
0.3113	T1	0.3100	2.5262e-07	2.5719e-07	165	1.9
0.5005		0.5002	5.9385e-07	5.9488e-07	18	0.6
0.9155		0.9136	6.8832e-06	7.0892e-06	1	0.9
1.7456		1.7429	7.0937e-06	7.5996e-06	2	0.3
2.6672	T5	2.6687	9.2164e-07	9.4622e-07	15	0.4
2.9846	T6	2.9818	7.7498e-08	8.1956e-08	1	0.3

RMS-acc	RMS-vel	RMS-dsp
3.325e-02	1.225e-02	8.179e-03

FIGURE C-3

BUILDING A - Power and Phase Spectra of Measured Acceleration

Measurement	Date	August 15, 1991
Measurement	Sensor Location	52nd Floor, East
Reference	Sensor Location	52nd Floor, West
	Sensor Direction	North-South

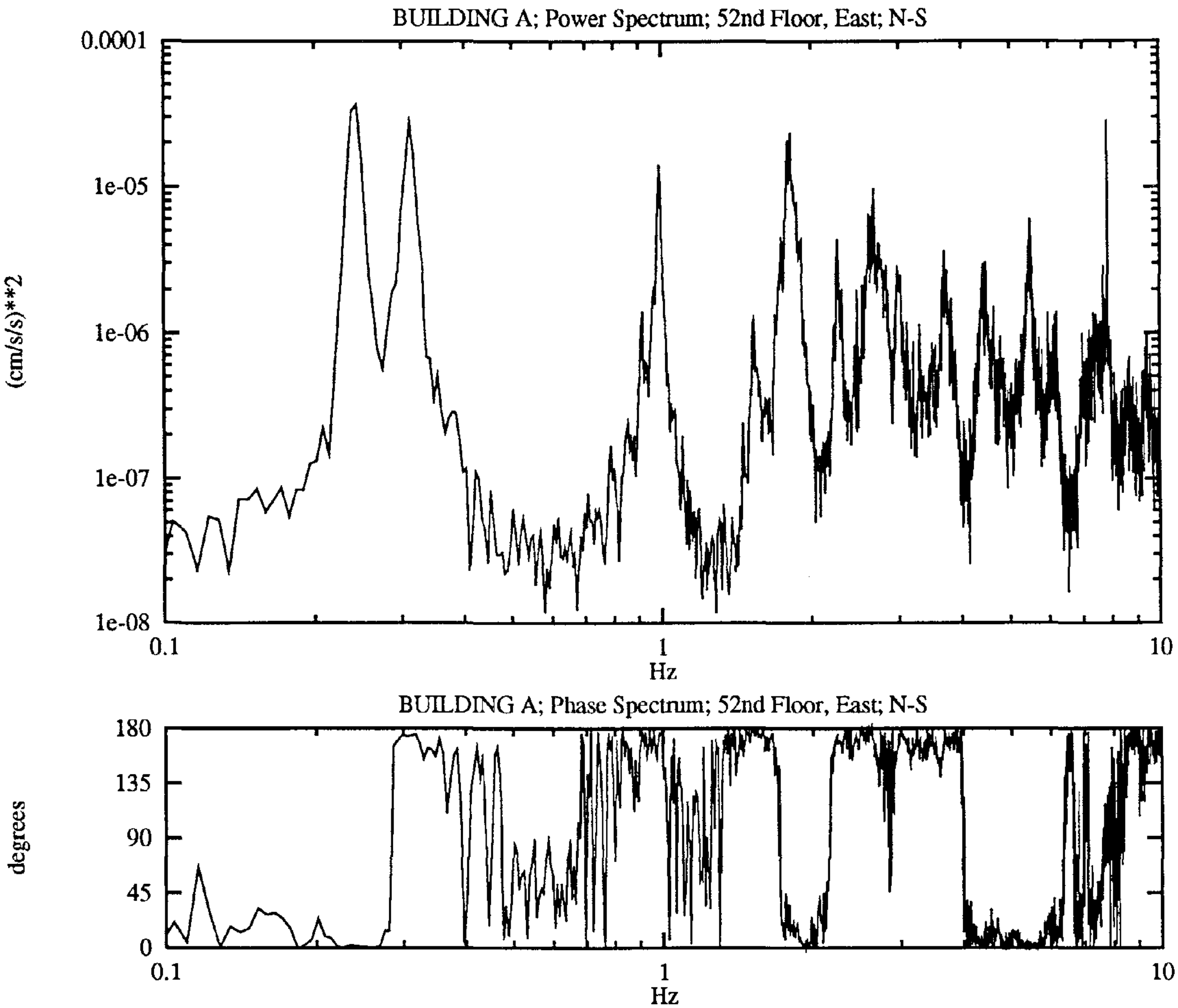

Peaks In G52ewn

Hz-data		Hz-fit	Amp^2-data	Amp^2-fit	Phase	Damping %
0.2441		0.2419	3.6481e-05	3.8264e-05	1	2.3
0.3113	T1	0.3116	2.7772e-05	2.7809e-05	174	2.0
0.9888	T2	0.9894	1.4237e-05	1.4290e-05	175	0.6
1.5320	T3	1.5304	1.2274e-06	1.2377e-06	174	0.8
1.8188		1.8184	2.3365e-05	2.3365e-05	13	0.4
2.2522	T4	2.2520	4.4082e-06	4.4256e-06	170	0.4
2.6672	T5	2.6672	9.7687e-06	9.7156e-06	168	0.3
2.9785	T6	2.9808	2.6913e-06	2.7344e-06	172	1.2

RMS-acc	RMS-vel	RMS-dsp
4.330e-02	8.567e-03	5.207e-03

FIGURE C-4

BUILDING B - Power and Phase Spectra of Measured Acceleration

Measurement	Date	August 15, 1991
Measurement	Sensor Location	10th Floor, Center
Reference	Sensor Location	40th Floor, Center
	Sensor Direction	North-South

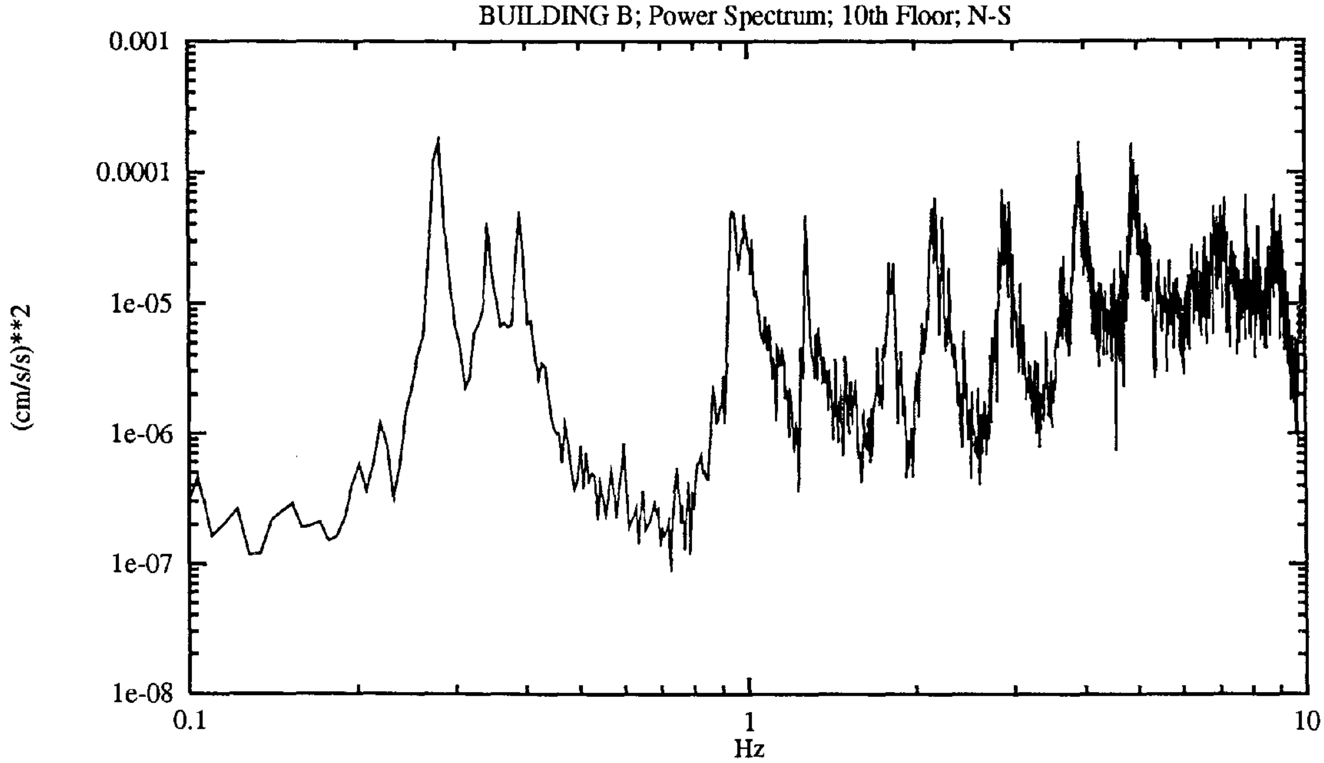

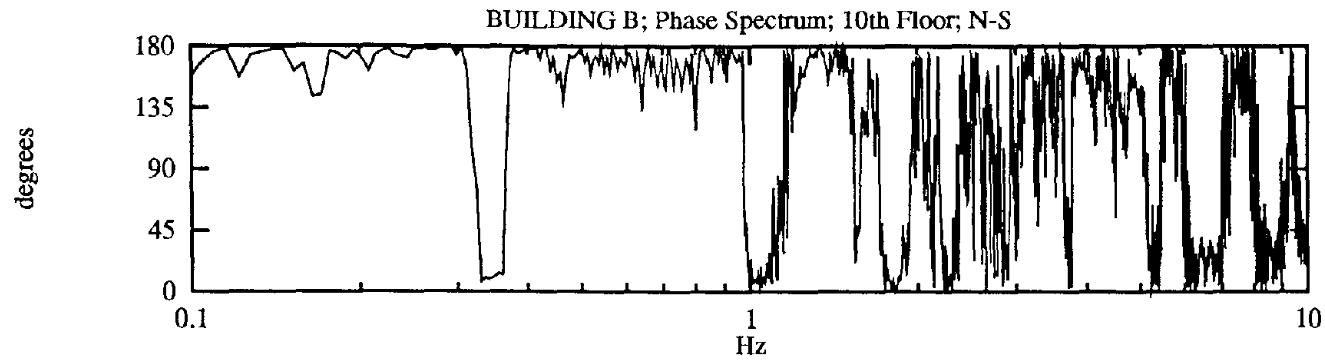

Peaks In G1040n

Hz-data		Hz-fit	Amp^2-data	Amp^2-fit	Phase	Damping %
0.2808		0.2794	1.7395e-04	1.7871e-04	180	1.3
0.3418		0.3423	4.1376e-05	4.1530e-05	9	1.3
0.3906		0.3906	4.9758e-05	4.9755e-05	176	1.3
0.9399		0.9423	5.0123e-05	5.0642e-05	172	1.5
0.9888	T1	0.9894	4.7610e-05	4.7743e-05	18	1.3
1.2756		1.2762	4.6701e-05	4.6790e-05	172	0.6
1.7944		1.7944	2.0362e-05	2.0325e-05	2	0.4
2.1729		2.1728	6.3866e-05	6.3419e-05	169	0.4
2.8687	T4	2.8687	7.4298e-05	7.5340e-05	17	0.3
3.9307		3.9306	1.7064e-04	1.7548e-04	162	0.1
4.8828		4.8800	1.5445e-04	1.5831e-04	156	0.2

RMS-acc	RMS-vel	RMS-dsp
2.180e-01	1.549e-02	7.966e-03

FIGURE C-5

BUILDING B - Power and Phase Spectra of Measured Acceleration

Measurement	Date	August 15, 1991
Measurement	Sensor Location	36th Floor, East
Reference	Sensor Location	10th Floor, Center
	Sensor Direction	North-South

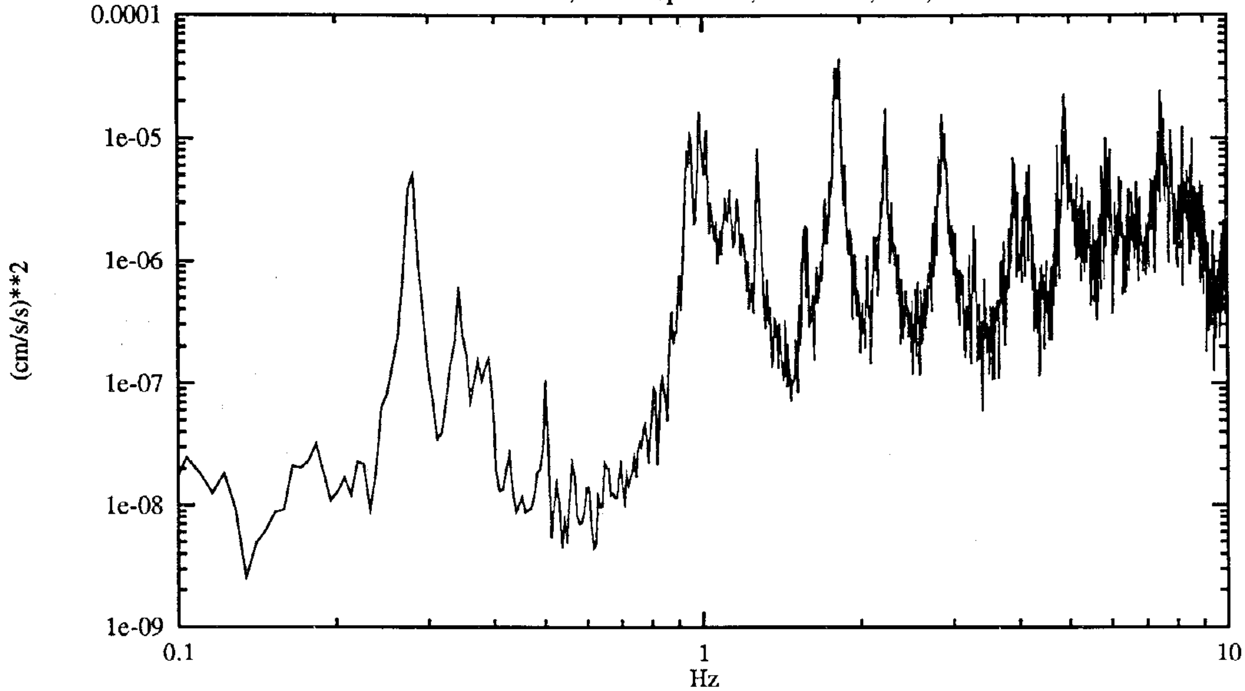

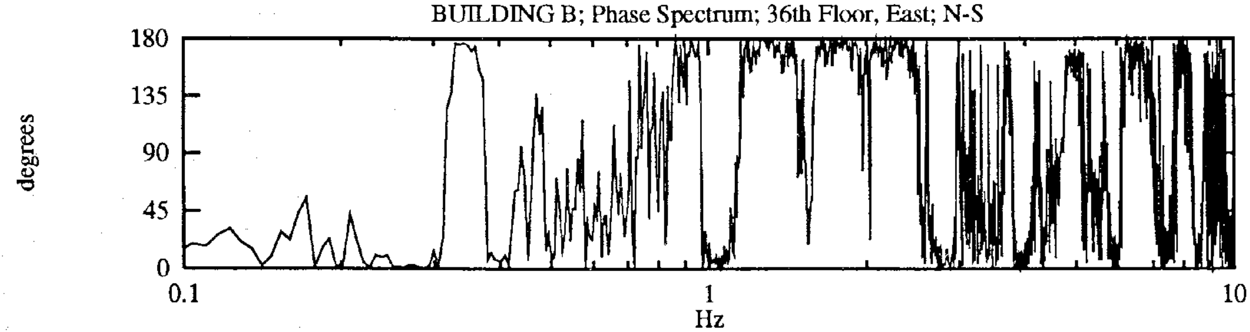

Peaks In G36e10n

Hz-data		Hz-fit	Amp^2-data	Amp^2-fit	Phase	Damping %
0.2808		0.2791	5.1004e-06	5.2908e-06	1	1.2
0.3418		0.3419	6.1939e-07	6.1956e-07	176	1.3
0.3906		0.3890	1.6010e-07	1.6406e-07	7	1.7
0.5005		0.5005	1.0596e-07	1.0600e-07	7	0.7
0.9460		0.9483	1.0672e-05	1.1001e-05	166	0.8
0.9888	T1	0.9883	1.6407e-05	1.6436e-05	12	0.7
1.0193	T2	1.0174	1.1486e-05	1.1936e-05	7	0.5
1.1047		1.1049	3.3119e-06	3.3081e-06	39	0.7
1.1292		1.1287	3.8387e-06	3.8445e-06	40	0.7
1.1658	T3	1.1657	3.0323e-06	3.0333e-06	134	0.9
1.2756		1.2758	8.1588e-06	8.1360e-06	179	0.5
1.5747		1.5731	1.8998e-06	1.9595e-06	53	0.3
1.8311	T4	1.8286	4.4506e-05	4.7088e-05	180	0.3
2.2400		2.2385	1.7490e-05	1.8001e-05	160	0.2
2.8687		2.8687	1.5584e-05	1.5557e-05	3	0.4
3.9001		3.9018	6.9523e-06	7.0333e-06	4	0.2
4.1870	T5	4.1879	5.9891e-06	5.8413e-06	72	0.3
4.8828		4.8800	2.1977e-05	2.2888e-05	170	0.2

FIGURE C-6

BUILDING B - Power and Phase Spectra of Measured Acceleration

Measurement	Date	August 15, 1991
Measurement	Sensor Location	40th Floor, Center
Reference	Sensor Location	10th Floor, Center
	Sensor Direction	North-South

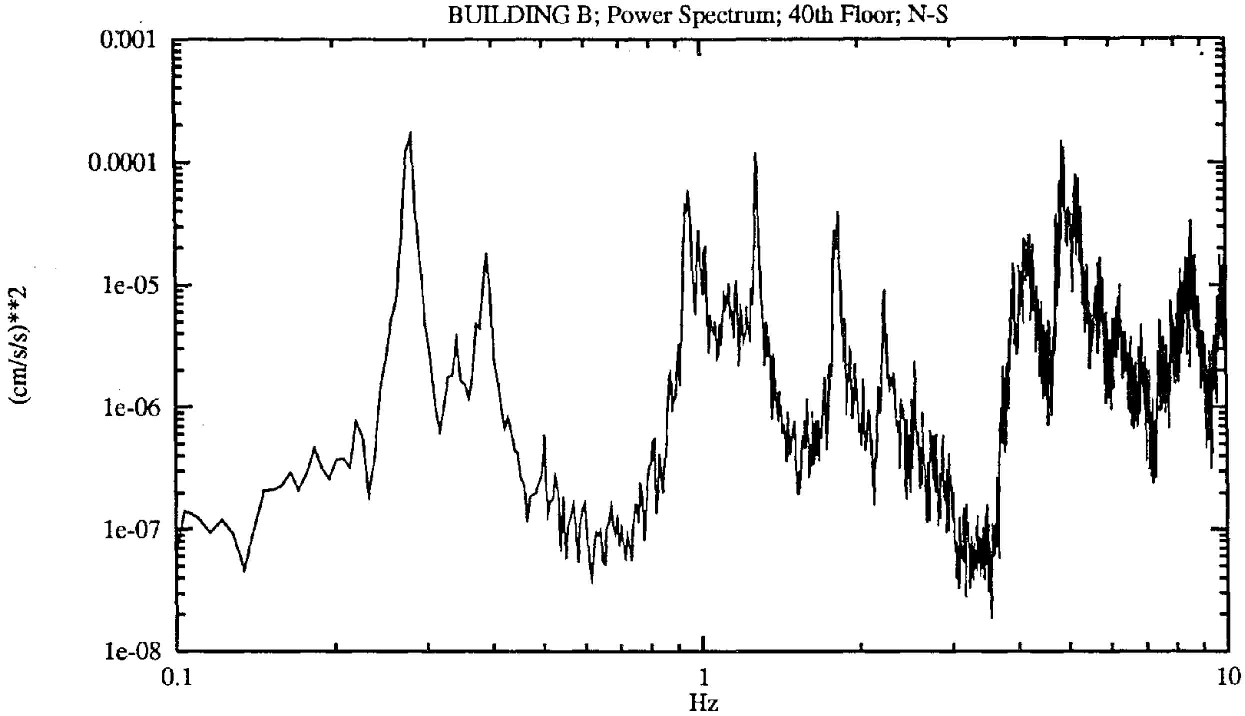

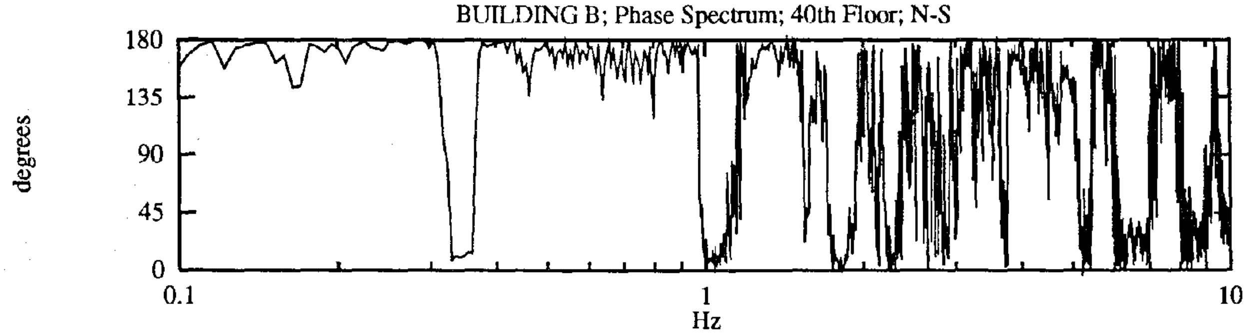

Peaks In G4010n

Hz-data		Hz-fit	Amp^2-data	Amp^2-fit	Phase	Damping %
0.2808		0.2792	1.6510e-04	1.7114e-04	180	1.2
0.3418		0.3417	3.6197e-06	3.6210e-06	9	1.6
0.3906		0.3903	1.8138e-05	1.8161e-05	176	1.4
0.5005		0.4999	5.9891e-07	6.0233e-07	179	0.7
0.9460		0.9472	5.4627e-05	5.4985e-05	168	0.9
0.9888	T1	0.9878	2.7728e-05	2.7955e-05	18	0.7
1.0193	T2	1.0167	1.9907e-05	2.1294e-05	9	0.5
1.1292	T3	1.1281	1.0298e-05	1.0394e-05	42	0.7
1.1658		1.1653	1.0770e-05	1.0796e-05	39	0.8
1.2756		1.2757	1.1819e-04	1.1802e-04	172	0.6
1.8311	T4	1.8289	3.9541e-05	4.1246e-05	2	0.3
2.2400		2.2376	9.0358e-06	9.4771e-06	35	0.3
4.2297	T5	4.2291	2.5202e-05	2.5034e-05	173	0.2
4.8767		4.8788	1.4886e-04	1.5259e-04	156	0.3

RMS-acc	RMS-vel	RMS-dsp
1.199e-01	1.331e-02	7.066e-03

FIGURE C-7

BUILDING B - Power and Phase Spectra of Measured Acceleration

Measurement	Date	August 15, 1991
Measurement	Sensor Location	10th Floor, Center
Reference	Sensor Location	40th Floor, Center
	Sensor Direction	East-West

BUILDING B; Power Spectrum; 10th Floor; E-W

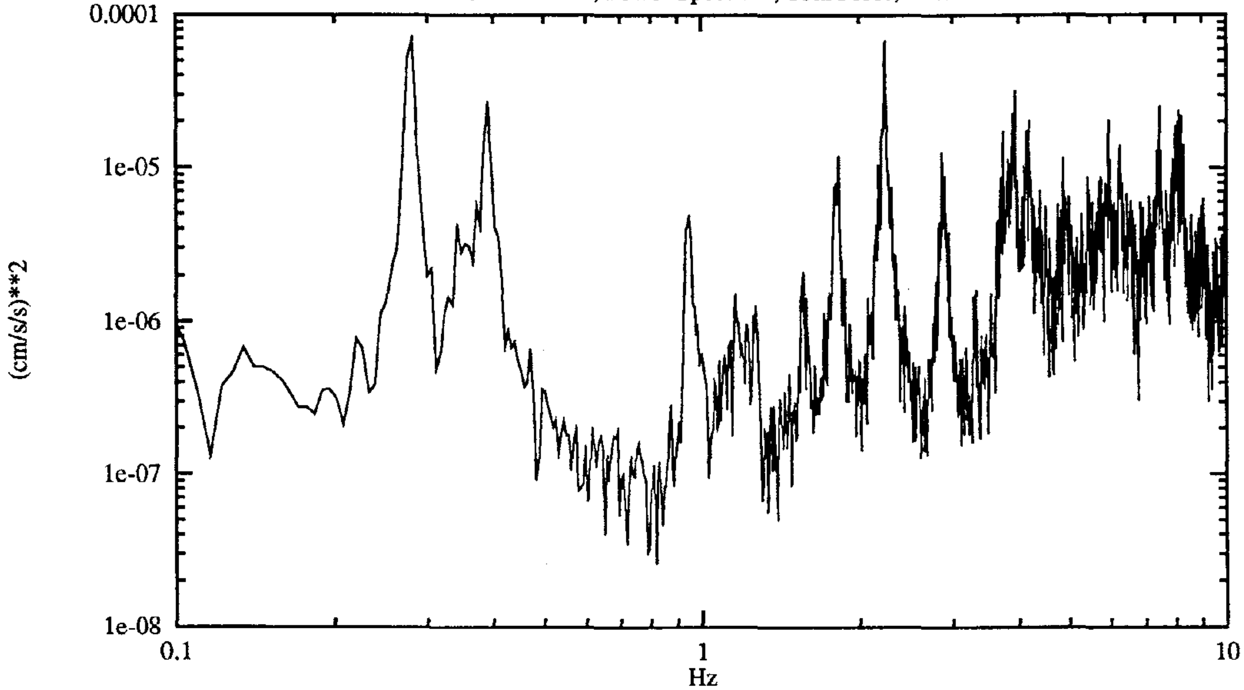

BUILDING B; Phase Spectrum; 10th Floor; E-W

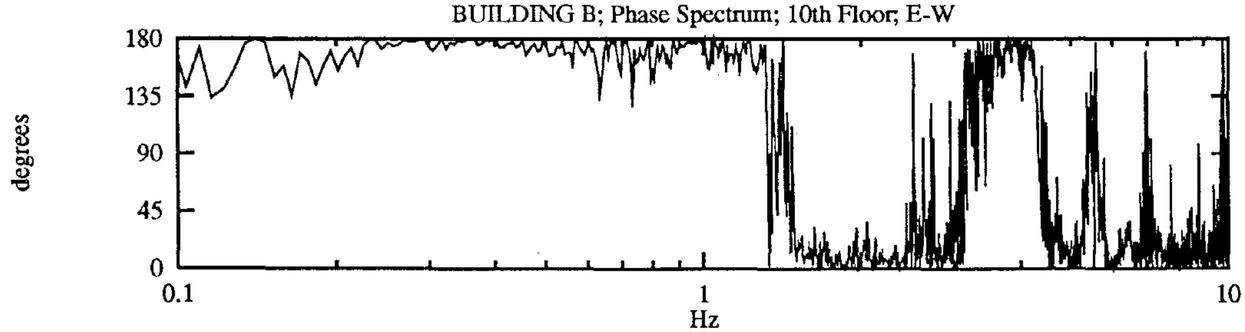

Peaks In G1040e

Hz-data		Hz-fit	Amp^2-data	Amp^2-fit	Phase	Damping %
0.2808		0.2791	6.9478e-05	7.2129e-05	177	1.2
0.3418		0.3428	4.3055e-06	4.3698e-06	179	1.8
0.3906		0.3905	2.7249e-05	2.7262e-05	178	1.4
0.9460		0.9451	4.7272e-06	4.7404e-06	177	1.1
1.1597	T3	1.1600	1.5128e-06	1.5125e-06	169	0.7
1.2695		1.2700	1.2770e-06	1.2778e-06	157	1.1
1.5625		1.5600	1.9912e-06	2.0619e-06	8	0.7
1.8311	T4	1.8287	1.1918e-05	1.2577e-05	1	0.3
2.2400		2.2385	6.8093e-05	6.9857e-05	5	0.3
2.8687		2.8686	1.2595e-05	1.2636e-05	27	0.3
3.7415		3.7424	1.7382e-05	1.7405e-05	166	0.2
3.9429		3.9431	3.2101e-05	3.4332e-05	177	0.1
4.1870	T5	4.1878	2.0377e-05	2.0027e-05	168	0.2
4.8767		4.8775	1.1698e-05	1.1921e-05	11	0.2

RMS-acc	RMS-vel	RMS-dsp
1.049e-01	1.147e-02	8.392e-03

FIGURE C-8

BUILDING B - Power and Phase Spectra of Measured Acceleration

Measurement	Date	August 15, 1991
Measurement	Sensor Location	36th Floor, East
Reference	Sensor Location	10th Floor, Center
	Sensor Direction	East-West

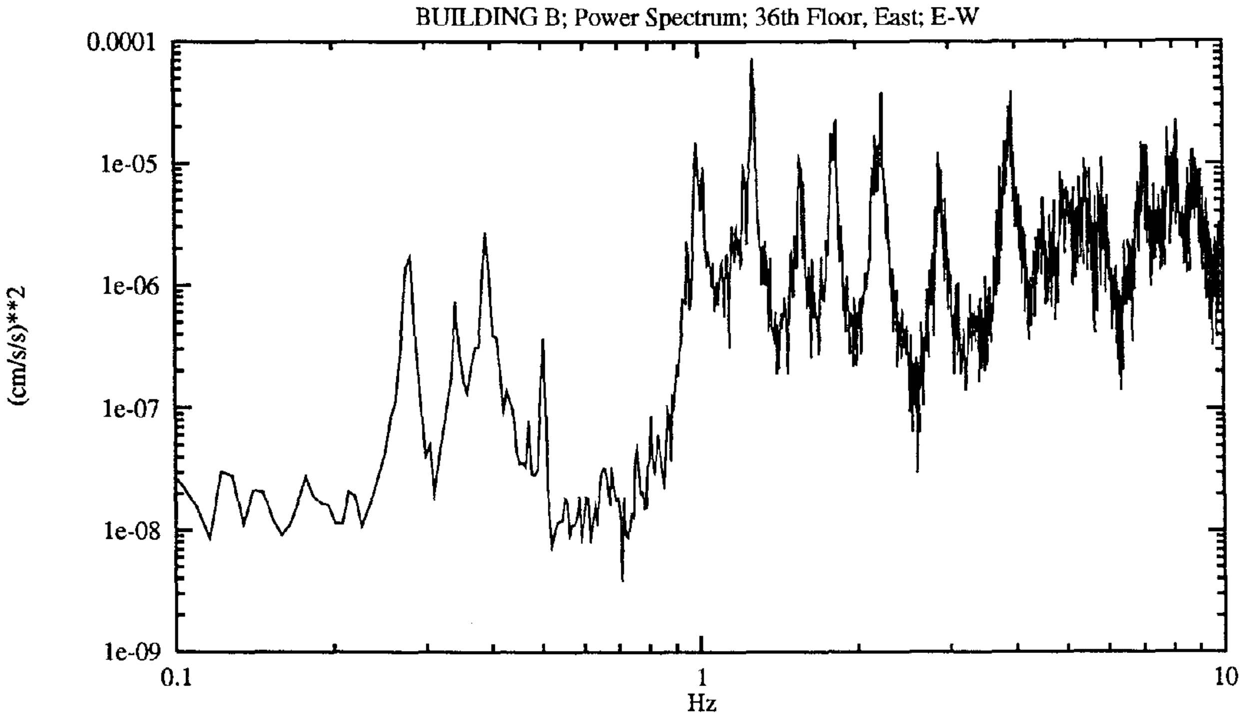

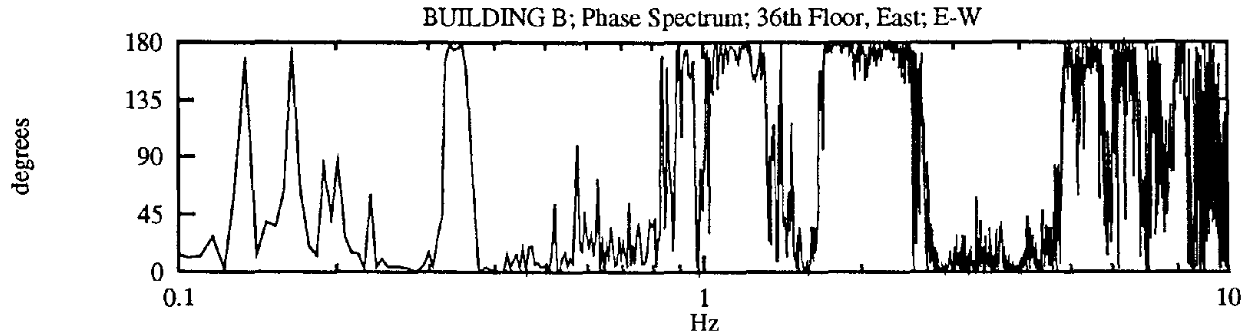

Peaks In G36e10e

Hz-data		Hz-fit	Amp^2-data	Amp^2-fit	Phase	Damping %
0.2808		0.2789	1.7068e-06	1.7844e-06	0	1.3
0.3418		0.3421	7.2849e-07	7.3016e-07	175	1.3
0.3906		0.3905	2.6772e-06	2.6776e-06	2	1.3
0.5005		0.5003	3.6844e-07	3.6880e-07	6	0.7
0.9460		0.9481	2.2606e-06	2.3637e-06	152	0.6
0.9888	T1	0.9884	1.4703e-05	1.4722e-05	80	0.7
1.0193	T2	1.0176	9.1861e-06	9.5144e-06	173	0.5
1.2756		1.2756	7.2635e-05	7.2598e-05	157	0.7
1.5625		1.5641	1.0616e-05	1.0788e-05	2	0.4
1.8311	T4	1.8283	2.1242e-05	2.2709e-05	178	0.3
2.2400		2.2389	3.7712e-05	3.8266e-05	174	0.4
2.8687		2.8684	1.2039e-05	1.2100e-05	4	0.3
3.9429		3.9432	3.8747e-05	3.9101e-05	1	0.1
4.5227		4.5228	5.2128e-06	5.0068e-06	33	0.1
4.8828		4.8825	8.4336e-06	8.1062e-06	152	0.2

RMS-acc	RMS-vel	RMS-dsp
1.037e-01	4.598e-03	1.828e-03

FIGURE C-9

BUILDING B - Power and Phase Spectra of Measured Acceleration

Measurement	Date	August 15, 1991
Measurement	Sensor Location	40th Floor, Center
Reference	Sensor Location	10th Floor, Center
	Sensor Direction	East-West

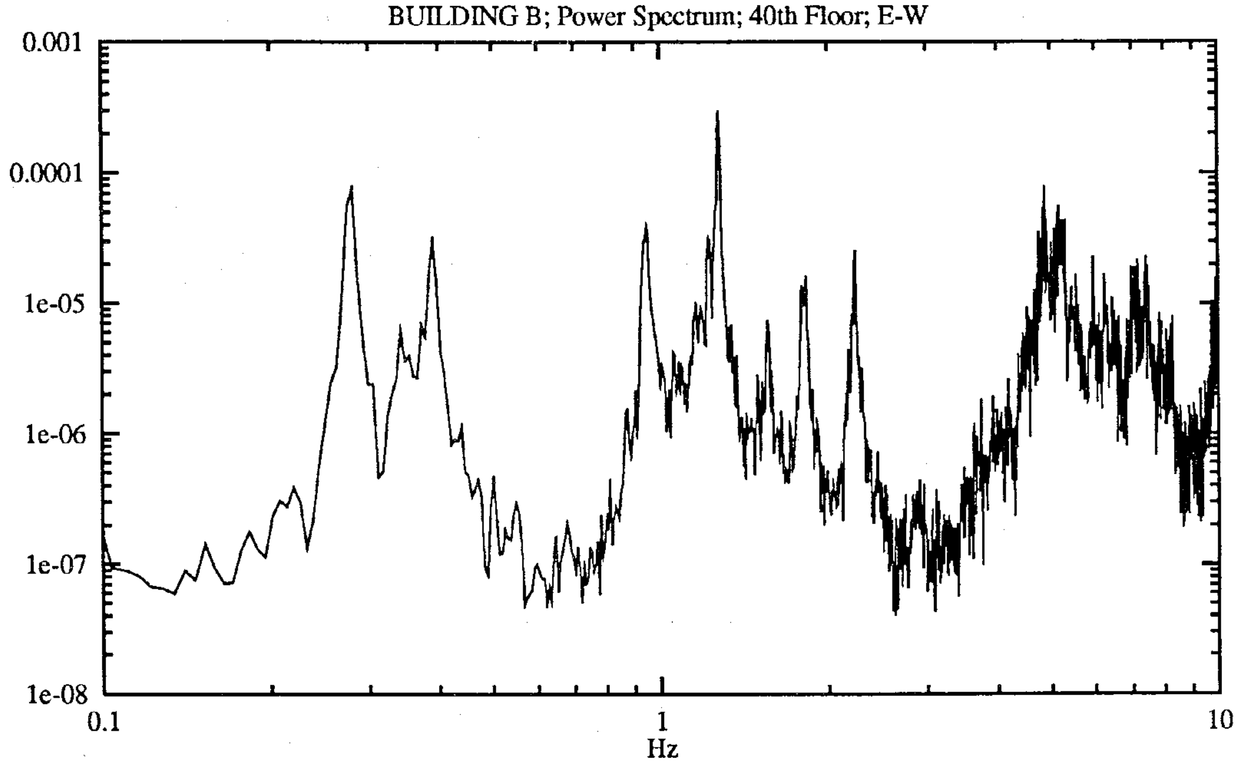

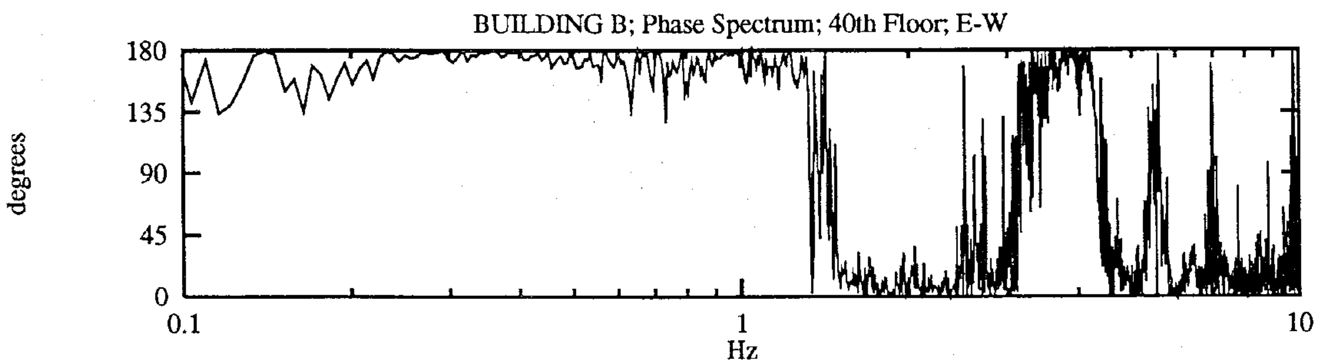

Peaks In G4010e

Hz-data	Hz-fit	Amp^2-data	Amp^2-fit	Phase	Damping %
0.2808	0.2792	7.5738e-05	7.8365e-05	177	1.2
0.3418	0.3423	6.2898e-06	6.3088e-06	179	1.8
0.3906	0.3904	3.2550e-05	3.2596e-05	178	1.3
0.9460	0.9465	3.8941e-05	3.8981e-05	177	0.9
1.0559 T2	1.0584	4.1825e-06	4.3809e-06	175	0.8
1.0803	1.0800	3.5445e-06	3.5465e-06	171	0.7
1.1597	1.1589	1.0171e-05	1.0207e-05	169	0.8
1.1841	1.1841	9.0985e-06	9.1009e-06	169	1.6
1.2756	1.2755	2.9857e-04	2.9898e-04	160	0.6
1.5625	1.5636	7.3950e-06	7.4506e-06	8	0.8
1.8311 T4	1.8291	1.6281e-05	1.6868e-05	1	0.3
2.2400	2.2383	2.5475e-05	2.5988e-05	5	0.4
4.8767	4.8782	7.8683e-05	8.0109e-05	11	0.2

RMS-acc	RMS-vel	RMS-dsp
1.229e-01	1.126e-02	5.976e-03

FIGURE C-10

BUILDING B - Power and Phase Spectra of Measured Acceleration

Measurement	Date	August 15, 1991
Measurement	Sensor Location	36th Floor, West
Reference	Sensor Location	36th Floor, East
	Sensor Direction	North-South

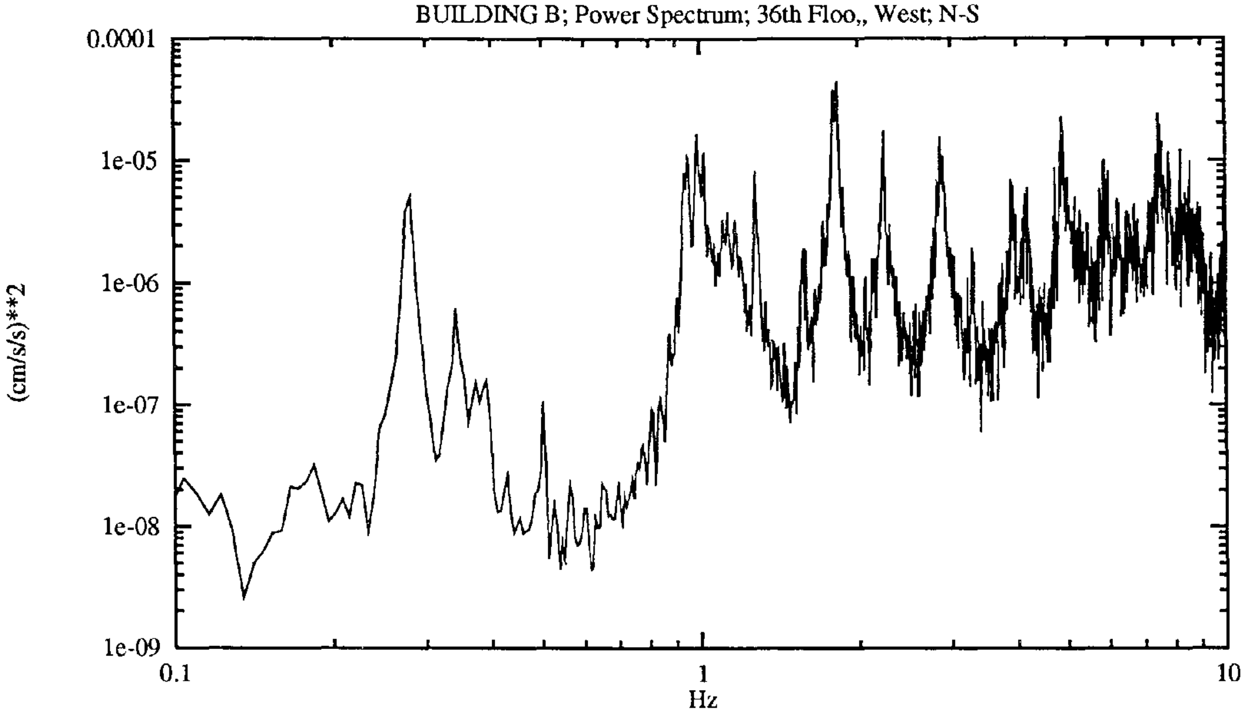

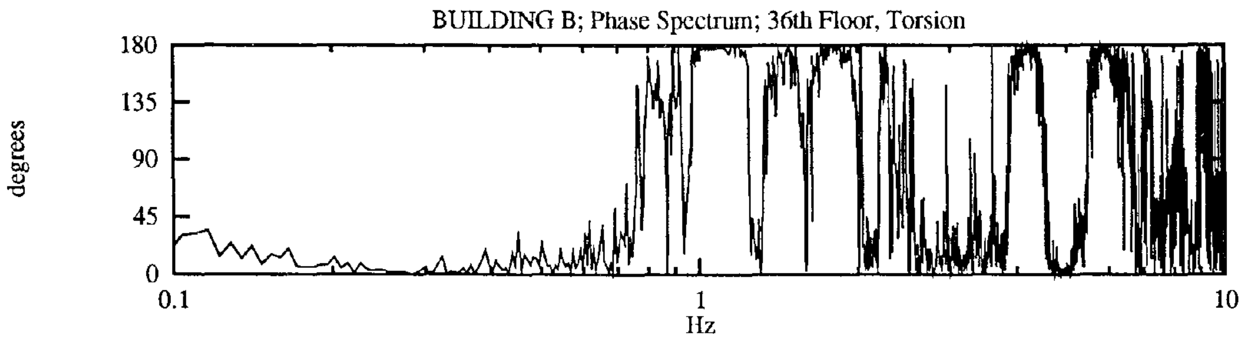

Peaks In G36w36en

Hz-data		Hz-fit	Amp^2-data	Amp^2-fit	Phase	Damping %
0.2808		0.2791	5.1004e-06	5.2908e-06	0	1.2
0.3418		0.3419	6.1940e-07	6.1956e-07	1	1.3
0.3906		0.3890	1.6010e-07	1.6403e-07	19	1.7
0.5005		0.5005	1.0596e-07	1.0594e-07	23	0.7
0.9460		0.9483	1.0672e-05	1.1001e-05	61	0.8
0.9888	T1	0.9883	1.6407e-05	1.6436e-05	175	0.7
1.0193	T2	1.0174	1.1486e-05	1.1936e-05	177	0.5
1.1292	T3	1.1287	3.8387e-06	3.8445e-06	175	0.7
1.2756		1.2758	8.1588e-06	8.1360e-06	21	0.5
1.5747		1.5731	1.8998e-06	1.9595e-06	127	0.3
1.8311	T4	1.8286	4.4506e-05	4.6968e-05	175	0.3
2.2400		2.2385	1.7490e-05	1.8001e-05	137	0.2
2.8687		2.8687	1.5584e-05	1.5557e-05	13	0.4
3.9001		3.9018	6.9523e-06	7.0333e-06	115	0.2
4.1870	T5	4.1879	5.9891e-06	5.8413e-06	172	0.3
4.8828		4.8800	2.1977e-05	2.2888e-05	0	0.2

RMS-acc	RMS-vel	RMS-dsp
7.776e-02	4.319e-03	1.990e-03

APPENDIX D
SOURCE CODE LISTING FOR COMPUTER PROGRAM AMB

The computer program AMB make extensive use of the numerical analysis libraries from Numerical Recipes in C: The Art of Scientific Computing [Press et. al 1988]. These routines are copyright (C) 1987,1988,1992 Numerical Recipes Software and are reproduced by permission, from the book Numerical Recipes: The Art of Scientific Computing, published by Cambridge University Press. Comments in the code indicate page numbers from the book where the routines came from. Some routines from this book were taken verbatim, whereas others required some modification.

D.1 Input

Program AMB is interactive with the user, but requires no special graphics interface. The compiled version of the program has no command line arguments. Control information, such as sample rate and desired frequency resolution are supplied interactively.

D.1.1 Example of Terminal Session

```
reeltime 15% amb
 Reference data file name: duane.52e.n
 Response  data file name: duane.52c.n
 Number of data points: 60000
 Sample rate (Hz): 50
 Maximum frequency in the spectrum (Hz): 25.00
 Target  frequency interval (Hz): 0.01
 Actual  frequency interval (Hz): 0.012207
 Points per spectrum: 2048
 Number of  averages: 28
 Amplitude / Phase file name: G52cen
reeltime 16%
```

The input files must be in ASCII format. The entries in the input files must be separated by tabs, blank space, or carriage returns (new lines). The time axis of the data must be omitted. The data files require no special headers. The time histories from the measurement location sensor and the reference location sensor must be in separate files. (The UNIX command "more" displays a file page by page.)

D.1.2 Example of Input Files

```
reeltime 16% more duane.52e.n
-2.889475e-02
-1.002818e-02
1.206781e-02
```

... following data deleted ...

```
reeltime 17% more duane.52c.n
4.691148e-02
4.844121e-02
2.226596e-02
```

... following data deleted ...

D.2 Output

Program AMB creates a single output file of three-column, tab delimited, ASCII data. The first column contains the frequency axis data. The second column contains the power spectrum data as computed by equation (5.6). The third column contains the phase spectrum data as computed by equation (5.9).

D.2.1 Example of Output File

```
reeltime 18% more G52cen
1.22070313e-02   3.8438816e-06   1.3000222e+01
2.44140625e-02   3.1228686e-07   7.0814271e+00
3.66210938e-02   2.0304019e-07   1.2047212e+00
```

... following data deleted ...

```
/***************************************************************************/
/* Program amb.c  -  Ambient  Vibration  Spectral  Analysis              */
/* calculates the power spectra Gx, Gy, and Gxy using data sets x & y   */
/* Averaging and Windowing are Incorporated.                              */
/* W.H. Press et al. Numerical Recipes In C. Cambridge Press - Ch. 12   */
/*                                                                        */
/* to compile: cc -O -o amb amb.c fft.c nrutil.c                         */
/* (c)  H.P. Gavin, Dept. of Civil Eng., Princeton University, 2-91     */
/***************************************************************************/

#define  MXLN   85
#include <math.h>
#include <stdio.h>

main()
{
        char    x_filename[MXLN],
                y_filename[MXLN],
                G_filename[MXLN],
                c;

        FILE    *fpx,*fpy,      /* file pointers to x & y data files    */
                *fpG;           /* file pointer to the spectra file     */

        float   *gx,*gy,        /* power spectra of x & y data files    */
                *gxyr,*gxyi,    /* real & imaginary parts of cross spct */
                *Coh,           /* coherence spectrum                   */
                *Pha,           /*  phase    spectrum                   */
                sr,df,          /* sample rate and frequency interval   */
                w2,             /* circular frequency in rad/sec squared*/
                data,
                *vector();

        int     m = 2,          /* number of frequency values / segment */
                tg_pts,         /* target number of freq vals / segment */
                k,              /* number of segments to be averaged    */
                j,              /* counter                              */
                ovrlap = 1,     /* 1: overlap segments; 0: no overlap   */
                points = 0;     /* number of data points ( 10,000 )     */

        void    spectra(),      /* returns spectra and cross spectra    */
                coh(),          /* returns coherence and phase          */
                free_vector();

        printf (" Reference data file name: ");
        scanf ("%s",x_filename);
        if (( fpx=fopen(x_filename,"r"))==NULL) {
                printf ("  error: cannot open %s\n",x_filename);
                exit (0);
        }
        printf (" Response  data file name: ");
        scanf ("%s",y_filename);
```

```
if (( fpy=fopen(y_filename,"r"))==NULL) {
        printf ("  error: cannot open %s\n",y_filename);
        exit (0);
}

        /*      Size  The  Data         */

printf (" Number of data points: ");
scanf ("%d",&points);
if (points == 0) {
        while ( (c=fscanf(fpx,"%f",&data)) != EOF ) ++points;
        printf (" %d X data points\n",points);
        points = 0;
        while ( (c=fscanf(fpy,"%f",&data)) != EOF ) ++points;
        printf (" %d Y data points\n",points);
        rewind (fpx);
        rewind (fpy);
}

        /*      Choose  Frequency  Resolution   */

printf (" Sample rate (Hz): ");
scanf ("%f",&sr);
printf (" Maximum frequency in the spectrum (Hz): %.2f\n", sr/2);
printf (" Target  frequency interval (Hz): ");
scanf ("%f",&df);
tg_pts = sr/df;
while (m < tg_pts) m <<= 1; m >>= 2;
k = points/m - 1;
df = sr / (2*m);
printf (" Actual  frequency interval (Hz): %f\n", df);
printf (" Points per spectrum: %d\n", m);
printf (" Number of  averages: %d\n", k);
if (k < 1) {
        printf ("  error: %d is too small\n", k);
        exit(0);
}

gx = vector(1,m);
gy = vector(1,m);
gxyr = vector(1,m);
gxyi = vector(1,m);

spectra (fpx,fpy,gx,gy,gxyr,gxyi,m,k,ovrlap);

fclose (fpx);
fclose (fpy);

Coh = vector(1,m);
Pha = vector(1,m);

coh (gx,gy,gxyr,gxyi,Coh,Pha,m);
```

```
        /*      Print the Spectra       */

    printf (" Amplitude / Phase file name: ");
    scanf ("%s", G_filename);
    if (( fpG=fopen(G_filename,"w"))==NULL) {
            printf ("  error: cannot open %s\n",G_filename);
            exit (1);
    }
    for (j=2;j<=m;j++)
            fprintf (fpG,"%e\t%e\t%7.2f\n",(j-1)*df,gy[j],Pha[j]);
    fclose (fpG);

    free_vector(Coh,1,m);
    free_vector(Pha,1,m);
    free_vector(gx,1,m);
    free_vector(gy,1,m);
    free_vector(gxyr,1,m);
    free_vector(gxyi,1,m);
}


    /*              Function spectra()                      */
    /* Power Spectra Using The Fast Fourier Transform       */
    /* Adapted from Numerical Recipes in C - Ch 12          */
    /* normalization: SUM(gx[i]) i=1..m = variance(x)       */

static float sqrarg;
#define SQR(a) (sqrarg=(a), sqrarg*sqrarg)
#define tpi 6.28318530717959

#define WINDOW(j,c,b) (0.5-0.5*cos(tpi*((j)-1)*(c)))    /* Hanning      */
/* #define WINDOW(j,a,b) (1.0-fabs((((j)-1)-(a))*(b)))  /* Parzen       */
/* #define WINDOW(j,a,b) (1.0-SQR((((j)-1)-(a))*(b)))   /* Welch        */
/* #define WINDOW(j,a,b) 1.0                            /* Square       */

void spectra(fpx,fpy,gx,gy,gxyr,gxyi,m,k,ovrlap)
FILE *fpx,*fpy;
float gx[],gy[],gxyr[],gxyi[];
int m,k,ovrlap;
{
        int n,tn,tn3,tn4,kk,j,tj;               /* Useful Quantities    */
        float a,b,c,sumw=0.0,den=0.0;
        float *x1,*x2,*y1,*y2;                  /* Operating vectors    */
        float *Sx,*Sy;                          /* FFT'd vectors        */
        float *vector();
        void segments(),twofft(),free_vector();

        tn4 = (tn3 = (tn = n+(n=m+m))+3)+1;
        a = m - 0.5;
        b = 1.0/(m+0.5);
        c = 1.0/(n-1.0);
```

```
        x1 = vector(1,m);
        x2 = vector(1,n);
        y1 = vector(1,m);
        y2 = vector(1,n);
        Sx = vector(1,tn);
        Sy = vector(1,tn);
        for (j=1; j<=n; j++) sumw += SQR(WINDOW(j,c,b));
        for (j=1; j<=m; j++) gx[j]=gy[j]=gxyr[j]=gxyi[j]=0.0;
        if (ovrlap)             /* Initialize the "save" half-buffer.   */
                for (j=1; j<=m; j++) {
                        fscanf(fpx,"%f",&x1[j]);
                        fscanf(fpy,"%f",&y1[j]);
                }
        for (kk=1; kk<=k; kk++) {
                segments(fpx,x1,x2,a,b,c,m,ovrlap);
                segments(fpy,y1,y2,a,b,c,m,ovrlap);
                                /* Fourier transform the windowed data  */
                twofft(x2,y2,Sx,Sy,n,1);
                        /* Sum the results into the previous segments   */
                gx[1] += (SQR(Sx[1]) + SQR(Sx[2]));
                gy[1] += (SQR(Sy[1]) + SQR(Sy[2]));
                for (j=2; j<=m; j++) {
                        tj = j+j;
                        gx[j] += (SQR(Sx[tj-1]) + SQR(Sx[tj])
                                + SQR(Sx[tn3-tj]) + SQR(Sx[tn4-tj]));
                        gy[j] += (SQR(Sy[tj]) + SQR(Sy[tj-1])
                                + SQR(Sy[tn3-tj]) + SQR(Sy[tn4-tj]));
                        gxyr[j] += (Sx[tj-1]*Sy[tj-1] + Sx[tj]*Sy[tj]
                                    + Sx[tn3-tj]*Sy[tn3-tj]
                                    + Sx[tn4-tj]*Sy[tn4-tj]);
                        gxyi[j] += (Sx[tj]*Sy[tj-1] - Sx[tj-1]*Sy[tj]
                                    - Sx[tn4-tj]*Sy[tn3-tj]
                                    + Sx[tn3-tj]*Sy[tn4-tj]);
                }
                den += sumw;
        }
        den *= n;                           /* Correct normalization.        */
        for (j=1; j<=m; j++) {
                gx[j] /= den;
                gy[j] /= den;
                gxyr[j] /= den;
                gxyi[j] /= den;
        }
        free_vector(x1,1,m);
        free_vector(x2,1,n);
        free_vector(y1,1,m);
        free_vector(y2,1,n);
        free_vector(Sx,1,tn);
        free_vector(Sy,1,tn);
        return;
}
```

```
        /*              Function segments()                          */
        /* Gets two complete segments into the work space            */
        /*              Numerical Recipes in C p446                  */

void segments(fp,z1,z2,a,b,c,m,ovrlap)
FILE    *fp;
float   *z1,*z2;
float   a,b,c;
int     m,ovrlap;
{
        int     j;
        if (ovrlap) {
                for (j=1; j<=m; j++) z2[j]=z1[j];
                for (j=1; j<=m; j++) fscanf(fp,"%f",&z1[j]);
                for (j=1; j<=m; j++) z2[m+j]=z1[j];
        } else {
                for (j=1; j<=m+m; j++)
                        fscanf(fp,"%f",&z2[j]);
        }
        for (j=1; j<=m+m; j++)          /* Apply the window to the data.*/
                z2[j] *= WINDOW(j,c,b);
        return;
}


        /*              Function coh()                               */
        /* Computes the coherence and the phase functions using */
        /* the power spectra gx and gy and the cross spectrum gxy*/

void coh(gx,gy,gxyr,gxyi,Coh,Pha,m)
float   *gx,*gy,*gxyr,*gxyi,
        *Coh,*Pha;
int     m;
{
        int     j;
        float   den1, den2;

        for (j=1; j<=m; j++) {
                den1 = SQR(gxyr[j]) + SQR(gxyi[j]);
                if (den2 = (gx[j]*gy[j]) != 0.0)
                        Coh[j] = den1/den2;
                else    Coh[j] = 0.0;
                if (gxyi[j] != 0.0)
                        Pha[j] = fabs(atan2(gxyi[j],gxyr[j])) * 57.29578;
                else    Pha[j] = Pha[j-1];
        }
        return;
}
```

```
/*                           FILE fft.c                                 */
/* Fast Fourier Transform routines from Numerical Recipes in C, by Press*/
/* et al. Cambridge University Press, 1988                              */

#include <math.h>

        /*              Function four1()                        */
        /* Fast Fourier Transform - Numerical Recipes in C p411.*/

#define SWAP(a,b) tempr=(a);(a)=(b);(b)=tempr

void four1(data,nn,isign)
float   data[];
int     nn,isign;
{
        int     n,mmax,m,j,istep,i;
        double  wtemp,wr,wpr,wpi,wi,theta;
        float   tempr,tempi;

        n=nn << 1;
        j=1;
        for (i=1;i<n;i+=2) {                            /* Bit Reversal */
                if (j > i) {
                        SWAP(data[j],data[i]);
                        SWAP(data[j+1],data[i+1]);
                }
                m=n >> 1;
                while (m >= 2 && j > m) {
                        j -= m;
                        m >>= 1;
                }
                j += m;
        }
        mmax=2;
        while (n > mmax) {
                istep = 2*mmax;
                theta = 6.28318530717959 / (isign*mmax);
                wtemp = sin(0.5*theta);
                wpr = -2.0*wtemp*wtemp;
                wpi = sin(theta);
                wr = 1.0;
                wi = 0.0;
                for (m=1; m<mmax; m+=2) {
                        for (i=m; i<=n; i+=istep) {
                                j = i + mmax;           /* Danielson-Lanczo
                                tempr = wr*data[j] - wi*data[j+1];
                                tempi = wr*data[j+1] + wi*data[j];
                                data[j] = data[i] - tempr;
                                data[j+1] = data[i+1] - tempi;
                                data[i] += tempr;
                                data[i+1] += tempi;
                        }                       /* Trigonometric Recurrence
```

```
                        wr = (wtemp=wr)*wpr - wi*wpi + wr;
                        wi = wi*wpr + wtemp*wpi + wi;
                }
                mmax = istep;
        }
        return;
}


        /*                function twofft()                     */
        /* The simultaneous FFT of two real valued functions    */
        /*        from  Numerical Recipes In C  p 415           */

void twofft(data1,data2,fft1,fft2,n)
float data1[],data2[],fft1[],fft2[];
int n;
{
        int nn3,nn2,jj,j;
        float rep,rem,aip,aim;
        void four1();

        nn3=1+(nn2=2+n+n);
        for (j=1,jj=2;j<=n;j++,jj+=2) {
                fft1[jj-1]=data1[j];
                fft1[jj]=data2[j];
        }
        four1(fft1,n,1);
        fft2[1]=fft1[2];
        fft1[2]=fft2[2]=0.0;
        for (j=3;j<=n+1;j+=2) {
                rep=0.5*(fft1[j]+fft1[nn2-j]);
                rem=0.5*(fft1[j]-fft1[nn2-j]);
                aip=0.5*(fft1[j+1]+fft1[nn3-j]);
                aim=0.5*(fft1[j+1]-fft1[nn3-j]);
                fft1[j]=rep;
                fft1[j+1]=aim;
                fft1[nn2-j]=rep;
                fft1[nn3-j] = -aim;
                fft2[j]=aip;
                fft2[j+1] = -rem;
                fft2[nn2-j]=aip;
                fft2[nn3-j]=rem;
        }
        return;
}


        /*                function realft()                           */
        /* The FFT of 2n real valued discrete function pointS         */
        /*        from  Numerical Recipes In C  p 417                 */

void realft(data,n,isign)
```

```
float data[];
int n,isign;
{
        int i,i1,i2,i3,i4,n2p3;
        float c1=0.5,c2,h1r,h1i,h2r,h2i;
        double wr,wi,wpr,wpi,wtemp,theta;
        void four1();

        theta=3.141592653589793/(double) n;
        if (isign == 1) {
                c2 = -0.5;
                four1(data,n,1);
        } else {
                c2=0.5;
                theta = -theta;
        }
        wtemp=sin(0.5*theta);
        wpr = -2.0*wtemp*wtemp;
        wpi=sin(theta);
        wr=1.0+wpr;
        wi=wpi;
        n2p3=2*n+3;
        for (i=2;i<=n/2;i++) {
                i4=1+(i3=n2p3-(i2=1+(i1=i+i-1)));
                h1r=c1*(data[i1]+data[i3]);
                h1i=c1*(data[i2]-data[i4]);
                h2r = -c2*(data[i2]+data[i4]);
                h2i=c2*(data[i1]-data[i3]);
                data[i1]=h1r+wr*h2r-wi*h2i;
                data[i2]=h1i+wr*h2i+wi*h2r;
                data[i3]=h1r-wr*h2r+wi*h2i;
                data[i4] = -h1i+wr*h2i+wi*h2r;
                wr=(wtemp=wr)*wpr-wi*wpi+wr;
                wi=wi*wpr+wtemp*wpi+wi;
        }
        if (isign == 1) {
                data[1] = (h1r=data[1])+data[2];
                data[2] = h1r-data[2];
        } else {
                data[1]=c1*((h1r=data[1])+data[2]);
                data[2]=c1*(h1r-data[2]);
                four1(data,n,-1);
        }
}
```

```
/*                      FILE nrutil.c                                    */
/* Memory allocation functions from Numerical Recipes in C, by Press,    */
/* Cambridge University Press, 1988                                      */

/* #include <malloc.h> */
#include <stdio.h>

typedef struct FCOMPLEX {float r,i;} fcomplex; /* */

void nrerror(error_text)        /* print error message to stderr        */
char error_text[];
{
        void exit();

        fprintf(stderr,"Numerical Recipes run-time error...\n");
        fprintf(stderr,"%s\n",error_text);
        fprintf(stderr,"...now exiting to system...\n");
        exit(1);
}


float *vector(nl,nh)    /* allocate storage for a vector        */
int nl,nh;
{
        float *v;

        v=(float *)malloc((unsigned) (nh-nl+1)*sizeof(float));
        if (!v) nrerror("allocation failure in vector()");
        return v-nl;
}

fcomplex *Cvector(nl,nh)
int nl,nh;              /* allocate storage for a complex vector        */
{
        fcomplex *v;

        v=(fcomplex *)malloc((unsigned) (nh-nl+1)*sizeof(fcomplex));
        if (!v) nrerror("allocation failure in Cvector()");
        return v-nl;
}

double *dvector(nl,nh)  /* allocate storage for a vector        */
int nl,nh;
{
        double *v;

        v=(double *)malloc((unsigned) (nh-nl+1)*sizeof(double));
        if (!v) nrerror("allocation failure in dvector()");
        return v-nl;
}

int *ivector(nl,nh)     /* allocate storage for a vector        */
```

```
int nl,nh;
{
        int *v;

        v=(int *)malloc((unsigned) (nh-nl+1)*sizeof(int));
        if (!v) nrerror("allocation failure in ivector()");
        return v-nl;
}

float **matrix(nrl,nrh,ncl,nch) /* allocate storage for a matrix        */
int nrl,nrh,ncl,nch;
{
        int     i;
        float   **m;

        m=(float **) malloc((unsigned) (nrh-nrl+1)*sizeof(float*));
        if (!m) nrerror("allocation failure 1 in matrix()");
        m -= nrl;
        for (i=nrl;i<=nrh;i++) {
                m[i]=(float *) malloc((unsigned) (nch-ncl+1)*sizeof(float))
                if (!m[i]) nrerror("allocation failure 2 in matrix()");
                m[i] -= ncl;
        }
        return m;
}

fcomplex **Cmatrix(nrl,nrh,ncl,nch)
int nrl,nrh,ncl,nch;    /* allocate storage for a Complex matrix        */
{
        int     i;
        fcomplex **m;

        m=(fcomplex **)malloc((unsigned) (nrh-nrl+1)*sizeof(fcomplex*));
        if (!m) nrerror("allocation failure 1 in Cmatrix()");
        m -= nrl;
        for (i=nrl;i<=nrh;i++) {
                m[i]=(fcomplex *)malloc((unsigned)(nch-ncl+1)*sizeof(fcompl
                if (!m[i]) nrerror("allocation failure 2 in Cmatrix()");
                m[i] -= ncl;
        }
        return m;
}

double **dmatrix(nrl,nrh,ncl,nch)   /* allocate storage for a matrix    */
int nrl,nrh,ncl,nch;
{
        int     i;
        double  **m;

        m=(double **) malloc((unsigned) (nrh-nrl+1)*sizeof(double*));
        if (!m) nrerror("allocation failure 1 in dmatrix()");
        m -= nrl;
```

```
	for (i=nrl;i<=nrh;i++) {
		m[i]=(double *) malloc((unsigned) (nch-ncl+1)*sizeof(double
		if (!m[i]) nrerror("allocation failure 2 in dmatrix()");
		m[i] -= ncl;
	}
	return m;
}

int **imatrix(nrl,nrh,ncl,nch)  /* allocate storage for a matrix        */
int nrl,nrh,ncl,nch;
{
	int	i;
	int	**m;

	m=(int **) malloc((unsigned) (nrh-nrl+1)*sizeof(int*));
	if (!m) nrerror("allocation failure 1 in imatrix()");
	m -= nrl;
	for (i=nrl;i<=nrh;i++) {
		m[i]=(int *) malloc((unsigned) (nch-ncl+1)*sizeof(int));
		if (!m[i]) nrerror("allocation failure 2 in imatrix()");
		m[i] -= ncl;
	}
	return m;
}

float **submatrix(a,oldrl,oldrh,oldcl,oldch,newrl,newcl)
float **a;
int oldrl,oldrh,oldcl,oldch,newrl,newcl;
{
	int i,j;
	float **m;

	m=(float **) malloc((unsigned) (oldrh-oldrl+1)*sizeof(float*));
	if (!m) nrerror("allocation failure in submatrix()");
	m -= newrl;

	for(i=oldrl,j=newrl;i<=oldrh;i++,j++) m[j]=a[i]+oldcl-newcl;

	return m;
}


void free_vector(v,nl,nh)
float *v;
int nl,nh;
{
	free((char*) (v+nl));
}

void free_Cvector(v,nl,nh)
fcomplex *v;
int nl,nh;
```

```
{
        free((char*) (v+nl));
}

void free_dvector(v,nl,nh)
double *v;
int nl,nh;
{
        free((char*) (v+nl));
}

void free_ivector(v,nl,nh)
int *v;
int nl,nh;
{
        free((char*) (v+nl));
}

void free_matrix(m,nrl,nrh,ncl,nch)
float **m;
int nrl,nrh,ncl,nch;
{
        int     i;

        for(i=nrh;i>=nrl;i--) free((char*) (m[i]+ncl));
        free((char*) (m+nrl));
}

void free_Cmatrix(m,nrl,nrh,ncl,nch)
fcomplex **m;
int nrl,nrh,ncl,nch;
{
        int     i;

        for(i=nrh;i>=nrl;i--) free((char*) (m[i]+ncl));
        free((char*) (m+nrl));
}

void free_dmatrix(m,nrl,nrh,ncl,nch)
double **m;
int nrl,nrh,ncl,nch;
{
        int     i;

        for(i=nrh;i>=nrl;i--) free((char*) (m[i]+ncl));
        free((char*) (m+nrl));
}

void free_imatrix(m,nrl,nrh,ncl,nch)
int **m;
int nrl,nrh,ncl,nch;
{
```

```
        int     i;

        for(i=nrh;i>=nrl;i--) free((char*) (m[i]+ncl));
        free((char*) (m+nrl));
}

void free_submatrix(b,nrl,nrh,ncl,nch)
float **b;
int nrl,nrh,ncl,nch;
{
        free((char*) (b+nrl));
}

float **convert_matrix(a,nrl,nrh,ncl,nch)
float *a;
int nrl,nrh,ncl,nch;
{
        int i,j,nrow,ncol;

        float **m;

        nrow=nrh-nrl+1;
        ncol=nch-ncl+1;

        m = (float **) malloc((unsigned) (nrow)*sizeof(float*));
        if (!m) nrerror("allocation failure in convert_matrix()");
        m -= nrl;
        for(i=0,j=nrl;i<=nrow-1;i++,j++) m[j]=a+ncol*i-ncl;
        return m;
}

void free_convert_matrix(b,nrl,nrh,ncl,nch)
float **b;
int nrl,nrh,ncl,nch;
{
        free((char*) (b+nrl));
}
```

APPENDIX E
SOURCE CODE LISTING FOR COMPUTER PROGRAM PEAK

E.1 Input

Input to program PEAK is interactive. The program is invoked with a command line argument which is the name of the file created by program AMB. The rest of the input, such as the frequency band-width for peak searching, the number of peaks searched for, and the name of the output file, is entered interactively by the user.

E.2 Output

The output of the file is in the form of a table. Examples of these tables are given in Appendices B and C.

E.3 Example of Terminal Session

```
reeltime 8% peak G52cen
 Number of Peaks: 4
 Minimum frequency for peak-picking: 0.1
 Maximum frequency for peak-picking: 2
 Closest peak spacing (Hz): 0.25
 Results file name: r52cen
reeltime 9%
reeltime 9% more r52cen
                    Peaks In G52cen

Hz-data    Hz-fit     Amp^2-data     Amp^2-fit     Phase Damping %
 0.2441     0.2426    8.4451e-05     8.5265e-05       1    2.8
 0.9888     0.9891    4.7639e-06     4.7664e-06       2    1.3
 1.5259     1.5243    1.4874e-07     1.4911e-07     158    1.8
 1.8066     1.8102    1.3160e-05     1.3314e-05       3    2.2

          RMS-acc         RMS-vel         RMS-dsp
          3.057e-02       9.156e-03       6.181e-03


reeltime 10%
```

```
/*************************************************************************/
/* Program peak.c  -  Spectral  Peak  Picking  For  Ambient  Data       */
/* Use data from the output of program amb.c for ambient parameter est. */
/* Finds amplitudes and phases using peak picking methods.              */
/* Estimates frequencies and damping using a quadratic curve-fit and    */
/* a band-width method combining raw data with the estimated frequency. */
/* RMS-displacement computation de-emphasizes low frequencies: line 71  */
/*                                                                      */
/* to compile:  cc -O -o peak peak.c gaussj.c nrutil.c                  */
/* to run:      peak 'amplitude / phase filename'                       */
/* (c)  H.P. Gavin, Dept. of Civil Eng., Princeton University, 2-91     */
/*************************************************************************/

#include <stdio.h>
#include <math.h>

main(argc,argv)
int     argc;
char    *argv[];
{
        char    filename[85],   /* output file name                       */
                c;

        FILE    *fp;            /* file pointer                           */

        float   frq, amp, pha,  /* frequency, amplitude, and phase        */
                frq_old,        /* previous frequency                     */
                amp_old,        /* previous amplitude                     */
                pha_old,        /* previous phase                         */
                f_tol,          /* closest spacing of 2 peaks             */
                f_min,          /* minimum frequency for peak picking     */
                f_max,          /* maximum frequency for peak picking     */
                df,             /* frequency interval                     */
                rms_a = 0.0,    /* rms acceleration                       */
                rms_v = 0.0,    /* rms velocity                           */
                rms_d = 0.0,    /* rms displacement                       */
                **pk_data,      /* data in a high peak region             */
                **C,            /* power polynomial coefficients          */
                **matrix();     /* allocates matrix storage               */

        int     n_pk,           /* number of peaks to pick                */
                slope,          /* sign of [ dG(f) / df ] (+/- 1)         */
                slope_old,      /* previous slope                         */
                slp_cond,       /* 1: change in slope, 0: same slope      */
                amp_cond,       /* 1: next largest amplitude, 0: not      */
                frq_cond,       /* 1: far from a peak, 0: close to pk     */
                i,j,k,n;        /* current peak number                    */

        struct  peak {float f,a,p,d,F,A;} pk[20];

        void    poly_fit(),     /* general least squares polynomial fit */
                dter_fit(),     /* deterministic curve fitting            */
```

```
        free_matrix();  /* deallocates matrix storage              */


if (( fp = fopen(argv[1],"r")) == NULL ) {
        printf (" error: cannot open %s\n", argv[1]);
        printf (" usage: peak 'amplitude/phase filename'\n");
        exit (0);
}

/*               Find The RMS Values              */
/* Change These Lines If The Data Is Velocity     */

while ((c = fscanf(fp,"%f %f %f", &frq,&amp,&pha)) != EOF ) {
        if(frq < 0.15) frq=0.16;/* filter low frequency noise    */
        frq *= 2.0*acos(-1.0);  /* w = 2.pi.f                    */
        frq *= frq;             /* w^2 = w.w                     */
        rms_a += amp;           /* a^2 = a^2  or  a^2 = v^2*w^2 */
        rms_v += amp/frq;       /* v^2 = a^2/w^2  or  v^2 = v^2 */
        rms_d += amp/(frq*frq); /* d^2 = a^2/w^4 or d^2 = v^2/w^2*/
}
rms_a = sqrt(rms_a);
rms_v = sqrt(rms_v);
rms_d = sqrt(rms_d);
rewind(fp);

printf (" Number of Peaks: ");
scanf ("%d", &n_pk);
printf (" Minimum frequency for peak-picking: ");
scanf ("%f", &f_min);
printf (" Maximum frequency for peak-picking: ");
scanf ("%f", &f_max);
printf (" Closest peak spacing (Hz): ");
scanf ("%f", &f_tol);

pk_data = matrix(1,20,1,2);
C = matrix(1,3,1,1);

        /*      Find  The  Peaks  By  Amplitude */

i=1;
pk[1].a = 0.0;
while ((c = fscanf(fp,"%f %f %f", &frq,&amp,&pha)) != EOF ) {
        if (frq > f_max) break;
        if (frq > f_min)
                if (pk[1].a < amp) {
                        pk[1].f = frq;
                        pk[1].a = amp;
                        pk[1].p = pha;
                }
        if (i) {
                df = frq;
                i=0;
```

```
        }
}
rewind(fp);

for (i=2; i <= n_pk; i++) {
        frq_old = amp_old = pk[i].a = slope = slope_old = 0;
        while ((c = fscanf(fp,"%f %f %f", &frq,&amp,&pha)) != EOF )
                if (frq > f_max) break;
                if (frq > f_min) {

                        slp_cond = 0;
                        if (amp > amp_old) slope = 1;
                        if (amp < amp_old) slope = -1;
                        if (slope_old == 1 && slope == -1) slp_cond

                        amp_cond = 0;
                        if (pk[i].a < amp_old && amp_old < pk[i-1].
                                amp_cond = 1;

                        frq_cond = 1;
                        for(k=1; k<i; k++)
                                if (fabs(frq_old - pk[k].f) < f_tol
                                        frq_cond = 0;

                        if (slp_cond && amp_cond && frq_cond) {
                                pk[i].f = frq_old;
                                pk[i].a = amp_old;
                                pk[i].p = pha_old;
                        }
                        frq_old = frq;
                        amp_old = amp;
                        pha_old = pha;
                        slope_old = slope;
                }
        }
        rewind(fp);
}

        /*      Sort  The  Peaks  By  Frequency */

for (i=2; i<=n_pk; i++) {
        frq = pk[i].f;
        amp = pk[i].a;
        pha = pk[i].p;
        k=i-1;
        while (k > 0 && pk[k].f > frq) {
                pk[k+1].f = pk[k].f;
                pk[k+1].a = pk[k].a;
                pk[k+1].p = pk[k].p;
                k--;
        }
        pk[k+1].f = frq;
```

```
        pk[k+1].a = amp;
        pk[k+1].p = pha;
}

        /*      Curve-fit  The  Peaks  With  A  Quadratic        */

amp_cond=0; n=i=1;
while ((c = fscanf(fp,"%f %f %f", &frq,&amp,&pha)) != EOF ) {
        if (i > n_pk || frq > f_max) break;
        if (frq > pk[i].f - 1.1*df) n = amp_cond = 1;

        while (amp_cond) {
                pk_data[n][1] = frq;
                pk_data[n][2] = amp;
                if (frq > pk[i].f + 0.9*df) amp_cond = 0;
                fscanf(fp,"%f %f %f", &frq,&amp,&pha);
                n++;
        }
        n--;
        if (frq > pk[i].f && n > 2) {

                if (n == 3)     dter_fit (pk_data,n,C);
                else            poly_fit (pk_data,n,2,C);

                pk[i].A = C[1][1] - C[2][1]*C[2][1] / (4.0*C[3][1])
                pk[i].F = -0.5*C[2][1]/C[3][1];
                i++;

        } else  if (frq > pk[i].f) {
                        pk[i].F = pk[i].f;
                        pk[i].A = pk[i].a;
                        i++;
                }
}

        /*      Estimate  The  Damping  With  Raw  Data */

rewind(fp);
i=1;
while ((c = fscanf(fp,"%f %f %f", &frq,&amp,&pha)) != EOF ) {
        if (i > n_pk || frq > f_max) break;
        if (frq == pk[i].f) {
                while (amp > 0.7*pk[i].a) {
                        fscanf(fp, "%f %f %f", &frq, &amp, &pha);
                        pk[i].d = 100.0 * fabs(frq - pk[i].F) /
                                (pk[i].F * sqrt(pow((frq/pk[i].F),4
                                        pk[i].A/amp - 1.0));
                }
                i++;
        }
}
fclose (fp);
```

```
        /*      Print  The  Results     */

    printf (" Results file name: ");
    scanf ("%s", filename);
    if (( fp=fopen(filename,"w")) == NULL ) {
            printf ("  error: cannot open %s\n", filename);
            exit (0);
    }

    fprintf (fp, "\t\t\t\tPeaks In %s\n\n", argv[1]);
    fprintf (fp, "Hz-data\t\tHz-fit\t\tAmp^2-data\tAmp^2-fit\t");
    fprintf (fp, "Phase\tDamping %%\n");

    for (i=1; i <= n_pk; i++)
            fprintf (fp, "%7.4f\t\t%7.4f\t\t%.4e\t%.4e\t%4.0f\t%5.1f\n"
            pk[i].f,pk[i].F,pk[i].a,pk[i].A,pk[i].p,pk[i].d);
    fprintf (fp, "\n");
    fprintf (fp, "\t\tRMS-acc\t\tRMS-vel\t\tRMS-dsp\n");
    fprintf (fp, "\t\t%.3e\t%.3e\t%.3e\n", rms_a, rms_v, rms_d);
    fprintf (fp, "\n\n");

    free_matrix(pk_data,1,20,1,2);
    free_matrix(C,1,3,1,1);

    fclose (fp);
}


    /*              Function dter_fit()                 */
    /* Fit a power polynomial to data deterministically      */

void dter_fit (data,n,C)
float   **data,         /* the data to be fit                                */
        **C;            /* the power polynomial coeffs & [X]t {y}            */
int     n;              /* the number of data points                         */
{
        float   **X,    /* the power poly basis function matrix */
                **matrix();

        int     i,j;

        void    gaussj(),       /* gauss-jordan elimination      */
                free_matrix();

        X = matrix(1,n,1,n);

        for (i=1; i<=n; i++) {
                X[i][1] = 1.0;
                for (j=2; j<=n; j++)
                        X[i][j] = X[i][j-1]*data[i][1];
                C[i][1] = data[i][2];
```

```
        }

        gaussj (X,n,C,1);

        free_matrix(X,1,n,1,n);
        return;
}


        /*              Function poly_fit()                          */
        /* Fit a power polynomial to a set of data using             */
        /* linear least squares & gauss-jordan inversion             */

void poly_fit (data,n,order,C)
float   **data,         /* the data to be fit                                  */
        **C;            /* the power polynomial coeffs & [X]t {y}              */
int     order,          /* the order of the fit                                */
        n;              /* the number of data points > order                   */
{
        float   **X,    /* the power poly basis function matrix */
                **A,    /*      [X]t [X]                        */
                **matrix();

        int     i,j,k;

        void    gaussj(),       /* gauss-jordan elimination     */
                free_matrix();

        A = matrix(1,order+1,1,order+1);
        X = matrix(1,n,1,order+1);

        printf ("%d\n",n);
        for (i=1; i<=n; i++) printf ("%e\t%e\n", data[i][1], data[i][2]);

        for (i=1; i<=n; i++) {
                X[i][1] = 1.0;
                for (j=2; j<=order+1; j++)
                        X[i][j] = X[i][j-1]*data[i][1];
        }
        for (k=1; k<=order+1; k++)
                for (j=k; j<=order+1; j++) {
                        A[k][j] = 0.0;
                        for (i=1; i<=n; i++)
                             A[k][j] += X[i][k]*X[i][j];
                        A[j][k] = A[k][j];
                }
        for (k=1; k<=order+1; k++) {
                C[k][1] = 0.0;
                for (i=1; i<=n; i++)
                        C[k][1] += X[i][k]*data[i][2];
        }
```

```
        gaussj (A,order+1,C,1);

        free_matrix(X,1,n,1,order+1);
        free_matrix(A,1,order+1,1,order+1);
        return;
}
```

```
/*                        FILE gaussj.c                                    */
/*      Gauss-Jordan Elimination from Numerical Recipes in C               */

#include <math.h>

#define SWAP(a,b) {float temp=(a);(a)=(b);(b)=temp;}

void gaussj(a,n,b,m)
float **a,**b;
int n,m;
{
        int *indxc,*indxr,*ipiv,*ivector();
        int i,icol,irow,j,k,l,ll;
        float big,dum,pivinv;
        void nrerror(),free_ivector();

        indxc=ivector(1,n);
        indxr=ivector(1,n);
        ipiv=ivector(1,n);
        for (j=1;j<=n;j++) ipiv[j]=0;
        for (i=1;i<=n;i++) {
                big=0.0;
                for (j=1;j<=n;j++)
                        if (ipiv[j] != 1)
                                for (k=1;k<=n;k++) {
                                        if (ipiv[k] == 0) {
                                                if (fabs(a[j][k]) >= big) {
                                                        big=fabs(a[j][k]);
                                                        irow=j;
                                                        icol=k;
                                                }
                                        } else if (ipiv[k] > 1)
                                        nrerror("GAUSSJ: Singular Matrix-1"
                                }
                ++(ipiv[icol]);
                if (irow != icol) {
                        for (l=1;l<=n;l++) SWAP(a[irow][l],a[icol][l])
                        for (l=1;l<=m;l++) SWAP(b[irow][l],b[icol][l])
                }
                indxr[i]=irow;
                indxc[i]=icol;
                if (a[icol][icol] == 0.0) nrerror("GAUSSJ: Singular Matrix-
                pivinv=1.0/a[icol][icol];
                a[icol][icol]=1.0;
                for (l=1;l<=n;l++) a[icol][l] *= pivinv;
                for (l=1;l<=m;l++) b[icol][l] *= pivinv;
                for (ll=1;ll<=n;ll++)
                        if (ll != icol) {
                                dum=a[ll][icol];
                                a[ll][icol]=0.0;
                                for (l=1;l<=n;l++) a[ll][l] -= a[icol][l]*d
                                for (l=1;l<=m;l++) b[ll][l] -= b[icol][l]*d
```

```
                        }
                }
                for (l=n;l>=1;l--) {
                        if (indxr[l] != indxc[l])
                                for (k=1;k<=n;k++)
                                        SWAP(a[k][indxr[l]],a[k][indxc[l]]);
                }
                free_ivector(ipiv,1,n);
                free_ivector(indxr,1,n);
                free_ivector(indxc,1,n);
}
```

NATIONAL CENTER FOR EARTHQUAKE ENGINEERING RESEARCH
LIST OF TECHNICAL REPORTS

The National Center for Earthquake Engineering Research (NCEER) publishes technical reports on a variety of subjects related to earthquake engineering written by authors funded through NCEER. These reports are available from both NCEER's Publications Department and the National Technical Information Service (NTIS). Requests for reports should be directed to the Publications Department, National Center for Earthquake Engineering Research, State University of New York at Buffalo, Red Jacket Quadrangle, Buffalo, New York 14261. Reports can also be requested through NTIS, 5285 Port Royal Road, Springfield, Virginia 22161. NTIS accession numbers are shown in parenthesis, if available.

NCEER-87-0001 "First-Year Program in Research, Education and Technology Transfer," 3/5/87, (PB88-134275/AS).

NCEER-87-0002 "Experimental Evaluation of Instantaneous Optimal Algorithms for Structural Control," by R.C. Lin, T.T. Soong and A.M. Reinhorn, 4/20/87, (PB88-134341/AS).

NCEER-87-0003 "Experimentation Using the Earthquake Simulation Facilities at University at Buffalo," by A.M. Reinhorn and R.L. Ketter, to be published.

NCEER-87-0004 "The System Characteristics and Performance of a Shaking Table," by J.S. Hwang, K.C. Chang and G.C. Lee, 6/1/87, (PB88-134259/AS). This report is available only through NTIS (see address given above).

NCEER-87-0005 "A Finite Element Formulation for Nonlinear Viscoplastic Material Using a Q Model," by O. Gyebi and G. Dasgupta, 11/2/87, (PB88-213764/AS).

NCEER-87-0006 "Symbolic Manipulation Program (SMP) - Algebraic Codes for Two and Three Dimensional Finite Element Formulations," by X. Lee and G. Dasgupta, 11/9/87, (PB88-219522/AS).

NCEER-87-0007 "Instantaneous Optimal Control Laws for Tall Buildings Under Seismic Excitations," by J.N. Yang, A. Akbarpour and P. Ghaemmaghami, 6/10/87, (PB88-134333/AS).

NCEER-87-0008 "IDARC: Inelastic Damage Analysis of Reinforced Concrete Frame - Shear-Wall Structures," by Y.J. Park, A.M. Reinhorn and S.K. Kunnath, 7/20/87, (PB88-134325/AS).

NCEER-87-0009 "Liquefaction Potential for New York State: A Preliminary Report on Sites in Manhattan and Buffalo," by M. Budhu, V. Vijayakumar, R.F. Giese and L. Baumgras, 8/31/87, (PB88-163704/AS). This report is available only through NTIS (see address given above).

NCEER-87-0010 "Vertical and Torsional Vibration of Foundations in Inhomogeneous Media," by A.S. Veletsos and K.W. Dotson, 6/1/87, (PB88-134291/AS).

NCEER-87-0011 "Seismic Probabilistic Risk Assessment and Seismic Margins Studies for Nuclear Power Plants," by Howard H.M. Hwang, 6/15/87, (PB88-134267/AS).

NCEER-87-0012 "Parametric Studies of Frequency Response of Secondary Systems Under Ground-Acceleration Excitations," by Y. Yong and Y.K. Lin, 6/10/87, (PB88-134309/AS).

NCEER-87-0013 "Frequency Response of Secondary Systems Under Seismic Excitation," by J.A. HoLung, J. Cai and Y.K. Lin, 7/31/87, (PB88-134317/AS).

NCEER-87-0014 "Modelling Earthquake Ground Motions in Seismically Active Regions Using Parametric Time Series Methods," by G.W. Ellis and A.S. Cakmak, 8/25/87, (PB88-134283/AS).

NCEER-87-0015 "Detection and Assessment of Seismic Structural Damage," by E. DiPasquale and A.S. Cakmak, 8/25/87, (PB88-163712/AS).

NCEER-87-0016 "Pipeline Experiment at Parkfield, California," by J. Isenberg and E. Richardson, 9/15/87, (PB88-163720/AS). This report is available only through NTIS (see address given above).

NCEER-87-0017 "Digital Simulation of Seismic Ground Motion," by M. Shinozuka, G. Deodatis and T. Harada, 8/31/87, (PB88-155197/AS). This report is available only through NTIS (see address given above).

NCEER-87-0018 "Practical Considerations for Structural Control: System Uncertainty, System Time Delay and Truncation of Small Control Forces," J.N. Yang and A. Akbarpour, 8/10/87, (PB88-163738/AS).

NCEER-87-0019 "Modal Analysis of Nonclassically Damped Structural Systems Using Canonical Transformation," by J.N. Yang, S. Sarkani and F.X. Long, 9/27/87, (PB88-187851/AS).

NCEER-87-0020 "A Nonstationary Solution in Random Vibration Theory," by J.R. Red-Horse and P.D. Spanos, 11/3/87, (PB88-163746/AS).

NCEER-87-0021 "Horizontal Impedances for Radially Inhomogeneous Viscoelastic Soil Layers," by A.S. Veletsos and K.W. Dotson, 10/15/87, (PB88-150859/AS).

NCEER-87-0022 "Seismic Damage Assessment of Reinforced Concrete Members," by Y.S. Chung, C. Meyer and M. Shinozuka, 10/9/87, (PB88-150867/AS). This report is available only through NTIS (see address given above).

NCEER-87-0023 "Active Structural Control in Civil Engineering," by T.T. Soong, 11/11/87, (PB88-187778/AS).

NCEER-87-0024 "Vertical and Torsional Impedances for Radially Inhomogeneous Viscoelastic Soil Layers," by K.W. Dotson and A.S. Veletsos, 12/87, (PB88-187786/AS).

NCEER-87-0025 "Proceedings from the Symposium on Seismic Hazards, Ground Motions, Soil-Liquefaction and Engineering Practice in Eastern North America," October 20-22, 1987, edited by K.H. Jacob, 12/87, (PB88-188115/AS).

NCEER-87-0026 "Report on the Whittier-Narrows, California, Earthquake of October 1, 1987," by J. Pantelic and A. Reinhorn, 11/87, (PB88-187752/AS). This report is available only through NTIS (see address given above).

NCEER-87-0027 "Design of a Modular Program for Transient Nonlinear Analysis of Large 3-D Building Structures," by S. Srivastav and J.F. Abel, 12/30/87, (PB88-187950/AS).

NCEER-87-0028 "Second-Year Program in Research, Education and Technology Transfer," 3/8/88, (PB88-219480/AS).

NCEER-88-0001 "Workshop on Seismic Computer Analysis and Design of Buildings With Interactive Graphics," by W. McGuire, J.F. Abel and C.H. Conley, 1/18/88, (PB88-187760/AS).

NCEER-88-0002 "Optimal Control of Nonlinear Flexible Structures," by J.N. Yang, F.X. Long and D. Wong, 1/22/88, (PB88-213772/AS).

NCEER-88-0003 "Substructuring Techniques in the Time Domain for Primary-Secondary Structural Systems," by G.D. Manolis and G. Juhn, 2/10/88, (PB88-213780/AS).

NCEER-88-0004 "Iterative Seismic Analysis of Primary-Secondary Systems," by A. Singhal, L.D. Lutes and P.D. Spanos, 2/23/88, (PB88-213798/AS).

NCEER-88-0005 "Stochastic Finite Element Expansion for Random Media," by P.D. Spanos and R. Ghanem, 3/14/88, (PB88-213806/AS).

NCEER-88-0006 "Combining Structural Optimization and Structural Control," by F.Y. Cheng and C.P. Pantelides, 1/10/88, (PB88-213814/AS).

NCEER-88-0007 "Seismic Performance Assessment of Code-Designed Structures," by H.H-M. Hwang, J-W. Jaw and H-J. Shau, 3/20/88, (PB88-219423/AS).

NCEER-88-0008 "Reliability Analysis of Code-Designed Structures Under Natural Hazards," by H.H-M. Hwang, H. Ushiba and M. Shinozuka, 2/29/88, (PB88-229471/AS).

NCEER-88-0009 "Seismic Fragility Analysis of Shear Wall Structures," by J-W Jaw and H.H-M. Hwang, 4/30/88, (PB89-102867/AS).

NCEER-88-0010 "Base Isolation of a Multi-Story Building Under a Harmonic Ground Motion - A Comparison of Performances of Various Systems," by F-G Fan, G. Ahmadi and I.G. Tadjbakhsh, 5/18/88, (PB89-122238/AS).

NCEER-88-0011 "Seismic Floor Response Spectra for a Combined System by Green's Functions," by F.M. Lavelle, L.A. Bergman and P.D. Spanos, 5/1/88, (PB89-102875/AS).

NCEER-88-0012 "A New Solution Technique for Randomly Excited Hysteretic Structures," by G.Q. Cai and Y.K. Lin, 5/16/88, (PB89-102883/AS).

NCEER-88-0013 "A Study of Radiation Damping and Soil-Structure Interaction Effects in the Centrifuge," by K. Weissman, supervised by J.H. Prevost, 5/24/88, (PB89-144703/AS).

NCEER-88-0014 "Parameter Identification and Implementation of a Kinematic Plasticity Model for Frictional Soils," by J.H. Prevost and D.V. Griffiths, to be published.

NCEER-88-0015 "Two- and Three- Dimensional Dynamic Finite Element Analyses of the Long Valley Dam," by D.V. Griffiths and J.H. Prevost, 6/17/88, (PB89-144711/AS).

NCEER-88-0016 "Damage Assessment of Reinforced Concrete Structures in Eastern United States," by A.M. Reinhorn, M.J. Seidel, S.K. Kunnath and Y.J. Park, 6/15/88, (PB89-122220/AS).

NCEER-88-0017 "Dynamic Compliance of Vertically Loaded Strip Foundations in Multilayered Viscoelastic Soils," by S. Ahmad and A.S.M. Israil, 6/17/88, (PB89-102891/AS).

NCEER-88-0018 "An Experimental Study of Seismic Structural Response With Added Viscoelastic Dampers," by R.C. Lin, Z. Liang, T.T. Soong and R.H. Zhang, 6/30/88, (PB89-122212/AS). This report is available only through NTIS (see address given above).

NCEER-88-0019 "Experimental Investigation of Primary - Secondary System Interaction," by G.D. Manolis, G. Juhn and A.M. Reinhorn, 5/27/88, (PB89-122204/AS).

NCEER-88-0020 "A Response Spectrum Approach For Analysis of Nonclassically Damped Structures," by J.N. Yang, S. Sarkani and F.X. Long, 4/22/88, (PB89-102909/AS).

NCEER-88-0021 "Seismic Interaction of Structures and Soils: Stochastic Approach," by A.S. Veletsos and A.M. Prasad, 7/21/88, (PB89-122196/AS).

NCEER-88-0022 "Identification of the Serviceability Limit State and Detection of Seismic Structural Damage," by E. DiPasquale and A.S. Cakmak, 6/15/88, (PB89-122188/AS). This report is available only through NTIS (see address given above).

NCEER-88-0023 "Multi-Hazard Risk Analysis: Case of a Simple Offshore Structure," by B.K. Bhartia and E.H. Vanmarcke, 7/21/88, (PB89-145213/AS).

NCEER-88-0024 "Automated Seismic Design of Reinforced Concrete Buildings," by Y.S. Chung, C. Meyer and M. Shinozuka, 7/5/88, (PB89-122170/AS). This report is available only through NTIS (see address given above).

NCEER-88-0025 "Experimental Study of Active Control of MDOF Structures Under Seismic Excitations," by L.L. Chung, R.C. Lin, T.T. Soong and A.M. Reinhorn, 7/10/88, (PB89-122600/AS).

NCEER-88-0026 "Earthquake Simulation Tests of a Low-Rise Metal Structure," by J.S. Hwang, K.C. Chang, G.C. Lee and R.L. Ketter, 8/1/88, (PB89-102917/AS).

NCEER-88-0027 "Systems Study of Urban Response and Reconstruction Due to Catastrophic Earthquakes," by F. Kozin and H.K. Zhou, 9/22/88, (PB90-162348/AS).

NCEER-88-0028 "Seismic Fragility Analysis of Plane Frame Structures," by H.H-M. Hwang and Y.K. Low, 7/31/88, (PB89-131445/AS).

NCEER-88-0029 "Response Analysis of Stochastic Structures," by A. Kardara, C. Bucher and M. Shinozuka, 9/22/88, (PB89-174429/AS).

NCEER-88-0030 "Nonnormal Accelerations Due to Yielding in a Primary Structure," by D.C.K. Chen and L.D. Lutes, 9/19/88, (PB89-131437/AS).

NCEER-88-0031 "Design Approaches for Soil-Structure Interaction," by A.S. Veletsos, A.M. Prasad and Y. Tang, 12/30/88, (PB89-174437/AS). This report is available only through NTIS (see address given above).

NCEER-88-0032 "A Re-evaluation of Design Spectra for Seismic Damage Control," by C.J. Turkstra and A.G. Tallin, 11/7/88, (PB89-145221/AS).

NCEER-88-0033 "The Behavior and Design of Noncontact Lap Splices Subjected to Repeated Inelastic Tensile Loading," by V.E. Sagan, P. Gergely and R.N. White, 12/8/88, (PB89-163737/AS).

NCEER-88-0034 "Seismic Response of Pile Foundations," by S.M. Mamoon, P.K. Banerjee and S. Ahmad, 11/1/88, (PB89-145239/AS).

NCEER-88-0035 "Modeling of R/C Building Structures With Flexible Floor Diaphragms (IDARC2)," by A.M. Reinhorn, S.K. Kunnath and N. Panahshahi, 9/7/88, (PB89-207153/AS).

NCEER-88-0036 "Solution of the Dam-Reservoir Interaction Problem Using a Combination of FEM, BEM with Particular Integrals, Modal Analysis, and Substructuring," by C-S. Tsai, G.C. Lee and R.L. Ketter, 12/31/88, (PB89-207146/AS).

NCEER-88-0037 "Optimal Placement of Actuators for Structural Control," by F.Y. Cheng and C.P. Pantelides, 8/15/88, (PB89-162846/AS).

NCEER-88-0038 "Teflon Bearings in Aseismic Base Isolation: Experimental Studies and Mathematical Modeling," by A. Mokha, M.C. Constantinou and A.M. Reinhorn, 12/5/88, (PB89-218457/AS). This report is available only through NTIS (see address given above).

NCEER-88-0039 "Seismic Behavior of Flat Slab High-Rise Buildings in the New York City Area," by P. Weidlinger and M. Ettouney, 10/15/88, (PB90-145681/AS).

NCEER-88-0040 "Evaluation of the Earthquake Resistance of Existing Buildings in New York City," by P. Weidlinger and M. Ettouney, 10/15/88, to be published.

NCEER-88-0041 "Small-Scale Modeling Techniques for Reinforced Concrete Structures Subjected to Seismic Loads," by W. Kim, A. El-Attar and R.N. White, 11/22/88, (PB89-189625/AS).

NCEER-88-0042 "Modeling Strong Ground Motion from Multiple Event Earthquakes," by G.W. Ellis and A.S. Cakmak, 10/15/88, (PB89-174445/AS).

NCEER-88-0043 "Nonstationary Models of Seismic Ground Acceleration," by M. Grigoriu, S.E. Ruiz and E. Rosenblueth, 7/15/88, (PB89-189617/AS).

NCEER-88-0044 "SARCF User's Guide: Seismic Analysis of Reinforced Concrete Frames," by Y.S. Chung, C. Meyer and M. Shinozuka, 11/9/88, (PB89-174452/AS).

NCEER-88-0045 "First Expert Panel Meeting on Disaster Research and Planning," edited by J. Pantelic and J. Stoyle, 9/15/88, (PB89-174460/AS).

NCEER-88-0046 "Preliminary Studies of the Effect of Degrading Infill Walls on the Nonlinear Seismic Response of Steel Frames," by C.Z. Chrysostomou, P. Gergely and J.F. Abel, 12/19/88, (PB89-208383/AS).

NCEER-88-0047 "Reinforced Concrete Frame Component Testing Facility - Design, Construction, Instrumentation and Operation," by S.P. Pessiki, C. Conley, T. Bond, P. Gergely and R.N. White, 12/16/88, (PB89-174478/AS).

NCEER-89-0001 "Effects of Protective Cushion and Soil Compliancy on the Response of Equipment Within a Seismically Excited Building," by J.A. HoLung, 2/16/89, (PB89-207179/AS).

NCEER-89-0002 "Statistical Evaluation of Response Modification Factors for Reinforced Concrete Structures," by H.H-M. Hwang and J-W. Jaw, 2/17/89, (PB89-207187/AS).

NCEER-89-0003 "Hysteretic Columns Under Random Excitation," by G-Q. Cai and Y.K. Lin, 1/9/89, (PB89-196513/AS).

NCEER-89-0004 "Experimental Study of 'Elephant Foot Bulge' Instability of Thin-Walled Metal Tanks," by Z-H. Jia and R.L. Ketter, 2/22/89, (PB89-207195/AS).

NCEER-89-0005 "Experiment on Performance of Buried Pipelines Across San Andreas Fault," by J. Isenberg, E. Richardson and T.D. O'Rourke, 3/10/89, (PB89-218440/AS).

NCEER-89-0006 "A Knowledge-Based Approach to Structural Design of Earthquake-Resistant Buildings," by M. Subramani, P. Gergely, C.H. Conley, J.F. Abel and A.H. Zaghw, 1/15/89, (PB89-218465/AS).

NCEER-89-0007 "Liquefaction Hazards and Their Effects on Buried Pipelines," by T.D. O'Rourke and P.A. Lane, 2/1/89, (PB89-218481).

NCEER-89-0008 "Fundamentals of System Identification in Structural Dynamics," by H. Imai, C-B. Yun, O. Maruyama and M. Shinozuka, 1/26/89, (PB89-207211/AS).

NCEER-89-0009 "Effects of the 1985 Michoacan Earthquake on Water Systems and Other Buried Lifelines in Mexico," by A.G. Ayala and M.J. O'Rourke, 3/8/89, (PB89-207229/AS).

NCEER-89-R010 "NCEER Bibliography of Earthquake Education Materials," by K.E.K. Ross, Second Revision, 9/1/89, (PB90-125352/AS).

NCEER-89-0011 "Inelastic Three-Dimensional Response Analysis of Reinforced Concrete Building Structures (IDARC-3D), Part I - Modeling," by S.K. Kunnath and A.M. Reinhorn, 4/17/89, (PB90-114612/AS).

NCEER-89-0012 "Recommended Modifications to ATC-14," by C.D. Poland and J.O. Malley, 4/12/89, (PB90-108648/AS).

NCEER-89-0013 "Repair and Strengthening of Beam-to-Column Connections Subjected to Earthquake Loading," by M. Corazao and A.J. Durrani, 2/28/89, (PB90-109885/AS).

NCEER-89-0014 "Program EXKAL2 for Identification of Structural Dynamic Systems," by O. Maruyama, C-B. Yun, M. Hoshiya and M. Shinozuka, 5/19/89, (PB90-109877/AS).

NCEER-89-0015 "Response of Frames With Bolted Semi-Rigid Connections, Part I - Experimental Study and Analytical Predictions," by P.J. DiCorso, A.M. Reinhorn, J.R. Dickerson, J.B. Radziminski and W.L. Harper, 6/1/89, to be published.

NCEER-89-0016 "ARMA Monte Carlo Simulation in Probabilistic Structural Analysis," by P.D. Spanos and M.P. Mignolet, 7/10/89, (PB90-109893/AS).

NCEER-89-P017 "Preliminary Proceedings from the Conference on Disaster Preparedness - The Place of Earthquake Education in Our Schools," Edited by K.E.K. Ross, 6/23/89.

NCEER-89-0017 "Proceedings from the Conference on Disaster Preparedness - The Place of Earthquake Education in Our Schools," Edited by K.E.K. Ross, 12/31/89, (PB90-207895). This report is available only through NTIS (see address given above).

NCEER-89-0018 "Multidimensional Models of Hysteretic Material Behavior for Vibration Analysis of Shape Memory Energy Absorbing Devices, by E.J. Graesser and F.A. Cozzarelli, 6/7/89, (PB90-164146/AS).

NCEER-89-0019 "Nonlinear Dynamic Analysis of Three-Dimensional Base Isolated Structures (3D-BASIS)," by S. Nagarajaiah, A.M. Reinhorn and M.C. Constantinou, 8/3/89, (PB90-161936/AS). This report is available only through NTIS (see address given above).

NCEER-89-0020 "Structural Control Considering Time-Rate of Control Forces and Control Rate Constraints," by F.Y. Cheng and C.P. Pantelides, 8/3/89, (PB90-120445/AS).

NCEER-89-0021 "Subsurface Conditions of Memphis and Shelby County," by K.W. Ng, T-S. Chang and H-H.M. Hwang, 7/26/89, (PB90-120437/AS).

NCEER-89-0022 "Seismic Wave Propagation Effects on Straight Jointed Buried Pipelines," by K. Elhmadi and M.J. O'Rourke, 8/24/89, (PB90-162322/AS).

NCEER-89-0023 "Workshop on Serviceability Analysis of Water Delivery Systems," edited by M. Grigoriu, 3/6/89, (PB90-127424/AS).

NCEER-89-0024 "Shaking Table Study of a 1/5 Scale Steel Frame Composed of Tapered Members," by K.C. Chang, J.S. Hwang and G.C. Lee, 9/18/89, (PB90-160169/AS).

NCEER-89-0025 "DYNA1D: A Computer Program for Nonlinear Seismic Site Response Analysis - Technical Documentation," by Jean H. Prevost, 9/14/89, (PB90-161944/AS). This report is available only through NTIS (see address given above).

NCEER-89-0026 "1:4 Scale Model Studies of Active Tendon Systems and Active Mass Dampers for Aseismic Protection," by A.M. Reinhorn, T.T. Soong, R.C. Lin, Y.P. Yang, Y. Fukao, H. Abe and M. Nakai, 9/15/89, (PB90-173246/AS).

NCEER-89-0027 "Scattering of Waves by Inclusions in a Nonhomogeneous Elastic Half Space Solved by Boundary Element Methods," by P.K. Hadley, A. Askar and A.S. Cakmak, 6/15/89, (PB90-145699/AS).

NCEER-89-0028 "Statistical Evaluation of Deflection Amplification Factors for Reinforced Concrete Structures," by H.H.M. Hwang, J-W. Jaw and A.L. Ch'ng, 8/31/89, (PB90-164633/AS).

NCEER-89-0029 "Bedrock Accelerations in Memphis Area Due to Large New Madrid Earthquakes," by H.H.M. Hwang, C.H.S. Chen and G. Yu, 11/7/89, (PB90-162330/AS).

NCEER-89-0030 "Seismic Behavior and Response Sensitivity of Secondary Structural Systems," by Y.Q. Chen and T.T. Soong, 10/23/89, (PB90-164658/AS).

NCEER-89-0031 "Random Vibration and Reliability Analysis of Primary-Secondary Structural Systems," by Y. Ibrahim, M. Grigoriu and T.T. Soong, 11/10/89, (PB90-161951/AS).

NCEER-89-0032 "Proceedings from the Second U.S. - Japan Workshop on Liquefaction, Large Ground Deformation and Their Effects on Lifelines, September 26-29, 1989," Edited by T.D. O'Rourke and M. Hamada, 12/1/89, (PB90-209388/AS).

NCEER-89-0033 "Deterministic Model for Seismic Damage Evaluation of Reinforced Concrete Structures," by J.M. Bracci, A.M. Reinhorn, J.B. Mander and S.K. Kunnath, 9/27/89.

NCEER-89-0034 "On the Relation Between Local and Global Damage Indices," by E. DiPasquale and A.S. Cakmak, 8/15/89, (PB90-173865).

NCEER-89-0035 "Cyclic Undrained Behavior of Nonplastic and Low Plasticity Silts," by A.J. Walker and H.E. Stewart, 7/26/89, (PB90-183518/AS).

NCEER-89-0036 "Liquefaction Potential of Surficial Deposits in the City of Buffalo, New York," by M. Budhu, R. Giese and L. Baumgrass, 1/17/89, (PB90-208455/AS).

NCEER-89-0037 "A Deterministic Assessment of Effects of Ground Motion Incoherence," by A.S. Veletsos and Y. Tang, 7/15/89, (PB90-164294/AS).

NCEER-89-0038 "Workshop on Ground Motion Parameters for Seismic Hazard Mapping," July 17-18, 1989, edited by R.V. Whitman, 12/1/89, (PB90-173923/AS).

NCEER-89-0039 "Seismic Effects on Elevated Transit Lines of the New York City Transit Authority," by C.J. Costantino, C.A. Miller and E. Heymsfield, 12/26/89, (PB90-207887/AS).

NCEER-89-0040 "Centrifugal Modeling of Dynamic Soil-Structure Interaction," by K. Weissman, Supervised by J.H. Prevost, 5/10/89, (PB90-207879/AS).

NCEER-89-0041 "Linearized Identification of Buildings With Cores for Seismic Vulnerability Assessment," by I-K. Ho and A.E. Aktan, 11/1/89, (PB90-251943/AS).

NCEER-90-0001 "Geotechnical and Lifeline Aspects of the October 17, 1989 Loma Prieta Earthquake in San Francisco," by T.D. O'Rourke, H.E. Stewart, F.T. Blackburn and T.S. Dickerman, 1/90, (PB90-208596/AS).

NCEER-90-0002 "Nonnormal Secondary Response Due to Yielding in a Primary Structure," by D.C.K. Chen and L.D. Lutes, 2/28/90, (PB90-251976/AS).

NCEER-90-0003 "Earthquake Education Materials for Grades K-12," by K.E.K. Ross, 4/16/90, (PB91-113415/AS).

NCEER-90-0004 "Catalog of Strong Motion Stations in Eastern North America," by R.W. Busby, 4/3/90, (PB90-251984)/AS.

NCEER-90-0005 "NCEER Strong-Motion Data Base: A User Manual for the GeoBase Release (Version 1.0 for the Sun3)," by P. Friberg and K. Jacob, 3/31/90 (PB90-258062/AS).

NCEER-90-0006 "Seismic Hazard Along a Crude Oil Pipeline in the Event of an 1811-1812 Type New Madrid Earthquake," by H.H.M. Hwang and C-H.S. Chen, 4/16/90(PB90-258054).

NCEER-90-0007 "Site-Specific Response Spectra for Memphis Sheahan Pumping Station," by H.H.M. Hwang and C.S. Lee, 5/15/90, (PB91-108811/AS).

NCEER-90-0008 "Pilot Study on Seismic Vulnerability of Crude Oil Transmission Systems," by T. Ariman, R. Dobry, M. Grigoriu, F. Kozin, M. O'Rourke, T. O'Rourke and M. Shinozuka, 5/25/90, (PB91-108837/AS).

NCEER-90-0009 "A Program to Generate Site Dependent Time Histories: EQGEN," by G.W. Ellis, M. Srinivasan and A.S. Cakmak, 1/30/90, (PB91-108829/AS).

NCEER-90-0010 "Active Isolation for Seismic Protection of Operating Rooms," by M.E. Talbott, Supervised by M. Shinozuka, 6/8/9, (PB91-110205/AS).

NCEER-90-0011 "Program LINEARID for Identification of Linear Structural Dynamic Systems," by C-B. Yun and M. Shinozuka, 6/25/90, (PB91-110312/AS).

NCEER-90-0012 "Two-Dimensional Two-Phase Elasto-Plastic Seismic Response of Earth Dams," by A.N. Yiagos, Supervised by J.H. Prevost, 6/20/90, (PB91-110197/AS).

NCEER-90-0013 "Secondary Systems in Base-Isolated Structures: Experimental Investigation, Stochastic Response and Stochastic Sensitivity," by G.D. Manolis, G. Juhn, M.C. Constantinou and A.M. Reinhorn, 7/1/90, (PB91-110320/AS).

NCEER-90-0014 "Seismic Behavior of Lightly-Reinforced Concrete Column and Beam-Column Joint Details," by S.P. Pessiki, C.H. Conley, P. Gergely and R.N. White, 8/22/90, (PB91-108795/AS).

NCEER-90-0015 "Two Hybrid Control Systems for Building Structures Under Strong Earthquakes," by J.N. Yang and A. Danielians, 6/29/90, (PB91-125393/AS).

NCEER-90-0016 "Instantaneous Optimal Control with Acceleration and Velocity Feedback," by J.N. Yang and Z. Li, 6/29/90, (PB91-125401/AS).

NCEER-90-0017 "Reconnaissance Report on the Northern Iran Earthquake of June 21, 1990," by M. Mehrain, 10/4/90, (PB91-125377/AS).

NCEER-90-0018 "Evaluation of Liquefaction Potential in Memphis and Shelby County," by T.S. Chang, P.S. Tang, C.S. Lee and H. Hwang, 8/10/90, (PB91-125427/AS).

NCEER-90-0019 "Experimental and Analytical Study of a Combined Sliding Disc Bearing and Helical Steel Spring Isolation System," by M.C. Constantinou, A.S. Mokha and A.M. Reinhorn, 10/4/90, (PB91-125385/AS).

NCEER-90-0020 "Experimental Study and Analytical Prediction of Earthquake Response of a Sliding Isolation System with a Spherical Surface," by A.S. Mokha, M.C. Constantinou and A.M. Reinhorn, 10/11/90, (PB91-125419/AS).

NCEER-90-0021 "Dynamic Interaction Factors for Floating Pile Groups," by G. Gazetas, K. Fan, A. Kaynia and E. Kausel, 9/10/90, (PB91-170381/AS).

NCEER-90-0022 "Evaluation of Seismic Damage Indices for Reinforced Concrete Structures," by S. Rodriguez-Gomez and A.S. Cakmak, 9/30/90, PB91-171322/AS).

NCEER-90-0023 "Study of Site Response at a Selected Memphis Site," by H. Desai, S. Ahmad, E.S. Gazetas and M.R. Oh, 10/11/90, (PB91-196857/AS).

NCEER-90-0024 "A User's Guide to Strongmo: Version 1.0 of NCEER's Strong-Motion Data Access Tool for PCs and Terminals," by P.A. Friberg and C.A.T. Susch, 11/15/90, (PB91-171272/AS).

NCEER-90-0025 "A Three-Dimensional Analytical Study of Spatial Variability of Seismic Ground Motions," by L-L. Hong and A.H.-S. Ang, 10/30/90, (PB91-170399/AS).

NCEER-90-0026 "MUMOID User's Guide - A Program for the Identification of Modal Parameters," by S. Rodriguez-Gomez and E. DiPasquale, 9/30/90, (PB91-171298/AS).

NCEER-90-0027 "SARCF-II User's Guide - Seismic Analysis of Reinforced Concrete Frames," by S. Rodriguez-Gomez, Y.S. Chung and C. Meyer, 9/30/90, (PB91-171280/AS).

NCEER-90-0028 "Viscous Dampers: Testing, Modeling and Application in Vibration and Seismic Isolation," by N. Makris and M.C. Constantinou, 12/20/90 (PB91-190561/AS).

NCEER-90-0029 "Soil Effects on Earthquake Ground Motions in the Memphis Area," by H. Hwang, C.S. Lee, K.W. Ng and T.S. Chang, 8/2/90, (PB91-190751/AS).

NCEER-91-0001 "Proceedings from the Third Japan-U.S. Workshop on Earthquake Resistant Design of Lifeline Facilities and Countermeasures for Soil Liquefaction, December 17-19, 1990," edited by T.D. O'Rourke and M. Hamada, 2/1/91, (PB91-179259/AS).

NCEER-91-0002 "Physical Space Solutions of Non-Proportionally Damped Systems," by M. Tong, Z. Liang and G.C. Lee, 1/15/91, (PB91-179242/AS).

NCEER-91-0003 "Seismic Response of Single Piles and Pile Groups," by K. Fan and G. Gazetas, 1/10/91, (PB92-174994/AS).

NCEER-91-0004 "Damping of Structures: Part 1 - Theory of Complex Damping," by Z. Liang and G. Lee, 10/10/91, (PB92-197235/AS).

NCEER-91-0005 "3D-BASIS - Nonlinear Dynamic Analysis of Three Dimensional Base Isolated Structures: Part II," by S. Nagarajaiah, A.M. Reinhorn and M.C. Constantinou, 2/28/91, (PB91-190553/AS).

NCEER-91-0006 "A Multidimensional Hysteretic Model for Plasticity Deforming Metals in Energy Absorbing Devices," by E.J. Graesser and F.A. Cozzarelli, 4/9/91, (PB92-108364/AS).

NCEER-91-0007 "A Framework for Customizable Knowledge-Based Expert Systems with an Application to a KBES for Evaluating the Seismic Resistance of Existing Buildings," by E.G. Ibarra-Anaya and S.J. Fenves, 4/9/91, (PB91-210930/AS).

NCEER-91-0008 "Nonlinear Analysis of Steel Frames with Semi-Rigid Connections Using the Capacity Spectrum Method," by G.G. Deierlein, S-H. Hsieh, Y-J. Shen and J.F. Abel, 7/2/91, (PB92-113828/AS).

NCEER-91-0009 "Earthquake Education Materials for Grades K-12," by K.E.K. Ross, 4/30/91, (PB91-212142/AS).

NCEER-91-0010 "Phase Wave Velocities and Displacement Phase Differences in a Harmonically Oscillating Pile," by N. Makris and G. Gazetas, 7/8/91, (PB92-108356/AS).

NCEER-91-0011 "Dynamic Characteristics of a Full-Size Five-Story Steel Structure and a 2/5 Scale Model," by K.C. Chang, G.C. Yao, G.C. Lee, D.S. Hao and Y.C. Yeh," 7/2/91.

NCEER-91-0012 "Seismic Response of a 2/5 Scale Steel Structure with Added Viscoelastic Dampers," by K.C. Chang, T.T. Soong, S-T. Oh and M.L. Lai, 5/17/91 (PB92-110816/AS).

NCEER-91-0013 "Earthquake Response of Retaining Walls; Full-Scale Testing and Computational Modeling," by S. Alampalli and A-W.M. Elgamal, 6/20/91, to be published.

NCEER-91-0014 "3D-BASIS-M: Nonlinear Dynamic Analysis of Multiple Building Base Isolated Structures," by P.C. Tsopelas, S. Nagarajaiah, M.C. Constantinou and A.M. Reinhorn, 5/28/91, (PB92-113885/AS).

NCEER-91-0015 "Evaluation of SEAOC Design Requirements for Sliding Isolated Structures," by D. Theodossiou and M.C. Constantinou, 6/10/91, (PB92-114602/AS).

NCEER-91-0016 "Closed-Loop Modal Testing of a 27-Story Reinforced Concrete Flat Plate-Core Building," by H.R. Somaprasad, T. Toksoy, H. Yoshiyuki and A.E. Aktan, 7/15/91, (PB92-129980/AS).

NCEER-91-0017 "Shake Table Test of a 1/6 Scale Two-Story Lightly Reinforced Concrete Building," by A.G. El-Attar, R.N. White and P. Gergely, 2/28/91, (PB92-222447/AS).

NCEER-91-0018 "Shake Table Test of a 1/8 Scale Three-Story Lightly Reinforced Concrete Building," by A.G. El-Attar, R.N. White and P. Gergely, 2/28/91.

NCEER-91-0019 "Transfer Functions for Rigid Rectangular Foundations," by A.S. Veletsos, A.M. Prasad and W.H. Wu, 7/31/91.

NCEER-91-0020 "Hybrid Control of Seismic-Excited Nonlinear and Inelastic Structural Systems," by J.N. Yang, Z. Li and A. Danielians, 8/1/91, (PB92-143171/AS).

NCEER-91-0021 "The NCEER-91 Earthquake Catalog: Improved Intensity-Based Magnitudes and Recurrence Relations for U.S. Earthquakes East of New Madrid," by L. Seeber and J.G. Armbruster, 8/28/91, (PB92-176742/AS).

NCEER-91-0022 "Proceedings from the Implementation of Earthquake Planning and Education in Schools: The Need for Change - The Roles of the Changemakers," by K.E.K. Ross and F. Winslow, 7/23/91, (PB92-129998/AS).

NCEER-91-0023 "A Study of Reliability-Based Criteria for Seismic Design of Reinforced Concrete Frame Buildings," by H.H.M. Hwang and H-M. Hsu, 8/10/91, (PB92-140235/AS).

NCEER-91-0024 "Experimental Verification of a Number of Structural System Identification Algorithms," by R.G. Ghanem, H. Gavin and M. Shinozuka, 9/18/91, (PB92-176577/AS).

NCEER-91-0025 "Probabilistic Evaluation of Liquefaction Potential," by H.H.M. Hwang and C.S. Lee," 11/25/91, (PB92-143429/AS).

NCEER-91-0026 "Instantaneous Optimal Control for Linear, Nonlinear and Hysteretic Structures - Stable Controllers," by J.N. Yang and Z. Li, 11/15/91, (PB92-163807/AS).

NCEER-91-0027 "Experimental and Theoretical Study of a Sliding Isolation System for Bridges," by M.C. Constantinou, A. Kartoum, A.M. Reinhorn and P. Bradford, 11/15/91, (PB92-176973/AS).

NCEER-92-0001 "Case Studies of Liquefaction and Lifeline Performance During Past Earthquakes, Volume 1: Japanese Case Studies," Edited by M. Hamada and T. O'Rourke, 2/17/92, (PB92-197243/AS).

NCEER-92-0002 "Case Studies of Liquefaction and Lifeline Performance During Past Earthquakes, Volume 2: United States Case Studies," Edited by T. O'Rourke and M. Hamada, 2/17/92, (PB92-197250/AS).

NCEER-92-0003 "Issues in Earthquake Education," Edited by K. Ross, 2/3/92, (PB92-222389/AS).

NCEER-92-0004 "Proceedings from the First U.S. - Japan Workshop on Earthquake Protective Systems for Bridges," 2/4/92, to be published.

NCEER-92-0005 "Seismic Ground Motion from a Haskell-Type Source in a Multiple-Layered Half-Space," A.P. Theoharis, G. Deodatis and M. Shinozuka, 1/2/92, to be published.

NCEER-92-0006 "Proceedings from the Site Effects Workshop," Edited by R. Whitman, 2/29/92, (PB92-197201/AS).

NCEER-92-0007 "Engineering Evaluation of Permanent Ground Deformations Due to Seismically-Induced Liquefaction," by M.H. Baziar, R. Dobry and A-W.M. Elgamal, 3/24/92, (PB92-222421/AS).

NCEER-92-0008 "A Procedure for the Seismic Evaluation of Buildings in the Central and Eastern United States," by C.D. Poland and J.O. Malley, 4/2/92, (PB92-222439/AS).

NCEER-92-0009 "Experimental and Analytical Study of a Hybrid Isolation System Using Friction Controllable Sliding Bearings," by M.Q. Feng, S. Fujii and M. Shinozuka, 5/15/92.

NCEER-92-0010 "Seismic Resistance of Slab-Column Connections in Existing Non-Ductile Flat-Plate Buildings," by A.J. Durrani and Y. Du, 5/18/92.

NCEER-92-0011 "The Hysteretic and Dynamic Behavior of Brick Masonry Walls Upgraded by Ferrocement Coatings Under Cyclic Loading and Strong Simulated Ground Motion," by H. Lee and S.P. Prawel, 5/11/92, to be published.

NCEER-92-0012 "Study of Wire Rope Systems for Seismic Protection of Equipment in Buildings," by G.F. Demetriades, M.C. Constantinou and A.M. Reinhorn, 5/20/92.

NCEER-92-0013 "Shape Memory Structural Dampers: Material Properties, Design and Seismic Testing," by P.R. Witting and F.A. Cozzarelli, 5/26/92.

NCEER-92-0014 "Longitudinal Permanent Ground Deformation Effects on Buried Continuous Pipelines," by M.J. O'Rourke, and C. Nordberg, 6/15/92.

NCEER-92-0015 "A Simulation Method for Stationary Gaussian Random Functions Based on the Sampling Theorem," by M. Grigoriu and S. Balopoulou, 6/11/92, (PB93-127496/AS).

NCEER-92-0016 "Gravity-Load-Designed Reinforced Concrete Buildings: Seismic Evaluation of Existing Construction and Detailing Strategies for Improved Seismic Resistance," by G.W. Hoffmann, S.K. Kunnath, J.B. Mander and A.M. Reinhorn, 7/15/92, to be published.

NCEER-92-0017 "Observations on Water System and Pipeline Performance in the Limón Area of Costa Rica Due to the April 22, 1991 Earthquake," by M. O'Rourke and D. Ballantyne, 6/30/92, (PB93-126811/AS).

NCEER-92-0018 "Fourth Edition of Earthquake Education Materials for Grades K-12," Edited by K.E.K. Ross, 8/10/92.

NCEER-92-0019 "Proceedings from the Fourth Japan-U.S. Workshop on Earthquake Resistant Design of Lifeline Facilities and Countermeasures for Soil Liquefaction," Edited by M. Hamada and T.D. O'Rourke, 8/12/92.

NCEER-92-0020 "Active Bracing System: A Full Scale Implementation of Active Control," by A.M. Reinhorn, T.T. Soong, R.C. Lin, M.A. Riley, Y.P. Wang, S. Aizawa and M. Higashino, 8/14/92, (PB93-127512/AS).

NCEER-92-0021 "Empirical Analysis of Horizontal Ground Displacement Generated by Liquefaction-Induced Lateral Spreads," by S.F. Bartlett and T.L. Youd, 8/17/92.

NCEER-92-0022 "IDARC Version 3.0: Inelastic Damage Analysis of Reinforced Concrete Structures," by S.K. Kunnath, A.M. Reinhorn and R.F. Lobo, 8/31/92, to be published.

NCEER-92-0023 "A Semi-Empirical Analysis of Strong-Motion Peaks in Terms of Seismic Source, Propagation Path and Local Site Conditions, by M. Kamiyama, M.J. O'Rourke and R. Flores-Berrones, 9/9/92.

NCEER-92-0024 "Seismic Behavior of Reinforced Concrete Frame Structures with Nonductile Details, Part I: Summary of Experimental Findings of Full Scale Beam-Column Joint Tests," by A. Beres, R.N. White and P. Gergely, 9/30/92, to be published.

NCEER-92-0025 "Experimental Results of Repaired and Retrofitted Beam-Column Joint Tests in Lightly Reinforced Concrete Frame Buildings," by A. Beres, S. El-Borgi, R.N. White and P. Gergely, 10/29/92, to be published.

NCEER-92-0026 "A Generalization of Optimal Control Theory: Linear and Nonlinear Structures," by J.N. Yang, Z. Li and S. Vongchavalitkul, 11/2/92.

NCEER-92-0027 "Seismic Resistance of Reinforced Concrete Frame Structures Designed Only for Gravity Loads: Part I - Design and Properties of a One-Third Scale Model Structure," by J.M. Bracci, A.M. Reinhorn and J.B. Mander, 12/1/92, to be published.

NCEER-92-0028 "Seismic Resistance of Reinforced Concrete Frame Structures Designed Only for Gravity Loads: Part II - Experimental Performance of Subassemblages," by L.E. Aycardi, J.B. Mander and A.M. Reinhorn, 12/1/92, to be published.

NCEER-92-0029 "Seismic Resistance of Reinforced Concrete Frame Structures Designed Only for Gravity Loads: Part III - Experimental Performance and Analytical Study of a Structural Model," by J.M. Bracci, A.M. Reinhorn and J.B. Mander, 12/1/92, to be published.

NCEER-92-0030 "Evaluation of Seismic Retrofit of Reinforced Concrete Frame Structures: Part I - Experimental Performance of Retrofitted Subassemblages," by D. Choudhuri, J.B. Mander and A.M. Reinhorn, 12/8/92, to be published.

NCEER-92-0031 "Evaluation of Seismic Retrofit of Reinforced Concrete Frame Structures: Part II - Experimental Performance and Analytical Study of a Retrofitted Structural Model," by J.M. Bracci, A.M. Reinhorn and J.B. Mander, 12/8/92, to be published.

NCEER-92-0032 "Experimental and Analytical Investigation of Seismic Response of Structures with Supplemental Fluid Viscous Dampers," by M.C. Constantinou and M.D. Symans, 12/21/92.

NCEER-92-0033 "Reconnaissance Report on the Cairo, Egypt Earthquake of October 12, 1992," by M. Khater, 12/23/92.

NCEER-92-0034 "Low-Level Dynamic Characteristics of Four Tall Flat-Plate Buildings in New York City," by H. Gavin, S. Yuan, J. Grossman, E. Pekelis and K. Jacob, 12/28/92.